Photophysical Studies of Metalloporphyrins for Sensitized Noncoherent Photon Upconversion

A Thesis Submitted to

The College of Graduate Studies and Research

In Partial Fulfillment of the Requirements

For the Degree of Doctor of Philosophy

In the Department of Chemistry

University of Saskatchewan

Saskatoon

By

Sunish Kaniyamparambil Sugunan

Permission to Use

In presenting this thesis in partial fulfilment of the requirements for a Postgraduate degree from the University of Saskatchewan, I agree that the Libraries of this University may make it freely available for inspection. I further agree that permission for copying of this thesis in any manner, in whole or in part, for scholarly purposes may be granted by the Professors Ronald P. Steer and Matthew F. Paige who supervised my thesis work or, in their absence, by the Head of the Department of Chemistry or the Dean of the College of Graduate Studies and Research of University of Saskatchewan. It is understood that any copying or publication or use of this thesis or parts thereof for financial gain shall not be allowed without my written permission. It is also understood that due recognition shall be given to me and to the University of Saskatchewan in any scholarly use which may be made of any material in my thesis.

Requests for permission to copy or to make other use of material in this thesis in whole or part should be addressed to:

The Head

Department of Chemistry

University of Saskatchewan

Saskatoon, Saskatchewan S7N 5C9

Canada

Abstract

Noncoherent photon upconversion (NCPU) realized by means of triplet-triplet annihilation (TTA) is of significant recent interest because of the possibility of using this phenomenon for increasing the efficiency of dye-sensitized solar cells (DSSCs). Efficiencies can be achieved if the near-IR parts of the solar spectrum can be absorbed and used in TTA. However, realizing this potential is not trivial. Dual absorption and TTA usually populates a higher excited singlet state (S_n, $n \geq 2$) of the absorber molecule and the fate of this state can be a critical factor controlling efficiencies and hence the potential efficiency improvements in DSSCs.

With a motivation to understand the photophysical processes that decides the fate of the product state of TTA, the role of the S_2 state of a metalloporphyrin and a fullerene in solution-phase NCPU has been investigated using photophysical techniques. TTA in the model porphyrin, zinc(II) meso-tetraphenylporphine (ZnTPP) realized by excitation with a green laser, was found to occur through a short-range Dexter-type energy transfer mechanism. It was also found, contrary to a previous suggestion, that a Förster-type energy transfer cannot occur from the short-lived S_2 state of ZnTPP to an acceptor molecule. It was hypothesized that prior aggregation of ZnTPP and the acceptor molecule should exist to enable such an energy transfer. For blue emitter (BE) molecules with triplet energies lower than that of ZnTPP, a triplet-triplet energy transfer (TTET) from ZnTPP to the BE followed by TTA in the BE populates its S_1 state. However, this is not

possible for BEs with triplet energies significantly greater than that of ZnTPP. In this case, it is proposed that the triplet ZnTPP forms a triplet exciplex with a ground state BE. The triplet exciplex then annihilates with a second triplet ZnTPP to form the S_1 state of the BE. For the studies of the NCPU in C_{60}, the BEs chosen were having triplet energies similar or slightly lower than that of C_{60}. The NCPU in these systems follows the well-established mechanism of TTET from C_{60} to the BE followed by TTA in the BE to produce its S_1 state. However, for systems in which the triplet energies of C_{60} and BE are similar, the NCPU process is controlled by entropic factors which in turn can be controlled by the concentration of the BE. Compared to this system, NCPU in a system in which the triplet of C_{60} lies slightly higher than that of the BE was found to be more efficient. The involvement of the higher excited singlet states of C_{60} (S_n, $n \geq 2$) can be considered as insignificant because of the proximity of these states to the S_1 state and the large rates of internal conversion from these states to the S_1 state.

Because triplets can be quenched by molecular oxygen, the rate of oxygen diffusion in devices based on NCPU needs to be evaluated. With this objective, upconverted S_2 emission from ZnTPP produced by TTA was used as a tool to measure the rate of oxygen diffusion in a thin polymer film. It was found that the oxygen permeability is controlled by the characteristics of the polymer matrix, including its water content and its distribution.

C_{60} has been evaluated as a possible electron acceptor for the TTA-produced S_2 state of ZnTPP. Quenching of the S_2 and S_1 fluorescence of ZnTPP by added C_{60}, with more

efficient quenching for the Soret-excited ZnTPP+C_{60} species, was demonstrated. Significant ground state aggregation between ZnTPP and C_{60} was proven. However this factor could not account for the observed difference in the rates of quenching of the S_2 and S_1 fluorescence of the excited porphyrin. The difference in the rates of quenching was attributed to differences in the free energies of electron transfer from the S_2 and S_1 states of ZnTPP to C_{60}. Conclusive evidence for this was obtained from transient absorption studies carried out at the University of Melbourne, which demonstrated the formation of a long-lived charge transfer state upon Soret-excitation of the porphyrin-C_{60} complex. However, the involvement of short-range Dexter type energy transfer could not be ruled out in this system.

Acknowledgements

This thesis would not have been in this form without the inspiration, intellectual contributions, technical helps, professional and personal supports and unconditional love and friendship of so many people.

First and foremost, I would like to express my deepest gratitude to my supervisors, Professors Ron Steer and Matthew Paige. They have been the source of inspiration for me. They challenged me to think independently, identify problems and tackle them. I learnt a lot from them! I would not have been able to complete this thesis without their guidance, I am sure!

I would like to thank my scientific advisory committee members, Professors Safa Kasap, Ian Burgess and Stephen Urquhart. Their monitoring of my research progress helped me to get up to this point. Thanks to Dr. Stephen Urquhart for letting me work on the ellipsometer in his lab.

I have had the privilege to work with a number of group members from both Ron's lab and Paige's lab. Technical and scientific help from Umakanta, Suresh, Jędrzej, Mani, Xia, Brook, Conie, Ryan and Chelsea are gratefully acknowledged.

Scientific assistance from Saskatchewan Structural Science Center (SSSC) and technical help of Dr. Sophie Brunet on TCSPC are gratefully acknowledged.

I express my gratitude to Department of Chemistry and University of Saskatchewan for allowing me to do my PhD here.

I thank my teachers from Mahatma Gandhi University and S.B. College who taught me the basics of Chemistry, Physics and Mathematics.

Friends from in and out of the lab deserve special mention here. Coffee session with Mani was the most relaxing time of my academic time here. Mani, you are like my brother, it would be inappropriate to thank you. I will see you, Shipra and Anwesha in

UK. Coffee time and chit-chat with Conie, Neeraj, Hessam and Ala was real fun; thanks Conie for brewing the coffee for me.

My Saskatoon friends cheered my days here. Tarek Bhai, you were the best friend I had in Saskatoon. I will never forget your wittiness, sarcasm and bugging me for not teaching you HPLC! You have a golden heart. Thanks to your friendship and thanks to your wife for the delicious dinners at your place. Vivekettan was the best roommate ever; he was the coolest graduate student I've ever seen. Thanks to my later roommates Jijin, Prashobh and Pranav for their cheerful company. Thanks to Vijay for helping me through my visa renewal.

My closest friends Binoy, Mathew, Vibin and Swaroop have been always on my side during my PhD, they were of great help and care. Only a graduate student can understand another graduate student; talking with Vibin almost every day was the buster of my daily life boredom. Friends, I cannot express how much I owe you.

Family is the greatest gift of life; I am what I am because of my family. Without their unconditional love, understanding, support and inspiration, I would not be the person I am now. My parents have been the greatest inspirations in my life. They taught me that one can find rays of hope and happiness among all the struggles of life. My brothers are my first and best friends. I know you both miss me. The lady love of my life, my wife, has been the greatest support during my PhD. None of my days in Saskatoon passed without calling you. You cheered my doomed-days and lit hope in me. Without your love, understanding and faith in me, I would not have survived staying away from you for this long-time. I cannot wait to see my family.

Finally, I thank all the scientists who laid the foundations of science to date and who work hard to make it progressing. Without them, the world would not be the same as I see today.

Dedicated To:

Dearest Achachan, Ammachi, Anuchettayi, Kocherukkan & my Paru

For the love and joy they bring in my life.

Table of Contents

List of Figures

List of Tables

List of Schemes

List of Abbreviations and Units

A	Absorption or ampere
Abs	Absorption
ADC	Analog to digital converter
AM1	Austin model 1
AM 1.5	Air mass coefficient 1.5 (Solar energy)
An	Anthanthrene
a.u.	Arbitrary units
BBO	β-Bariumborate, β-BaB_2O_4
BE	Blue-emitter
C343	Coumarin 343
C_{60}	Buckminsterfullerene
CFD	Constant fraction discriminator
Corr	Corrected
cw	Continuous wave
DSSC	Dye-sensitized solar cell
E	Energy
EA	Electron affinity
Elec	Electronic
Em	Emission
ET	Electron transfer
eV	Electron-volt
Ex or Exc	Excitation
F	Fluorescence
FRET	Förster resonance energy transfer
fs	Femtoseconds
FWHM	Full width at half maximum

g	Gerade symmetry or spin statistical factor
GC	Gas chromatography
HeNe	Helium-neon
HOMO	Highest occupied molecular orbital
HPLC	High performance liquid chromatography
IC	Internal conversion
IP	Ionization potential
IR	Infrared
IRF	Instrument response function
ISC	Intersystem crossing
IVR	Intramolecular vibrational relaxation
J	Joules
LFP	Laser flash photolysis
LUMO	Lowest unoccupied molecular orbital
MCA	Multichannel analyzer
MCP	Microchannel plate
MO	Molecular orbitals
MP	Metalloporphyrin
ms	Milliseconds
MS	Mass spectroscopy
NCPU	Noncoherent photon upconversion
Nd:YAG	Neodymium-doped yttrium aluminum garnet, Nd:$Y_3Al_5O_{12}$
NIR	Near-infrared
nm	nanometer
Norm.	Normalized
ns	Nanoseconds
OD	Optical density
OLED	Organic light emitting diode
OPA	Optical parametric amplifier

Ox	Oxidation
P	Phosphorescence or Polarizer or Perylene
Pa	Pascal
PdOEP	β-octaethylporphyrin palladium
PEMA	Poly(ethyl methacrylate)
PMMA	Poly(methyl methacrylate)
PMT	Photomultiplier tube
ps	Picoseconds
PTI	Photon technology international
PtOEP	β-octaethylporphyrin palladium
PVA	Poly(vinyl alcohol)
Q	Quencher
Red	Reduction
RegA	Regenerative amplifier
Rot	Rotational
rpm	Revolutions per minute
S	Singlet state
Sen	Sensitizer
SHG	Second harmonic generation
SSET	Singlet-singlet energy transfer
STP	Standard conditions for temperature and pressure
T	Triplet or temperature
TAC	Time to amplitude converter
TCSPC	Time-correlated single photon counting
TDDFT	Time-dependent density functional theory
TEM	Transverse electromagnetic
Ti:Sapphire	Titanium:Sapphire, Ti:Al_2O_3
TTA	Triplet-triplet annihilation
TTBET	Triplet-triplet back energy transfer

TTET	Triplet-triplet energy transfer
u	Ungerade symmetry
UC	Upconverted
Vib	Vibrational
W	Watts
ZnTPP	Zinc tetraphenyl porphyrin

List of Symbols and Mathematical Terms

A	Absorbance or acceptor molecule or amplitude or pre-exponential factor
B	Pre-exponential factor
C	Constant or concentration
c	speed of light
D	Diffusion coefficient or donor molecule
Da	Dalton
d	Interionic distance or thickness
d_M	Degeneracy of the accepting vibrational states
e	Electron charge
F	Correction factor for the fluorescence spectrum or fraction of the total light absorbed
f	Oscillator strength
G	Gibbs free energy
h	Planck constant
Hz	Hertz
I	Intensity of light
J	Spectral overlap integral
$\hat{J}_N$	Nuclear kinetic energy operator
k	Rate constant
k_B	Boltzmann constant
K_H	Henry's constant
L	Bohr radius
l	Thickness of the light absorbing medium (path length)
m	Mass of an electron
n	Refractive index of the medium
N_A	Avogadro's constant

R	Distance between the donor and acceptor molecules
R_0	Förster distance
r	Ionic radii
Å	Angstrom
α	Luminescence quenching probability
β	Fraction of the initial triplet decay due to TTA
β_e	Electronic coupling energy for electronic states
ΔE	Energy gap between two electronic states
Δ_M	Dimensionless displacement parameter of the vibrational modes
ε	Molar extinction coefficient or dielectric constant of the solvent
ε_0	Permittivity of the free space
η	Efficiency of a photophysical process or solvent viscosity
ϕ	Angle of incidence of light
ϕ_f	Fluorescence quantum yield
Γ	Symmetry representation
$\hbar\omega_M$	Angular frequency of the accepting vibrational modes
κ	Constant with the dimension of energy in the Dexter energy transfer equation
κ^2	Orientation parameter of the transition dipole moments
λ	Wavelength of light in nm
λ_i	Nuclear energy barrier to electron transfer
λ_o	Solvent reorganization energy
μ	Micro
$\hat{\mu}$	Transition dipole moment operator
ν	Frequency in Hz
$\bar{\nu}$	Frequency in cm^{-1}
Ω	Ohms
ψ	Wavefunction
ρ_v	Density of vibrational states

σ	Absorption cross-section or diameter of an encounter complex
τ	Lifetime

Chapter 1: Introduction and Literature Review

The science, technology and applications of organic dye-sensitized solar cells (DSSCs) are rapidly developing research fields. Proposed as key elements of alternative energy technologies, DSSCs can convert solar energy into electricity to meet global energy demands.[1] These devices are attractive because of their low-cost of production and flexible roll-to-roll manufacturing process which makes them thin and light weight. In standard DSSC devices,[2] dye molecules adsorbed or chemisorbed onto a semiconductor material such as TiO_2, absorb sunlight and produce an excited electronic state from which electrons can be injected into the conduction band of the semiconductor. Electrons from the conduction band of the semiconductor flow through an external circuit where they can perform electrical work. The electrons then flow to a cathode to reduce the oxidized form of a redox couple such as I_3^-/I^- in a suitable electrolyte. The dye is then rapidly regenerated by extracting electrons from the reduced form of the redox couple.

DSSCs generally contain organic fluorescing molecules or polymers as the light absorbing units. Most of the dye molecules used in DSSCs absorb solar radiation in the visible region of the electromagnetic spectrum (i.e. 400 – 750 nm wavelength range). However, the solar spectrum shows significant photon flux in the near-IR wavelength range (i.e. $\lambda > 750$ nm) which is usually wasted in conventional DSSCs. Recently, low-power, noncoherent photon upconversion (NCPU) via triplet-triplet annihilation (TTA) has been proposed to solve this problem.[3] Therefore, it is essential to explore new

materials and understand the mechanism of triplet exciton fusion and annihilation in DSSCs.

The motivation of the research work in this thesis originates from the need to understand the mechanisms and the kinetics of the photophysical processes associated with TTA-NCPU, to explore the possibility of using upper excited singlet states for increasing the efficiency and output yield of these processes, to optimize the performance of NCPU in the solution and solid phases and to employ new molecules to achieve these goals. In the following parts of the introduction chapter, a detailed review of the basic theories of photophysics required to understand the results described in the research chapters will be provided.

1.1 Introduction to light-induced photophysical processes in polyatomic molecules

When electromagnetic radiation falls on a molecule, the molecule absorbs the radiation if the electric field associated with the molecule oscillates with the same frequency as that of the electric field associated with the incident radiation under resonating conditions.[4] The interaction of the magnetic field of the radiation with closed shell ground state organic molecules is usually very weak, therefore it does not affect the absorption process.[4] According to Bohr's theory,[4,5] absorption of the light results in the excitation of the molecule from a lower energy state to a higher energy state if the energy spacing between the upper and lower energy states satisfies the condition, $\Delta E = h\nu$, where h is the Planck's constant and ν is the frequency of the incident radiation. The molecule may interact with electromagnetic radiation spanning the range from γ-rays to

radiofrequency waves (~ 1.0×10^{-2} nm – 1.0×10^{12} nm). This thesis mainly deals with electric dipole transitions induced by radiation in the uv-visible (uv-vis) region of the spectrum (~ 200 nm – 750 nm). When a frequency (ν_{nm}) is absorbed to promote a molecule from a state n to m, the rate of absorption (R_{abs}) is correlated with the Einstein coefficient of absorption (B_{nm}) defined by the equation,

$$R_{abs} = B_{nm} N_n \rho_{nm} \qquad (1.1)$$

where N_n is the population of molecules in the n state that absorbs radiation and ρ_{nm} is the radiation density defined as the energy of radiation per unit volume.

When an organic polyatomic molecule absorbs radiation in the uv-vis region of the electromagnetic spectrum, the molecule is excited from a lower electronic energy state to a higher electronic energy state. Each electronic state of a molecule can be represented by an anharmonic oscillator-type potential energy surface. Each of these electronic energy states contains a set of vibrational energy states and each of these vibrational energy states in turn contains of a set of rotational energy states so that the total energy of the molecule is given by, $E_{Total} = E_{elec} + E_{vib} + E_{rot}$. However, the Born-Oppenheimer approximation suggests that the electronic, vibrational and rotational energy states are energetically separable. Therefore, $E_{elec} >> E_{vib} >> E_{rot}$. Thus, electronic transitions are usually induced by uv-vis radiation, vibrational transitions are induced by infrared radiation and rotational transitions are induced by microwave radiation. In electronic spectroscopy of polyatomic molecules in solution, electronic transitions are characterized by broad spectral bands which envelop the vibrational transitions which are resolvable

under adequate spectral resolution. Rotational spectral features are not resolvable under normal experimental conditions of solution state electronic spectroscopy; however, they may be observed in gas phase spectroscopy carried out at very low temperatures.

The molecule which is excited to a higher electronic state (m) may emit light while it relaxes back to the ground singlet state (n). The rate of emission is given by,

$$R_{em} = A_{mn}N_m + B_{mn}N_m\rho_{mn} \qquad (1.2)$$

where A_{mn} is the Einstein coefficient of spontaneous emission, B_{mn} is Einstein's coefficient of induced emission, N_m is the population of molecules in the m state that emits radiation and ρ_{mn} is the radiation density.

The feasibility and strength of an electronic transition depends upon the magnitude of the transition moment integral, i.e., $M = \int \psi^* \hat{\mu} \psi d\tau \neq 0$, where ψ^* and ψ are the electronic wavefunctions of the excited state and ground state, respectively and $\hat{\mu}$ is the transition dipole moment operator.[5] The wavefunction, ψ, is composed of the vibrational (ψ_v) and electronic (ψ_{es}) wavefunctions. The electronic wavefunction (ψ_{es}) contains the orbital (ψ_e) and spin (ψ_s) wavefunctions. Therefore, the total wavefunction is given by, $\psi = \psi_v\psi_{es} = \psi_v\psi_e\psi_s$. Pauli's exclusion principle requires that ψ^2 be unchangeable to the exchange of electrons which in turn requires the wavefunction ψ_{es} to be antisymmetric to the electron exchange operation. This requires that both ψ_e and ψ_s cannot be symmetric or antisymmetric at the same time and that either of them is antisymmetric if the other is symmetric. This condition requires the wavefunctions to be orthonormal (orthogonal and normalized). The transition dipole moment operator

depends on the nuclear and electronic coordinates so that $\hat{\mu} = \hat{\mu}_n + \hat{\mu}_e$. The transition probability is given by,

$$P \propto |M|^2 = \left[\int (\psi_v^* \psi_e^* \psi_s^*)(\hat{\mu}_n + \hat{\mu}_e)(\psi_v \psi_e \psi_s) d\tau\right]^2 \qquad (1.3)$$

i.e. $$P \propto [\int \psi_v^* \psi_v \, d\tau_v \int \psi_e^* \hat{\mu}_e \psi_e d\tau_e \int \psi_s^* \psi_s d\tau_s]^2 + (Other\ terms = 0) \qquad (1.4)$$

The second term on the right hand side of equation (1.4) is zero because of the orthogonal nature of electronic wavefunctions. The electronic and vibrational factors in equation (1.4) being separable is a consequence of the Born-Oppenheimer approximation. The orbital and spin integrals are separated based on the assumption that $\hat{\mu}_e$ acts only on the orbital wavefunctions, not on the spin wavefunctions. This approximation generally holds true for organic compounds when there is no spin-orbit interaction, however, it can be violated if there is spin-orbit coupling.

In equation (1.4), the first integral contains wavefunctions that belong to different electronic states and does not need to be orthogonal. The square of this integral is called the Franck-Condon factor which represents the overlap of vibrational wavefunctions. The Franck-Condon principle suggests that electronic transitions are much faster than the vibrational transitions; the intramolecular vibrational motions are essentially frozen during an electronic transition. Therefore the electronic transitions are represented by vertical transitions in an energy level diagram. The second integral represents the orbital contribution and the third integral is the spin contribution to the electronic transition. These terms form the basis of orbital and spin selection rules for light-induced transitions.

Light-induced transitions are described by the following selection rules. (i) Orbital selection rule: the transition moment integral must be non-zero ($\int \psi_e^* \hat{\mu}_e \psi_e d\tau_e \neq 0$) and should not be changed with respect to symmetry operations on the molecule. This implies that the product $\Gamma(\psi_e^*) \times \Gamma(\hat{\mu}_e) \times \Gamma(\psi_e)$ must contain the totally symmetric irreducible representation of the symmetry point group of the molecule.[5b] (ii) Electron spin conservation rule: the spin integral in equation (1.4) must be nonzero for the transition to be allowed, i.e. $\int \psi_s^* \psi_s d\tau_s \neq 0$. This is a consequence of the orthogonality requirement of the electronic wavefunctions. Therefore photon-induced transitions between electronic states of the same electron spin multiplicity are allowed whereas transitions between states with different multiplicity are forbidden. However, strong spin-orbit coupling of two electronic states with different spin multiplicities can generate perturbed electronic wavefunctions that may contain the characteristics of both the states which can still provide a mechanism for both weak radiative and radiationless transitions between them.[6] (iii) Laporte selection rule: quantum mechanics demonstrates that for centrosymmetric molecules, electric dipole transitions are only allowed between states having different parity. Therefore transitions between states of different symmetry are allowed (*gerade* ↔ *ungerade*, *g* ↔ *u*) whereas transitions between states with similar symmetry are forbidden (*gerade* ↮ *gerade*, *g* ↮ *g* and *ungerade* ↮ *ungerade*, *u* ↮ *u*). For radiationless transitions, the Laporte selection rules are just the opposite of radiative transitions.[4] However, a disruption of the center of symmetry through either asymmetric vibrations or Jahn-Teller distortions and the availability of an accepting vibrational mode with

appropriate symmetry would still allow for transitions that are otherwise Laporte forbidden.

1.1.1 Jabłoński diagram: Radiative and nonradiative transitions

Aleksander Jabłoński has laid out a model for the fundamental photophysical processes that could occur in a polyatomic molecule upon absorption of uv-vis radiation. The resulting energy level diagram is known as Jabłoński diagram (Fig 1.1). In this simplified Jabłoński diagram, electronic energy states are denoted based on the electron spin multiplicities of the molecule in that state. When the electron spins are paired (s = +1/2 and -1/2), it is called a singlet state (spin multiplicity = [2S+1] = 1), denoted by "S" and when the spins are unpaired (s = +1/2), it is called a triplet state (spin multiplicity = [2S+1] = 3), denoted by "T". Since the total electronic wavefunction has to be antisymmetric to the electron exchange operations, the orbital wavefunction is symmetric and the spin wavefunction is antisymmetric for the singlet states. In contrast, the orbital factor and the spin factors of the total electronic wavefunctions of the triplet states are antisymmetric and symmetric, respectively.

For most closed-shell organic molecules the ground singlet electronic state is represented by S_0, the first excited singlet state by S_1, the second excited singlet state by S_2 and so on. The same notation holds for the triplet states also, except that the lowest triplet energy state is the T_1 state rather than a T_0 state. It must be noted that the energy of the triplet state T_1 is slightly lower than the energy of the first excited singlet state, S_1. This is a direct consequence of the Hund's rule which states that states with lower net

spin lies at higher energy than those with greater net spin and the Pauli's exclusion principle which instructs two unpaired electrons in the triplet state to avoid each other, resulting in better correlation of the electron spins to avoid electron-electron repulsion.[7]

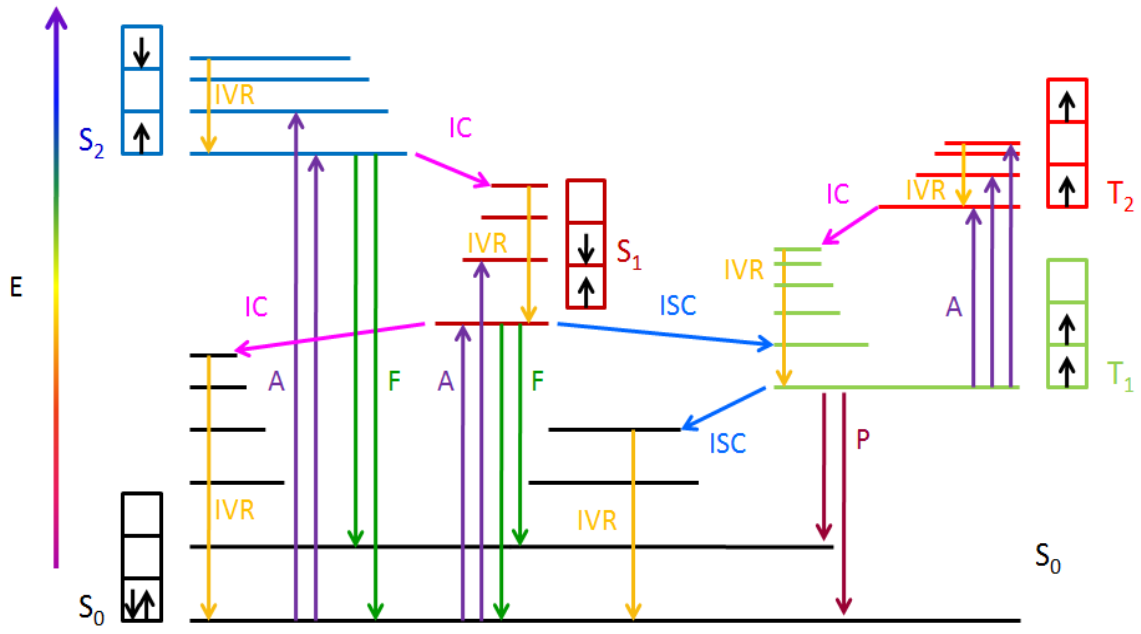

Fig. 1.1 Jabłoński diagram demonstrating the fundamental photophysical processes in a closed-shell molecule. The labels denote the following: E = Energy, A = Absorption, F = Fluorescence, P = Phosphorescence, IVR = Intramolecular vibration relaxation, IC = Internal conversion, ISC = Intersystem crossing. [Adapted and modified from Fundamentals of Photochemistry, Rohatgi Mukherjee].[4]

The singlet excited states of organic molecules are usually short-lived with lifetimes of a few microseconds to sub-picoseconds. Radiative transition from these states to the ground singlet state is called fluorescence. The radiative transitions from the triplet state to the ground singlet state are generally spin-forbidden, and are made possible by spin-orbit coupling. Therefore, the triplet states of organic molecules are generally long-lived

compared to the singlet states, with lifetimes ranging from a few milliseconds to microseconds to sub-microseconds. The emission from these states to the ground singlet state is called phosphorescence. Kasha's rule states that the emitting states of an organic molecule are the lowest excited singlet state (S_1) and the lowest triplet state (T_1).[8] However, a violation of Kasha's rule was observed for the first time when the anomalous emission from the S_2 state of azulene was detected.[9] S_2 emission has been observed from many molecules, including derivatives of azulenes,[10] aromatic thiocarbonyls,[11] metalloporphyrins,[12] polyacenes[13] and linear conjugated polyenes such as tetradecaheptane.[14] These molecules have relatively large S_2-S_1 energy differences and small Franck-Condon factors for S_2-S_1 internal conversion which controls the quantum yield of S_2 fluorescence from these molecules.[14]

When the highest vibrational level in the vibrational manifold of an electronic state is populated due to an absorption or emission process, it will relax back to the lowest vibrational level through a cascade of vibrational transitions without emitting photons. This type of transitions are called intramolecular vibrational relaxation (IVR) and usually occurs on sub-picosecond time scales ($<< 10^{-12}$ s) and when the excess vibrational energy is deposited in the surrounding medium, it is called intermolecular vibrational relaxation (VR). Once the lowest vibrational level of an excited electronic state is populated, it can relax back to a higher vibrational level of a lower electronic state with the same spin multiplicity without emitting photons. This process is called internal conversion (IC) and it depends upon the Franck-Condon factors. Intersystem crossing (ISC) from the singlet state to the triplet state or vice-versa is a radiationless process and is spin-forbidden.

However, strong spin-orbit coupling facilitated by, for example, the presence of a heavy atom can enhance the rates of ISC. Finally, sequential or simultaneous multi-photon absorption and emission are some other possible photophysical processes, the selection rules of which depend upon the symmetry of the molecule.

For rigid aromatic molecules, such as metalloporphyrins, the excited state is expected to have a similar geometry as that of the ground state. This will result in the same shape of vibrational features in the absorption and the emission spectrum, which will result in a mirror image relationship (Levschin's rule) between the absorption and emission spectrum.[4] Because of the Franck-Condon principle and intramolecular vibrational relaxation in the excited state, the fluorescence emission will be slightly shifted towards longer wavelengths (red shift or bathochromic shift) compared to the absorption spectrum. The difference between the absorption maximum and the emission maximum is called the Stokes shift. The degree of Stokes shift is determined by several factors. A large displacement of the excited state potential energy surface with respect to the ground state potential surface would increase the Stokes shift. This could happen because of various reasons such as a structural change of the molecule in the excited state due to a photochemical reaction or a physical process such as a conformational change, relaxation of the locally excited state to another potential surface corresponding to an exciplex or a charge transfer complex, and stabilization of the locally excited state or the exciplex or the charge-transfer complex by the medium. The stabilization of the excited state potential energy surface by a solvent depends upon the structure and excited state dipole moment of the molecule as well as the structure and polarity of the solvent molecules.

For unaggregated structurally rigid aromatic molecules, like metalloporphyrins, the Stokes shift is usually very small which leads to considerable overlap of the longer wavelength tail of the absorption spectrum with the onset region of the emission spectrum. This overlap leads to fluorescence-reabsorption effects.

1.1.2 Theory of radiative transitions

The intensity of light being absorbed can be correlated with the number of molecules that absorbs the light over the distance it travels using the famous Lambert-Beer law. i.e.

$$A = \log_{10}\left(\frac{I_0}{I_t}\right) = \varepsilon C l \qquad (1.5)$$

where A is the absorbance, I_0 is the incident light intensity on the sample, I_t is the transmitted light intensity, ε is the molar extinction coefficient expressed in $M^{-1}cm^{-1}$, C is the concentration of the sample in M and l is the length over which light travels through the sample, known as the pathlength (cm).

The integrated absorption spectrum is represented by the transition probability integral,

$$A = \int \varepsilon(\bar{\nu})\mathrm{d}\,\bar{\nu} = \frac{8\pi^3}{3h^2}\frac{N_A h\nu}{2.303c}\left|\int \psi^* \hat{\mu}\psi \mathrm{d}\tau\right|^2 \qquad (1.6)$$

where $\varepsilon(\bar{\nu})$ is the molar extinction coefficient measured as a function of frequency in cm^{-1}, N_A is Avogadro's number, c is the velocity of light and the integration limits are the wavenumbers of the highest and lowest energy features of the electronic transition.

The probability of a one-electron transition can also be expressed in terms of its oscillator strength, f, which is defined as the ratio of the experimental transition probability to the transition probability of an ideal harmonic oscillator.

$$f = \frac{[\int \varepsilon(\bar{\nu})\mathrm{d}\,\bar{\nu}]_{exp}}{[\int \varepsilon(\bar{\nu})\mathrm{d}\,\bar{\nu}]_{ideal}} = \frac{8\pi^2 mc\bar{\nu}}{3he^2}\left|\int \psi^* \hat{\mu}\psi \mathrm{d}\tau\right|^2 = 4.33 \times 10^{-9} \int \varepsilon(\bar{\nu})\mathrm{d}\,\bar{\nu} \qquad (1.7)$$

where m is the mass of an electron having a charge e.

An ensemble of excited molecules decay back to the ground singlet state by emitting light with a time-dependent intensity given by the equation,

$$I_t = I_0 \exp(-t/\tau) = I_0 \exp(-kt) \qquad (1.8)$$

where I_0 and I_t are the intensity of emitted light observed at time $t = 0$ and $t = t$, τ is the 1/e lifetime of an ensemble of excited molecules, the time required for an ensemble of excited molecules to decay to 1/e of an initial population. The radiative lifetime can be estimated using the Strickler-Berg equation,[15]

$$k_{rad} = \frac{1}{\tau_{rad}} = 2.88 \times 10^{-9} n^2 \langle \bar{\nu}_f^{-3} \rangle_{\mathrm{av}}^{-1} \left(\frac{g_1}{g_2}\right) \int \varepsilon(\bar{\nu})\mathrm{d}\ln\bar{\nu} \qquad (1.9)$$

where n is the refractive index of the medium, g_1 and g_2 are spin statistical factors for the lower and upper energy states respectively. For singlet → singlet transitions, $g_1/g_2 = 1$ and for triplet → singlet transition, $g_1/g_2 = 1/3$.

The quantum yield of emission is defined as the ratio of number of photons emitted to the number of photons absorbed and is related to the rate of these processes through the following relation,

$$\phi_f = \frac{k_{rad}}{k_{rad} + \sum k_{nonrad}} = \frac{\tau}{\tau_{rad}} \qquad (1.10)$$

where $k_{rad} = (\phi_f/\tau)$ is the rate constant for the radiative transition, $\sum k_{nonrad} = (1 - \phi_f/\tau)$ is the sum of all the nonradiative transitions, τ is the measured radiative lifetime governed by the deactivation processes such as radiative and nonradiative transitions and τ_{rad} is the natural lifetime given by equation (1.9).

1.1.3 Theory of nonradiative transitions

For nonradiative transitions, the nuclear kinetic energy operator, $\hat{\jmath}_N$ couples the excited and ground state electronic wavefunctions such that the transition moment integral is given by,

$$M = \int \psi^* \hat{\jmath}_N \psi \mathrm{d}\tau = \int \psi_v^* \psi_v \, \mathrm{d}\tau \int \psi_e^* \hat{\jmath}_N \psi_e \mathrm{d}\tau \int \psi_s^* \psi_s \mathrm{d}\tau \qquad (1.11)$$

Therefore the probability of a radiationless transition can be written as,

$$P \propto \left| \int \psi_v^* \psi_v \, \mathrm{d}\tau \int \psi_e^* \hat{\jmath}_N \psi_e \mathrm{d}\tau \int \psi_s^* \psi_s \mathrm{d}\tau \right|^2 \qquad (1.12)$$

where the square of the first term is the Franck-Condon factor, the second term reflects that the perturbation acts only on the electronic wavefunctions and the third term is the electron spin integral (which is 1 for singlet-singlet transition).

The rate of radiationless transition depends upon three factors: (i) the density of states, ρ_v, defined as the number of vibrational energy levels of the final accepting state per unit energy interval in cm^{-1}, (ii) electronic energy gap between the electronic states between which the transition takes place and (iii) the Franck-Condon factor. The exact expression for this relation is,[4,16]

$$k_{nonrad} = \left(\frac{4\pi^2}{h}\rho_v\right)\beta_e^2\left(\int \psi_v^* \psi_v \, d\tau\right)^2 \qquad (1.13)$$

The first term in the brackets represents the density of states factor, the second term β_e^2 represents the electronic interaction energy between the two states and is a constant for a series of structurally similar molecules like metalloporphyrins and the third term is the Franck-Condon factor which depends upon the energy gap between the two states. Equation (1.13) is called the Fermi Golden rule. The relation between the nonradiative rate constant and the energy gap, ΔE, for weakly-coupled states was proposed by Englman and Jortner[17] and is given by,[18]

$$k_{nonrad} = \left[(2\pi)^{1/2}\beta_e^2/\hbar(\hbar\omega_M \Delta E)^{1/2}\right]\exp[-(\gamma/\hbar\omega_M)\Delta E] \qquad (1.14)$$

$$\gamma = \ln(2\Delta E/d_M \hbar\omega_M \Delta_M^2) - 1 \qquad (1.15)$$

where $\hbar\omega_M$ is the angular frequency of the accepting vibrational modes, d_M is degeneracy of the accepting vibrational states and Δ_M is a dimensionless displacement parameter.

Differentiation of $\log_{10}(k_{nr})$ with respect to ΔE gives the following expression,

$$\frac{\mathrm{d}\left(\log_{10}(k_{nr})\right)}{\mathrm{d}(\Delta E)} = -\frac{1}{4.6\Delta E} - \frac{\gamma + 1}{2.3\hbar\omega_M} \qquad (1.16)$$

Equation (1.16) predicts a plot of $\log_{10}(k_{nr})$ versus ΔE to be approximately linear when ΔE is large. Such plots are called energy gap law plots, and the interstate coupling energy, β_e, can be calculated from their slopes.

1.2 Photophysical properties of metalloporphyrins

With a recent report of a zinc porphyrin derivative sensitized DSSC achieving a record power conversion efficiency of 12.3% and photovoltage approaching 1 volt under simulated AM 1.5 solar irradiation,[19] it is now clear that metalloporphyrins are candidates for efficient light sensitization in DSSCs. In addition, it has already been established that metalloporphyrins can be used as sensitizers and upconverters in TTA and associated NCPU to utilize the parts of the solar spectrum that are otherwise unutilized in traditional solar cells (*vide infra*). Our objective is to study the involvement of the second excited singlet (S_2) state of porphyrins in TTA-NCPU processes. Therefore it is essential to understand the photophysical properties of the metalloporphyrins, especially the properties of their S_2 states.

Diamagnetic metalloporphyrins such as ZnTPP (D_{4h} symmetry) have two absorption band systems in the uv-visible region of the spectrum called the B band or Soret band in the violet region and Q band in the visible region. Excitation in the B band of ZnTPP populates the S_2 state (2^1E_u in D_{4h} symmetry, τ_{S2} ~ (1.3 - 2.5) ps in different solvents) causing weak emission ($\phi_{f\text{-}S2} \sim 10^{-3}$) from this state while the molecule decays back to the ground state.[18b,20] Q band excitation of ZnTPP populates the S_1 state (1^1E_u in D_{4h} symmetry, τ_{S1} ~ 2 ns in various solvents) which decays back to the ground state by emitting fluorescence with a quantum yield of $\phi_{f\text{-}S1} \sim 10^{-2}$.[21] The separately normalized absorption and emission spectra of ZnTPP is given in Fig. 1.2.

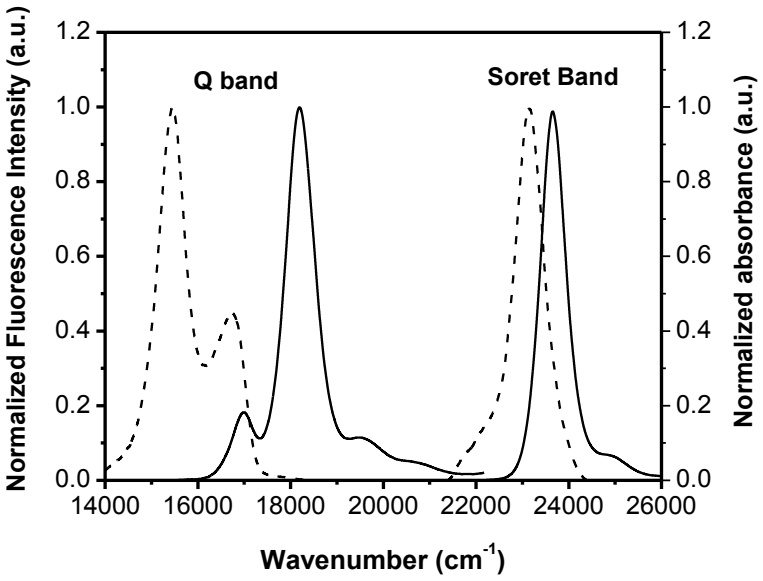

Fig. 1.2 Normalized absorption (—) and fluorescence (---) spectra of ZnTPP in benzene.

The absorption spectral characteristics of metalloporphyrins were first explained by the four-orbital model proposed by M. Gouterman.[22] According to this model, electronic

transitions from two nearly degenerate highest occupied molecular orbitals, HOMO and HOMO-1 (the a_{1u} and a_{2u} orbitals) to a degenerate set of two lowest unoccupied molecular orbitals, LUMO (the e_g orbitals), i.e. the $^1a_{1u}$-^1e_g and $^1a_{2u}$-^1e_g transitions, give rise to two excited states with ^1E_u character. Mixing of the orbitals corresponding to these one electron transitions defines the relative energies of the transitions and hence the spectral characteristic of the B band and Q band. The transition dipole moments for the two transitions, $^1a_{1u}$-^1e_g and $^1a_{2u}$-^1e_g lie in the plane of the metalloporphyrins D_{4h} macrocycle. These transition moments are parallel for the S_2-S_0 transition, giving rise to an intense absorption and they are anti-parallel for the S_1-S_0 transition, giving rise to a weak absorption. The four-orbital model suggests that the nature of the central metal and the substituents on the porphyrin macrocycle affect the relative energies of these transitions.

The energy gap of ZnTPP, $\Delta E(S_2\text{-}S_1)$, is influenced by the large differences in the polarizabilities of the S_2 and S_1 states and can be controlled by the solvation environment.[20-21] The energy gap law plot of the nonradiative rate constants for the S_2 state versus the $\Delta E(S_2\text{-}S_1)$ energy gap of ZnTPP in various solvents is linear, demonstrating that S_2-S_1 internal conversion is the dominant nonradiative relaxation pathway for the Soret excited ZnTPP in all the solvents.[18,20] The rate of internal conversion varies from ~ $(4 - 7) \times 10^{11}$ s^{-1} in different solvents[18,21] with quantum efficiency close to 1. The energy gap law plot suggests that the interstate coupling energy of ZnTPP is greater than that suggested for a weak-coupling limit.[18] The observed radiative and nonradiative decay rates from the S_2 state of ZnTPP have been rationalized

based on the Franck-Condon vibronic coupling and the coupling energy of the S_2 and S_1 states.[18a]

1.3 Photophysical properties of the fullerene, C_{60}

Because of its icosahedral symmetry (I_h), the distribution of the electronic states and hence the electronic spectroscopy of C_{60} is complicated. A detailed review of the electronic structure and the optical spectroscopy of C_{60} has been prepared by Orlandi.[23] C_{60} has 120 occupied MOs and 120 unoccupied MOs. Of these molecular orbitals, 60 (30 occupied and 30 unoccupied) have π character. For C_{60}, the lowest energy electronic dipole-allowed transition is between the A_g ground state and the T_{1u} excited state. HOMO-LUMO excitations corresponding to the lowest excited states are symmetry forbidden and can occur only by means of vibronic coupling induced by non-totally-symmetric vibrations. This results in the lower energy parts of the electronic absorption spectrum having weak oscillator strengths and in weak emission with a low fluorescence quantum yield. The absorption spectrum and fluorescence spectrum of C_{60} are shown in Fig. 1.3.

In the absorption spectrum, the band observed at around 29,500 cm^{-1} is due to transitions from the ground state to a higher excited state with T_{1u} symmetry and is one of the bands in the uv-region with the highest oscillator strength. The weak bands in the region 22,500-25,000 cm^{-1} are due to transitions to the lowest excited state with T_{1u} symmetry. The weak bands in the spectral region 15,000-22,500 cm^{-1} are due to transitions to the lowest excited states with *gerade* symmetry. These transitions are

forbidden and have very low oscillator strengths. The intensity of the weak bands is provided by the intensity borrowing from the symmetry-allowed transitions through Herzberg-Teller mechanism and vibronic coupling induced by Jahn-Teller distortions. The fluorescence spectrum is due to emission from the S_1 state with symmetry of $^1T_{1g}$ contaminated with T_{2g} and G_g characters and thus is forbidden. It was proposed that the S_1, S_2 and S_3 states are equally spaced ($\Delta\nu \sim 50$ cm^{-1}) with symmetries T_{1g}, T_{2g} and G_g respectively and are quasidegenerate.[24] Most of the vibronic structures in the emission spectrum are due to intensity borrowing from the higher T_{1u} states.

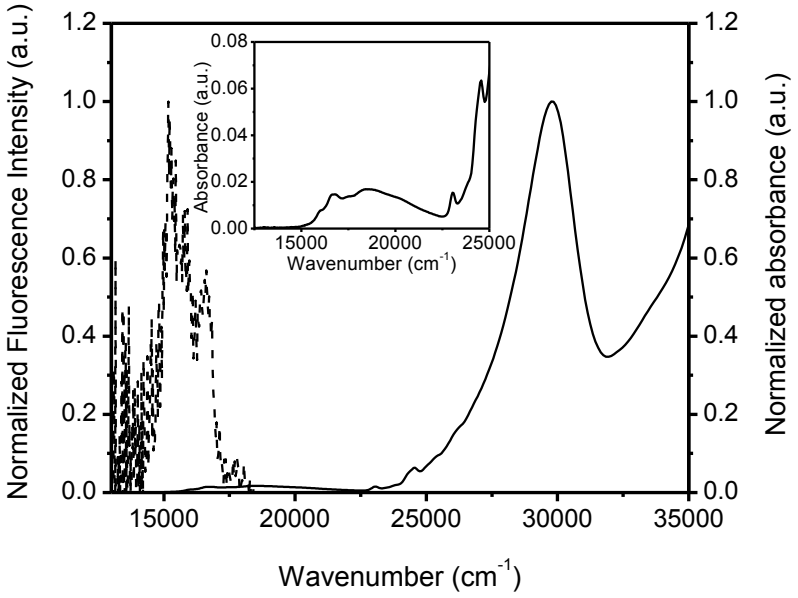

Fig. 1.3 Normalized absorption (—) and fluorescence (---) spectrum of C_{60} in toluene. The inset shows the absorption spectrum in the region 13,000 – 25,000 cm^{-1} in detail.

Time-resolved fluorescence measurements of C_{60} in argon matrix shows that S_3 with G_g character populates the S_2 and S_1 states with time constants of 90 and 60 ps,

respectively. Emission from S_1, S_2 and S_3 states was characterized by similar time constants, approximately 1.5 ns.[24] The S_1 fluorescence decay time and the S_n-S_1 rise time of C_{60} toluene have been reported to be about 1.2 ns and $\leq$ 20 ps.[24] The transient absorption spectrum of C_{60} in toluene excited at 402 nm revealed a rise time of 200 fs which was attributed to the internal conversion from the S_n state to an S_n' state which then decays to the S_3 state with a time constant of $\leq$ 20 ps. The state, S_3, decays to the S_2 or S_1 state with a time constant of 70 – 170 ps.[25]

The intersystem crossing from the S_1 state to the T_1 state is highly efficient with a near unit quantum yield and a time constant of τ_{ISC} = (600 ± 100) ps.[26] Calculations suggest that the lowest triplet state belongs to the T_{2g} irreducible representation. The T_1-S_0 transition is symmetry and spin forbidden resulting in very weak phosphorescence.[23] The second excited triplet state is approximately 0.4 eV above the lowest triplet state.

1.4 Fluorescence quenching

Any process that reduces the intensity of the fluorescence of an ensemble of excited molecules can be considered as a fluorescence quenching process.[27] These processes include energy transfer, electron transfer, collisional quenching, ground-state complex formation, excited-state complex formation, excited state reactions and molecular rearrangements. Molecular oxygen,[28] heavy atoms such as iodine,[29] electron scavengers such as protons[30] are often reported as efficient fluorescence quenchers.

Fluorescence quenching can proceed through one of the well-known dynamic or static quenching mechanisms or through a combination of both mechanisms. Dynamic quenching usually involves the diffusion of the quencher to the fluorophore within its excited state lifetime followed by a collisional quenching to reduce its fluorescence intensity. The average distance a quencher can diffuse during the excited state lifetime of the donor is given by, $\langle x \rangle = (2D\tau)^{1/2}$, where D is the diffusion coefficient of the quencher and τ is the excited state lifetime of the fluorophore in the absence of the quencher. The dynamic quenching usually results in a reduction in both the intensity and the excited state lifetime of the fluorophore with an increase in the concentration of the quencher. The dynamic Stern-Volmer equation describing this process can be given as,

$$\frac{I_0}{I_q} = \frac{\tau_0}{\tau_q} = 1 + k_q \tau_0 [Q] = 1 + K_D [Q] \qquad (1.17)$$

where I_0 and τ_0 are the unquenched fluorescence intensity and the excited state lifetime of the fluorophore in the absence of the quencher, I_q and τ_q are the quenched fluorescence intensity and the excited state lifetime of the fluorophore in the presence of the quencher, k_q is the bimolecular quenching rate constant, $K_D = k_q \tau_0$ is the Stern-Volmer constant and $[Q]$ is the concentration of the quencher. Therefore, for a single fluorophore, a plot of (I_0/I_q) and (τ_0/τ_q) will provide a straight line with a slope = $K_D = k_q \tau_0$, from which the bimolecular quenching rate constant can be extracted if the value of τ_0 is known. These types of plots are called Stern-Volmer plots. However, if there are two types of fluorophores with one of them inaccessible to the quencher, the resulting Stern-Volmer plot will no longer be linear and will deviate towards the x-axis.

Static quenching involves the ground state complexation of the fluorophore and the quencher. Excitation of this complex causes the excited state to relax to the ground state without emitting photons, resulting in quenching of the fluorescence. During a static quenching process, only the free fluorophores which are not bound to the quencher emit fluorescence and hence are observable in a fluorescence lifetime measurement. Therefore the observed lifetimes of the uncomplexed fluorophores will be the unperturbed excited state lifetimes of the fluorophore, resulting in $\tau_0/\tau_q = 1$. Therefore, the Stern-Volmer equation for a static quenching process is given by,

$$\frac{I_0}{I_q} = 1 + K_S[Q] \qquad (1.18)$$

where the Stern-Volmer constant (K_S) for a static quenching process can frequently be associated with the association (binding) constant (K_a) of the fluorophore and the quencher, i.e. $K_S = K_a$.

Therefore the static and dynamic quenching processes can be distinguished based on the lifetime measurements of the fluorophore with and without the quencher added. In addition, they can be differentiated with varying the temperature of the medium in which the fluorphore and the quencher are dissolved. The molecules will diffuse faster at higher temperature (apparently at lower viscosity), resulting in a greater rate of collisional quenching and hence will result in a deviation of the Stern-Volmer plot towards the y-axis. However, higher temperatures will usually increase dissociation of the complexes of

the fluorophore and the quencher, resulting in lower net rates of static quenching and an inclination of the Stern-Volmer plot towards the x-axis.

In some circumstances, both dynamic and static mechanisms can quench the fluorescence of a molecule. In such a case, the equation describing the quenching process is given as,

$$\frac{I_0}{I_q} = (1 + K_D[Q])(1 + K_S[Q]) \qquad (1.19)$$

which is quadratic in [Q]. The values of K_D and K_S can be extracted by plotting K_{app} versus [Q], where $K_{app} = (K_D + K_S) + K_D K_S[Q]$.

1.5 Brief review of energy transfer

Excitation energy transfer in solid and condensed phases is an intensively progressing research area[31] since the pioneering works by Th. Förster[32] and D. L. Dexter.[33] Excitation energy transfer has been found to be responsible for sensitized luminescence in solutions and solid phases,[33-34] and has become a key tool for studying photosynthesis,[35] and processes in biological[36] and polymer molecules.[37] The theoretical background for these phenomena is based on the electric-dipole-dipole,[32,33] electric dipole-quadrupole,[33] and electron-exchange interactions.[33] Of these three mechanisms, the first two depend on the classical interaction between the oscillating electric fields of the donor and acceptor molecules whereas the last one is dependent on the overlap of the electronic wavefunctions of the donor and the acceptor molecules.[38]

Nonradiative electronic energy transfer from an excited donor molecule to an unexcited acceptor molecule can occur with higher efficiency through a resonant dipole-dipole interaction called the Förster resonance energy transfer (FRET).[39] FRET is a classical electrodynamic phenomenon[27] in which both the excited donor and the ground state acceptor are considered as oscillating electric dipoles and FRET occurs through a classical resonant interaction between these two dipoles. A simplified schematic diagram depicting the FRET process is shown in Fig. 1.4.

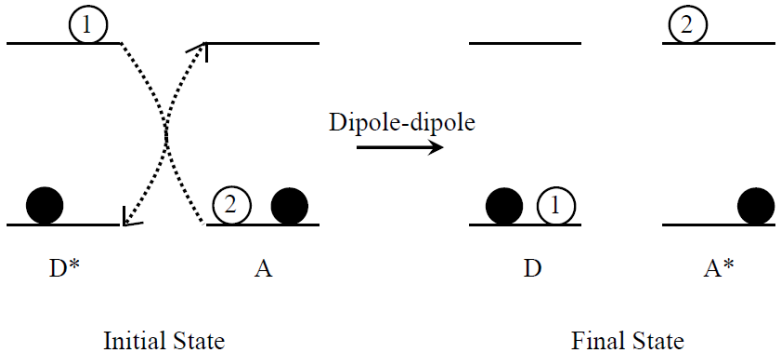

Fig. 1.4 Schematic diagram demonstrating the FRET process. The dotted arrows indicate the dipole-dipole coupled energy transfer process. Both the dark-colored circles and the numbered open circles indicate electrons. The numbers help to identify the electrons undergoing FRET.

FRET is a radiationless process and the rate of FRET is dependent upon the spectral overlap between the emission spectrum of the donor and the absorption spectrum of the acceptor, the fluorescence quantum yield of the donor, the relative orientation of the donor and the acceptor and the distance between the donor and the acceptor molecules.[27]

The efficiency of FRET is expressed as the fraction of photons absorbed by the donor to that are transferred to the acceptor and is given by,

$$E = \frac{k(R)}{\tau_D^{-1} + k(R)} = \frac{1}{\tau_D}\left(\frac{R_0}{R}\right)^6 \qquad (1.20)$$

where *k(R)* is the distance dependent rate of energy transfer from the donor to the acceptor, τ_D is the fluorescence lifetime of the donor in the absence of the acceptor, *R* is the distance between the donor and the acceptor and R_0 is the distance between the donor and acceptor at which the FRET efficiency is 50% and is called the Förster distance. Therefore at the Förster distance, the rate of energy transfer will be equal to the rate of decay of the donor excited state in the absence of the acceptor. The rate of energy transfer is given by the following equation,

$$k(R) = \left(\frac{\phi_D \kappa^2}{\tau_D R^6}\right)\left(\frac{9000(\ln 10)}{128\pi^5 N_A n^4}\right)\int_0^\infty F_D(\bar{\nu})\varepsilon_A(\bar{\nu})\mathrm{d}(\bar{\nu})/(\bar{\nu})^4 \qquad (1.21)$$

where ϕ_D is the fluorescence quantum yield of the donor, N_A is Avogadro's number and n is the refractive index of the medium. κ^2 is called the orientation factor which describes the relative spatial orientation of the transition dipole moments of the emission of the donor and the absorption of the acceptor and is given by the following expressions,[27]

$$\begin{aligned}\kappa^2 &= (\cos\theta_T - 3\cos\theta_D \cos\theta_A)^2 \\ &= (\sin\theta_D \sin\theta_A \cos\phi - 2\cos\theta_D \cos\theta_A)^2 \end{aligned} \qquad (1.22)$$

where θ_T is the angle between the transition dipole moments for the emission of the donor and the absorption of the acceptor, θ_D and θ_A are the angle between these dipoles and the vector joining the geometric centers of the donor and the acceptor and ϕ is the angle between the planes in which these transition dipole moments lie. For a random orientation of the transition dipole moments, the time average value of κ^2 is taken as 2/3.[27]

The integral in equation (1.21) represents the extent of overlap between the donor emission spectrum and the acceptor absorption spectrum and is called the overlap integral *J*. A pictorial representation of the overlap integral is shown in Fig. 1.5.

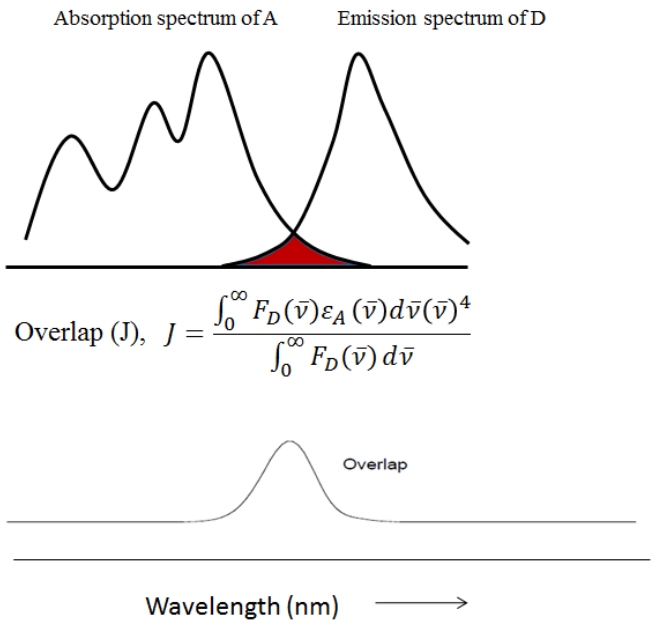

Fig. 1.5 Schematic diagram demonstrating the spectral overlap for the FRET process.

The spectral overlap integral can be mathematically represented as,

$$J(\bar{\nu}) = \int_0^{\infty} F_D(\bar{\nu})\varepsilon_A(\bar{\nu})\mathrm{d}\bar{\nu}/(\bar{\nu})^4 = \frac{\int_0^{\infty} F_D(\bar{\nu})\varepsilon_A(\bar{\nu})\mathrm{d}\bar{\nu}/(\bar{\nu})^4}{\int_0^{\infty} F_D(\bar{\nu})\,\mathrm{d}\bar{\nu}} \qquad (1.23)$$

where $\bar{\nu}$ is the wavenumber expressed in cm^{-1}, $F_D(\bar{\nu})$ is the corrected donor emission fluorescence spectrum with the total area normalized to unity, $\varepsilon_A(\bar{\nu})$ is the absorption spectrum of the acceptor and expressed in terms of its molar extinction coefficient ($M^{-1}cm^{-1}$). In the middle term of equation (1.23), $F_D(\bar{\nu})$ is already normalized before calculating $J(\bar{\nu})$ whereas in the third term on the right side of equation (1.23), $J(\bar{\nu})$ is calculated and normalized to unity by the area under the corrected emission spectrum of the donor.

FRET usually results in a reduction in the emission intensity of the donor molecule and an enhancement in the emission intensity of the acceptor molecule (if it fluoresces) with an increase in concentration of the acceptor molecules. Förster developed an equation to relate the donor intensity with the acceptor concentration which is given below,

$$\frac{I_0}{I_q} = \left(1 - \left(\frac{\pi}{2}\right)\left(\frac{C}{C_0}\right)\exp\left[\left(\frac{\pi}{4}\right)\left(\frac{C}{C_0}\right)^2\right]\left[1 - \mathrm{erfc}\left\{\left(\frac{\sqrt{\pi}}{2}\right)\left(\frac{C}{C_0}\right)\right\}\right]\right)^{-1} \qquad (1.24)$$

where I_0 is the unquenched luminescence intensity of the donor in the absence of the acceptor, I_q is the luminescence intensity in the presence of the acceptor, *erfc* is the complimentary error function, C is the added acceptor concentration and C_0 is a critical transfer concentration which depends on the rate of energy transfer.

The efficiency of FRET is dependent upon the inverse sixth power of the distance between the donor and the acceptor molecules. Therefore FRET has evolved as a powerful tool for measuring the distance between two sites in macromolecules such as proteins when the center-to-center distance between the donor and acceptor are substantially greater than the sum of their van der Waals radii.[27] FRET distances of 10 – 90 Å has been reported for proteins.[27,40]

Terenin and Ermolaev[38] first observed sensitized phosphorescence through triplet energy transfer and explained it in terms of electron exchange interactions. They found that in the presence of an acceptor molecule: (i) the donor luminescence yield does not follow equation (1.24), rather it follows a *exp(-aC)* relation where *a* is a positive constant and *C* is the concentration of the acceptor, (ii) the donor decay time-constant is reduced much more slowly as a function of increased acceptor concentration compared to the trend predicted by the Förster mechanism, and (iii) the efficiency of energy transfer is independent of the oscillator strength of the acceptor molecule. Inokuti and Hirayama[38] proposed that the triplet energy transfer process follows the electron exchange mechanism originally proposed by Dexter.[33] A simplified schematic representation of the Dexter-type electron exchange energy transfer process is shown in Fig. 1.6.

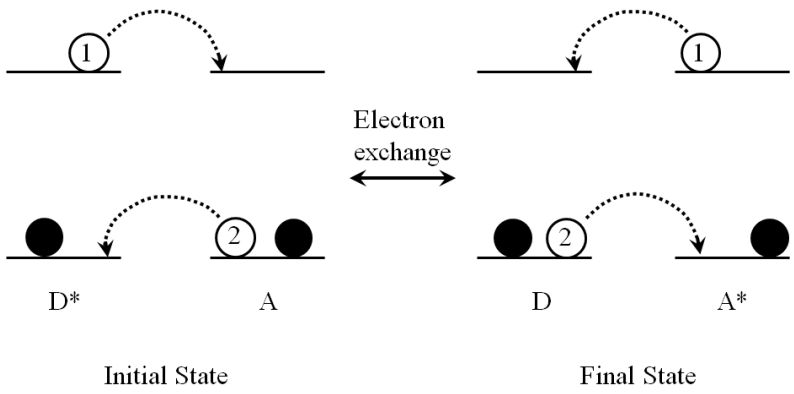

Fig. 1.6 Schematic illustration of the Dexter-type electron exchange energy transfer. The dotted arrows indicate the electron exchange process. Both the dark-colored circles and the numbered open circles indicate electrons. The numbers serve to identify the electrons undergoing the Dexter-mechanism.

The rate of this type of energy transfer can be expressed as,

$$k(R) = KJ\exp(-2R/L) \qquad (1.25)$$

where R is the distance between the donor and acceptor molecules, L is the effective average Bohr radius for the donor and the acceptor molecules. K is a constant given by the equation, $K = (2\pi/\hbar)\kappa^2$, where κ is a constant with the dimension of energy. The spectral overlap integral J is given by the equation,

$$J(\bar{\nu}) = \int_0^\infty F_D(\bar{\nu})\varepsilon_A(\bar{\nu})\mathrm{d}\bar{\nu} \qquad (1.26)$$

where the donor emission spectrum and the acceptor absorption spectrum are separately normalized, i.e.

$$\int_0^\infty F_D(\bar{\nu})\mathrm{d}\bar{\nu} = \int_0^\infty \varepsilon_A(\bar{\nu})\mathrm{d}\bar{\nu} = 1 \qquad (1.27)$$

Here, the term *K*.exp(-*2R/L*) is an asymptotic form of an exchange integral for the donor-acceptor system and denotes the specific orbital interaction between them. Therefore the exponential dependence of the rate constant is a direct consequence of the exponential decay of the molecular wavefunction. The rate of Dexter-type energy transfer can also be expressed as,[38]

$$k(R) = \left(\frac{1}{\tau_D}\right)\exp\left\{\gamma\left[1-\left(\frac{R}{R_0}\right)\right]\right\} \qquad (1.28)$$

where τ_D is the lifetime of the donor in the absence of the acceptor, R_0 is the critical transfer distance at which energy transfer process is equally efficient as the spontaneous decay of the donor and $\gamma = 2\,R_0/L$.

1.6 Brief review of electron transfer

Photo-induced electron transfer in which an electron is transferred from a donor molecule to an acceptor molecule creating a radical ion pair or a charge-transfer complex has been an intensive research area since early 1960s.[41] If a fluorescing, sensitizer molecule is acting as the electron donor or acceptor, the electron transfer process can quench the fluorescence of the sensitizer. The basic classical theories of electron transfer reactions were developed by R. A. Marcus.[42] Photo-induced electron transfer from a donor molecule in the ground state to an acceptor molecule in its excited singlet or triplet state, or from the donor molecule in the excited singlet or triplet state to the acceptor

molecule in the ground state will form a charge-separated species. Depending upon the polarity of the medium, the charge-separated species can be stabilized or form solvent-separated ion-pairs. The charge-separated species can undergo a number or possible reactions: (i) charge recombination to reform the neutral donor and acceptor molecules, (ii) ionic dissociation to form donor cation and acceptor anion, and (iii) formation of other stable photochemical products.[41] The possible reaction pathways are given below.

$$^{1}D + {}^{1,3}A^{*} \rightarrow {}^{1,3}(D^{\cdot+}\cdots A^{\cdot-}) \rightarrow {}^{1}D + {}^{1}A \text{ or } D^{\cdot+} + A^{\cdot-} \text{ or photochemical products}$$

$$^{1,3}D^{*} + {}^{1}A \rightarrow {}^{1,3}(D^{\cdot+}\cdots A^{\cdot-}) \rightarrow {}^{1}D + {}^{1}A \text{ or } D^{\cdot+} + A^{\cdot-} \text{ or photochemical products}$$

In general, photo-induced electron transfer can occur through: (i) the formation of encounter complexes or exciplexes of the donor and the acceptor, and (ii) a hopping process. Following excitation, the donor and acceptor molecules can undergo multiple collisions and can form encounter complexes in solution. The donor and acceptor molecules in these complexes will be solvated and can be separated by a small distance (~7 Å is typical). The lifetime of the collision complexes can be of the order ~ 10^{-9}s. The vibrational changes within the complex occur on the time-scale of ~ 10^{-12} s. Therefore, if the free energy factor is favorable, electron transfer can occur in the quenching complex before the donor and acceptor molecules are separated by the solvent molecules, forming a contact ion pair. Electron transfer in a complex slightly separated by the solvent molecules can form a solvent-separated ion pair. Both the contact ion pair and solvent-separated ion pair can be further stabilized by the solvent molecules.[43] Following excitation, the donor and acceptor molecules can make stable, long-lived complexes

called exciplexes. Electron transfer within exciplexes will render them charge transfer character and they can emit broad, structureless emission.[44] These exciplexes can dissociate to radical ion pairs or contact ion pairs or sometimes can undergo energy transfer. An excellent review of various aspects of electron transfer and charge transfer processes in exciplexes has been written by Mataga et al.[45]

In some cases of a rigid intramolecular system where the donor and acceptor molecules are separated by a spacer and where the separation distance is greater than the collision-encounter distance, electron transfer can still occur through a hopping process.[46] In this case, the spacer can be a linker molecule connecting the donor and the acceptor and can act as a charge carrier through which the electrons hop from the donor to the acceptor. Such an intramolecular electron transfer can produce exciplexes or charge separated species, the yield of which will be dependent upon the structure and the conformations of the connecting link. Electron transfer through hopping can also occur in intermolecular systems in which the solvent molecules can act as the charge carriers.

In order to be feasible, an electron transfer reaction has to be exergonic ($\Delta G < 0$).[47] The free energy change for electron transfer between two ground state molecules in the gas phase is given by,[41]

$$\Delta G = IP_D - EA_A \qquad (1.30)$$

where IP_D is the ionization potential of the donor and EA_A is the electron affinity of the acceptor. If one of the molecules is electronically excited, the IP or the EA values will be reduced by the magnitude of the excitation energy. i.e.

$$\Delta G = (IP_D - E_D^*) - EA_A \qquad \text{if the donor is excited}$$

$$\Delta G = IP_D - (EA_A + E_A^*) \qquad \text{if the acceptor is excited}$$

The change in free energy for an electron transfer process creating a charge transfer complex in solution which will be stabilized by Coulombic interactions between the donor and the acceptor and by the solvent molecules can be given by,[47-48]

$$\Delta G = E_{ox}(D) - E_{red}(A) - E^* + \lambda_o \qquad (1.31)$$

where $E_{ox}(D)$ is the oxidation potential of the donor, $E_{red}(A)$ is the reduction potential of the acceptor and E^* is the excitation energy of the donor or the acceptor. λ_o is the solvent reorganization energy needed to stabilize the charge separated species and is given by,[48a]

$$\lambda_o = \frac{e}{8\pi\varepsilon_0}\left(\frac{1}{r_+} - \frac{1}{r_-}\right)\left(\frac{1}{\varepsilon_s} - \frac{1}{\varepsilon_m}\right) - \frac{e}{4\pi\varepsilon_0}\left(\frac{1}{\varepsilon_s d}\right) \qquad (1.32)$$

where e is the charge of the electron, ε_0 is the permittivity of the free space, r_+ and r_- are the ionic radii of the radical cation and the anion respectively, ε_s is the dielectric constant of the solvent in which charge separation occurs, ε_m is the dielectric constant of the medium in which the redox potentials of the donor and the acceptor are measured and d is the interionic distance.

The rate constant for an electron transfer reaction can be correlated with the standard free energy of the reaction through the following equations,[42i,j]

$$k = A \exp\left(\frac{-\Delta G^*}{k_B T}\right) \qquad (1.33)$$

$$\Delta G^* = \left(\frac{\lambda}{4}\right)\left(1 + \frac{\Delta G^0}{\lambda}\right)^2 \qquad (1.34)$$

where the pre-exponential character A depends upon the nature of the electron transfer, ΔG^0 is the standard free energy of the reaction, k_B is the Boltzmann constant and T is the temperature. $\lambda = \lambda_i + \lambda_o$, where λ_i and λ_o are intrinsic barriers due to nuclear motions within the reactants (inner coordination sphere) and nuclear motions induced by solvent reorganization (outer coordination sphere), respectively.

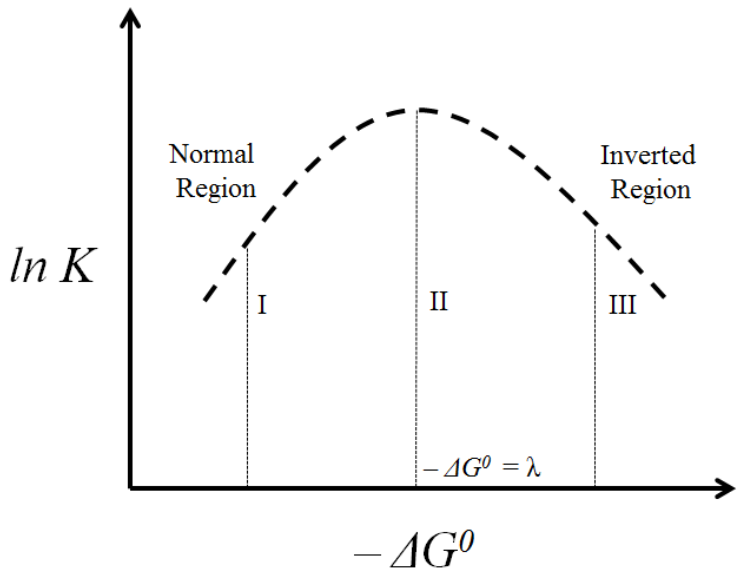

Fig. 1.7 Marcus plot of (*ln k*) versus $-\Delta G^0$ for a bimolecular electron transfer reaction.

A plot of logarithm of the rate constant (*ln k*) versus $-\Delta G^0$ results in a parabolic plot and is called a Marcus plot. Marcus predicted two regions in this plot: (i) the normal region in which an increase of $-\Delta G^0$ results in an increase of the net electron transfer reaction rate which maximizes at $-\Delta G^0 = \lambda$, and (ii) the inverted region in which an

increase in free energy beyond the point $-\Delta G^0 = \lambda$ results in a decrease of the electron transfer reaction rate.

1.7 Introduction to noncoherent photon upconversion via triplet-triplet annihilation

Photon upconversion is a process in which photons of lower energy are absorbed and converted into photons of higher energy.[49] Sequential or simultaneous two-photon absorption is a well-established method for achieving this goal. However, photon upconversion triggered by two-photon absorption usually requires a coherent excitation source such as lasers with a high incident laser power density and absorbing molecules with large two-photon absorption cross sections.[49] Realizing upconversion through two-photon absorption with noncoherent light sources such as sunlight is thus improbable. However, sensitized triplet-triplet annihilation (TTA) has been proposed as a method for achieving photon upconversion using low-power, noncoherent excitation sources. Basically, TTA is a process where two triplet molecules annihilate according to the Dexter-type electron exchange mechanism to form an intermediate complex which then dissociates to form an excited singlet state and a singlet ground state. i.e.,

$$T_1 + T_1 \rightarrow {}^{1,3,5}(T_1 \ldots T_1) \rightarrow S_n + S_0,\ n \geq 1 \qquad \text{(i)}$$

The phenomenon of delayed fluorescence due to TTA was first ever reported in the 1960s in a series of publications by Parker.[50] During the same period, a theoretical study of delayed fluorescence from an excited singlet state due to TTA in some aromatic hydrocarbons was reported by Krishna.[51] This report demonstrated that, in solution, the rates of nonradiative transitions from the bimolecular singlet and triplet states formed due

to TTA is much faster than the rate of quenching of the triplet states and that the nonradiative transitions from the quintent state may compete with the triplet state quenching. This was followed by reports of TTA-induced delayed fluorescence from the S_2 state of metalloporphyrins[52] and from the $K_4[Pt_2(P_2O_5H_2)_4]$ complex, all published in the 1980s.[53]

Research in this field had not been active until the first decade of 21st century when, in 2004, Kozlov and Castellano reported the anti-Stokes shifted delayed fluorescence due to TTA in metal-organic bichromophores in solution.[54] Since then, noncoherent photon upconversion (NCPU) realized by triplet-triplet annihilation (TTA) by visible to near-infrared sensitization using a low-power light source has been emerged as an active area of research. Recent reviews about the developments in this field include the following. (i) A detailed description of sensitized TTA and NCPU processes in different molecular systems by Singh-Rachford and Castellano.[3] (ii) The possibility of enhancing the efficiency of TTA by increasing the photon absorption of the sensitizer by incorporating supramolecular functional groups was discussed in a mini-review by Ceroni.[49] (iii) A theoretical model which could guide optimization of the efficiency of the TTA process and its evaluation methods have recently been proposed by Monguzzi et al.[55]

TTA and its associated delayed fluorescence are of great interest mainly because of the possibility of using this phenomenon: (i) for enhancing the efficiency of dye-sensitized organic solar cells (DSSCs),[56] (ii) in oxygen sensors,[57] other flexible, transparent optoelectronic devices including organic light emitting diodes (OLEDs)[58] and

multicolor displays,[59] (iii) for generating white-light emission[60] and (iv) as a fluorescent probe for bioimaging.[49,61] Compared to conventional visible light-absorbing dyes commonly used in DSSCs, molecules capable of NCPU offer the following distinct advantages. (i) They can use photons in the near-IR part of the solar spectrum that are otherwise unutilized. (ii) Such dyes can exploit electronic states that are otherwise not used (e.g. higher singlet states) or considered as energy sinks (e.g. triplet states). Therefore a solar cell with an upconverter and a conventional dye unit in tandem would be expected to enhance the ability of the cell to absorb over a wider range of the solar spectrum. The efficiency of p-n junction solar cells is limited to the theoretical value, 30%, known as the Shockley-Queisser limit[62] and incorporating a TTA-NCPU unit with the single-threshold solar cells may increase the efficiency above this limit. In fact, recent research shows that solar cells involving a rear photon upconverting unit sandwiched with a conventional silicon thin film unit do increase the peak efficiency by a modest factor of (1.0 ± 0.2) % under irradiation conditions similar to solar AM 1.5.[63] With the application of a back-scattering layer, the peak efficiency was increased to ~ 2% with a record upconversion figure of merit (current enhancement per area per sunsquared with units $mA.cm^{-2}.sun^{-2}$).[64]

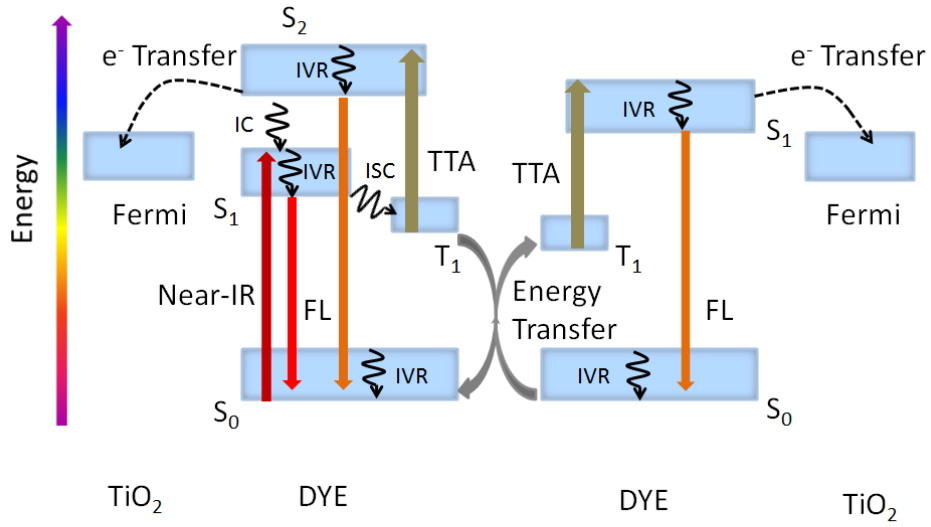

Fig. 1.8 Schematic illustration of the possible mechanistic pathways associated with TTA, consequent NCPU process and electron transfer to a semiconductor.

Most reports concerning NCPU outline a general mechanism for the upconversion process; a sensitizer molecule (Sen) such as a metalloporphyrin absorbs a noncoherent source of light and is excited to a singlet state (S_1) which then undergoes efficient intersystem crossing to a triplet state (T_1). When this molecule encounters a second molecule (BE, a blue-emitter) with a lower-lying triplet state, triplet-triplet energy transfer (TTET) occurs if the triplet state of BE is sufficiently long-lived. TTA can ensue causing the blue emitter to populate its S_n state (n = 1 in most cases). This requires the condition, $\Delta E(S_n\text{-}S_0) \geq 2 \times \Delta E(T_1\text{-}S_0)$. TTA thus results in an emission that is blue-shifted with respect to the excitation wavelength, hence the term non-coherent photon

upconversion (NCPU). The proposed mechanisms are given below and are depicted in Fig. 1.8.

$$S_0(Sen) + h\nu_{VIS\text{-}NIR} \rightarrow S_1(Sen) \quad \text{(ii)}$$

$$S_1(Sen) \rightarrow T_1(Sen) \quad \text{(iii)}$$

$$T_1(Sen) + S_0(BE) \rightarrow S_0(Sen) + T_1(BE) \quad \text{(iv)}$$

$$2\ T_1(BE) \rightarrow S_1(BE) + S_0(BE) \quad \text{(v)}$$

$$S_1(BE) \rightarrow S_0(BE) + h\nu_{UC\text{-}BLUE} \quad \text{(vi)}$$

An alternative, less efficient mechanism was also proposed by Baluschev et al.[65] In this mechanism, the sensitizer itself acts as an upconverter so that after light absorption and T_1 formation, TTA populates the S_n state ($n \geq 2$) of the sensitizer, which then can act as an energy donor to the BE. The BE then emits the upconverted photon. i.e.

$$S_0(Sen) + h\nu_{VIS\text{-}NIR} \rightarrow S_1(Sen) \quad \text{(vii)}$$

$$S_1(Sen) \rightarrow T_1(Sen) \quad \text{(viii)}$$

$$2\ T_1(Sen) \rightarrow S_n(Sen) + S_0(Sen) \quad \text{(ix)}$$

$$S_n(Sen) + S_0(BE) \rightarrow S_0(Sen) + S_1(BE) \quad \text{(x)}$$

$$S_1(BE) \rightarrow S_0(BE) + h\nu_{UC\text{-}BLUE} \quad \text{(xi)}$$

However, this mechanism had been somewhat controversial[56,66] for reasons discussed later in this thesis.

Significant efforts have been made during the last few years to explore different methods to enhance the efficiency of NCPU. Research in this field has mainly progressed in two directions: (i) employing various combinations of sensitizer molecules and upconverter molecules having different photophysical properties, and (ii) understanding the mechanisms and kinetics of NCPU of these systems in both solution and the solid state studied. A list of the sensitizers and upconverters reported in the literature up to 2010 can be found in the review by Singh-Rachford and Castellano.[3]

Baluschev and co-workers were the first to observe the NCPU process upon excitation using the green wavelengths of sunlight.[67] They have mainly used Pd(II) and Pt(II) porphyrins as the sensitizers and polyfluorenes and other aromatic hydrocarbons such as 9,10-diphenylanthracene (DPA) and rubrene as the BEs.[59,65,67-68] They have demonstrated (i) that NCPU can be used in 2-D multicolor diplay devices,[59] (ii) that under ultralow excitation intensities, surface plasmon resonance enhanced efficient NCPU can be realized in polymer-BE blended thin films with a metalloporphyrin sensitizer near a silver surface,[68f] (iii) that NCPU can be realized in a micellar environment in aqueous medium[69] and, (iv) that mechanism (II) for TTA does occur in PtOEP + polyfluorene or pentaphenylene systems, but only if the sensitizer and the emitter are aggregated in the ground state.[66c]

Castellano and co-workers[3] have mainly focused on trying various combinations of sensitizers and upconverters to obtain the maximum peak-to-peak anti-Stokes shift for the upconverted emission and to obtain maximum quantum efficiency under high excitation

intensity conditions, i.e. where the upconverted emission intensity shows a linear dependence on the excitation intensity.[3,54,70] It was also demonstrated that simultaneous two-photon excitation of a Ru(II) triplet sensitizer complex yielded delayed fluorescence from 9,10-diphenylanthracene with a quartic incident light power dependence.[70d] Also, they demonstrated that NCPU through TTA can be achieved in polymer matrices[71] where the temperature can affect the NCPU process.[72] In addition, they have demonstrated that TTA can be used for photochemical and photoelectrochemical reactions. Photochemical dimerization of anthracene molecules has been achieved by visible sensitization of anthracene by a ruthenium complex.[73] TTA in anthracene produced an excited anthracene singlet state which dimerized with another anthracene molecule to form an anthracene dimer. Recently, upconversion supported photoelectrochemistry was demonstrated using a sub-band gap laser source in which a photocurrent was generated from nanostructured WO_3 photoanodes by an upconverting sensitizer.[74]

Detailed investigations of the mechanistic and kinetic aspects of the NCPU process have been conducted by Monguzzi et al.[55,75] and Schmidt et al.[76] The effect of temperature and hence the viscosity of the medium on the NCPU yield has been studied by Monguzzi et al.[75b,c] They found that at 77 K, the efficiency of energy transfer from the sensitizer triplet to the annihilator triplet depended on Dexter-type energy transfer in the Perrin approximation. In this approximation, it is assumed that the rate of energy transfer is fast when $R << L$ and that the rate of energy transfer is negligible when $R > L$, where R and L are distance between the sensitizer and annihilator and the effective Bohr radius, respectively. The enhanced energy transfer rate when the temperature was increased to

300 K was attributed to the enhanced rate of diffusion of the molecules. Based on a kinetic analysis, the quadratic behavior of the dependence of the upconverted emission intensity on the incident light intensity was attributed to dominance of spontaneous decay of the triplets at low laser illumination power and bimolecular TTA at high incident intensities.[75a] The incident light power where the TTA starts to dominate is the threshold excitation power to have efficient NCPU. The parameters that affect the efficiency of NCPU in terms of the threshold excitation intensity and the intrinsic photophysical properties of the molecules are discussed in a recent paper by Monguzzi.[55] The effect of an applied magnetic field on the upconverted emission intensity demonstrated that TTA in solid films is controlled by the migration of triplet excitons rather than the probability of annihilation, that TTA is a diffusion-limited process and that the probability of TTA approaches unity after the collision of the excitons.[75e] Finally, it was shown that the reduced efficiency of TTA in solid matrices due to limited exciton diffusion can be circumvented by incorporating the NCPU system in polymer nanoparticles where each nanoparticle acts as a single, isolated high-efficiency upconverting unit.[77]

Early studies suggested that the efficiency of TTA is limited by spin statistics rule, i.e. only one out of the possible nine spin states (1/9) of the encounter complexes formed during a TTA process can give rise to singlet state products that could emit the upconverted emission, thus limiting the efficiency to 11%. Schmidt et al. used a kinetic analysis to prove that no such upper limit of TTA efficiency exists and observed that more than 60% of triplet molecules annihilated in a rubrene system. As a result a TTA efficiency that exceeds 40% at the highest upconverter concentration is possible, and this

has been attributed to recycling of the triplet states that are produced as a result of the decay of the triplet and quintet encounter complexes.[76a,76c,d] The rate of NCPU from a BE which has its triplet state lying slightly above the triplet state of the triplet sensitizer was shown to be controlled by the concentration of the BE due to entropic factors in the triplet energy transfer process. A record peak-to-peak anti-Stokes shift of 0.94 eV for the upconverted emission was reported.[76b] Intriguingly, singlet oxygen which is usually considered as a quencher of the triplet states was shown in this system to act as a triplet energy transmitter, enhancing rather than reducing the efficiency of TTA in an NCPU process.[78] The molecules are chosen such that $\Delta E(T_1\text{-}S_0)_{(Sensitizer)} > \Delta E(^1\Delta_g\text{-}^3\Sigma^-_g)_{(Oxygen)} > \Delta E(T_1\text{-}S_0)_{(BE)}$. Here triplet energy transfer from the sensitizer to the oxygen occurs populating the $^1\Delta_g$ state of oxygen. The singlet oxygen formed thus can transfer energy to the triplet state of the BE and the triplet BEs can then annihilate to form the S_1 state of the BE, and emit delayed fluorescence. Alternatively, the triplet BE can undergo heteromolecular TTA with a second singlet oxygen to form the S_1 state of the BE.

Other attempts to generate upconverted emission includes using systems of Pt(II), Ir(III), Re(I) and Ru(II) organometallic complexes as sensitizers combined with organic BEs.[54,70a,70k,79,57b,80] Zhao et al.[57b,c,80a-n,80p,81] demonstrated that NCPU in their systems can be used for oxygen sensing in solution. NCPU in non-volatile, non-flammable ionic liquids was reported by Murakami[82] who found that the upconversion quantum yields saturate rapidly under very low incident laser powers. This observation was attributed to complete triplet energy transfer in degassed samples where efficient removal of oxygen was made possible by taking advantage of negligible vapor pressures of the ionic liquids.

Recently, NCPU from a Pt(II)porphyrin+DPA pair on nanocrystalline sensitized mesoporous ZrO_2 was reported and the triplet energy (exciton?) migration was proposed to occur via a static Dexter-type energy transfer.[83]

1.8 Photophysics of metalloporphyrin-fullerene systems

The photophysical and electrochemical properties of metalloporphyrins and fullerenes in supramolecular self-assembled, host-guest, covalent- and coordinate-bound structures are the subjects of a large number of articles published over the last few years and a list of reviews of these studies can be found in references (23) and (83).[23,84] Excitation of combinations of porphyrins and fullerenes have been found to generate long-lived charge transfer states, which are of critical importance in applications such as organic optoelectronic devices and organic solar cells.[85] The charge transfer in these systems is usually facilitated by selective one-photon excitation of the porphyrin. However, in some cases excitation of a fullerene has also triggered charge transfer events. In any case, these supramolecular constructs take advantage of the excellent electron donating nature of the porphyrins and the electron accepting behavior of the fullerenes, as illustrated by the favorable oxidation and reduction potentials of these molecules.

The ground state association energies of fullerenes and metalloporphyrins are often large in self-assembled systems because of the attraction between the central metal of the metalloporphyrin and the electron-rich π bonds of the fullerenes.[86] In some host-guest complex structures, fullerenes are trapped in a cage of self-assembled or chemically assembled (through coordinate or covalent linkage) metalloporphyrins, thus allowing

efficient electron transfer to generate the charge-separated states.[84b,87] Fullerenes encapsulated in porphyrin nanorods have also been found to have efficient electron transfer characteristics.[88]

Molecular wires which exhibit efficient charge transport properties have been developed by the covalent linking of fullerenes through unsaturated π-electron rich functional groups.[89] Efficient electron transfer has been observed in systems in which Hamilton-type molecular wires were formed through hydrogen bonding between chemically functionalized porphyrins and fullerenes.[90] Alternatively, fullerenes and porphyrins can be linked through very long saturated chains where the linker adopts a conformation such that the poprhyrin and fullerene will be close enough to allow an intermolecular through-space electron transfer.[91] In coordinately linked dyads or triads, the fullerene is functionalized with a group such as an electron-rich nitrogen bearing pyrrolidine[84a,84c] that can link to the central metal atom of the porphyrin, or a functional group bearing a cationic moiety such as $-NH_3^+$ that can link to a crown ether group functionalized on the porphyrin macrocyclic structure.[92]

Most of the reported studies of electron transfer and energy transfer between porphyrins and fullerenes deal with porphyrins excited in their Q-band region. Other than these studies, electron transfer and energy transfer between the triplet states of self-assembled porphyrins and fullerenes have been reported by Ito and co-workers.[84a] They found[93] that selective excitation of a porphyrin resulted in electron transfer from the triplet state of the porphyrin to the C_{60} and C_{70} fullerenes. Contrary to this, selective

excitation of the fullerene resulted in electron transfer from the ground state of the porphyrin to the triplet state of the fullerenes.

Kesti et al.[94] reported the dynamics of relaxation of the Soret-excited covalently linked porphyrin-C_{60} or $-C_{70}$ dyads. They attributed the relaxation of the S_2 state of the porphyrin in these systems to rapid S_2-S_1 internal conversion in the porphyrin and energy transfer from the porphyrin to the fullerene. Other than this single report, reports of the photophysics of Soret-excited porphyrin-fullerene systems are rare in the literature.

1.9 Motivation and objectives of the present work

Metalloporphyrins are commonly used as sensitizers in the NCPU processes reported to date. The possibility of homomolecular TTA within the metallporphyrin or heteromolecular TTA of the porphyrin with a BE to populate a higher excited singlet state of the porphyrin is possible if some preconditions are met. In fact, delayed fluorescence from the S_2 state of metalloporphyrins produced as result of homolecular TTA was reported decades ago.[52] Thus the product state of TTA in metalloporphyrins, in principle, can act as an energy donor or electron donor provided that this state is sufficiently long-lived to compete with other nonradiative energy wasting processes. The radiative and nonradiative upper excited singlet (S_2) state dynamics of several classes of molecules including aromatic thiocarbonyls,[95] azulenes[96] and metalloporphyins[97] has been a long-standing interest for our group. This interest has focused our attention on metalloporphyrins and other molecules such as fullerenes which have higher excited

singlet states (S_n, $n \geq 2$) that can act as the product state of TTA and in turn can act as an energy or electron donor in a DSSC.

With this background we have focused our attention to the mechanisms of TTA-NCPU proposed by Baluschev et al.[65] The Pt (II) and Pd (II) porphyrins used as sensitizers in most of their studies of NCPU are nonfluorescent from their S_2 states and have sub-picosecond (< 1 ps) S_2 state lifetimes in agreement with the reported literature values[97] of the S_2 lifetimes of unaggregated diamagnetic metalloporphyrins in solution. The S_2 state could still be the product state for the homolecular TTA process within the porphyrin. However, it is highly unlikely that the short-lived S_2 state in these porphyrins can act as an energy donor to the S_1 state of the BE through a standard FRET mechanism because FRET depends upon the fluorescence quantum yield and lifetime of the donor as well as the spectral overlap of the donor emission with the acceptor absorption.[32]

A Dexter-type electron exchange energy transfer from the S_2 of porphyrin to the BE is also possible, however, this requires the overlap of the electronic wavefunctions[33] which demands aggregation of the porphyrin and the BE in either the ground state or in the excited state. Baluschev et al. considered ground state aggregation of the porphyrin, aggregation of the porphyrin with the BE and aggregation within the BE as undesired phenomena in TTA-NCPU. However, ground state aggregation is a well-established property of metalloporphyrins which are reported to aggregate even at micromolar concentrations in solution.[98] Steer proposed that[66a] if the NCPU process is to occur through energy transfer from the S_2 state of porphyrin to the S_1 state of the BE, either

triplet exciton annihilation in porphyrin aggregates or prior aggregation of the porphyrin and the BE should be a prerequisite. In addition, it was proposed that[66a] involvement of heteromolecular TTA between a porphyrin and the BE and the possibility of the involvement of a long-lived intermediate charge-transfer state formed by intramolecular ligand-metal charge transfer in the porphyrin to BE energy transfer should be considered.

In order to clarify these discrepancies, we have undertaken to study the NCPU process in model metalloporphyrin + BE systems in solution; this is the first major research topic and forms chapter 3 of this thesis. The porphyrin selected was meso-tetraphenylporphine zinc (II), ZnTPP, in which the zinc has a closed d shell, thus eliminating the possibility of intramolecular ligand-metal charge transfer.[99] The S_2 state of ZnTPP is fluorescent with a lifetime of about 1.4 ps.[97] Therefore both the S_2 and S_1 fluorescence of ZnTPP can be used to characterize the NCPU process.

In search of molecules like metalloporphyrins which are capable of undergoing homomolecular TTA to produce an upper excited singlet state, we found that the fullerene may be used as a sensitizer and an upconverter. C_{60} and its derivatives can undergo efficient triplet energy transfer with a number of organic molecules[84a,100] including other fullerenes such as C_{70}.[101] This underpins the ability of C_{60} as a potential triplet sensitizer in mechanism (I) of TTA.[102] More interestingly, C_{60} itself has been reported to undergo efficient homomolecular TTA.[103] However, on energetic backgrounds, the product state of TTA in C_{60} is the one which corresponds to an electric dipole allowed one-electron transition,[23] even though the oscillator strength for this

transition is too small. As a preliminary step before investigating the dynamics of the possible involvement of this state in a singlet energy transfer mechanism, it is necessary to understand the kinetics of TTA in C_{60} and where C_{60} can act as a triplet sensitizer with a BE. Therefore we have studied the detailed kinetics of TTA of C_{60} and two BEs in a nonpolar solvent, the topic of Chapter 4 of the thesis.

Luminescence quenching is an established, reliable and accurate method used for finding the rate of oxygen diffusion in polymer thin films that can be used as barrier membranes for several applications. Fluorescence quenching monitored using a fluorimeter or phosphorescence quenching monitored using a phosporimeter is the most frequently used oxygen sensing techniques. Here, our goal was to show proof-of-principle that TTA-induced delayed fluorescence can be used as a technique for measuring the oxygen diffusion process in polymer thin films and this is the subject of Chapter 5 of the thesis.

Fullerenes are reported as efficient electron acceptors of metalloporphyrins in covalently or coordinately linked supramolecular structures. However, reports of the dynamics of Soret-excited metalloporphyrins in the presence of untethered, unsubstituted fullerenes are rare. If fullerenes are to be used as electron acceptors when the TTA-populated short-lived S_2 state of a porphyrin is the donor, it is necessary to study the picosecond to sub-picosecond excited state dynamics of a model metalloporphyrin (ZnTPP in our case) with a fullerene. We are interested in the photophysical processes of self-assembled systems and have therefore attempted to study the photophysics of Soret-

excited ZnTPP and C_{60} in nonpolar (toluene) and polar (benzonitrile) solutions. This is the core topic of Chapter 6 of this thesis.

References

(1) Hagfeldt, A.; Boschloo, G.; Sun, L. C.; Kloo, L.; Pettersson, H. *Chem. Rev.* **2010**, *110*, 6595.

(2) (a) Gratzel, M. *Nature* **2001**, *414*, 338. (b) Gratzel, M. *J. Photochem. Photobiol. C-Photochem. Rev.* **2003**, *4*, 145. (c) Gratzel, M. *Chem. Lett.* **2005**, *34*, 8.

(3) Singh-Rachford, T. N.; Castellano, F. N. *Coord. Chem. Rev.* **2010**, *254*, 2560.

(4) Rohatgi-Mukherjee, K. K. *Fundamentals of Photochemistry Revised Edition*; New Age International (P) Limited: New Delhi, 1986.

(5) (a) Barrow, G. M. *Introduction to Molecular Spectroscopy*; McGraw-Hill Kongakusha, Ltd. : Tokyo, 1962. (b) Harris, D. C.; Bertolucci, M. D. *Symmetry and Spectroscopy: An Introduction to Vibrational and Electronic Spectroscopy*; Oxford University press: New York, 1978.

(6) Simons, J. *Energetic Principles of Chemical Reactions*; Jones and Bartlett Publishers, Inc.: Massachusetts, 1983.

(7) Turro, N. J. *Modern Molecular Photochemistry*; University Science Books: California, 1991.

(8) Kasha, M. *Discuss. Faraday Soc.* **1950**, 14.

(9) Beer, M.; Longuethiggins, H. C. *J. Chem. Phys.* **1955**, *23*, 1390.

(10) (a) Maurata, S.; Iwanaga, C.; Toda, T.; Kokubun, H. *Chem. Phys. Lett.* **1972**, *13*, 101. (b) Eber, G.; Schneider, S.; Dorr, F. *Chem. Phys. Lett.* **1977**, *52*, 59.

(11) Maciejewski, A.; Steer, R. P. *Chem. Rev.* **1993**, *93*, 67.

(12) (a) Bajema, L.; Gouterma.M; Rose, C. B. *J. Mol. Spectrosc.* **1971**, *39*, 421. (b) Kurabayashi, Y.; Kikuchi, K.; Kokubun, H.; Kaizu, Y.; Kobayashi, H. *J. Phys. Chem.* **1984**, *88*, 1308.

(13) (a) Leupin, W.; Berens, S. J.; Magde, D.; Wirz, J. *J. Phys. Chem.* **1984**, *88*, 1376. (b) Plummer, B. F.; Alsaigh, Z. Y.; Arfan, M. *Chem. Phys. Lett.* **1984**, *104*, 389.

(14) Snyder, R.; Arvidson, E.; Foote, C.; Harrigan, L.; Christensen, R. L. *J. Am. Chem. Soc.* **1985**, *107*, 4117.

(15) Strickler, S. J.; Berg, R. A. *J. Chem. Phys.* **1962**, *37*, 814.

(16) Freed, K. F. *Acc. Chem. Res.* **1978**, *11*, 74.

(17) Englman, R.; Jortner, J. *Mol. Phys.* **1970**, *18*, 145.

(18) (a) Liu, X.; Tripathy, U.; Bhosale, S. V.; Langford, S. J.; Steer, R. P. *J. Phys. Chem. A* **2008**, *112*, 8986. (b) Tripathy, U.; Kowalska, D.; Liu, X.; Velate, S.; Steer, R. P. *J. Phys. Chem. A* **2008**, *112*, 5824.

(19) Yella, A.; Lee, H. W.; Tsao, H. N.; Yi, C. Y.; Chandiran, A. K.; Nazeeruddin, M. K.; Diau, E. W. G.; Yeh, C. Y.; Zakeeruddin, S. M.; Gratzel, M. *Science* **2011**, *334*, 629.

(20) Velate, S.; Liu, X.; Steer, R. P. *Chem. Phys. Lett.* **2006**, *427*, 295.

(21) (a) Liu, X.; Yeow, E. K. L.; Velate, S.; Steer, R. P. *Phys. Chem. Chem. Phys.* **2006**, *8*, 1298. (b) Karolczak, J.; Kowalska, D.; Lukaszewicz, A.; Maciejewski, A.; Steer, R. P. *J. Phys. Chem. A* **2004**, *108*, 4570.

(22) (a) Gouterman, M. *J. Mol. Spectrosc.* **1961**, *6*, 138. (b) Gouterman, M. *The Porphyrins*; Academic Press: New York, 1978. (c) Gouterman, M.; Snyder, L. C.; Wagniere, G. H. *J. Mol. Spectrosc.* **1963**, *11*, 108.

(23) Orlandi, G.; Negri, F. *Photochem. Photobiol. Sci.* **2002**, *1*, 289.

(24) Sassara, A.; Zerza, G.; Chergui, M.; Ciulin, V.; Ganiere, J. D.; Deveaud, B. *J. Chem. Phys.* **1999**, *111*, 689.

(25) Stepanov, A. G.; Portella-Oberli, M. T.; Sassara, A.; Chergui, M. *Chem. Phys. Lett.* **2002**, *358*, 516.

(26) McBranch, D.; Klimov, V.; Smilowitz, L.; Grigorova, M.; Robinson, J. M.; Koskelo, A.; Mattes, B. R.; Wang, H.; Wudl, F. *Femtosecond excited-state absorption dynamics and optical limiting in fullerene solutions, sol-gel glasses, and thin films*; SPIE - Int Soc Optical Engineering: Bellingham, 1996.

(27) Lakowicz, J. R. *Principles of Fluorescence Spectroscopy*; Springer: New York, 2006.

(28) Kautsky, H. *Trans. Faraday Soc.* **1939**, *35*, 0216.

(29) Kasha, M. *J. Chem. Phys.* **1952**, *20*, 71.

(30) Steiner, R. F.; Kirby, E. P. *J. Phys. Chem.* **1969**, *73*, 4130.

(31) Allinger, K.; Blumen, A. *J. Chem. Phys.* **1980**, *72*, 4608.

(32) (a) Forster, T. *Ann. Physik.* **1948**, *2*, 55. (b) Forster, T. *Disc. Faraday Soc.* **1959**, 7.

(33) Dexter, D. L. *J. Chem. Phys.* **1953**, *21*, 836.

(34) Loring, R. F.; Andersen, H. C.; Fayer, M. D. *J. Chem. Phys.* **1982**, *76*, 2015.

(35) (a) Pearlstein, R. M. *Proc. Natl. Acad. Sci. U. S. A.* **1964**, *52*, 824. (b) Porter, G. *Proc. R. Soc. London Ser. A-Math. Phys. Eng. Sci.* **1978**, *362*, 281. (c) Markvart, T. *J. Theor. Biol.* **1978**, *72*, 91.

(36) Haas, E.; Wilchek, M.; Katchalskikatzir, E.; Steinberg, I. Z. *Proc. Natl. Acad. Sci. U. S. A.* **1975**, *72*, 1807.

(37) Klopffer, W. *Ann. NY Acad. Sci.* **1981**, *366*, 373.

(38) Inokuti, M.; Hirayama, F. *J. Chem. Phys.* **1965**, *43*, 1978.

(39) Jang, S. J.; Shin, K. J.; Lee, S. Y. *J. Chem. Phys.* **1995**, *102*, 815.

(40) Stryer, L. *Annu. Rev. Biochem.* **1978**, *47*, 819.

(41) Kavarnos, G. J.; Turro, N. J. *Chem. Rev.* **1986**, *86*, 401.

(42) (a) Marcus, R. A. *J. Chem. Phys.* **1956**, *24*, 966(b) Marcus, R. A. *J. Chem. Phys.* **1957**, *26*, 867. (c) Marcus, R. A. *J. Chem. Phys.* **1957**, *26*, 872. (d) Marcus, R. A. *Can. J. Chem.-Rev. Can. Chim.* **1959**, *37*, 155. (e) Marcus, R. A. *Discussions of the Faraday Society* **1960**, 21. (f) Marcus, R. A. *J. Phys. Chem.* **1963**, *67*, 853. (g) Marcus, R. A. *J. Chem. Phys.* **1965**, *43*, 679. (h) Marcus, R. A. *J. Chem. Phys.* **1965**, *43*, 2654. (i) Marcus, R. A. *Angew. Chem.-Int. Edit. Engl.* **1993**, *32*, 1111. (j) Marcus, R. A.; Sutin, N. *Biochim. Biophys. Acta* **1985**, *811*, 265. (k) Sumi, H.; Marcus, R. A. *J. Chem. Phys.* **1986**, *84*, 4894.

(43) Sutin, N. *Accounts Chem. Res.* **1982**, *15*, 275.

(44) Beens, H.; Knibbe, H.; Weller, A. *J. Chem. Phys.* **1967**, *47*, 1183.

(45) Mataga, N.; Chosrowjan, H.; Taniguchi, S. *J. Photochem. Photobiol. C-Photochem. Rev.* **2005**, *6*, 37.

(46) Mataga, N.; Migita, M.; Nishimura, T. *J. Mol. Struct.* **1978**, *47*, 199.

(47) Rehm, D.; Weller, A. *Isr. J. Chem.* **1970**, *8*, 259.

(48) (a) Danger, B. R.; Bedient, K.; Maiti, M.; Burgess, I. J.; Steer, R. P. *J. Phys. Chem. A* **2010**, *114*, 10960. (b) Rehm, D.; Weller, A. *Ber. Bunsenges. Phys. Chem.* **1969**, *73*, 834. (c) Braslavsky, S. E. *Pure Appl. Chem.* **2007**, *79*, 293.

(49) Ceroni, P. *Chem.-Eur. J.* **2011**, *17*, 9560.

(50) (a) Parker, C. A.; Hatchard, C. G. *P. Chem. Soc. London* **1962**, 386. (b) Parker, C. A.; Hatchard, C. G. *P. Roy. Soc. Lond. A-Math.* **1962**, *269*, 574. (c) Parker, C. A. *Nature* **1963**, *200*, 331(d) Parker, C. A. *P. Roy. Soc. Lond. A-Math.* **1963**, *276*, 125. (e) Parker, C. A. *Spectrochim. Acta* **1963**, *19*, 989. (f) Parker, C. A.; Hatchard, C. G. *Trans. Faraday Soc.* **1963**, *59*, 284. (g) Parker, C. A.; Hatchard, C. G.; Joyce, T. A. *J. Mol. Spectrosc.* **1964**, *14*, 311. (h) Parker, C. A. *Trans. Faraday Soc.* **1964**, *60*, 1998. (i) Parker, C. A.; Hatchard, C. G.; Joyce, T. A. *Analyst* **1965**, *90*, 1. (j) Parker, C. A.; Hatchard, C. G.; Joyce, T. A. *Nature* **1965**, *205*, 1282. (k) Parker, C. A.; Joyce, T. A. *J. Chem. Soc. A* **1966**, 821. (l) Parker, C. A.; Joyce, T. A. *Nature* **1966**, *210*, 701. (m) Parker, C. A.; Joyce, T. A. *Chem. Commun.* **1966**, 234. (n) Parker, C. A.; Joyce, T. A. *Trans. Faraday Soc.* **1966**, *62*, 2785. (o) Parker, C. A.; Joyce, T. A. *Chem. Commun.* **1967**, 744. (p) Parker, C. A.; Joyce, T. A. *Chem. Commun.* **1967**, 1138. (q) Parker, C. A.; Joyce, T. A. *Photochem. Photobiol.* **1967**, *6*, 395.

(51) Krishna, V. G. *J. Chem. Phys.* **1967**, *46*, 1735.

(52) (a) Stelmakh, G. F.; Tsvirko, M. P. *Opt. Spektrosk.* **1980**, *49*, 511. (b) Stelmakh, G. F.; Tsvirko, M. P. *ACS Sym. Ser.* **1986**, *321*, 118. (c) Ksenofontova, N. M.; Stelmakh, G. F.; Tsvirko, M. P. *Dokl. Akad. Nauk SSSR+* **1986**, *289*, 405.

(53) Tanaka, Y.; Azumi, T. *Inorg. Chem.* **1986**, *25*, 247.

(54) Kozlov, D. V.; Castellano, F. N. *Chem. Commun.* **2004**, 2860.

(55) Monguzzi, A.; Tubino, R.; Hoseinkhani, S.; Campione, M.; Meinardi, F. *Phys. Chem. Chem. Phys.* **2012**, *14*, 4322.

(56) Sugunan, S. K.; Tripathy, U.; Brunet, S. M. K.; Paige, M. F.; Steer, R. P. *J. Phys. Chem. A* **2009**, *113*, 8548.

(57) (a) Sugunan, S. K.; Paige, M. F.; Steer, R. P. *Can. J. Chem.-Rev. Can. Chim.* **2011**, *89*, 195. (b) Sun, H. Y.; Guo, H. M.; Wu, W. T.; Liu, X.; Zhao, J. Z. *Dalton Transactions* **2011**, *40*, 7834(c) Wu, W. T.; Wu, W. H.; Ji, S. M.; Guo, H. M.; Zhao, J. Z. *Dalton T.* **2011**, *40*, 5953.

(58) King, S. M.; Cass, M.; Pintani, M.; Coward, C.; Dias, F. B.; Monkman, A. P.; Roberts, M. *J. Appl. Phys.* **2011**, *109*.

(59) Miteva, T.; Yakutkin, V.; Nelles, G.; Baluschev, S. *New J. Phys.* **2008**, *10*.

(60) (a) Chen, H. C.; Hung, C. Y.; Wang, K. H.; Chen, H. L.; Fann, W. S.; Chien, F. C.; Chen, P. L.; Chow, T. J.; Hsu, C. P.; Sun, S. S. *Chem. Commun.* **2009**, 4064. (b) Monguzzi, A.; Riva, F.; Tubino, R.; Meinardi, F. *Chem. Phys. Lett.* **2012**, *521*, 17.

(61) Wohnhaas, C.; Turshatov, A.; Mailander, V.; Lorenz, S.; Baluschev, S.; Miteva, T.; Landfester, K. *Macromol. Biosci.* **2011**, *11*, 772.

(62) Shockley, W.; Queisser, H. J. *J. Appl. Phys.* **1961**, *32*, 510.

(63) Cheng, Y. Y.; Fuckel, B.; MacQueen, R. W.; Khoury, T.; Clady, R.; Schulze, T. F.; Ekins-Daukes, N. J.; Crossley, M. J.; Stannowski, B.; Lips, K.; Schmidt, T. W. *Energy Environ. Sci.* **2012**, *5*, 6953.

(64) Schulze, T. F.; Cheng, Y. Y.; Fuckel, B.; MacQueen, R. W.; Danos, A.; Davis, N.; Tayebjee, M. J. Y.; Khoury, T.; Clady, R.; Ekins-Daukes, N. J.; Crossley, M. J.; Stannowski, B.; Lips, K.; Schmidt, T. W. *Aust. J. Chem.* **2012**, *65*, 480.

(65) Baluschev, S.; Yakutkin, V.; Wegner, G.; Minch, B.; Miteva, T.; Nelles, G.; Yasuda, A. *J. Appl. Phys.* **2007**, *101*.

(66) (a) Steer, R. P. *J. Appl. Phys.* **2007**, *102*. (b) Baluschev, S.; Yakutkin, V.; Wegner, G.; Minch, B.; Miteva, T.; Nelles, G.; Yasuda, A. *J. Appl. Phys.* **2007**, *102*. (c) Keivanidis, P. E.; Laquai, F.; Robertson, J. W. F.; Baluschev, S.; Jacob, J.; Mullen, K.; Wegner, G. *J. Phys. Chem. Lett.* **2011**, *2*, 1893.

(67) Baluschev, S.; Miteva, T.; Yakutkin, V.; Nelles, G.; Yasuda, A.; Wegner, G. *Phys. Rev. Lett.* **2006**, *97*, 143903/1.

(68) (a) Baluschev, S.; Jacob, J.; Avlasevich, Y. S.; Keivanidis, P. E.; Miteva, T.; Yasuda, A.; Nelles, G.; Grimsdale, A. C.; Mullen, K.; Wegner, G. *Chem. Phys. Chem.* **2005**, *6*, 1250. (b) Baluschev, S.; Keivanidis, P. E.; Wegner, G.; Jacob, J.; Grimsdale, A. C.; Mullen, K.; Miteva, T.; Yasuda, A.; Nelles, G. *Appl. Phys. Lett.* **2005**, *86*. (c) Baluschev, S.; Yakutkin, V.; Miteva, T.; Avlasevich, Y.; Chernov, S.; Aleshchenkov, S.; Nelles, G.; Cheprakov, A.; Yasuda, A.; Mullen, K.; Wegner, G. *Angew. Chem. Int. Edit.* **2007**, *46*, 7693. (d) Baluschev, S.; Yakutkin,

V.; Miteva, T.; Wegner, G.; Roberts, T.; Nelles, G.; Yasuda, A.; Chernov, S.; Aleshchenkov, S.; Cheprakov, A. *New J. Phys.* **2008**, *10*. (e) Baluschev, S.; Yakutkin, V.; Wegner, G.; Miteva, T.; Nelles, G.; Yasuda, A.; Chernov, S.; Aleshchenkov, S.; Cheprakov, A. *Appl. Phys. Lett.* **2007**, *90*. (f) Baluschev, S.; Yu, F.; Miteva, T.; Ahl, S.; Yasuda, A.; Nelles, G.; Knoll, W.; Wegner, G. *Nano Lett.* **2005**, *5*, 2482.

(69) Turshatov, A.; Busko, D.; Baluschev, S.; Miteva, T.; Landfester, K. *New J. Phys.* **2011**, *13*.

(70) (a) Islangulov, R. R.; Kozlov, D. V.; Castellano, F. N. *Chem. Commun.* **2005**, 3776. (b) Singh-Rachford, T. N.; Castellano, F. N. *J. Phys. Chem. A* **2008**, *112*, 3550. (c) Singh-Rachford, T. N.; Castellano, F. N. *Inorg. Chem.* **2009**, *48*, 2541. (d) Singh-Rachford, T. N.; Castellano, F. N. *J. Phys. Chem. A* **2009**, *113*, 9266. (e) Singh-Rachford, T. N.; Castellano, F. N. *J. Phys. Chem. A* **2009**, *113*, 5912. (f) Singh-Rachford, T. N.; Castellano, F. N. *J. Phys. Chem. Lett.* **2010**, *1*, 195. (g) Singh-Rachford, T. N.; Islangulov, R. R.; Castellano, F. N. *J. Phys. Chem. A* **2008**, *112*, 3906. (h) Singh-Rachford, T. N.; Nayak, A.; Muro-Small, M. L.; Goeb, S.; Therien, M. J.; Castellano, F. N. *J. Am. Chem. Soc.* **2010**, *132*, 14203. (i) Singh-Rachford, T. N.; Nayak, A.; Muro-Small, M. L.; Goeb, S.; Therien, M. J.; Castellano, F. N. *J. Am. Chem.l Soc.* **2011**, *133*, 2791. (j) Haefele, A.; Blumhoff, J.; Khnayzer, R. S.; Castellano, F. N. *J. Phys. Chem. Lett.* **2012**, *3*, 299. (k) Zhao, W.; Castellano, F. N. *J. Phys. Chem. A* **2006**, *110*, 11440.

(71) (a) Islangulov, R. R.; Lott, J.; Weder, C.; Castellano, F. N. *J. Am. Chem. Soc.* **2007**, *129*, 12652. (b) Kim, J.-H.; Deng, F.; Castellano, F. N.; Kim, J.-H. *Chem. Mater.* **2012**, *24*, 2250.

(72) Singh-Rachford, T. N.; Lott, J.; Weder, C.; Castellano, F. N. *J. Am. Chem. Soc.* **2009**, *131*, 12007.

(73) Islangulov, R. R.; Castellano, F. N. *Angew. Chem. Int. Edit.* **2006**, *45*, 5957.

(74) Khnayzer, R. S.; Blumhoff, J.; Harrington, J. A.; Haefele, A.; Deng, F.; Castellano, F. N. *Chem. Commun.* **2012**, *48*, 209.

(75) (a) Monguzzi, A.; Mezyk, J.; Scotognella, F.; Tubino, R.; Meinardi, F. *Phys. Rev. B* **2008**, *78*. (b) Monguzzi, A.; Tubino, R.; Meinardi, F. *Phys. Rev. B* **2008**, *77*. (c) Monguzzi, A.; Tubino, R.; Meinardi, F. *Int. J. Photoenergy* **2008.** (d) Monguzzi, A.; Tubino, R.; Meinardi, F. *J. Phys. Chem. A* **2009**, *113*, 1171. (e) Mezyk, J.; Tubino, R.; Monguzzi, A.; Mech, A.; Meinardi, F. *Phys. Rev. Lett.* **2009**, *102*.

(76) (a) Auckett, J. E.; Chen, Y. Y.; Khoury, T.; Clady, R. G. C. R.; Ekins-Daukes, N. J.; Crossley, M. J.; Schmidt, T. W. *J. Phys. Conf. Ser.* **2009**, *185*, 012002. (b) Cheng, Y. Y.; Fuckel, B.; Khoury, T.; Clady, R.; Ekins-Daukes, N. J.; Crossley, M. J.; Schmidt, T. W. *J. Phys. Chem. A* **2011**, *115*, 1047. (c) Cheng, Y. Y.; Fuckel, B.; Khoury, T.; Clady, R.; Tayebjee, M. J. Y.; Ekins-Daukes, N. J.; Crossley, M. J.; Schmidt, T. W. *J. Phys. Chem. Lett.* **2010**, *1*, 1795. (d) Cheng, Y. Y.; Khoury, T.; Clady, R.; Tayebjee, M. J. Y.; Ekins-Daukes, N. J.; Crossley, M. J.; Schmidt, T. W. *Phys. Chem. Chem. Phys.* **2010**, *12*, 66.

(77) Monguzzi, A.; Frigoli, M.; Larpent, C.; Tubino, R.; Meinardi, F. *Adv. Funct. Mater.* **2012**, *22*, 139.

(78) Fuckel, B.; Roberts, D. A.; Cheng, Y. Y.; Clady, R.; Piper, R. B.; Ekins-Daukes, N. J.; Crossley, M. J.; Schmidt, T. W. *J. Phys. Chem. Lett.* **2011**, *2*, 966.

(79) Du, P. W.; Eisenberg, R. *Chem. Sci.* **2010**, *1*, 502.

(80) (a) Wu, W. T.; Zhao, J. Z.; Wu, W. H.; Chen, Y. H. *J. Organomet. Chem.* **2012**, *713*, 189. (b) Ji, S. M.; Wu, W. H.; Zhao, J. Z.; Guo, H. M.; Wu, W. T. *Eur. J. Inorg. Chem.* **2012**, 3183. (c) Sun, J. F.; Wu, W. H.; Zhao, J. Z. *Chem.-Eur. J.* **2012**, *18*, 8100. (d) Wu, W. H.; Ji, S. M.; Wu, W. T.; Shao, J. Y.; Guo, H. M.; James, T. D.; Zhao, J. Z. *Chem.-Eur. J.* **2012**, *18*, 4953. (e) Wu, W. H.; Zhao, J. Z.; Guo, H. M.; Sun, J. F.; Ji, S. M.; Wang, Z. L. *Chem.-Eur. J.* **2012**, *18*, 1961. (f) Guo, H. M.; Li, Q. T.; Ma, L. H.; Zhao, J. Z. *J. Mater. Chem.* **2012**, *22*, 15757. (g) Yi, X. Y.; Zhao, J. Z.; Wu, W. H.; Huang, D. D.; Ji, S. M.; Sun, J. F. *Dalton T.* **2012**, *41*, 8931. (h) Li, Q. T.; Guo, H. M.; Ma, L. H.; Wu, W. H.; Liu, Y. F.; Zhao, J. Z. *J. Mater. Chem.* **2012**, *22*, 5319. (i) Zhao, J. Z.; Ji, S. M.; Wu, W. H.; Wu, W. T.; Guo, H. M.; Sun, J. F.; Sun, H. Y.; Liu, Y. F.; Li, Q. T.; Huang, L. *RSC Adv.* **2012**, *2*, 1712. (j) Liu, Y. F.; Li, Q. T.; Zhao, J. Z.; Guo, H. M. *RSC Adv.* **2012**, *2*, 1061. (k) Wu, W. T.; Guo, H. M.; Wu, W. H.; Ji, S. M.; Zhao, J. Z. *Inorg. Chem.* **2011**, *50*, 11446. (l) Huang, L.; Zeng, L.; Guo, H. M.; Wu, W. H.; Wu, W. T.; Ji, S. M.; Zhao, J. Z. *Eur. J. Inorg. Chem.* **2011**, 4527. (m) Sun, J. F.; Wu, W. H.; Guo, H. M.; Zhao, J. Z. *Eur. J. Inorg. Chem.* **2011**, 3165. (n) Ji, S. M.; Guo, H. M.; Wu, W. T.; Wu, W. H.; Zhao, J. Z. *Angew. Chem. Int. Edit.*

2011, *50*, 8283. (o) Wu, W. T.; Wu, W. H.; Ji, S. M.; Guo, H. M.; Zhao, J. Z. *Dalton T.* **2011**, *40*, 5953. (p) Wu, W. H.; Sun, J. F.; Ji, S. M.; Wu, W. T.; Zhao, J. Z.; Guo, H. M. *Dalton T.* **2011**, *40*, 11550.

(81) (a) Sun, J. F.; Wu, W. H.; Guo, H. M.; Zhao, J. Z. *Eur. J. Inorg. Chem.* **2011**, 3165. (b) Ji, S. M.; Guo, H. M.; Wu, W. T.; Wu, W. H.; Zhao, J. Z. *Angew. Chem. Int. Edit.* **2011**, *50*, 8283. (c) Ji, S. M.; Wu, W. H.; Wu, W. T.; Guo, H. M.; Zhao, J. Z. *Angew. Chem. Int. Edit.* **2011**, *50*, 1626. (d) Liu, Y.; Wu, W.; Zhao, J.; Zhang, X.; Guo, H. *Dalton T.* **2011**, *40*, 9085.

(82) Murakami, Y. *Chem. Phys. Lett.* **2011**, *516*, 56.

(83) Lissau, J. S.; Gardner, J. M.; Morandeira, A. *J. Phys. Chem. C* **2011**, *115*, 23226.

(84) (a) El-Khouly, M. E.; Ito, O.; Smith, P. M.; D'Souza, F. *J. Photochem. Photobiol., C* **2004**, *5*, 79. (b) Boyd, P. D. W.; Reed, C. A. *Acc. Chem. Res.* **2005**, *38*, 235. (c) D'Souza, F.; Ito, O. *Coord. Chem. Rev.* **2005**, *249*, 1410. (d) Thomas, K. G.; George, M. V.; Kamat, P. V. *Helv. Chim. Acta* **2005**, *88*, 1291. (e) Tashiro, K.; Aida, T. *Chem. Soc. Rev.* **2007**, *36*, 189. (f) Drain, C. M.; Varotto, A.; Radivojevic, I. *Chem. Rev.* **2009**, *109*, 1630. (g) Beletskaya, I.; Tyurin, V. S.; Tsivadze, A. Y.; Guilard, R.; Stern, C. *Chem. Rev.* **2009**, *109*, 1659. (h) Accorsi, G.; Armaroli, N. *J. Phys. Chem. C* **2010**, *114*, 1385. (i) Grimm, B.; Hausmann, A.; Khant, A.; Seitz, W.; Spänig, F.; Guldi, D. M. *Handbook of Porphyrin Science, Vol. 1, Supramolecular Chemistry*; World Scientific: Singapore, 2010. (j) D'Souza, F.; Ito, O. *Handbook of Porphyrin Science, Vol. 1, Supramolecular Chemistry*; World Scientific: Singapore, 2010.

(85) (a) Bell, T. D. M.; Ghiggino, K. P.; Jolliffe, K. A.; Ranasinghe, M. G.; Langford, S. J.; Shephard, M. J.; Paddon-Row, M. N. *J. Phys. Chem. A* **2002**, *106*, 10079. (b) Milanesio, M. E.; Gervaldo, M.; Otero, L. A.; Sereno, L.; Silber, J. J.; Durantini, E. N. *J. Phys. Org. Chem.* **2002**, *15*, 844. (c) Vail, S. A.; Tome, J. P. C.; Krawczuk, P. J.; Dourandin, A.; Shafirovich, V.; Cavaleiro, J. A. S.; Schuster, D. I. *J. Phys. Org. Chem.* **2004**, *17*, 814. (d) Imahori, H. *Org. Biomol. Chem.* **2004**, *2*, 1425. (e) Nierengarten, J.-F. *New J. Chem.* **2004**, *28*, 1177. (f) Günes, S.; Neugebauer, H.; Sariciftci, N. S. *Chem. Rev.* **2007**, *107*, 1324. (g) Imahori, H.; Umeyama, T. *J. Phys. Chem. C* **2009**, *113*, 9029. (h) Megiatto, J. D.; Schuster, D. I.; Abwandner, S.; de, M. G.; Guldi, D. M. *J. Am. Chem. Soc.* **2010**, *132*, 3847. (i) Pal, S. K.; Kesti, T.; Maiti, M.; Zhang, F.; Inganaas, O.; Hellstroem, S.; Andersson, M. R.; Oswald, F.; Langa, F.; Oesterman, T.; Pascher, T.; Yartsev, A.; Sundstroem, V. *J. Am. Chem. Soc.* **2010**, *132*, 12440.

(86) (a) Liao, M.-S.; Watts, J. D.; Huang, M.-J. *Phys. Chem. Chem. Phys.* **2009**, *11*, 4365. (b) Liao, M.-S.; Watts, J. D.; Huang, M.-J. *J. Phys. Chem. B* **2007**, *111*, 4374.

(87) (a) Guldi, D. M. *Chem. Soc. Rev.* **2002**, *31*, 22. (b) Sun, D. Y.; Tham, F. S.; Reed, C. A.; Chaker, L.; Boyd, P. D. W. *J. Am. Chem. Soc.* **2002**, *124*, 6604. (c) Takai, A.; Chkounda, M.; Eggenspiller, A.; Gros, C. P.; Lachkar, M.; Barbe, J. M.; Fukuzumi, S. *J. Am. Chem. Soc.* **2010**, *132*, 4477. (d) Ayabe, M.; Ikeda, A.; Kubo, Y.; Takeuchi, M.; Shinkai, S. *Angew. Chem. Int. Edit.* **2002**, *41*, 2790.

(88) Hasobe, T.; Sandanayaka, A. S. D.; Wada, T.; Araki, Y. *Chem. Commun.* **2008**, 3372.

(89) Guldi, D. M.; Illescas, B. M.; Atienza, C. M.; Wielopolskia, M.; Martin, N. *Chem. Soc. Rev.* **2009**, *38*, 1587.

(90) (a) Wessendorf, F.; Gnichwitz, J. F.; Sarova, G. H.; Hager, K.; Hartnagel, U.; Guldi, D. M.; Hirsch, A. *J. Am. Chem. Soc.* **2007**, *129*, 16057. (b) Gnichwitz, J. F.; Wielopolski, M.; Hartnagel, K.; Hartnagel, U.; Guldi, D. M.; Hirsch, A. *J. Am. Chem. Soc*. **2008**, *130*, 8491. (c) Wessendorf, F.; Grimm, B.; Guldi, D. M.; Hirsch, A. *J. Am. Chem. Soc.* **2010**, *132*, 10786. (d) Maurer, K.; Grimm, B.; Wessendorf, F.; Hartnagel, K.; Guldi, D. M.; Hirsch, A. *Eur. J. Org. Chem*. **2010**, 5010.

(91) Martin, N.; Sanchez, L.; Illescas, B.; Perez, I. *Chem. Rev.* **1998**, *98*, 2527.

(92) D'Souza, F.; Chitta, R.; Gadde, S.; Zandler, M. E.; Sandanayaka, A. S. D.; Araki, Y.; Ito, O. *Chem. Commun.* **2005**, 1279.

(93) (a) El-Khouly, M. E.; Fujitsuka, M.; Ito, O. *J. Porphyr. Phthalocya*. **2000**, *4*, 590. (b) Nojiri, T.; Watanabe, A.; Ito, O. *J. Phys. Chem. A* **1998**, *102*, 5215.

(94) Kesti, T.; Tkachenko, N.; Yamada, H.; Imahori, H.; Fukuzumi, S.; Lemmetyinen, H. *Photochem. Photobiol. Sci.* **2003**, *2*, 251.

(95) Maciejewski, A.; Steer, R. P. *Chem. Rev.* **1993**, *93*, 67.

(96) (a) Yeow, E. K. L.; Ziolek, M.; Karolczak, J.; Shevyakov, S. V.; Asato, A. E.; Maciejewski, A.; Steer, R. P. *J. Phys. Chem. A* **2004**, *108*, 10980. (b) Yeow, E. K. L.; Steer, R. P. *Phys. Chem. Chem. Phys.* **2003**, *5*, 97. (c) Yeow, E. K. L.; Steer,

R. P. *Chem. Phys. Lett.* **2003**, *377*, 391. (d) Tetreault, N.; Muthyala, R. S.; Liu, R. S. H.; Steer, R. P. *J. Phys. Chem. A* **1999**, *103*, 2524.

(97) Tripathy, U.; Steer, R. P. *J. Porphyr. Phthalocya.* **2007**, *11*, 228.

(98) Lukaszewicz, A.; Karolczak, J.; Kowalska, D.; Maciejewski, A.; Ziolek, M.; Steer, R. P. *Chem. Phys.* **2007**, *331*, 359.

(99) Sorgues, S.; Poisson, L.; Raffael, K.; Krim, L.; Soep, B.; Shafizadeh, N. *J. Chem. Phys.* **2006**, *124*.

(100) (a) Fueno, H.; Takenaka, Y.; Tanaka, K. *Opt. Spectrosc.* **2011**, *111*, 248. (b) Iehl, J.; Vartanian, M.; Holler, M.; Nierengarten, J. F.; Delavaux-Nicot, B.; Strub, J. M.; Van Dorsselaer, A.; Wu, Y. L.; Mohanraj, J.; Yoosaf, K.; Armaroli, N. *J. Mater. Chem.* **2011**, *21*, 1562. (c) Biczok, L.; Linschitz, H.; Walter, R. I. *Chem. Phys. Lett.* **1992**, *195*, 339. (d) Taliani, C.; Ruani, G.; Zamboni, R.; Danieli, R.; Rossini, S.; Denisov, V. N.; Burlakov, V. M.; Negri, F.; Orlandi, G.; Zerbetto, F. *J. Chem. Soc.-Chem. Commun.* **1993**, 220. (e) Foote, C. S. *Electron Transfer I* **1994**, *169*, 347. (f) Lambert, C.; Redmond, R. W. *Chem. Phys. Lett.* **1994**, *228*, 495.

(101) Fraelich, M. R.; Weisman, R. B. *J. Phys. Chem.* **1993**, *97*, 11145.

(102) Wu, W. H.; Zhao, J. Z.; Sun, J. F.; Guo, S. *J. Org. Chem.* **2012**, *77*, 5305.

(103) Fujitsuka, M.; Ito, O. In *Encyclopedia of Nanoscience and Nanotechnology*; Nalwa, H. S., Ed., 2004; Vol. 8.

Chapter 2: Experimental Methods

2.1 Materials used and sample preparation

Low chlorin zinc (II) *meso*-tetraphenylporphine (ZnTPP), the model porphyrin used in our studies, the fullerene C_{60} (99.9% purity) and the blue emitting molecules perylene (P) (≥99.5% purity) and coumarin 343 (C343) (97% purity) were purchased from Sigma-Aldrich. Another blue emitting molecule, anthanthrene (An) (high purity, checked by GC/MS) was purchased from Accustandard. The steady state absorption and fluorescence spectra of these molecules in solution closely resembled the spectra reported previously[1] and showed that the samples were free of measurable impurities in the spectral range of interest. The polymers used in the oxygen diffusion studies, poly(ethyl methacrylate) (PEMA; average molecular weight ~ 515000 Da by gel permeation chromatogarphy) and poly(vinyl alcohol) (PVA; 99.7 mol% hydrolyzed, average molecular weight ~ 78000 Da) were purchased from Sigma-Aldrich and Polysciences respectively. The chemical structures of these compounds are shown in scheme 2.1. The solvents used in these studies, namely, benzene, toluene, pyridine, acetonitrile, dimethyl formamide (DMF) and benzonitrile were of HPLC grade (≥99.9%) and were purchased from Sigma-Aldrich. All these chemicals and solvents were used as received without any further purification procedures as they showed no indication of any fluorescent impurities. In most cases, the solvents were dried using appropriate molecular sieves. Sample preparations involving pyridine and DMF were carried out in a dry nitrogen environment in a glove box to avoid

any possible moisture contamination from the atmosphere. Ultrapure Millipore water (18 MΩ·cm) was used whenever required to make water based polymer films of PVA. Unless otherwise noted, experiments were carried out in aerated solutions.

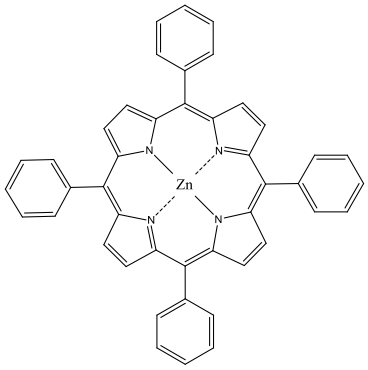

Zinc (II) *meso*-tetraphenylporphine (ZnTPP)

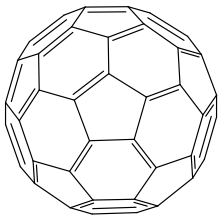

Fullerene (C_{60})

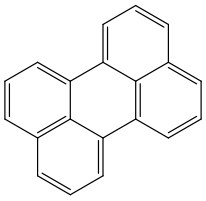

Perylene (P)

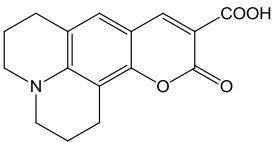

Coumarin 343 (C343)

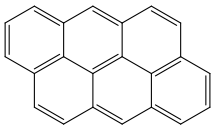

Anthanthrene (An)

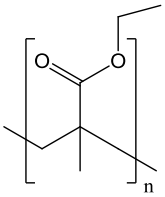

Poly(ethyl methacrylate) (PEMA)

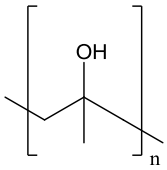

Poly(vinyl alcohol) (PVA)

Scheme 2.1 Chemical structures of the compounds studied in this thesis.

Solution samples for TTA experiments involving ZnTPP, P and C343 were subjected to degassing by at least four freeze-pump-thaw cycles on a grease-free high vacuum line. A custom made triangular or rectangular vacuum cuvette which can be attached to the side arm of a round bottom glass flask containing the sample was used. Once the sample

was completely degassed, it was thawed and transferred immediately from the round bottom flask to the vacuum cuvette, which was sealed under vacuum. Samples for triplet-triplet energy transfer measurements involving ZnTPP and C_{60} and for TTA associated energy transfer measurements involving C_{60} and P and An were initially subjected for purging with ultrahigh purity nitrogen for at least 45 minutes. The sample vial was then immediately placed in a dry nitrogen atmosphere in a glove box, then immediately transferred into a round bottom flask and attached to the vacuum cuvette. This sample was then degassed by subjecting it to at least ten freeze-pump-thaw cycles. For studying the photophysics of self-assembled mixtures of ZnTPP and C_{60} (*vide infra*), all the measurements were carried in air saturated toluene or benzonitrile solutions.

For oxygen diffusion measurements in thin polymer films, PEMA was chosen as the host polymer for ZnTPP in the sensor film because of the greater oxygen permeability of PEMA compared to the test polymer PVA.[2] PVA was selected as the test polymer film primarily because ZnTPP is insoluble in the water soluble polymer PVA. Any other attempts to use an organic soluble polymer as the test layer resulted in the dissolution and migration of ZnTPP from the sensor layer to the test layer.

The samples were prepared according to the following procedure. First, the sensor films were prepared by spin casting (800 rpm) 40 aliquots of a solution containing a mixture of 4.0 mM ZnTPP and 2.0% (w/v) PEMA in toluene sequentially onto thoroughly precleaned 1.2 mm thick glass slides (VWR). Approximately 50 μL of solution was used for each layer. The total absorbance of the resultant test film did not

scale exactly with the number of layers deposited, even though a linear relation was obtained for the total absorbance *versus* the number of layers (See appendix A.5.1). In addition, the total thickness of the resultant sensor layer was lesser than the sum of the thickness of the individual layers of ZnTPP and PEMA. This suggests that some dissolution and loss of ZnTPP occurred during the spin casting process. Thin films of PVA on the top of the sensor layer were prepared by spin casting (1000 rpm) aliquots of 100 μL per layer of PVA in Millipore water onto the sensor film.

2.2 Ellipsometry

The thickness of the PVA polymer test films for oxygen diffusion measurements was measured using an LSE Stokes ellipsometer from Gaertner Scientific Corporation. In ellipsometry measurements, the polarization state of plane polarized light reflected or transmitted from a sample surface is measured. A schematic illustration of a LSE Stokes ellipsometer is shown in Fig. 2.1.[3]

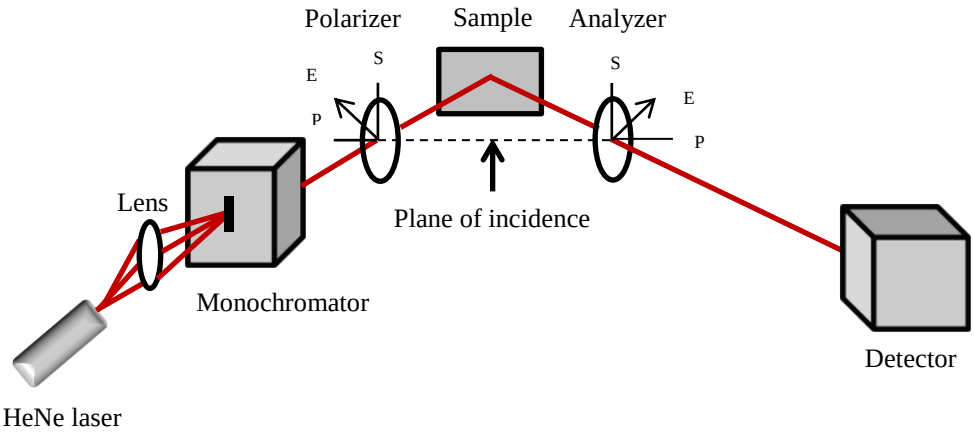

Fig. 2.1 Schematic diagram of an ellispometer working in the reflection-polarization mode.

In brief, a 632.8 nm HeNe laser beam having 1 mm diameter was passed through a polarizer to make it linearly polarized and directed onto the sample surface. Depending on the sample refractive index and its thickness, the light that is reflected from the surface of the sample will be in a different polarization state compared to the polarization of the incident light. This light was then passed through an analyzer and into a photodetector. In case of the ellipsometer used here, the light was partially reflected from four successive photodetectors at oblique angles of incidence and hits a fifth, final photodetector which is completely absorptive. Each of the photodetectors generates electric signals which are proportional to the fraction of the light it absorbs. Light which has a plane of polarization in the plane of incidence is called p-polarized light and the light which has a perpendicular plane of polarization with respect to the plane of incidence is called s-polarized light. The mathematical expression for Fresnel type reflection or transmission ellipsometric measurements is derived from Maxwell's relations and is given as a ratio of the normalized Fresnel coefficients of the reflected or transmitted p- and s-polarized light (r_p and r_s respectively),[4]

$$\rho = \frac{r_p}{r_s} = \tan(\Psi) \, . \, e^{i\Delta} \qquad (2.1)$$

where tan(Ψ) is the amplitude ratio of the reflected light and Δ is the relative phase shift of the amplitudes along the s and p planes.

For an isotropic single layer thin film of thickness d, the Fresnel coefficients are given by the Airy formula,[3]

$$r_{p,s} = \frac{r_{1,p,s} + r_{2,p,s}\mathrm{e}^{-2ib}}{1 + r_{1,p,s}r_{2,p,s}\mathrm{e}^{-2ib}} \qquad (2.2)$$

where the factor b is related to the thickness d of the film by the equation,

$$b = \frac{2\pi dn\cos\phi}{\lambda} \qquad (2.3)$$

where r_1 and r_2 represent the Fresnel coefficients for interfaces 1 and 2, n is the complex refractive index of the sample, ϕ is the angle of incidence determined by Snell's law and λ is the wavelength of the light used. For multiple isotropic layers of films, these calculations are usually represented using matrix methods.

2.3 Steady state spectroscopic techniques

2.3.1 UV-visible absorption spectroscopy

Steady state absorption spectroscopy was carried out using either a Varian-Cary 500 or a 6000i spectrophotometer in dual beam mode. The scans were done usually at a step size of 1 nm at a band pass of 2.0 nm. For more sensitive measurements, a step size of 0.1 nm and a band pass of 0.1 nm were employed. Measurements were usually taken with samples in a 2 mm × 10 mm cuvettes with light passing through the 2 mm path. For measurements involving highly concentrated samples, cuvettes having a dimension of 1 mm × 10 mm or 0.5 mm × 10 mm cuvettes were used with the light propagating along the short path of the cuvette in order to keep the absorbance in the linear range of the detector sensitivity. For sensitive measurements in the Q-band region of solutions of low

concentrations of porphyrin, 4 mm × 10 mm or 10 mm × 10 mm cuvettes were used. For most of the absorption measurements, a similar cuvette containing the pure solvent was used as the reference. For binary mixture solutions such as those containing ZnTPP and C_{60}, a cuvette containing the same concentration of C_{60} in the same solvent was used as a reference. When the absorption measurements were carried out for films of ZnTPP dissolved in a polymer on a glass substrate, pure polymer film having a similar thickness as the sample film on a similar glass substrate was used as the reference.

2.3.2 Steady-state fluorescence emission spectroscopy

Steady-state fluorescence emission measurements were performed using either a Jobin-Yvon Spex Fluorolog spectrophotometer or a PTI Quantamaster spectrofluorimeter, both equipped with double monochromators on both the excitation and emission sides. A schematic diagram of the PTI Quantamaster spectrofluorimeter is shown in Fig. 2.2. In normal fluorescence emission measurements, the excitation source used was a Xenon arc lamp. The continuous light produced from the lamp is passed through an excitation monochromator which can be computer controlled to select the desired wavelength of excitation. A calibrated photodiode on the excitation side was used to collect a small fraction of the excitation light prior to sample excitation to correct for the dependence of the excitation light intensity on the wavelength. The light was then passed through the sample and the fluorescence emission was collected at a 90 degree angle with respect to the excitation beam (rectangular geometry). The emission light was then passed through a computer-controlled emission monochromator and finally detected

using a photomultiplier tube (PMT) detector. A correction file supplied by the manufacturer was used for correcting the fall off in the efficiency of the photodetector towards longer wavelengths. Normally the slit width used on the excitation side was 2 nm, but variable slits were used on the emission side according to the requirements of the experiments. Whenever different slit widths were used for the measurements, if required, corrections were made to account for the nonlinear dependence of the fluorescence intensity on the slit widths.

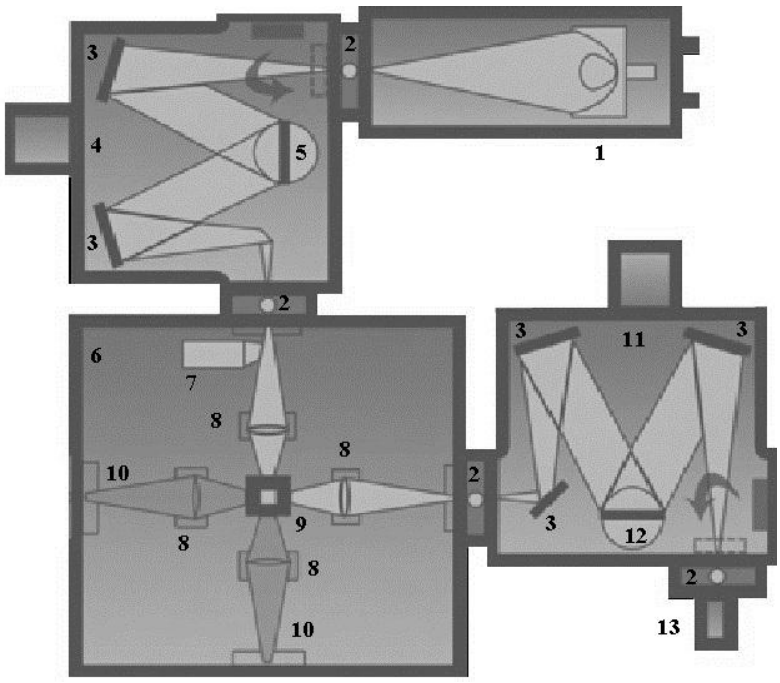

Fig. 2.2 Schematic set up of a PTI Quantamaster™ spectrofluorimeter adapted from the reference manual of Quantamaster™ 30 spectrofluorimeter.[5] The optical and mechanical components of the spectrofluorimeter are listed as follows. 1. Xenon lamp housing, 2. Adjustable slits, 3. Mirrors, 4. Excitation Monochromator, 5. Excitation grating, 6. Sample compartment, 7. Excitation correction, 8. Focusing lens, 9. Sample holder, 10. External excitation source such as an Nd:YAG laser, 11. Emission Monochromator, 12. Emission grating and 13. Photodetector.

In order to perform triplet-triplet annihilation measurements, an external excitation source such as low power frequency doubled 532 nm (TEM_{00}) Nd:YAG laser (WSTech, TECGL-30) was used. Whenever necessary, a 10-step calibrated neutral density filter from Edmund Optics was used to attenuate the power of the incident laser. The total power density ($W.cm^{-2}$) of the laser transmitted through the neutral density filter was calculated by measuring laser power and the 1/e spot size from the divergence of the laser beam. A 532 nm notch filter was placed in the emission path before the monochromator to attenuate the scattered excitation light.

Measurements involving air saturated solutions were usually carried out using 2 mm × 10 mm quartz cuvettes with the sample being excited along the long path of the cuvette whereas the fluorescence emission was collected along the short path for minimizing the effects due to secondary inner filter effects (*vide infra*). In order to minimize the effects of reabsorption by the sample itself, sample solutions of low concentration were used whenever possible. TTA measurements were usually carried out by either (i) exciting at the front face of a sealed triangular evacuable cell containing the degassed sample solution and collecting the emission from the front face at an angle ~ 30^0 with respect to the excitation beam to reduce the effect re-absorption, or (ii) in rectangular geometry for samples in rectangular vacuum cells where the emission was collected at 90^0 with respect to the excitation beam.

For oxygen diffusion measurements, the samples were prepared as described in the sample preparation section and the polymer-coated glass slides were mounted as

windows on the front side of an evacuated triangular brass cell in such a way that the sample film is facing towards the inner side of the evacuated cell. By connecting the brass cell to a grease-free glass vacuum line, the sample film was allowed to outgas for at least an hour prior to any measurements.

A mechanical beam shutter from (Edmund Optics) was used in front of the graded neutral density filter to chop the 532 nm Nd:YAG laser every 30 s to minimize any photochemical damage which could occur to the sample from prolonged exposure to the laser light. The sample was excited at less than the critical angle of incidence of ~30^0 to minimize scattering and to avoid total reflection of the excitation beam, and the emission was collected in front-face geometry. The typical power density of the incident 532 nm laser excitation beam was 0.38 $W.cm^{-2}$. The sample was subjected to continuous irradiation with the 532 nm laser prior to any measurements until a stable emission intensity was achieved at the Soret emission maximum of ZnTPP (~435 nm) as a function of time. The porphyrin S_2 emission intensity was found to be reduced slightly during this procedure, most probably because of photo-oxidation of ZnTPP by residual oxygen in the sensor layer and due to the slight outgassing of water vapor because of the mild thermal heating by the incident laser. A pre-evacuated glass gas mixing chamber was attached to the vacuum line. Different pre-defined proportions of dry N_2 and O_2 gases were mixed together in this mixing chamber by gentle heating and were exposed to the degassed sample film at time t = 0 s. The total pressure of both N_2 and O_2 was kept constant and slightly below 1 atm pressure. The S_2 fluorescence decay induced by the quenching of the triplet states of ZnTPP by oxygen was monitored as a function of time until the

fluorescence intensity reached a steady value. Continuous outgassing of the sample after the measurements usually brought the S_2 fluorescence intensity back to within a few percent of the initial fluorescence intensity.

2.3.2.1 Corrections for primary and secondary inner filter effects and competitive absorption

In order to obtain an error-free fluorescence emission spectrum, the raw spectrum must be corrected for both primary and secondary inner filter effects. First, any signal from the solvent, which could be due to Raman scattering or any impurity emission has to be corrected and subtracted from the sample solution emission spectrum. Second, corrections to account for the reabsorption of fluorescence by the sample itself have to be performed. Reabsorption effects become significant when there is a considerable overlap between the sample absorption spectrum and the emission spectrum which is particularly severe in the allowed Soret band region of porphyrins. Third, for fluorescence measurements involving binary or higher mixtures of fluorophores, efforts should be made to correct for the reduced fluorescence intensity due to both competitive absorption at the excitation wavelength and competitive reabsorption at the emission wavelength by molecules other than the emitting species of interest.

Whenever a rectangular cuvette was used to take the spectra in right angle geometry, corrections to the fluorescence spectra were made using the correction factors described by Liu et al.[6] First, the background solvent emission spectrum was corrected for the reduced incident intensity at the excitation wavelength by multiplying by the correction

factor, $F = (1\text{-}10^{-A_{exc}})/2.303A_{exc}$, where A_{ex} is the absorbance of the sample in the same solvent at the excitation wavelength. Care was taken to scale the absorption values properly whenever the light path length for the absorption measurements was different from the excitation beam penetration length for the emission measurements. This corrected background spectrum was then subtracted from the sample emission spectrum to get the spectrum $F_0(\bar{\nu})$. Then, the following correction factor was used to correct for the primary and secondary inner filter effects;

$$F_{corr}(\bar{\nu}) = F_0(\bar{\nu}) \times 10^{(A_{ex}l_{ex}+A_{em}l_{em})} \quad (2.4)$$

where $F_{corr}(\bar{\nu})$ is the corrected fluorescence intensity, A_{ex} is the absorbance at the excitation wavelength, l_{ex} is the penetration depth of the light into the sample, A_{em} is the absorbance over the emission wavelength and l_{em} is the emission path length. Following the report by Liu et al., l_{ex} = 0.44 cm and l_{em} = 0.05 cm were used for experiments using a 2 × 10 mm cuvette in a Spex fluorolog spectrofluorimeter. For the experiments using PTI Quantamaster spectrofluorometer, l_{ex} = 0.40 cm and l_{em} = 0.1 cm were used.[6]

In the case of the fluorescence measurements involving solutions containing two fluorophores a and b, the equation will take the form,

$$F_{corr}(\bar{\nu}) = F_0(\bar{\nu}) \times 10^{\{(A_{ex(a)}+A_{exc(b)})l_{ex}+(A_{em(a)}+A_{em(b)})l_{em}\}} \quad (2.5)$$

where A_{em} is the absorbance over the emission wavelength range, l_{ex} is the excitation penetration distance into the sample and l_{em} is the emission path length. Values of l_{ex} = 0.40 cm and l_{em} = 0.10 cm were used.

For front-face measurements involving triangular cuvettes illustrated in Fig. 2.3, a different correction procedure reported by Lopez[7] was used.

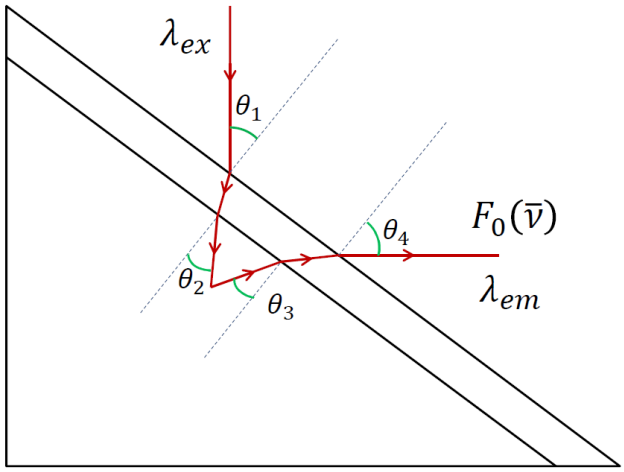

Fig. 2.3 Definitions of angles used in front-face illumination, triangular cell reabsorption correction.

In practice, $\theta_1 + \theta_2 = 45°$ for front-face illumination in the fluorimeter used. The corrected fluorescence intensity, *F*, is obtained from the measured fluorescence intensity, F_0, using the expression:

$$F_{corr}(\bar{\nu}) = F_0(\bar{\nu}) \times \left[\frac{\{\varepsilon_{ex}+\varepsilon(\bar{\nu})z\}}{\varepsilon_{ex}}\right] \times \left[\frac{1-\exp(-2.3\varepsilon_{ex}cl/\cos\theta_2}{1-\exp(-2.3(\varepsilon_{ex}+\varepsilon(\bar{\nu})z)cl/\cos\theta_2}\right] \times \left[\frac{\cos\theta_4}{n(n^2-\sin^2\theta_4)^{1/2}}\right] \quad (2.6)$$

Here the second and third terms in square brackets account for the absorption by ground state aggregates, ε_{ex} is the molar extinction coefficient at the excitation wavelength, $\varepsilon(\bar{\nu})$ is the molar extinction coefficient at wavenumber $\bar{\nu}$, $z = \cos\theta_2/\cos\theta_3$, where θ_2 and θ_3 are defined in the figure, *c* is the concentration of the sample, and *l* is the

penetration depth of the excitation beam into the sample. The fourth term in the equation takes into account the differences in the refractive indices when the excitation beam enters the sample from air. Here, θ_4 is again depicted in the figure and *n* is the refractive index of the solvent used for the sample.

Finally, for a binary mixture of a fluorophore (e.g. ZnTPP) with another molecule (e.g. C_{60}), corrections to account for competitive absorption and competitive reabsorption must be made if the added molecule absorbs at the excitation wavelength and/or the emission wavelength of the emitting molecule. The correction factor is given by the mathematical expression,

$$F_{corr}(\bar{\nu}) = F(\bar{\nu})\left(\frac{1-e^{-\varepsilon_{ex(a)}c_{ex(a)}l_{ex}}}{\varepsilon_{ex(a)}c_{ex(a)}}\right)\left(\frac{\varepsilon_{ex(a)}c_{ex(a)}+\varepsilon_{ex(b)}c_{ex(b)}}{1-e^{-(\varepsilon_{ex(a)}c_{ex(a)}+\varepsilon_{ex(a)}c_{ex(b)})l_{ex}}}\right)\left(\frac{\varepsilon_{em(b)}c_{em(b)}l_{em}}{1-e^{-(\varepsilon_{em(b)}c_{ex(b)})l_{em}}}\right) \quad (2.7)$$

where $\varepsilon_{ex(a)}$, $c_{ex(a)}$ and $\varepsilon_{ex(b)}$, $c_{ex(b)}$ are the molar extinction coefficients and concentrations of the components a (ZnTPP) and b (C_{60}) at the excitation wavelength (400 nm for the Soret band or 550 nm for the Q band), respectively, $\varepsilon_{em(b)}$, $c_{em(b)}$ are the molar extinction coefficient and concentration of C_{60} in the emission wavelength range (410 nm – 500 nm for the Soret band or 570 nm – 750 nm for the Q band) and l_{ex} and l_{em} are the excitation and emission path length respectively. Values of l_{ex} = 0.40 cm and l_{em} = 0.10 cm were used.

2.4 Time-resolved transient absorption spectroscopic techniques

Transient absorption data can provide detailed description of the excited state properties of molecules, even for those that are weakly fluorescent or weakly phosphorescent. In general, the molecules in the electronic ground state are excited to a higher energy electronic state using a pump pulse. Then, the absorption properties of the transient species are probed with a continuum light source called the probe light. These transient absorption data can give information about the excited state electronic properties, solvation environment around the excited molecule, electron transfer or energy transfer from the excited molecule, excited state quenching kinetics, etc.

2.4.1 Laser flash photolysis

An LP920 laser flash photolysis (LFP) spectrometer from Edinburgh Instruments was used to measure the triplet-triplet transient absorption kinetics and triplet decay of the molecules investigated in this thesis. The basic optical outline of the LFP instrument is shown in Fig 2.4.

In brief, a flash lamp-pumped, Q-switched Tempest 300 Nd:YAG laser capable of producing ~ 3-5 ns pulses, operating at a frequency of 10 Hz and a beam diameter of ~ 6 mm was used as the excitation source. Either the second harmonic wavelength, 532 nm (180 mJ) or the third harmonic wavelength, 355 nm (70 mJ) were used for exciting the samples. The initial laser intensity was cut off to ~ 40% and was defocussed slightly using a plano-concave lens (focal length ~ -13 mm, Edmund optics) to reduce the

incident laser power on the sample cell. The typical power on density delivered to the sample cell was 0.34 W/cm^2 (19 mJ / pulse).

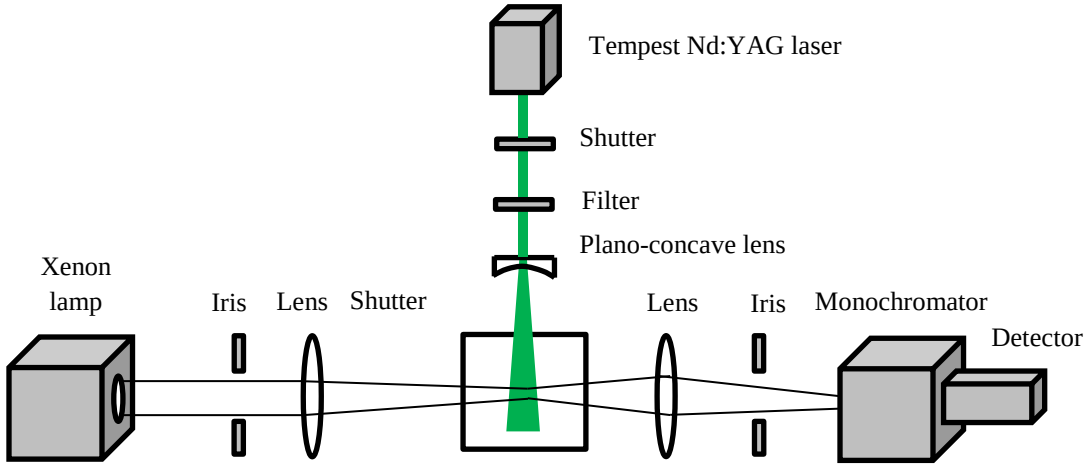

Fig 2.4 Generic optical layout of the laser flash photolysis setup.

The absorption spectrum and the time-dependent absorption kinetics of the transients formed upon excitation with the laser pulse were probed using a 450 W Xenon arc lamp (Xe920) producing either continuous or pulsed (pulse duration ~ 0.5 – 10 ms, repetition rate ~ 10 Hz) light in the spectral range of 190 – 2600 nm. The excitation beam and the probe beam cross each other at 90^0 in a 10 mm × 10 mm quartz cuvette containing the sample. The transmitted light was then focused onto a Czerny-Turner monochromator (TMS300) and finally detected using either a LP900 photomultiplier. This detector was used for taking spectra at single wavelength the spectral range 185 to 870 nm, and was supplemented by a Princeton PI-MAX ICCD camera which has a spectral detection range of 180 to 850 nm. A digital phosphor oscilloscope (Tektronix TDS3032C, 300 MHz

bandwidth) was used to record the real time signal from the detector. The time resolution of the instrument is *ca*. 7 ns. The measurements could be carried out either in the kinetic mode or the spectral mode. The data acquisition is facilitated using L900 software supplied by Edinburgh instruments.

2.4.1.1 The kinetics of flash photolysis measurements

The absorption of the transient species, namely the optical density (ΔOD), is recorded as a ratio of the incident light intensity to the transmitted light during and shortly after the formation of the transient molecules, T.

$$\Delta OD(t,\lambda) = \log\frac{I_0}{I_t(t,\lambda)} \qquad (2.8)$$

For a pure triplet-triplet transient absorption, ΔOD would take the form of the famous Beer-Lambert's law,

$$\Delta OD(t,\lambda) = \varepsilon_T(\lambda)C_T(t)l \qquad (2.9)$$

where l is the path length the probe light travels, ε_T is the molar extinction coefficient and C_T is the concentration of the triplet species absorbing the probe light.

For a first order transient decay kinetics having a rate equation,

$$\frac{-\mathrm{d}[T]}{\mathrm{dt}} = k_1[T] \qquad (2.10)$$

the change in the optical density is given by the equation,

$$\Delta OD(t) = \Delta OD_0 \mathrm{e}^{-k_1 t} \qquad (2.11)$$

where k_1 is the first order rate constant.

If the triplet transient is quenched by a relatively large concentration of a quencher, the quenching process is assumed to follow pseudo-first order decay, for which the rate equation is given by,

$$\frac{-\mathrm{d}[T]}{\mathrm{dt}} = k_1[T] + k_q[T][Q] \qquad (2.12)$$

where k_q is the bimolecular quenching rate constant and [Q] is the concentration of the quencher.

The pseudo-first order rate constant is given by,

$$k_2 = k_1 + k_q[Q] \qquad (2.13)$$

For bimolecular processes involving transients to take part in TTA, the rate equation is given by,

$$\frac{-\mathrm{d}[T]}{\mathrm{dt}} = k_1[T] + k_{TTA}[T]^2 \qquad (2.14)$$

where k_{TTA} is the bimolecular triplet-triplet annihilation rate constant.

For such a second order process, the change in optical density is calculated according to the equation,

$$\Delta OD(t) = \frac{\Delta OD_0}{(1 + k_2 t)} \mathrm{e}^{-k_1 t} \qquad (2.15)$$

where $k_2 = C_0 . k_{TTA}$ and C_0 is the initial triplet concentration.

2.4.1.2 Data analysis for Flash photolysis measurements

The kinetic absorption data obtained from flash photolysis is usually analyzed by fitting to exponential functions and extracting the rate constants.

$$R(t) = A + \sum_{i=1}^{4} B_i \mathrm{e}^{-t/\tau_i} \qquad (2.16)$$

where A is the amplitude, B is the pre-exponential factor and τ is the lifetime constant.

The factors, B and τ are usually extracted by fitting the raw data to equation 2.16 using a Marquardt-Levenberg iterative algorithm by minimizing the "goodness of the fit" factor, the reduced Chi-square. The reduced chi-square is given by,

$$\chi^2 = \sum_k W_k^2 \frac{[S_k - F_k]^2}{[n_2 - n_1 + 1 - P]} \qquad (2.17)$$

where W_k are the weighting factors for the individual raw data points, S_k are the fitting data, F_k are the experimental data points, n_1 and n_2 are the first and last number of channels of the region selected for fitting and P is the number variables in the fitting equation. For data which follows a Poisson-type distribution, the weighting factor is given by the expression, $W_k = 1/\sqrt{F_k}$. This results in the constraint that the value of reduced chi-square should be 1.0. However, in practice, reduced chi-square values up to

1.3 are acceptable. For LFP measurements, the data noise usually follows Gaussian noise statistics with a constant value of W_k rather than following the Poissonian statistics. This results in lesser reliability of the reduced chi-square for Gaussian data distribution compared to that for Poissonian data statistics.

The visual inspection of the quality of the fit is usually done by plotting the distribution of the weighted residuals, which is the difference between the fitted data and the experimental data weighted by the standard deviation of each data point. The residuals are given by the equation,

$$X_k = W_k(S_k - F_k) \qquad (2.18)$$

A good fit is usually indicated by a random distribution of the residual data around a value of zero.

In most of the LFP experiments, the data was usually fitted with a tail fit procedure where the fitting started at a point where the laser pulse disappears and the goodness of the fit is judged by monitoring the reduced chi-square value and a plot of the distribution of the weighted residuals.

2.4.2 Picosecond transient absorption spectroscopy

Picosecond transient absorption spectral measurements were carried out by Benjamin Robotham and Prof. Kenneth P. Ghiggino of the School of Chemistry, University of Melbourne, Australia. A detailed description of the instrumentation and methods is provided in the section Chapter 6 of the appendix.

2.5 Time-resolved fluorescence emission spectroscopic techniques

Time-resolved fluorescence emission measurements can provide detailed information about the excited state electronic properties of fluorescing molecules. Generally, a molecule is excited with a pulsed laser to its excited electronic state and the fluorescence decay of the molecule from that excited state is monitored as a function of time. Unimolecular fluorescence decay as a function of time is usually represented by an exponential function, $I(t) = I_0 e^{-t/\tau}$, where I_0 is the initial fluorescence intensity at time $t = 0$ and τ is the excited state population decay time. The lifetime of an ensemble of excited molecules is the inverse of the total decay rate, $\tau = (k_{rad} + k_{nonrad})^{-1}$, where k_{rad} is the radiative rate constant and k_{nonrad} is the non-radiative rate constant.[8] In this thesis, two types of time-resolved fluorescence spectroscopic techniques were employed, time-correlated single photon counting (TCSPC) and ultrafast fluorescence upconversion spectroscopy. The TCSPC technique was used to measure the ns S_1 state decay rates of the porphyrin used. Time-resolved fluorescence upconversion was used to measure the ps S_2 fluorescence decay rates as well as the corresponding S_1 fluorescence rise kinetics of the porphyrin (*vide infra*).

2.5.1 Time-correlated single photon counting (TCSPC)

Time-correlated single photon counting (TCSPC) is a popular technique for measuring the ns fluorescence lifetimes of electronically excited species. In TCSPC, single photons emitted by an ensemble of fluorescing molecules are counted and time-correlated with respect to the excitation pulse. A histogram of the number of photons in time-bin

addresses called “channels” usually follows Poissonian statistics and the histogram can be fitted using exponential decay functions to extract the ns excited state lifetimes. The schematic optical layout of the TCSPC setup used in this thesis is shown in Fig. 2.5.

A tunable Ti:Sapphire laser system (Mira 900-D, 700 – 1000 nm, 76 MHz) was continuously pumped with a 532 nm light from a solid state laser (Verdi V-10, 10 W) to produce mode-locked laser pulses operating in the picosecond mode. The picosecond laser was tunable to obtain the desired fundamental wavelength. An acousto-optic modulator in a “pulse picker” (Coherent 9200) was used to select a train of pulses having the desired repetition rate and intensity. A beam splitter directed a small fraction of this pulse train to a photodiode. The electrical signal from the photodiode was fed into a constant fraction discriminator (CFD) and a time to amplitude converter for generating a “stop” pulse. The larger fraction of the laser pulse train from the beam splitter was frequency doubled using a nonlinear second harmonic generator crystal (SHG, HG 9300). The frequency doubled output was focused onto the sample and the resulting fluorescence collected at right angle geometry. The relative polarization of the excitation beam and the emission light was set at the magic angle (54.7^0) using a polarizer on the emission side to avoid any artifacts due to rotational de-polarization of the fluorescing molecules. In most of the measurements, a cut off filter was used on the emission side to filter out any scattered radiation from the excitation pulse.

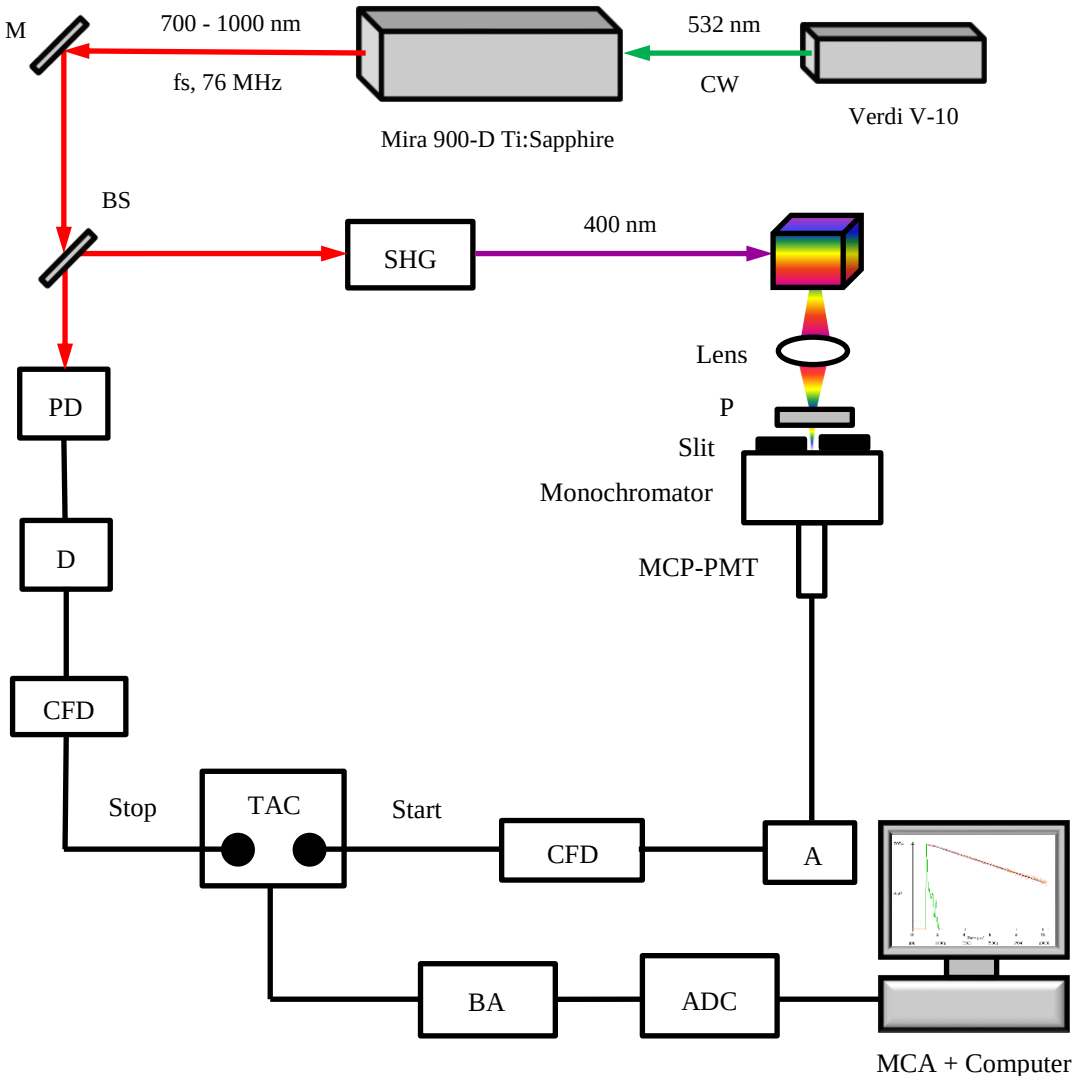

Fig. 2.5 Schematic diagram of the TCSPC setup (adapted and modified from reference 9).[9] M, mirror, BS, beam splitter, PD, photodiode, D, delay, CFD, constant fraction discriminator, TAC, time to amplitude converter, P, polarizer, MCP-PMT, microchannel plate photomultiplier tube, A, amplifier, BA, biased amplifier, ADC, analog to digital converter and MCA, multichannel analyzer.

The collected fluorescence emission was then passed through a Carl Zeiss prism monochromator (M4 QIIID) and focused to a cooled (-30^0C) MCP-PMT detector

(R3809-50U). The electrical signal from the MCP-PMT is then amplified using a high speed amplifier (C5594) and fed into a second CFD and then to the time to amplitude converter (TAC). The first single fluorescent photon reaching the TAC registers a "start" pulse in the TAC. Here, the TAC operates in the reverse start-stop mode where the start pulse is generated by the fluorescence detected and the stop pulse is generated by the excitation laser pulse detected by the stop-pulse photodiode. The start pulse initiates the charging of a capacitor and the stop pulse stops the charging of the capacitor. This process generates a voltage pulse in the TAC having an amplitude proportional to the magnitude of the charge generated in the capacitor. This signal, the magnitude of which is proportional to the time difference between the start and stop pulses, was again amplified using a biased amplifier (TC864 BA) and then stored as a count in an analogue-to-digital converter (ADC). This single photon event is stored in a specific address corresponding to the numerical value (called a channel) in a data acquisition multi-channel analyzer (MCA) and fed into a computer. This process was repeated until a histogram of the number of photons detected versus the channel number (i.e. time) representing the measured emission decay obtained in the experiment.

The temporal resolution of a TCSPC instrument is controlled by the excitation laser pulse width, and the time-dependent response of the detection system and the electronics. The temporal resolution of the instrument is measured from the instrumental response function (IRF). A scattering medium such as a Ludox (colloidal silica) solution was used to scatter the excitation light to measure the IRF. Data acquisition was performed using a Maestro-32 program or SPCM SPC-830 program from Becker & Hickl GmbH. When

using the Maestro-32 program, a suitable time window for the fluorescence decay was selected assuming that it should be at least 5 times the fluorescence lifetime under investigation. The time base was then calibrated by measuring the IRF at different time delays of the stop pulse. A plot of the difference between the channel numbers of adjacent IRF profiles versus the corresponding time delay resulted in a straight line. The slope of this line provides the time division/channel over the entire time window. Further trial experiments were then conducted to make sure that the emission decay of the sample was finished within the selected time window. When using the SPCM SPC-830 software, the time calibration was done by the SPCM data acquisition card and the stop pulse was delayed to insure that it is working in the reverse stop-pulse mode.

A minimum of three fluorescence decays were measured to determine the S_1 lifetime of the porphyrin by setting the monochromator emission wavelength to the maximum of its Q-band fluorescence, 650 nm was used in most of the measurements. Interference from scattered excitation light was unlikely because the emission wavelength set was far away from the excitation wavelength and a filter was used on the emission side to cut off the excitation laser pulse. However, if the experimental fluorescence decay is a convolution of the IRF and the actual decay of the sample, then deconvolution of the IRF from the experimental decay is required to extract the actual decay of the sample. Prior to deconvolution, a constant back ground due to electronic dark counts and stray light was subtracted from both the decay data and the IRF data. The experimental decay data collected at any time t' over the time period t, which was corrected for the background noise is given by,[9b]

$$I_0(t) = \int_0^t P_0(t')G(t-t')\mathrm{d}t' \qquad (2.19)$$

where, $P_0(t')$ is the background corrected instrument response function and $G(t-t')$ is the actual decay data of the sample.

Deconvolution was carried out using an iterative reconvolution procedure using in-house developed software called PsDecay 2000. This procedure minimizes the deviations between fitting data and the emission decay data. The goodness of the fit was decided by the chi-square value and the distribution of the weighted residuals as outlined in section 2.4.1.2.

2.5.2 Picosecond fluorescence upconversion

The TCSPC technique employed in this thesis can achieve a time resolution as low as 50 ps using standard MCP-PMT detectors.[9b] However, it cannot be used to measure ultrashort lifetimes such as the S_2 excited state lifetime of the porphyrins. For such measurements, a fluorescence upconversion set-up was used in which femtosecond pump pulses induce fluorescence from a sample that is collected and overlapped both spatially and temporally with a train of fs gate pulses in an upconversion crystal to generate a sum-frequency signal to provide the required time resolution.

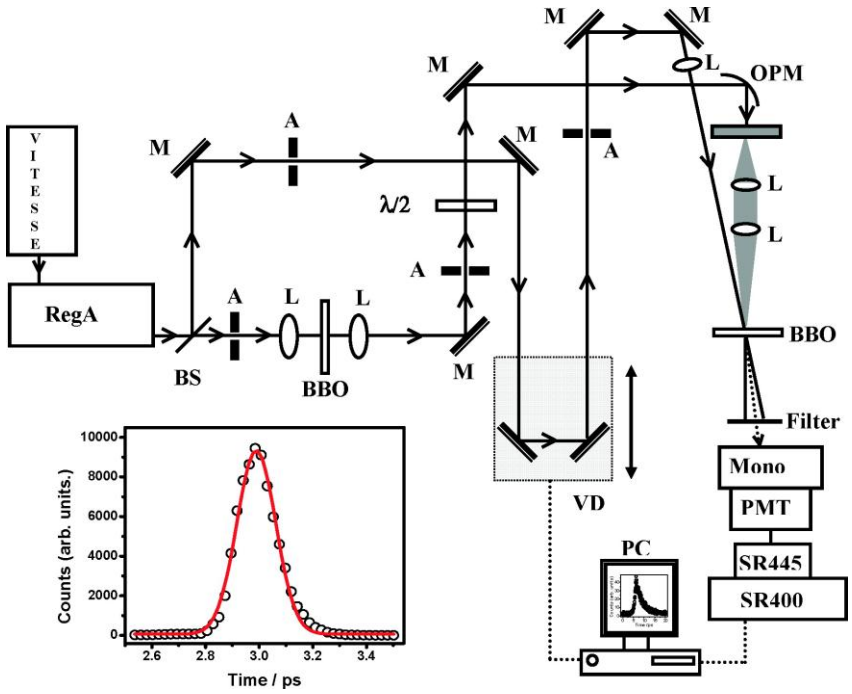

Fig 2.6 Schematic set-up of a picosecond fluorescence upconversion instrument. Reprinted with permission from reference 10.[10] Copyright © 2008 American Chemical Society. RegA, regenerative amplifier, BS, beam splitter, M, mirror, A, aperture, L, planoconvex lens, VD, variable delay, OPM, off-axis parabolic mirror, Mono, monochromator and PMT, photomultiplier tube. The inset shows the Gaussian-type cross-correlation function between the pump and the gate pulses.

The picosecond S_2 state decay time constants and the S_1 fluorescence rise time constants of ZnTPP were measured using the fluorescence upconversion set-up shown in Fig. 2.6. The excitation source consisted of a femtosecond Ti:Sapphire laser (Coherent, Vitesse Duo) and regenerative amplifier (Coherent, RegA 9000) capable of producing 800 nm femtosecond pulses at a pulse repitition rate of 100 KHz with an average output power of ~ 400 mW. The output pulse train from the RegA at 800 nm was split using an 80/20 beam splitter and a major fraction of this beam (the gate beam) was optically

delayed using a variable delay line (Newport, ILS150LP) and focused onto a sum-frequency generation BBO crystal. The other part of the laser (the pump beam) was then passed through a BBO crystal (Photop, UTO8201) at a phase-matching angle of 29.2^0 to generate the second harmonic wavelength at 400 nm. The second harmonic output was then passed through a half-wave plate λ/2 to rotate its plane of polarization by 90^0 and then focused onto the sample using a first surface, Al-coated, off-axis parabolic mirror (Edmund Optics, effective focal length = 101 mm). In order to avoid laser induced photochemical degradation, the sample was continuously flowed through a 200 μm thick quartz cell (Starna). The fluorescence originating in the sample was focused onto the BBO crystal where both the fluorescence light and the gate beam are overlapped, both spatially and temporally, to generate the sum-frequency signal at phase-matching angle of 38^0. Maximum overlap of both the pump beam and the gate beam in the BBO crystal was ensured by phase-matching them at an angle of 10^0. Frequency of the resulting sum-frequency signal is related to the frequencies of the fluorescence signal and the gate pulses by the following equation,

$$\bar{\nu}_{upconv} = \bar{\nu}_{fluor} + \bar{\nu}_{gate} \qquad (2.20)$$

where, $\bar{\nu}$ is the frequency of the light.

The pump beam and gate beam were filtered from the sum-frequency signal using an optical filter and the resulting upconverted signal was passed through a double monochromator (CM112, Spectral products) set to the maximum upconversion efficiency and detected using a photomultiplier tube (Hamamatsu, H7732P-01, C7169 power

supply). The signal from the PMT was amplified using a preamplifier (Stanford research, model SR445) and finally counted using a photon counter (Stanford research, model SR400). The data acquisition was carried out using in-house developed software in Labview (version 7.0). The pump-gate cross-correlation signal was characterized as a Gaussian function with a full width at half maximum (FWHM) of *ca*. 170 ~ 230 fs.

The instrument response function (IRF) of the fluorescence upconversion setup is normally broader than the cross-correlation signal because of the dispersion of the laser and the fluorescence signal due to the optics. In addition, the S_2 fluorescence of the porphyrin measured in the present work is a very fast decaying one. Therefore, the upconversion signal would be a convolution of the actual fluorescence decay and the IRF. Hence, routine measurement of the IRF and its deconvolution from the experimental fluorescence decay is required to obtain the actual fluorescence decay.

The experimental IRF can be measured using two methods. (i) Measuring the scattered Raman signal from the solvent due to the gate pulse and (ii) measuring the fast emission decay of a fluorophore and using it as IRF (such as measuring the ultrafast S_2 emission decay of zinc octaethylporphyrin (ZnOEP), the S_2 state lifetime of which is around 30 fs[9a]). However, an experimental IRF was not measured for the work described in this thesis. Instead, when the data was fitted using the program given in the section Chapter 6 of the appendix, a Gaussian-type IRF was assumed for the iterative fitting procedure.

The S_2 fluorescence decay of ZnTPP was measured by setting the observation wavelength to the S_2 fluorescence maximum emission wavelength (433 nm) and the S_1 state rise data was measured at an observation wavelength at the S_1 fluorescence maximum emission wavelength (655 nm). The temporal S_2 fluorescence decays and S_1 rise profiles were analyzed by an iterative reconvolution procedure with a Gaussian type instrument response function. S_2 fluorescence decays were satisfactorily fitted using a single exponential decay function whereas the S_1 rise data was fitted using two time constants, the first one of the order of ps to account for the S_1 population rise and the long lived second component to account for the S_1 state decay. The goodness of the fit was determined by compairing the S_2 excited state emission decay time constant with the corresponding S_1 fluorescence rise time constant. Even though the S_1 rise data was scattered compared to the S_2 decay data and hence had a lower signal-to-noise ratio, the lifetime constants extracted from the decay data and the rise data were similar within experimental error; thus substantiating the vailidity of the fitting procedure. The computer program used to fit the data is shown in the section Chapter 6 of the appendix. All the picosecond fluorescence upconversion measurements and the data analysis were carried out in collaboration with Dr. Jędrzej Szmytkowski.

2.6 Data analysis and curve fitting

Most of the data were analyzed using Origin 7.5 and 8.0 (OriginLab). Linear and polynomial fits to the data were carried out using a weighted least-square method. In this method, a Levenberg-Marquardt algorithm was used to minimize the sum of the squares

of the deviations between the calculated fitting curve and the experimental data for a range of independent variables. The goodness of the fit was decided by the values of "reduced χ^2" and the "coefficient of determination, R^2". R^2 usually ranges between 0 and 1. A value of R^2 close to 1 indicates good agreement between the theoretical fit and the experimental data. The output of the fitting procedure was usually reported as (output value ± standard error). It should be mentioned that the error bar for each of the data points in some of the plots in the following chapters demonstrates a 5% percentage y-error value of the data point in consideration.

References

(1) (a) Sugunan, S. K.; Tripathy, U.; Brunet, S. M. K.; Paige, M. F.; Steer, R. P. *J. Phys. Chem. A* **2009**, *113*, 8548. (b) Shah, B. K.; Neckers, D. C.; Shi, J. M.; Forsythe, E. W.; Morton, D. *J. Phys. Chem. A* **2005**, *109*, 7677. (c) Shah, B. K.; Neckers, D. C.; Shi, J. M.; Forsythe, E. W.; Morton, D. *Chem. Mater.* **2006**, *18*, 603. (d) Guldi, D. M.; Prato, M. *Acc. Chem. Res.* **2000**, *33*, 695. (e) Orlandi, G.; Negri, F. *Photoch. Photobio. Sci.* **2002**, *1*, 289. (f) Accorsi, G.; Armaroli, N. *J. Phys. Chem. C* **2010**, *114*, 1385.

(2) Sugunan, S. K.; Paige, M. F.; Steer, R. P. *Can. J. of Chem.* **2011**, *89*, 195.

(3) *Hand book of ellipsometry*; William Andrew, Inc, Springer-Verlag GmbH & Co. KG: United States of America, 2005.

(4) Woollam, J. A.; Johs, B.; Herzinger, C. M.; Hilfiker, J.; Synowicki, R.; Bungay, C. L. Optical metrology, 1999; p 1.

(5) *P.T.I. (PTI) Quantamaster™ UV VIS spectrofluorimeter Vol. 2008*.

(6) Liu, X.; Tripathy, U.; Bhosale, S. V.; Langford, S. J.; Steer, R. P. *J. Phys. Chem. A* **2008**, *112*.

(7) Lopez, A. I. *J. Photochem.* **1980**, *14*.

(8) Lakowicz, J. R. *Principles of Fluorescence Spectroscopy*; Springer: New York, 1999.

(9) (a) Liu, X. Ph.D. Thesis, University of Saskatchewan, Saskatchewan, 2009. (b) O'Connor, D. V.; Phillips, D. *Time Correlated Single Photon Counting*; Academic Press: London, 1984.

(10) Tripathy, U.; Kowalska, D.; Liu, X.; Velate, S.; Steer, R. P. *J. Phys. Chem. A* **2008**, *112*, 5824.

Chapter 3: Noncoherent photon upconversion in zinc metalloporphyrin–organic blue emitting molecule systems in solution

3.1 Introduction

Metalloporphyrins (MPs)[1,2,3,4] and transition metal complexes[4,5,6] are the two kinds of molecular systems in present use to produce noncoherent photon upconversion via triplet-triplet annihilation (TTA).[7] The first observation of delayed S_2 fluorescence due to TTA in metalloporphyrins has been made by Stelmakh and Tsvirko.[8] The metalloporphyrin used in the present TTA study, ZnTPP, has D_{4h} symmetry and it has two allowed optically induced electronic transitions in the visible region of the spectrum.[9] These transitions in ZnTPP give rise to a strong fluorescence from its first excited singlet state (Q-band, S_1, 1^1E_u in D_{4h} symmetry) with a fluorescence quantum yield, $\phi_{S1\text{-}S0} = 4.0 \times 10^{-2}$ and a weak fluorescence from the second excited singlet state (B-band or Soret band, S_2, 2^1E_u in D_{4h} symmetry), $\phi_{S2\text{-}S0} = 1.1 \times 10^{-3}$.[9,10] These two optical transitions arise from the one electron transitions within the same set of molecular orbitals, the near degenerate HOMO and HOMO-1 (a_{2u} and a_{1u} in D_{4h}) and a doubly degenerate LUMO (e_g in D_{4h}). It was evident from TDDFT calculations[11] that >95% and >85% of the oscillator strengths of the S_1-S_0 transitions and the S_2-S_0 electronic transitions are mainly contributed by the a_{2u}-e_g and a_{1u}-e_g one electron transitions, respectively. The S_2-S_0 transition is highly allowed with an oscillator strength $f \sim 1$.[12] The average excited state lifetimes of the S_2 and S_1 states are *ca*. 1.4 ps and 2.0 ns respectively with an S_2-S_1 internal conversion

efficiency of nearly unity, which results in more than 99% of the S_2 state population decay into the S_1 state on a sub-picosecond time scale.[9]

The singlet to triplet, S_1-T_1 internal conversion efficiency of ZnTPP is nearly one ($\eta_{ISC} \sim 1$)[13] and the triplet state of ZnTPP is long-lived with a lifetime of τ_{T1} = 0.6-1.2 ms in deaerated solution at room temperature.[14,15] The S_2-S_0 electronic energy spacing (ΔS_2-S_0 = 23,580 cm^{-1}) of ZnTPP is more than two times greater than the T_1-S_0 energy spacing (ΔT_1-S_0 = 12,850 cm^{-1}).[10] This condition satisfies the requirement for a triplet-triplet annihilation process in which the two ZnTPP molecules in their lowest triplet state (T_1) diffuse together and annihilate to form an excited singlet state (S_n, $n \geq 2$), which in the case of ZnTPP is the S_2 state.

It was proposed by Baluschev et al. that noncoherent photon upconversion (NCPU) via TTA can proceed through two different mechanisms.[1,16] In the first mechanism, heteromolecular triplet-triplet electronic energy transfer (TTET) occurs between a sensitizer molecule (metalloporphyrin, MP) and a blue emitter molecule (BE). This is followed by homomolecular TTA between two triplet sensitized blue emitting molecules which populates the S_n state ($n \geq 1$) of one of the blue emitting molecules. The excited blue emitting molecule then emits light at a higher energy than the light absorbed by the sensitizer, thus manifesting the process of upconversion. The mechanistic scheme for this type of NCPU is given below.

$$S_0(MP) + h\nu_{(VIS\text{-}NIR)} \longrightarrow S_1(MP) \qquad (i)$$

$$S_1(MP) \longrightarrow T_1(MP) \qquad \text{(ii)}$$

$$T_1(MP) + S_0(BE) \longrightarrow S_0(MP) + T_1(BE) \qquad \text{(iii)}$$

$$2\ T_1(BE) \longrightarrow S_1(BE) + S_0(BE) \qquad \text{(iv)}$$

$$S_1(BE) \longrightarrow S_0(BE) + h\nu_{UC} \qquad \text{(v)}$$

The second, and less efficient mechanism was proposed to operate in molecular systems in which the triplet energy of the BE is greater than that of the triplet sensitizer MP.[16c,16e] In this case, homomolecular TTA occurs on the MP itself to populate the S_2 state of the MP. If the BE has its S_1 state lying lower than the energy of the S_2 state of ZnTPP, a singlet-singlet electronic energy transfer (SSET) is proposed to be possible from the MP S_2 state to the S_1 state of the BE, followed by the generation of the upconverted emission from the BE. The proposed mechanism is given below.

$$2\ T_1(MP) \longrightarrow S_2(MP) + S_0(MP) \qquad \text{(vi)}$$

$$S_2(MP) + S_0(BE) \longrightarrow S_0(MP) + S_1(BE) \qquad \text{(vii)}$$

$$S_1(BE) \longrightarrow S_0(BE) + h\nu_{UC} \qquad \text{(viii)}$$

The mechanisms proposed by Baluschev et al. are controversial for the following reasons.[17,18] If the SSET mechanism has to occur through a standard Förster resonance energy transfer (FRET) mechanism, the excited state lifetime of the donor molecule should be long enough for energy transfer to compete with other excited state radiative and nonradiative decay processes. Efficient FRET has been reported in porphyrin

aggregates[9] and in tethered azulene-porphyrin dyads[19] in which the donor is relatively long lived. However, the metalloporphyrins used by Baluschev et al., β-octaethylporphyrin platinum (PtOEP) and palladium (PdOEP) do not emit fluorescence from the S_2 state and therefore, the second excited singlet state of these porphyrins must be very short-lived (<<1 ps).[20,21] Therefore, a diffusion controlled SSET mechanism operating between the short-lived S_2 state of the MPs and the S_1 state of the BEs is highly unlikely. In order for the SEET mechanism in solution to work, there should be strong ground state aggregation of the MPs to facilitate efficient homomolecular TTA to populate its S_2 state. Porphyrins are well-known for aggregating even at low concentrations in dilute solutions.[22] However, Baluschev et al.[1,16] did not account for the role of aggregation in solution-phase TTA, rather, they argued that solute aggregation is an unfavorable phenomenon for TTA processes.[18] In addition, heteromolecular TTA between the triplet MP and triplet BE was not considered as another potential pathway for producing the upconverted radiation.

In this context, a detailed study of the two proposed mechanisms is required to clarify the issues. ZnTPP was used as the sensitizing MP in the present study because the photophysical properties of ZnTPP are well characterized.[23] Another advantage of using ZnTPP is that its filled d shell orbitals eliminate the possibility of involvement of charge transfer states[24] in sensitized NCPU. In addition, ZnTPP can undergo homomolecular TTA to populate its fluorescent S_2 state. The S_2-S_0 fluorescence from ZnTPP can be used as a metric to study the SSET mechanism proposed by Baluschev et al.[1,16]

In order to scrutinize the two proposed mechanisms, two blue emitting molecules were selected, perylene (P) and coumarin 343 (C343). Table 3.1 shows that these two molecules are highly fluorescent from their S_1 states having ns lifetimes. Perylene has a long triplet lifetime, 0.3 - 1.1 ms,[25] while, literature data for the T_1 lifetime of C343 have not been reported. However, C343 is used as an efficient laser dye; and therefore should have a short triplet lifetime and a small intersystem crossing yield. Both the S_2 state and the T_1 state of ZnTPP have higher energies than the S_1 state and T_1 state of P, respectively. In principle, based on energetic, thermodynamic and kinetic information, this would allow for the following three mechanistic possibilities for producing the NCPU radiation from P in a ZnTPP-P binary solution. (i) Homomolecular TTA in ZnTPP to populate its S_2 state followed by SSET from that state (if the S_2 state is sufficiently long lived, which is not the actual case, *vide infra*) to the S_1 state of P, (ii) TTET from the T_1 state of ZnTPP to the T_1 state of P followed by homolecular TTA in P to populate its S_1 state and (iii) heteromolecular TTA between triplet ZnTPP and triplet P to generate the S_1 state of P. However, C343 is different in this respect as its T_1 state is substantially higher in energy than the T_1 state of ZnTPP, eliminating the possibilities of TTET or heteromolecular TTA between the triplet C343 and the triplet ZnTPP. However, the S_2 state of ZnTPP is higher in energy compared to the S_1 state of C343. Therefore, if one is to observe upconverted emission from the S_1 state of C343 upon excitation to the S_1 state of ZnTPP in a binary mixture solution of ZnTPP and C343, the plausible reasons would be mechanism (i); i.e. homomolecular TTA in ZnTPP and subsequent SSET from the S_2 state of ZnTPP. If mechanism (i) is impossible, a new alternate process must be involved.

A schematic representation of the energy levels of ZnTPP, P and C343 involved in the present study are shown in Scheme 3.1.

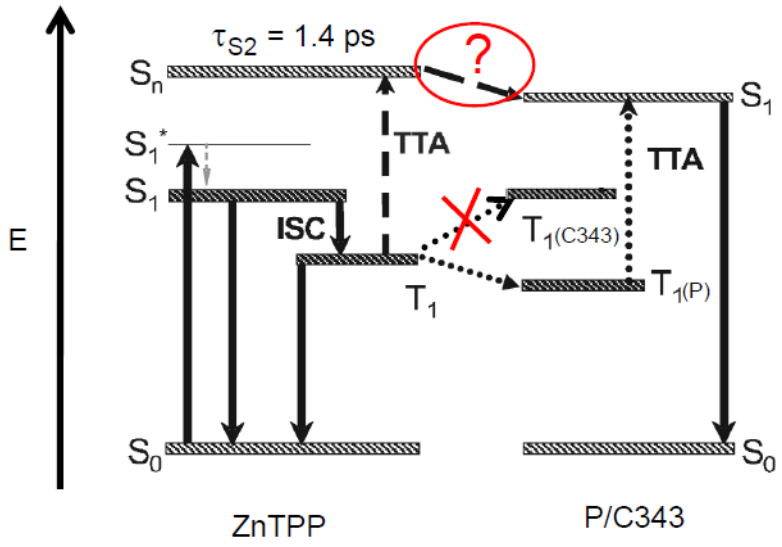

Scheme 3.1 Simplified energy level diagram of ZnTPP, P and C343 involved in NCPU (adapted and modified from reference 16c).[16c]

3.2 Results and discussion

The photophysical properties of ZnTPP and the BEs, P and C343 are tabulated in table 3.1.

Table 3.1 Photophysical properties of the compounds used in the present study.

	ZnTPP	Perylene	Coumarin 343	References
$E(S_2)$ (cm^{-1})	23,580	-	-	23
$E(S_1)$ (cm^{-1})	16,865	22,700	22,600	23, 25a-d, 26
$E(T_1)$ (cm^{-1})	12,850	12,371	16,581	27, 28, 29
$\tau(S_1)$ (ns)	2.0	5.5	4.0	29, 25a-d, 26
$\tau(T_1)$ (ms)	1.2, 0.6	1.1, 0.3	-	(14, 15), (25e, 25a-d)
η_{isc}	0.9	0.01	-	13, 25a-d
$\phi_{f,S2}$	1.1×10^{-3}	-	-	23
$\phi_{f,S1}$	0.04	0.98	0.63	30, 25a-d, 31

The absorption and fluorescence emission spectra of the different compounds are shown in Fig. 3.1(A) and 3.1(B) and closely resemble the spectra reported in dilute solutions, indicative of the absence of fluorescent impurities.[23,25a-d,26] From the absorption spectra of Fig. 3.1(A), it can be seen that only ZnTPP absorbs a major fraction of the light at the excitation wavelength (532 nm, 18,800 cm^{-1}) used for TTA and NCPU

experiments, whereas the BEs do not absorb at this wavelength. The concentration of ZnTPP used in the absorption measurement (0.1 mM) was exactly the same concentration as those used for typical TTA experiments in the present study. At these concentrations, porphyrins tend to form ground state aggregates[22] which is evident from the slight broadening of the absorption spectrum of the MP. However, this effect is somewhat offset by taking the absorption spectrum in benzene in which ZnTPP is readily soluble and aggregation is minimized.

The prompt emission spectra of benzene solutions of ZnTPP, P and C343 obtained by one-photon excitation at or near their absorption maxima are shown in Fig. 3.1(A). The spectra were taken in solution concentrations (0.1 mM in benzene) lying within the range of solution concentrations employed for TTA and NCPU experiments involving the BEs. Perylene was excited at the wavelength of its absorption maximum (442 nm, 22,600 cm^{-1}). Both ZnTPP and C343 were excited to the blue side of their absorption maxima (410 nm, 24,400 cm^{-1}) to minimize the interference from scattered excitation light. All of the spectra were corrected for both primary and secondary inner filter effects using the procedure discussed in section 2.3.2.1. All of the emission spectra are slightly broadened and the peak maxima are slightly red shifted when compared with the reported literature spectra measured in dilute solutions. This implies that slight solute aggregation of these molecules exists in the electronic ground state. However, the relative shapes of the peaks for the solution concentrations employed here are similar to the spectra measured in dilute solutions.[23,25a-d,26]

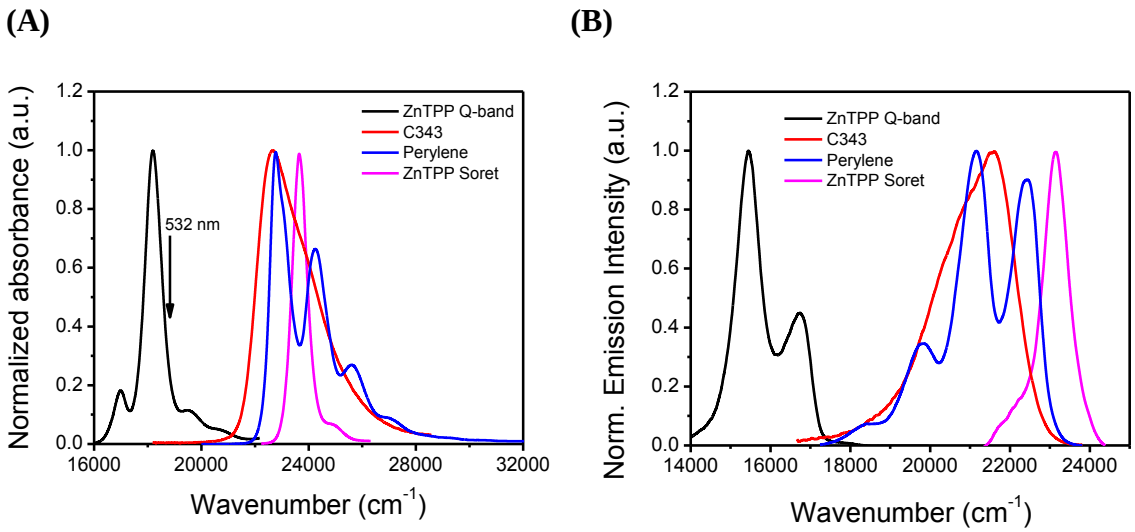

Fig. 3.1 (A) Separately normalized absorption spectra of ZnTPP, C343 and perylene. The sample solutions were all of the same concentration (1.0×10^{-4} M) in benzene and the absorbance was measured at a spectral bandwidth of 2.0 nm, and (B) Separately normalized, directly excited fluorescence spectra of ZnTPP, C343 and perylene. The sample solutions were all of the same concentration (1.0×10^{-4} M) in benzene. Perylene was excited at the wavelength of its absorption maximum, 442 nm. C343 and ZnTPP were excited at 410 nm, to the blue of the absorption maxima to minimize scattered light corrections. Fluorescence was collected with a PTI spectrophotometer with a bandpass of 2.0 nm on both the excitation and emission monochromators.

Interference by the emission from ZnTPP in the emission spectra of the BEs is unlikely because both the S_2 fluorescence and S_1 fluorescence spectra of ZnTPP are well separated and bracket the emission from the BEs. It should be noted that the absorption spectra of the BEs overlap significantly with the S_2 emission spectrum of ZnTPP, which would make it difficult to extract the true S_2 emission spectrum of ZnTPP in a binary mixture solution of ZnTTP and the BE. In addition, the spectral overlap between the absorption spectra and the emission spectra of the BEs themselves will be significant at high concentrations, thus making reabsorption effects significant. In order to minimize the artifacts in the emission spectra induced by the above mentioned issues, front-face

illumination of the sample in a custom made triangular glass cuvette was employed for TTA measurements, and the reabsorption corrections were done using the procedure described in section 2.3.2.1.

3.2.1 Mechanism of homomolecular TTA of ZnTPP in solution

TTA in solution is a bimolecular process in which two molecules in their triplet state diffuse together and annihilate. TTA in solution therefore should have a quadratic dependence on the incident excitation laser power (at low powers) because the concentration of the triplets formed is proportional to the incident laser flux.[1-5,32,33] The S_1-T_1 ISC quantum yield of ZnTPP is nearly one ($\phi_{ISC} \sim 0.9$).[13] Therefore, the allowed S_1 fluorescence of ZnTPP ($\phi_f \sim 0.04$ in benzene)[13,30] can be used as a relative measure of the initial population of the triplet state T_1 under various laser excitation conditions, and, it can be reasonably assumed that $I_f(S_1, \text{ZnTPP}) \propto [T_1]$. Clearly, the intensity of S_2 fluorescence produced as a result of TTA should bear a quadratic relationship with the triplet state concentration, i.e., $I_f(S_2, \text{ZnTPP}) \propto [T_1]^2$. Therefore, in the absence of any photon-wasting processes limiting the production of triplet states, one expects the ratio, $\log_{10}(I_f(S_2, \text{ZnTPP})/I_f(S_1, \text{ZnTPP})) = 2.0$. In the present experiments, a double logarithmic plot of $I_f(S_2, \text{ZnTPP})$ *vs* $I_f(S_1, \text{ZnTPP})$ as shown in Fig. 3.2, resulted in a slope of 2.0 in the low laser power range, thus establishing that the observed S_2 fluorescence of ZnTPP excited at 532 nm is a result of a bimolecular annihilation process between two triplet ZnTPP molecules. However, above this low power laser excitation threshold, the slope of the curve diminishes to a value that is less than 2, and we speculated that photon wasting

processes such as triplet-triplet transient absorption might be in operation at high laser powers on the basis of the fact that the transient absorption of the T_1 state of ZnTPP has a high oscillator strength in the visible region of the spectrum,[27] which would depopulate the T_1 state at higher excitation powers, resulting in lower yield of S_2 in the TTA process. However, recent reports[34] suggest that the region of slope 2 is the region where the first order radiative (phosphorescence) and nonradiative (triplet quenching and intersystem crossing from T_1 to S_0) processes dominate. It was proposed that[34] in the region where the slope 2 is declined to a slope of 1, the incident laser power is large enough to make a high triplet concentration such that each of these triplets in principle should find a triplet annihilation partner within the triplet lifetime and in the absence of quasi-first order decay processes, this would maximize the probability of annihilation. Therefore the delayed fluorescence intensity should be linear in relation to the triplet concentration which has a linear relation to the incident photon flux, hence a slope of 1. In addition, if excited state saturation occurs which would result in ground state bleaching, triplet state concentration will be saturated at higher laser powers.[34a] It was suggested that[35] the region where the slope deviates from quadratic to linear produces the highest TTA efficiency and all of the subsequent TTA experiments described in the present study have been carried out using laser power densities falling in the low power range of Fig. 3.2, most frequently by setting the laser power density at the upper end of the low power range, i.e., at *ca*. 0.28 $W.cm^{-2}$, the onset where the slope is about to decrease to a linear range. The solutions for the rate equations pertaining to these effects are provided in section Chapter 3 of the appendix.

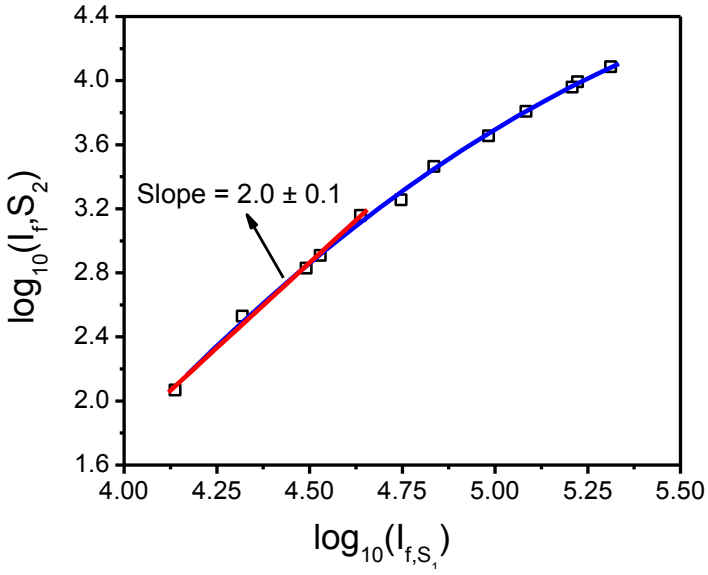

Fig. 3.2 Plot of $\log_{10}$ of delayed S_2 fluorescence intensity *versus* $\log_{10}$ of prompt S_1 fluorescence intensity as a function of increasing laser power using a 532 nm cw laser and front-face excitation of 1.0×10^{-4} M ZnTPP in degassed benzene. The red line represents intensities due to contributions from quasi-first order processes and the blue line represents intensities due to predominant contributions from TTA. $R^2 = 0.99$ for the least-squares fit.

In order to understand the mechanism of homomolecular TTA of ZnTPP in solution, the TTA induced upconverted S_2-S_0 emission spectra were obtained by exciting ZnTPP to its S_1 state in both coordinating and noncoordinating organic solvents using a 532 nm laser. These spectra are shown along with the respective prompt S_1 spectra taken under the same experimental conditions in Fig. 3.3. These emission spectra were corrected to same absorbance at the excitation wavelength; hence the apparent differences in the emission spectra are due to the solvent effect, and not to variations in concentration or absorbed light intensity.

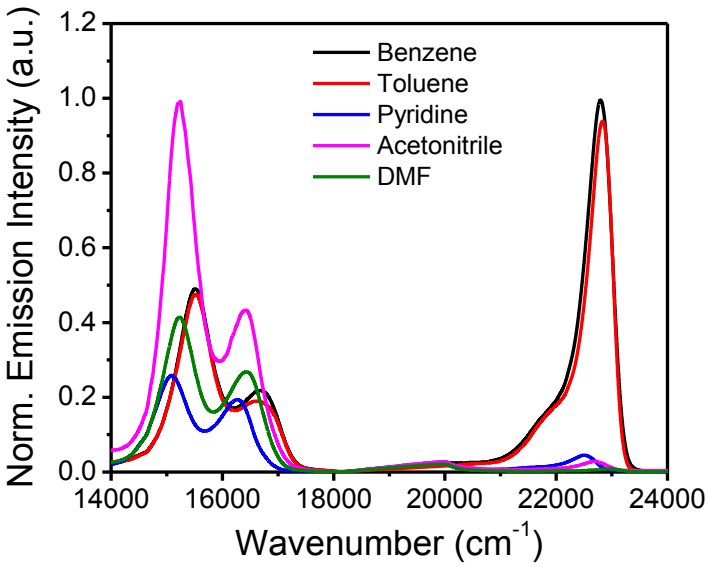

Fig. 3.3 Prompt S_1 fluorescence and delayed S_2 fluorescence obtained from front-face excitation of 1.0×10^{-4} M ZnTPP in degassed non-coordinating solvents (benzene and toluene) and coordinating solvents (pyridine, acetonitrile and *N*,*N*-dimethylformamide) with a 532 nm (18797 cm^{-1}) cw laser at an incident power density of 0.28 W/cm^2 and a fluorometer with a 3.6 nm emission bandpass.

The S_1-S_0 emission spectra of ZnTPP exhibit some degree of solvent dependency as reported previously[23] and are unremarkable. However, the intensity of the S_2-S_0 fluorescence of ZnTPP resulting from TTA is highly solvent dependent. It should be noted that the S_2-S_0 emission intensity is found to be a maximum in noncoordinating aromatic solvents such as benzene and toluene and is strongly suppressed in coordinating solvents such as pyridine, acetonitrile and DMF. Of the solvents used here, the smallest emission intensity observed was in DMF. Note in particular that the S_2 fluorescence spectral maximum is slightly shifted towards longer wavelengths by about 300 cm^{-1} when compared with the prompt S_2 fluorescence spectra obtained in dilute solutions. This

observed bathochromic effect of the fluorescence has been reported previously[8,36] and was explained in terms of the perturbation of the emitting S_2 state by a second, ground state porphyrin. The emitting S_2 state produced as a result of TTA of ZnTPP molecules must be reasonably short-lived (approximately a picosecond)[23] and therefore emits before the second, ground state ZnTPP molecule produced as a result of TTA has had a chance to diffuse away. The effect of perturbation is therefore only observed in the TTA-induced S_2 fluorescence.

The mechanism of TTA in solution follows a Dexter type short-range electron exchange energy transfer between two triplet molecules where the rate of encounter is diffusion controlled.[37] In the Dexter type of energy transfer, the rate of energy transfer decreases exponentially as the distance between the donor and the acceptor increases, resulting in a reduced wavefunction overlap between the donor and the acceptor.[38] The observed difference in the TTA-induced Soret emission spectra of ZnTPP in different degassed solvents may be analyzed in terms of the Dexter mechanism. The substantial diminution in the Soret emission intensity as a result of carrying out TTA in ZnTPP in coordinating solvents can be ascribed to the increased center-to-center distance between ZnTPP molecules. Axial coordination between the coordinating solvent and the Zn atom at the center of ZnTPP is known to occur in the ground state with association constants in the 10^3 M^{-1} to 10^5 M^{-1} range.[39] An experiment in which pyridine was quantitatively titrated into benzene solutions of ZnTPP was carried out to study the effect of this axial coordination on the TTA-produced S_2 fluorescence intensity. The results are shown in Fig. 3.4.

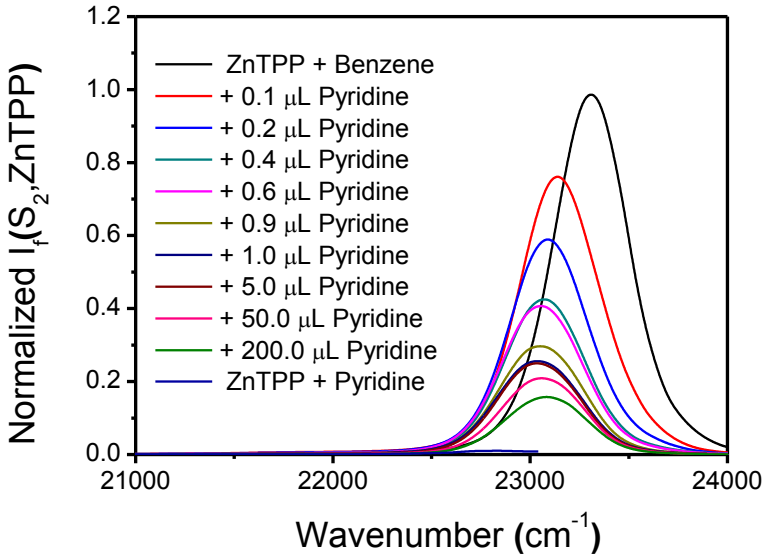

Fig. 3.4 Delayed S_2 fluorescence spectrum obtained from the titration of 1.0×10^{-4} M ZnTPP in degassed non-coordinating benzene solvent with incremental amounts of pyridine. Samples were excited in front-face geometry with a 532 nm cw laser at a constant power density of 0.28 Wcm^{-2}.

It should be noticed that Soret band intensity decreases significantly with the addition of tiny volume fractions of pyridine into benzene solutions of ZnTPP, while keeping the concentration of ZnTPP constant in all cases. Note, in addition, that the S_2 fluorescence maximum undergoes a gradual red-shift with the addition of pyridine. This bathochromic effect can be ascribed to the axial coordination of pyridine onto the metal center of ZnTPP. The bathochromic shift of Soret band emission in coordinating solvents has been previously reported in one photon prompt excitation of ZnTPP to the S_2 state and it is attributed to the axial coordination of pyridine to the metal center which stabilizes the excited state slightly more than the ground state.[40] The effect of axial coordination of a

coordinating solvent molecule on the rate of TTA can be analyzed in terms of a simplified model of the Dexter theory[37] using the following equation,

$$R_{calc} = \frac{k_{NC}}{k_c} = \frac{A_{NC}\exp(-2R_{NC}/L)}{A_C\exp(-2R_C/L)} \approx \frac{\eta_{NC}}{\eta_C}\exp\{-2(R_C - R_{NC})/L\} \qquad (3.1)$$

where, R_{calc} is the ratio of the rate of TTA in noncoordinating and coordinating solvents, k_{NC} and k_c are the rates of TTA in noncoordinating and coordinating solvents respectively, R_{NC} and R_C are the corresponding distances between the annihilating triplet porphyrins and L is the effective Bohr radius, which for ZnTPP is 0.48 nm.[41] A_{NC} and A_C are the pre-exponential factors and they include the overlap integral between the electronic wave functions of the donor and the acceptor and the diffusion rate constants. Here, it was assumed that the overlap integrals are similar for ZnTPP in both coordinating and noncoordinating solvents and that the diffusion coefficients vary inversely with the solvent viscosity (η). Semiempirical AM1 level calculations were used to estimate the center-to-center distances, R_C and R_{NC} between two ZnTPP molecules for a variety of possible relative orientations, and the differences in these distances, R_C-R_{NC} were estimated to be in a range of 0.98 to 1.14 nm for pyridine. Inserting these values in equation 3.1 yielded an estimated R_{calc} value in the range of 12-24 for noncoordinating benzene and coordinating pyridine solvents for which the ratio of diffusion coeffiecients is η_C/η_{NC} = 1.5. This calculated value should be compared with the measured experimental ratio of TTA fluorescence intensities of R_{obs} = 22 for ZnTPP in benzene relative to pyridine. Considering the uncertainties in determining L, errors associated with calculating the computed geometries and uncertainties associated with the approximation

of equating R_C and R_{NC} to the Zn…Zn center-to-center distance, the calculated value of R_{calc} is reasonable. Based on this analysis, it can be reasonably concluded that the TTA in ZnTPP occurs through a short range electron-exchange Dexter type energy transfer mechanism.

3.2.2 Mechanism of photon upconversion in the ZnTPP-Perylene system in solution

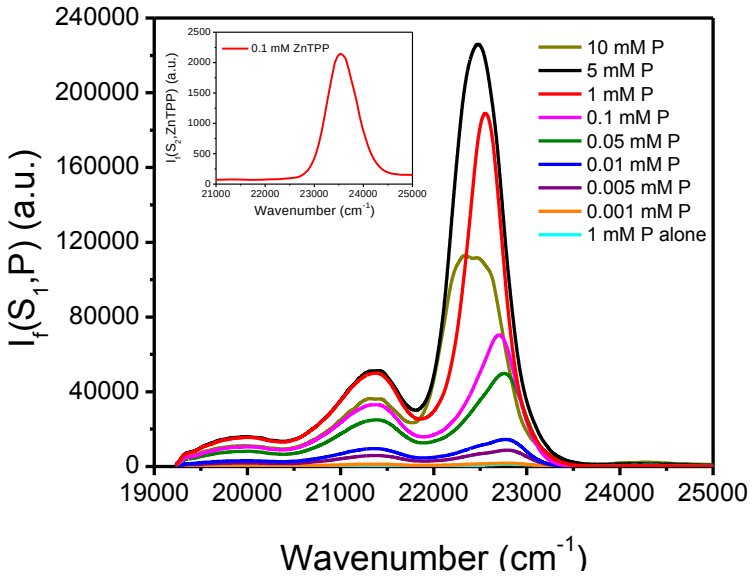

Fig. 3.5 Upconverted S_1 fluorescence obtained from various concentrations of perylene in a solution containing 1.0×10^{-4} M ZnTPP in degassed benzene. Samples were excited in front-face geometry with a 532 nm cw laser at a power density of 0.28 Wcm^{-2} and a spectrometer with a 1.0 nm emission band pass. The spectra were corrected for the detector response as a function of wavelength and for reabsorption by perylene, which is large in the > 22000 cm^{-1} region. The inset shows the corrected delayed S_2 emission spectrum obtained from 1.0×10^{-4} M ZnTPP in benzene in the absence of perylene under the same experimental conditions.

Fig 3.5 demonstrates the variation in the TTA-S_2 fluorescence of 0.1 mM ZnTPP in benzene as a function of the concentration of P when exciting the sample in the Q-band

of ZnTPP using a 532 nm laser at 0.28 $W.cm^{-2}$. The inset shows the S_2 fluorescence of ZnTPP as a result of TTA measured under the same experimental conditions. Note that the S_2 emission from ZnTPP is completely quenched with the addition of a small volume fraction of P, and that the S_1 fluorescence of P is enhanced with increasing P concentration. In the absence of ZnTPP, no S_1 fluorescence was observed even from a deoxygenated, highly concentrated (1.0 mM) solution of P excited at 532 nm. In addition, no S_1 fluorescence of P was observed from an air saturated solution of ZnTPP and P in benzene in which the triplet states of ZnTPP would be completely quenched by molecular oxygen. The energy of the electronic states of ZnTPP and P suggest that the mechanism of the observed S_1 fluorescence of P from the ZnTPP-P mixture in solution could be due to the well-established[1-5,16,32] mechanism of triplet-triplet energy transfer (TTET) from the ZnTPP triplet to the triplet state of P followed by homomolecular TTA in P.

Spectral overlap of the S_2 fluorescence of ZnTPP with the S_1 fluorescence of P made it difficult to extract the kinetic information about the upconversion process from the quenching kinetics of the S_2 fluorescence of ZnTPP. Moreover, the reabsorption of the upconverted emission by both ZnTPP and P distorted the initial part of the upconverted emission spectra. Correction factors suggested by Lopez[42] were used to correct for these artifacts. However, the correction factors became very large at P concentration $\geq$ 1.0 mM. Therefore, above this high concentration of P, the apparent decrease in the fluorescence intensity of P could not reliably be attributed to the ground state quenching induced by a second ground state P. Nevertheless, the corrected fluorescence intensities were used to

plot the dependence of the upconverted fluorescence intensity on the incident laser power and on the concentration of P employed, which are shown in Fig. 3.6(A) and 3.6(B).

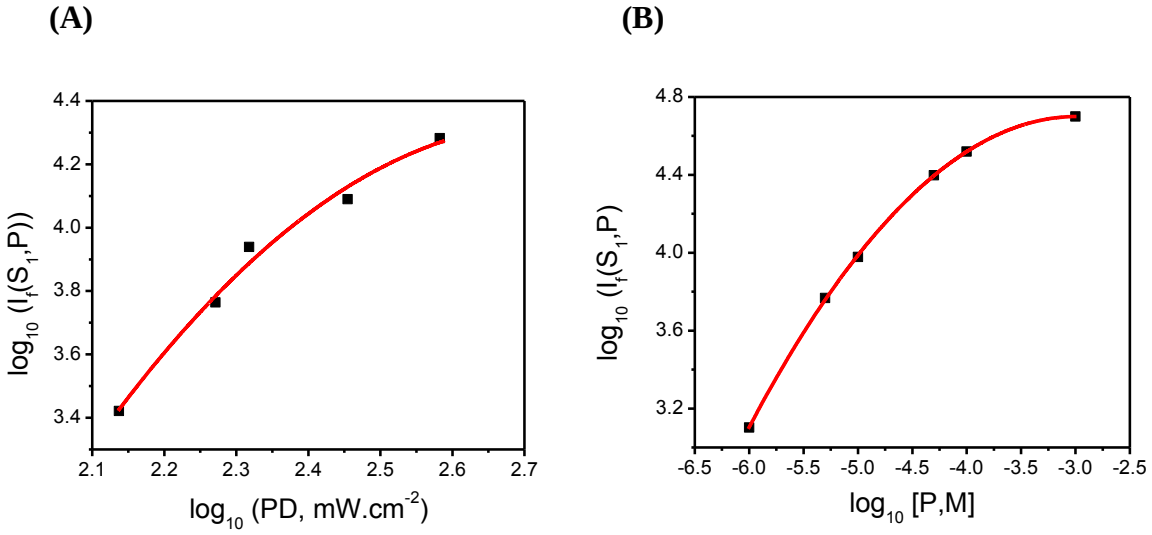

Fig. 3.6 (A) Plot of the $\log_{10}$ of the S_1 fluorescence intensity of perylene, P, *vs.* the $\log_{10}$ of the power density (PD) of the excitation laser for 532 nm cw illumination of a 1.0×10^{-4} M ZnTPP solution in degassed benzene containing 1.0×10^{-4} M perylene., and (B) Graph of $\log_{10}$ $I_f(S_1,P)$ (corrected intensities) *vs.* $\log_{10}$ [P]. Experimental conditions are the same as in Figure 3.6 (A) except that different concentrations of perylene were employed at a fixed excitation power density of 0.28 Wcm^{-2}.

In Fig. 6(A), the upconverted S_1 fluorescence originating from constant concentrations of ZnTPP and P was measured as a function of the incident laser power at 532 nm. This curve is slightly nonlinear and exhibits a tangential slope at lower laser power of *ca*. 2.0, which suggests that the S_1 emission produced from the ZnTPP-P solution is due to the TTET followed by the TTA in the P triplet state. However, the plot 3.6(B) of the upconverted fluorescence intensity as a function of increasing concentrations of P in constant concentration of ZnTPP in benzene obtained at a constant laser power, 0.28 $W.cm^{-2}$ showed considerable nonlinearity with a tangential slope reaching *ca*. 1.0 at

lower P concentrations. This could be due to the fact that higher concentrations of P ensures a complete quantitative TTET process which results in no further enhancement of the upconverted emission with still higher P concentrations. Based on the above results, it can be concluded that the mechanism of photon upconversion in the ZnTPP-P system in non-coordinating solvents is due to TTET and consequent TTA in the acceptor, i.e., the mechanism proposed by Baluschev et al.[1,16]

3.2.3 Mechanism of photon upconversion in the ZnTPP-C343 system in solution

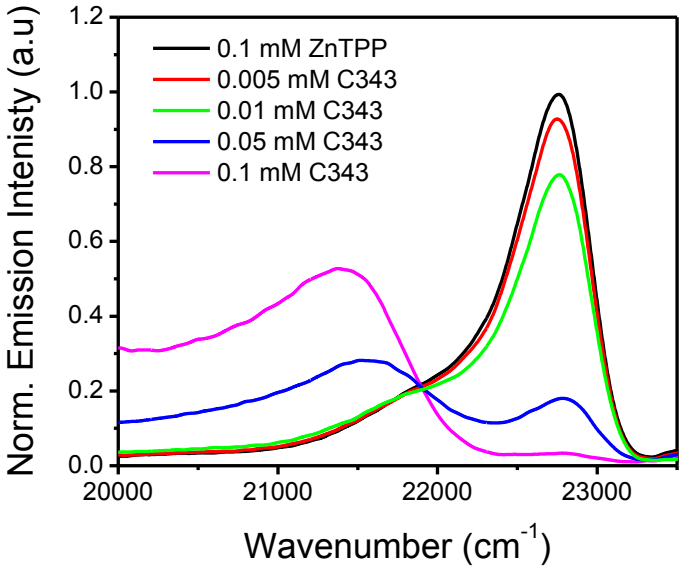

Fig. 3.7 Upconverted S_1 fluorescence spectra obtained from various concentrations of C343 in a solution containing 1.0×10^{-4} M ZnTPP in degassed benzene. Samples were excited in rectangular geometry with a 0.28 W/cm^2, 532 nm cw laser and a spectrometer with a 3.6 nm emission bandpass. The spectra were corrected for detector response and for reabsorption effects.

As noted in Table 3.1, the triplet state of C343 lies above the triplet of ZnTPP by a factor of about 3,000 cm^{-1} whereas its lowest excited singlet state (S_1) lies slightly below

the S_2 state of ZnTPP. Although, in principle, thermally activated TTET from ZnTPP to C343 could occur, the fractional population of the thermally activated triplets of ZnTPP 3,000 cm^{-1} above the zero point, $[T_1^*]/[T_1]$, would be $<10^{-6}$ at room temperature and would make the TTET process too slow to be competitive. Therefore, a TTET followed by TTA in C343 is not possible in the ZnTPP-C343 system. Photon upconversion measurements in solutions containing ZnTPP and C343 were conducted to unravel the mechanism of NCPU in these systems, with the expectation that the results might explain the role of the second excited singlet state of metalloporphyrins in the mechanism (II) proposed by Baluschev et al.[16c,16e]

Surprisingly, efficient NCPU was observed from ZnTPP-C343 system in degassed benzene solution when ZnTPP was excited using the 532 nm laser at modest power. Fig. 3.7 displays the quenching of the TTA-S_2 fluorescence of ZnTPP together with the concomitant increase of the S_1 fluorescence of C343 with increasing C343 concentration. An isoemissive point at 21,850 cm^{-1} is observed. The S_1 fluorescence of C343 alone measured in benzene by exciting at 532 nm is also shown in Fig. 3.7 and it can be seen that in the absence of ZnTPP, this fluorescence signal is negligibly small. All the spectra have been corrected for reabsorption effects. In addition, a negligibly small fluorescence signal was obtained in the 400 nm - 500 nm wavelength range when an air-saturated, equimolar (0.1 mM) solution of ZnTPP and C343 in benzene was excited at 532 nm and the emission was collected under identical experimental conditions. The $\log_{10}$ of the upconverted fluorescence intensity obtained from a solution of 0.1 mM ZnTPP and 0.05 mM C343 was plotted as a function of the log of the incident laser power, as shown in

Fig. 3.8, and resulted in a near-linear curve with a slope of 1.7, close to the value of 2 expected for a bimolecular process under weak annihilation limit, but tending towards a strong annihilation regime.

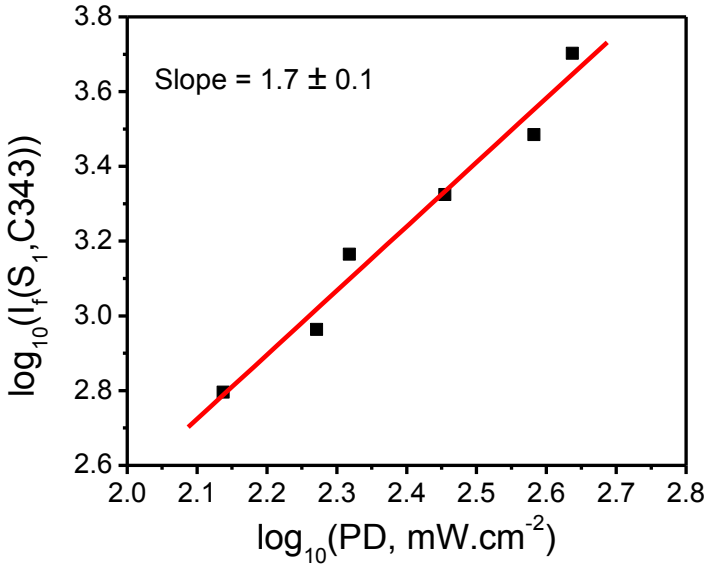

Fig. 3.8 Plot of the $\log_{10}$ of the S_1 fluorescence intensity of C343 *vs.* $\log_{10}$ of the power density of the excitation laser for a degassed solution containing 1.0×10^{-4} M ZnTPP and a 5.0×10^{-5} M C343 in benzene. Samples were excited in front-face geometry with a 532 nm cw laser and the intensities were recorded with a fluorometer with a 3.6 nm emission bandpass. $R^2 = 0.96$ for the least-squares fit.

It can be concluded that the observed fluorescence is originating largely from a bimolecular process in the ZnTPP-C343 system. Considering the assumptions that a TTET is not possible in ZnTPP-C343 system and that the S_2 state of ZnTPP lies higher in energy than the S_1 state of C343, the obtained result might tempt one to conclude that the observed fluorescence is due to the homomolecular TTA in ZnTPP followed by the SSET from the S_2 state of ZnTPP to the S_1 state of C343. However, the following analysis

indicates that the mechanism involved is not TTA followed by SSET. Rather it is a mechanism not previously mentioned by Baluschev et al.[16c,16e] or others who have previously investigated the NCPU phenomenon.

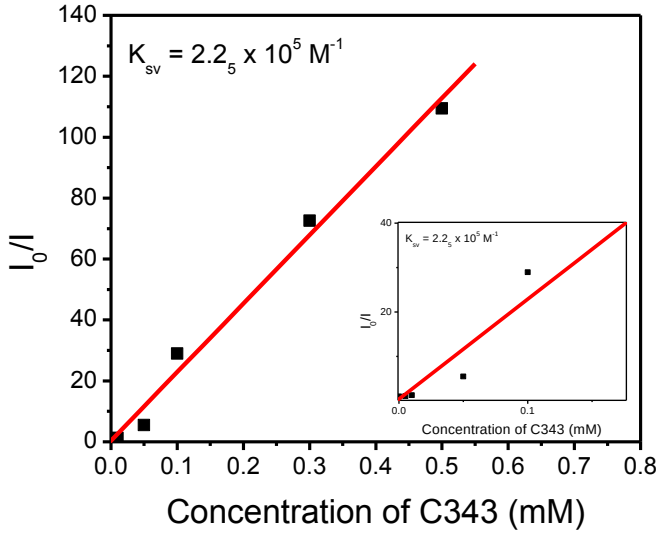

Fig. 3.9 Stern-Volmer plot of I_0/I *vs*. the concentration of C343 in a solution containing 1.0×10^{-4} M ZnTPP in benzene. Samples were excited in rectangular geometry by a 532 nm cw laser at a power density of 0.28 W/cm^2 and a spectrometer with a 3.6 nm emission bandpass. The insert shows the lower portion of the graph in greater detail. R^2 = 0.98 for the least-squares fit.

The TTA-S_2 fluorescence quenching data from Fig. 3.7 was cast in the form of a Stern-Volmer plot where the ratio of the unquenched fluorescence intensity to the quenched fluorescence intensity was plotted as a function of the added concentration of C343. The plot shown in Fig. 3.9 provided a linear curve with a slope resulting in a very large value of Stern-Volmer constant, $K_{SV} = k_Q \tau^0_D$ = 2.2(5) × 10^5 M^{-1}, where k_Q is the bimolecular diffusion controlled rate constant of quenching and τ^0_D is the excited state lifetime of the unquenched donor molecule. The lifetime of the perturbed TTA produced

S_2 state of ZnTPP is unknown, however, the S_2 lifetime of the one-photon Soret excited ZnTPP molecule is 1.4 ps.[23] Inserting this 1.4 ps as the S_2 lifetime of ZnTPP in the equation for the Stern-Volmer constant results in a quenching rate constant, $k_Q = 1.6 \times 10^{17}$ M^{-1} s^{-1}, which is about 7 orders of magnitude greater than the theoretical bimolecular diffusion controlled rate constant of ZnTPP and C343 in benzene at room temperature. Even if the S_2 state lifetime of ZnTPP in the unrelaxed encounter complex is assumed to be considerably different than the reported lifetime of one-photon Soret-excited ZnTPP in benzene, and even if the SSET is assumed to be considerably efficient over longer distances than the diffusion controlled hard-sphere distance, the calculated rate of quenching would still be unreasonably larger than the diffusion controlled rate constant. This suggests that the SSET mechanism from the S_2 state of ZnTPP is not responsible for the blue emission from the S_1 state of C343.

The SSET mechanism can further be ruled out based upon the rate of energy transfer derived from Förster resonance energy transfer (FRET)[43] parameters of SSET from the S_2 state of ZnTPP to C343 (energy transfer rate was calculated using the software PhotochemCAD).[44] From the absorption spectrum of C343 in benzene expressed in molar absorbance ($M^{-1}cm^{-1}$) *vs* wavenumber and from the normalized TTA-S_2 emission spectrum of ZnTPP in benzene, an overlap integral, $J = 1.65 \times 10^{-13}$ cm^6 is obtained, resulting in a Förster radius of $R_0 = 17.4$ Å and a rate constant of energy transfer, $k_{D*A} = 1.25 \times 10^{10}$ s^{-1}. This calculated rate constant should be compared with the radiative decay rate of unperturbed ZnTPP in the S_2 state, $1/\tau_D = 6.9 \times 10^{11}$ s^{-1} and therefore results in a calculated SSET efficiency of < 2%. Considering that the Pt and Pd porphyrins used by

Baluschev et al.[1,16] have S_2 state lifetimes that are at least two orders of magnitude shorter than the S_2 state lifetime of ZnTPP, a SSET mechanism giving rise to the upconverted emission intensities reported by Baluschev et al. is highly improbable.

Since the SSET mechanism can be eliminated for the reasons stated above, an alternative plausible mechanism must be described. The first possibility is to consider the formation of ground state complexes of ZnTPP and C343. However, this possibility is ruled out based on the fact that there was no significant change in the absorption spectrum of ZnTPP, particularly at 532 nm, even after the addition of 1.0 mM C343.

The next possibility is to consider the aggregation of ZnTPP and C343 when ZnTPP is in its triplet state. Based on the following information, a triplet exciplex formed between a triplet ZnTPP molecule and a ground state C343 molecule is proposed to be responsible for the upconverted fluorescence from ZnTPP-C343 system. Triplet exciplex formation in metalloporphyrins has been previously reported[45] and the photophysics well characterized.[46] The photophysical properties of these exciplexes include: (i) The quenching of triplet porphyrins in nonpolar solvents occurs via the formation of triplet exciplexes. (ii) Transient absorption spectroscopy suggests[45,46] that the lifetimes of a wide range of metalloporphyrin triplet exciplexes lie in the range of tens of microseconds to milliseconds. The lifetimes of the triplet exciplexes depend upon the nature of the porphyrin and the quencher. (iii) The lifetimes of triplet exciplexes have been correlated with the degree of charge transfer in the encounter complex. Complexes formed between good electron-donor porphyrins and weak electron-acceptor molecules tend to form long-

lived triplet exciplexes. (iv) A reduction in triplet lifetime is observed when porphyrin complexes are formed at lower quencher concentrations, whereas, a longer-lived species forms at a higher quencher concentration. This observation suggests that the lifetime of the initially-formed triplet exciplex might be shorter than the lifetime of the triplet porphyrin, that decay of the triplet exciplex results in deactivation of the triplet state and that further aggregation of the triplet exciplex with the quencher results in a longer-lived triplet species.

Evidence for the formation of a triplet exciplex between ZnTPP and C343 can be obtained from the Stern-Volmer plot in Fig. 3.7. From the Stern-Volmer constant, K_{SV} = 2.2(5) × 10^5 M^{-1} and from the diffusion controlled rate constant, $k_Q \leq k_{diff}$ = 1.0 × 10^{10} $M^{-1}s^{-1}$ in benzene, an upper limit of the triplet lifetime of ZnTPP was estimated to be, $\tau_D \geq 2.2 \times 10^{-5}$ s. This upper limit estimate is shorter than the range of triplet lifetimes reported for ZnTPP in fluid, deoxygenated solution which lies in the range of 0.6 - 1.2 ms[14-15] and is consistent with the range of triplet exciplexes lifetimes reported in literature and the fact that triplet exciplexes are shorter-lived than the triplet porphyrin itself.

A mechanism involving the formation of a triplet exciplex from triplet ZnTPP and ground state C343 followed by a three-center heteromolecular TTA between the triplet exciplex and a second triplet of ZnTPP is therefore proposed to be responsible for the formation of a C343 in its S_1 state. This product state then emits the upconverted radiation at around 21,400 cm^{-1}. The following scheme summarizes the steps in the mechanism.

$$T_1(MP) + S_0(BE) \rightleftharpoons {}^3(MP\cdots BE) \quad \text{(ix)}$$

$${}^3(MP\ldots BE) + T_1(MP) \longrightarrow 2S_0(MP) + S_1(BE) \quad \text{(x)}$$

$$S_1(BE) \longrightarrow S_0(BE) + h\nu_{UC} \quad \text{(xi)}$$

$${}^3(MP\ldots BE) \longrightarrow S_0(MP) + S_0(BE) \quad \text{(xii)}$$

This type of three-center energy pooling process is well-established for excited singlet states in mutichromophoric arrays and the theory of such processes has been described by Jenkins and Andrews.[47]

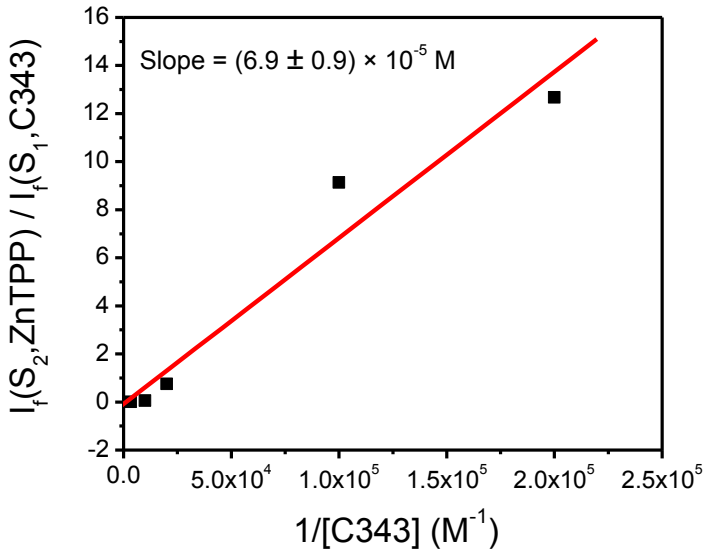

Fig. 3.10 Plot of the ratio, R_f, described in equation (3.2) *vs.* the inverse of the molar concentration of C343 in a 0.10 mM solution of ZnTPP in deoxygenated benzene at room temperature. The excitation conditions are the same as those described in Figure 3.9. R^2 = 0.93 for the least-squares fit.

If the exciplex formation and dissociation reactions are fast compared to: (i) the heteromolecular TTA process, as it should be at lower laser powers, and (ii) the rate of

nonradiative decay of the triplet exciplex, then the ratio of the intensity of S_2 fluorescence of ZnTPP produced as a result of TTA of triplet porphyrins and the intensity of S_1 fluorescence of C343 produced as a result of heteromolecular TTA of the triplet exciplex with a triplet porphyrin should be inversely proportional to the concentration of added C343. This relationship is derived in section Chapter 3 of the appendix and is given below.

$$R_f = \frac{I_{f,S2(ZnTPP)}}{I_{f,S1(C343)}} = \frac{\phi_{f,S2(ZnTPP)}}{\phi_{f,S1(C343)}} \frac{k_{\mathrm{vi}}}{k_{\mathrm{x}}} \frac{1}{K_{as}[BE]} \qquad (3.2)$$

where $\phi_{f,S2(ZnTPP)}$ and $\phi_{f,S1(C343)}$ are the quantum yields of TTA-S_2 fluorescence of ZnTPP and upconverted S_1 fluorescence of C343, k_{vi} is the rate of TTA in ZnTPP (equation vi), k_{x} is the rate of heteromolecular TTA between the triplet exciplex and triplet ZnTPP (equation x) and K_{as} is the bimolecular association constant for aggregation of triplet ZnTPP with ground state C343. A plot of ($I_{f,S2(ZnTPP)}/I_{f,S1(C343)}$) *versus* $[C343]^{-1}$, such as the one shown in Fig. 3.9, resulted in a slope of $(6.9 \pm 0.9) \times 10^{-5}$ which, together with the quantum yields, resulted in an association constant, $K_{as} = 24\ M^{-1}$ a reasonable value for a weakly aggregated triplet exciplex.[45-46] It should be noted that direct spectroscopic measurement for the formation of triplet exciplex and the rate of heteromolecular TTA between the triplet exciplex and the triplet ZnTPP would be complicated by the fact that both ZnTPP and C343 absorb strongly throughout the visible region of the spectrum and emit in the blue-green and red-near-infrared region of the spectrum.

3.2.4 Role of the second excited singlet state of porphyrins in photon upconversion

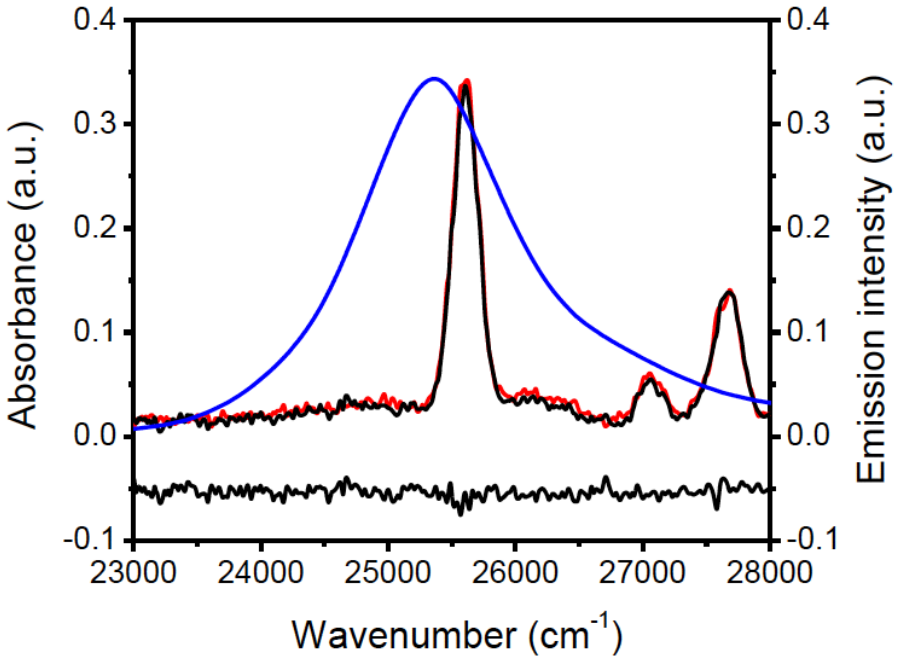

Fig. 3.11 Absorption spectrum (blue) of 14.4 x 10^{-6} M PdOEP in benzene. Raw background plus solvent Raman scatter spectrum (red) excited at 350 nm; background plus Raman scatter spectrum corrected for solute absorbance (black). Emission spectrum minus background plus corrected Raman scatter spectrum (offset in black).

The above results demonstrate conclusively that SSET transfer from the TTA-produced, short-lived S_2 state of ZnTPP cannot be responsible for NCPU in ZnTPP-BE systems in solution and that an alternate process, triplet exciplex formation followed by three-center heteromolecular TTA gives rise to the NCPU in ZnTPP-C343 system in solution. The PtOEP and PdOEP used by Baluschev et al. in their NCPU processes are nonfluorescent from their second excited singlet states.[1,16]

The Strickler-Berg equation,[48] can be used to calculate the radiative rate constant and the S_2 state lifetime of PdOEP. The absorption spectrum of PdOEP was measured in benzene solution (Fig. 3.11) and was used to calculate the Strickler-Berg parameters using the PhotochemCAD.[44] The absorption maximum was observed at 25,380 cm^{-1} in agreement with previous reports.[16d] A Raman spectrum (plus the background) lying to the blue side of the expected S_2 emission of the PdOEP was obtained when this sample was excited at 28,571 cm^{-1} and is shown as the red curve in Fig. 3.11. When the Raman spectrum (plus background) corrected for the solute absorbance (black) is subtracted from the Raman scattering spectrum the result is a noisy background offset (black). From this spectrum, the quantum yield of S_2-S_0 fluorescence was estimated to be $< 10^{-5}$. Using the molar absorptivity obtained from the integrated Soret absorption spectrum, the radiative decay rate of the S_2 state of PdOEP was estimated to be, $k_r \sim 5 \times 10^8$ s^{-1}. Using the well-established relationship between the radiative rate constant and the fluorescence quantum yield, $k_r = \phi_{f(S2)}/\tau_{(S2)}$, the S_2 state lifetime of PdOEP is estimated to be < 20 fs. Based on this reasoning, PtOEP is expected to have an S_2 lifetime of the order of tens of femtoseonds. These estimated lifetimes are at least 2 orders of magnitude shorter than the S_2 state lifetime of ZnTPP[23] which again suggests that without prior aggregation of the metalloporphryin with the BE in solution, NCPU via a SSET mechanism is improbable.

3.3 Conclusions

The mechanisms of NCPU in model ZnTPP-BE systems in solution were studied using steady state optical spectroscopy. For ZnTPP in solution, homomolecular TTA produces delayed emission from the S_2 state of ZnTPP, which was confirmed by the quadratic dependence of the emission intensity on the incident laser flux. This delayed Soret band emission is highly solvent sensitive and is quenched in coordinating solvents. It was confirmed that TTA in ZnTPP occurs through a short-range Dexter electron exchange energy transfer mechanism. For the ZnTPP-P system in benzene where the T_1 of P lies lower than the T_1 of ZnTPP, NCPU proceeds via a TTET from the triplet ZnTPP to the triplet P followed by homomolecular TTA in P. However, the ZnTPP-C343 system in solution, for which the triplet of C343 lies higher than the triplet of ZnTPP, follows neither the TTET mechanism nor the SSET mechanism. Rather, NCPU in such a system is proposed to occur via the formation of a weak triplet exciplex between triplet ZnTPP and ground state C343 followed by heteromolecular TTA between the triplet exciplex and a second triplet ZnTPP. Interestingly, very recent research in this field shows that the rate of NCPU in solution in which the triplet of the acceptor is slightly energetically higher than the triplet of sensitizer is controlled by entropic factors in part.[49] Enthalpic losses associated with TTET and subsequent TTA were found to be reduced with these types of donor-acceptor pairs. In these systems thermally activated TTET results in a gain in entropy due to the distribution of the triplet excitons between the triplet states of the donor and the acceptor molecules. However, a low efficiency of TTET was reported due

to the low yield of thermal population. Nonetheless, a significant excitation peak-to-upconversion peak margin of 0.9 eV was reported.

Metalloporhyrins such as ZnTPP used in the present study or PtOEP and PdOEP used by other groups cannot give rise to NCPU through a SSET mechanism owing to the short lifetime of the second excited singlet state of these porphyrins unless strong prior MP-BE ground state aggregation exists in solution. Prior aggregation of the MP with itself and with BE would still allow for SSET-supported NCPU in MP-BE in the solid state and thin polymer films. In any case, the annihilation of the triplet excitons[50] which is controlled by the state of aggregation of the MP with itself is likely to be responsible for the annihilation process to yield the upper excited singlet state of the MPs. In fact, a very recent report by Keivanidis et al.[51] showed: (i) that TTA followed by SSET occur in thin films of PtOEP mixed with either poly(fluorene) (PF26) or ladder-type pentaphenylene (L5Ph), (ii) that enhanced prior aggregation of PtOEP undergoing homomolecular TTA occurs in the films, (iii) that the mechanism of SSET can be attributed to an electron exchange energy transfer which occurs at short distances and (iv) that a charge transfer state may participate in the excited state energy transfer process.

References

(1) Baluschev, S.; Yakutkin, V.; Miteva, T.; Avlasevich, Y.; Chernov, S.; Aleshchenkov, S.; Nelles, G.; Cheprakov, A.; Yasuda, A.; Mullen, K.; Wegner, G. *Angew. Chem.Int. Edit.* **2007**, *46*, 7693.

(2) Singh-Rachford, T. N.; Castellano, F. N. *J. Phys. Chem. A* **2008**, *112*, 3550.

(3) Singh-Rachford, T. N.; Castellano, F. N. *Inorg. Chem.* **2009**, *48*, 2541.

(4) Singh-Rachford, T. N.; Castellano, F. N. *Coord. Chem. Rev.* **2010**, *254*, 2560.

(5) Islangulov, R. R.; Kozlov, D. V.; Castellano, F. N. *Chem. Commun.* **2005**, 3776.

(6) (a) Kozlov, D. V.; Castellano, F. N. *Chem. Commun.* **2004**, 2860. (b) Ji, S. M.; Wu, W. H.; Wu, W. T.; Guo, H. M.; Zhao, J. Z. *Angew. Chem. Int. Edit.* **2011**, *50*, 1626. (c) Ji, S. M.; Guo, H. M.; Wu, W. T.; Wu, W. H.; Zhao, J. Z. *Angew. Chem. Int. Edit.* **2011**, *50*, 8283. (d) Wu, W. T.; Wu, W. H.; Ji, S. M.; Guo, H. M.; Zhao, J. Z. *Dalton T.* **2011**, *40*, 5953. (e) Liu, Y.; Wu, W.; Zhao, J.; Zhang, X.; Guo, H. *Dalton T.* **2011**, *40*, 9085. (f) Sun, H.; Guo, H.; Wu, W.; Liu, X.; Zhao, J. *Dalton T.* **2011**, *40*, 7834. (g) Sun, H.; Guo, H.; Wu, W.; Liu, X.; Zhao, J. *Dalton T.* **2011**, *40*, 7834. (h) Sun, H. Y.; Guo, H. M.; Wu, W. T.; Liu, X.; Zhao, J. Z. *Dalton T.* **2011**, *40*, 7834. (i) Sun, J. F.; Wu, W. H.; Guo, H. M.; Zhao, J. Z. *Eur. J. Inorg. Chem.* **2011**, 3165.

(7) Wu, W. H.; Guo, H. M.; Wu, W. T.; Ji, S. M.; Zhao, J. Z. *J. Org. Chem.* **2011**, *76*, 7056.

(8) Stelmakh, G. F.; Tsvirko, M. P. *Opt. Spektrosk.* **1980**, *49*, 511.

(9) Tripathy, U.; Steer, R. P. *J. Porphyr. Phthalocya.* **2007**, *11*, 228.

(10) Sugunan, S. K.; Tripathy, U.; Brunet, S. M. K.; Paige, M. F.; Steer, R. P. *J. Phys. Chem. A* **2009**, *113*, 8548.

(11) Liu, X.; Yeow, E. K. L.; Velate, S.; Steer, R. P. *Phys. Chem. Chem. Phys.* **2006**, *8*, 1298.

(12) Sugunan, S. K.; Paige, M. F.; Steer, R. P. *Can. J. Chem.-Rev. Can. Chim.* **2011**, *89*, 195.

(13) Tagaki, S. S.; Inoue, H. *In Molecular and Supramolecular Photochemistry*; Dekker, M.: New York, 2000.

(14) Kalyanasundaram, K. *J. Chem. Soc., Faraday Trans. 2* **1983**, *79*, 383.

(15) Crouch, A. M.; Langford, C. H. *J. Photochem. Photobiol. A-Chem.* **1990**, *52*, 55.

(16) (a) Baluschev, S.; Jacob, J.; Avlasevich, Y. S.; Keivanidis, P. E.; Miteva, T.; Yasuda, A.; Nelles, G.; Grimsdale, A. C.; Mullen, K.; Wegner, G. *Chem. Phys. Chem* **2005**, *6*, 1250. (b) Baluschev, S.; Keivanidis, P. E.; Wegner, G.; Jacob, J.; Grimsdale, A. C.; Mullen, K.; Miteva, T.; Yasuda, A.; Nelles, G. *Appl. Phys. Lett.* **2005**, *86.* (c) Baluschev, S.; Miteva, T.; Yakutkin, V.; Nelles, G.; Yasuda, A.; Wegner, G. *Phys. Rev. Lett.* **2006**, *97.* (d) Baluschev, S.; Yakutkin, V.; Miteva, T.; Wegner, G.; Roberts, T.; Nelles, G.; Yasuda, A.; Chernov, S.; Aleshchenkov, S.; Cheprakov, A. *New J. Phys.* **2008**, *10.* (e) Baluschev, S.; Yakutkin, V.; Wegner, G.; Minch, B.; Miteva, T.; Nelles, G.; Yasuda, A. *J. Appl. Phys.* **2007**, *101.* (f) Baluschev, S.; Yakutkin, V.; Wegner, G.; Miteva, T.; Nelles, G.; Yasuda, A.; Chernov, S.; Aleshchenkov, S.; Cheprakov, A. *Appl. Phys. Lett.* **2007**, *90.* (g) Baluschev, S.; Yu,

F.; Miteva, T.; Ahl, S.; Yasuda, A.; Nelles, G.; Knoll, W.; Wegner, G. *Nano Lett.* **2005**, *5*, 2482.

(17) Steer, R. P. *J. Appl. Phys.* **2007**, *102*.

(18) Baluschev, S.; Yakutkin, V.; Wegner, G.; Minch, B.; Miteva, T.; Nelles, G.; Yasuda, A. *J. Appl. Phys.* **2007**, *102*.

(19) Yeow, E. K. L.; Ziolek, M.; Karolczak, J.; Shevyakov, S. V.; Asato, A. E.; Maciejewski, A.; Steer, R. P. *J. Phys. Chem. A* **2004**, *108*, 10980.

(20) Gouterman, M. *The Porphyrins*; Academic Press: New York, 1978.

(21) Bansal, A. K.; Holzer, W.; Penzkofer, A.; Tsuboi, T. *Chem. Phys.* **2006**, *330*, 118.

(22) Khairutdinov, R. F.; Serpone, N. *J. Phys. Chem. B* **1999**, *103*, 761.

(23) (a) Liu, X.; Tripathy, U.; Bhosale, S. V.; Langford, S. J.; Steer, R. P. *J. Phys. Chem. A* **2008**, *112*, 8986. (b) Tripathy, U.; Kowalska, D.; Liu, X.; Velate, S.; Steer, R. P. *J. Phys. Chem. A* **2008**, *112*, 5824. (c) Lukaszewicz, A.; Karolczak, J.; Kowalska, D.; Maciejewski, A.; Ziolek, M.; Steer, R. P. *Chem. Phys.* **2007**, *331*, 359. (d) Karolczak, J.; Kowalska, D.; Lukaszewicz, A.; Maciejewski, A.; Steer, R. P. *J. Phys. Chem. A* **2004**, *108*, 4570.

(24) Sorgues, S.; Poisson, L.; Raffael, K.; Krim, L.; Soep, B.; Shafizadeh, N. *J. Chem. Phys.* **2006**, *124*.

(25) (a) Komfort, M.; Lohmannsroben, H. G.; Salthammer, T. *J. Photochem. Photobiol. A-Chem.* **1990**, *51*, 215. (b) Lewitzka, F.; Lohmannsroben, H. G. *Z. Phys. Chem. Neue. Fol.* **1990**, *169*, 181. (c) Lewitzka, F.; Lohmannsroben, H. G. *Z. Phys. Chem. Neue. Fol.* **1990**, *169*, 203. (d) Lewitzka, F.; Lohmannsroben, H. G.; Strauch, M.;

Luttke, W. *J. Photochem. Photobiol. A-Chem.* **1991**, *61*, 191. (e) Pirotta, M.; Renn, A.; Werts, M. H. V.; Wild, U. P. *Chem. Phys. Lett.* **1996**, *250*, 576.

(26) (a) Wachtveitil, J.; Huber, R.; Sporlein, S.; Moser, J. E.; Gratzel, M. *Int. J. Photoenergy* **1999**, *1*, 153. (b) Hara, K.; Sato, T.; Katoh, R.; Furube, A.; Ohga, Y.; Shinpo, A.; Suga, S.; Sayama, K.; Sugihara, H.; Arakawa, H. *J. Phys. Chem. B* **2003**, *107*, 597.

(27) Tobita, S.; Kaizu, Y.; Kobayashi, H.; Tanaka, I. *J. Chem. Phys.* **1984**, *81*, 2962.

(28) Clarke, R. H.; Hochstra.Rm *J. Mol. Spectrosc.* **1969**, *32*, 309.

(29) McCarthy, P. K.; Blanchard, G. J. *J. Phys. Chem.* **1993**, *97*, 12205.

(30) (a) Harriman, A. *J. Chem. Soc., Faraday Trans. I* **1980**, *76*, 1978. (b) Harriman, A.; Porter, G.; Wilowska, A. *J. Chem.l Society., Faraday Trans. I* **1983**, *79*, 807.

(31) Reynolds, G. A.; Drexhage, K. H. *Opt. Commun.* **1975**, *13*, 222.

(32) (a) Islangulov, R. R.; Lott, J.; Weder, C.; Castellano, F. N. *J. Am. Chem. Soc.* **2007**, *129*, 12652. (b) Singh-Rachford, T. N.; Castellano, F. N. *J. Phys. Chem. A* **2009**, *113*, 9266. (c) Singh-Rachford, T. N.; Castellano, F. N. *J. Phys. Chem. A* **2009**, *113*, 5912. (d) Singh-Rachford, T. N.; Castellano, F. N. *J. Phys. Chem. Lett.* **2010**, *1*, 195. (e) Singh-Rachford, T. N.; Islangulov, R. R.; Castellano, F. N. *J. Phys. Chem. A* **2008**, *112*, 3906. (f) Singh-Rachford, T. N.; Lott, J.; Weder, C.; Castellano, F. N. *J. Am. Chem. Soc.* **2009**, *131*, 12007. (g) Singh-Rachford, T. N.; Nayak, A.; Muro-Small, M. L.; Goeb, S.; Therien, M. J.; Castellano, F. N. *J. Am. Chem. Soc.* **2010**, *132*, 14203. (h) Singh-Rachford, T. N.; Nayak, A.; Muro-Small, M. L.; Goeb, S.; Therien, M. J.; Castellano, F. N. *J. Am. Chem. Soc.* **2011**, *133*, 2791.

(33) Monguzzi, A.; Tubino, R.; Meinardi, F. *J. Phys. Chem. A* **2009**, *113*, 1171.

(34) (a) Cheng, Y. Y.; Khoury, T.; Clady, R.; Tayebjee, M. J. Y.; Ekins-Daukes, N. J.; Crossley, M. J.; Schmidt, T. W. *Phys. Chem. Chem. Phys.* **2010**, *12*, 66. (b) Monguzzi, A.; Mezyk, J.; Scotognella, F.; Tubino, R.; Meinardi, F. *Phys. Rev. B* **2008**, *78.* (c) Haefele, A.; Blumhoff, J.; Khnayzer, R. S.; Castellano, F. N. *J. Phys. Chem. Lett.* **2012**, *3*, 299. (d) Kim, J.-H.; Deng, F.; Castellano, F. N.; Kim, J.-H. *Chem. Mater*. **2012**, *24*, 2250.

(35) Auckett, J. E.; Chen, Y. Y.; Khoury, T.; Clady, R. G. C. R.; Ekins-Daukes, N. J.; Crossley, M. J.; Schmidt, T. W. *J. Phys. Conf. Ser.* **2009**, *185*, 012002.

(36) (a) Tsvirko, M. P.; Stelmakh, G. F. *ACS Sym. Ser.* **1986**, *321*, 118. (b) Ksenofontova, N. M.; Stelmakh, G. F.; Tsvirko, M. P. *Dokl. Akad. Nauk. SSSR+* **1986**, *289*, 405. (c) Sevchenko, A. N.; Stelmakh, G. F.; Tsvirko, M. P. *Opt. Spektrosk.* **1979**, *46*, 893.

(37) Monguzzi, A.; Tubino, R.; Meinardi, F. *Phys. Rev. B* **2008**, *77*.

(38) Dexter, D. L. *J. Chem. Phys.* **1953**, *21*, 836.

(39) Danger, B. R.; Bedient, K.; Maiti, M.; Burgess, I. J.; Steer, R. P. *J. Phys. Chem. A* **2010**, *114*, 10960.

(40) Nappa, M.; Valentine, J. S. *J. Am. Chem. Soc.* **1978**, *100*, 5075.

(41) Faure, S.; Stern, C.; Guilard, R.; Harvey, P. D. *J. Am. Chem. Soc.* **2004**, *126*, 1253.

(42) Lopez, A. I. *J. Photochem.* **1980**, *14*, 97.

(43) (a) Forster, T. *Disc. Faraday Soc.* **1959**, 7. (b) Tripathy, U.; Bisht, P. B. *J. Chem. Phys.* **2006**, *125*.

(44) (a) Du, H.; Fuh, R. C. A.; Li, J. Z.; Corkan, L. A.; Lindsey, J. S. *Photochem. Photobiol.* **1998**, *68*, 141. (b) Dixon, J. M.; Taniguchi, M.; Lindsey, J. S. *Photochem. Photobiol.* **2005**, *81*, 212.

(45) (a) Roy, J. K.; Carroll, F. A.; Whitten, D. G. *J. Am. Chem. Soc.* **1974**, *96*, 6349. (b) Roy, J. K.; Whitten, D. G. *J. Am. Chem. Soc.* **1972**, *46*, 7162.

(46) (a) Kapinus, E. I.; Aleksankina, M. M.; Staryi, V. P.; Boghillo, V. I.; Dilung, II *J. Chem. Society., Faraday Trans. 2* **1985**, *81*, 631. (b) Kapinus, E. I.; Aleksankina, M. M.; Dilung, I. *J. Photochem.* **1982**, *21*, 125.

(47) Jenkins, R. D.; Andrews, D. L. *J. Phys. Chem. A* **1998**, *102*, 10834.

(48) Strickler, S. J.; Berg, R. A. *J. Chem. Phys.* **1962**, *37*, 814.

(49) Cheng, Y. Y.; Fuckel, B.; Khoury, T.; Clady, R.; Ekins-Daukes, N. J.; Crossley, M. J.; Schmidt, T. W. *J. Phys. Chem. A* **2011**, *115*, 1047.

(50) Brun, A. M.; Atherton, S. J.; Harriman, A.; Heitz, V.; Sauvage, J. P. *J. Am. Chem. Soc.* **1992**, *114*, 4632.

(51) Keivanidis, P. E.; Laquai, F.; Robertson, J. W. F.; Baluschev, S.; Jacob, J.; Mullen, K.; Wegner, G. *J. Phys. Chem. Lett.* **2011**, *2*, 1893.

Chapter 4: Low-power noncoherent photon upconversion in fullerene-blue emitter systems in solution and thin polymer films

4.1 Introduction

In pursuit of exploring additional molecules (other than metalloporphyrins) possessing higher energy singlet states that are accessible by homomolecular TTA, we found the fullerene, C_{60} to be an excellent initial choice. The relevant photophysical properties of C_{60} are outlined in Table1. The triplet (T_1) energy of C_{60} is similar to the triplet energy of ZnTPP (E_T = 1.5 eV)[1] and C_{60} has a fairly long triplet lifetime (of the order of 0.1 ms).[2] It was proposed that the first electric-dipole allowed one electron transition to a singlet state of C_{60}, derived from the fluorescence excitation spectrum in a neon matrix at 4K, lies between 400 nm and 410 nm.[3] This transition peaks at 407 nm (3.04 eV) for C_{60} in toluene (toluene is the solvent chosen in most of our experiments because it doesn't form charge transfer complexes with C_{60}). The energy of this state is slightly lower than double the energy of the triplet state of C_{60}, which satisfies the energy conservation requirements of TTA. Thus the state which lies at 3.04 eV can, in principle, act as the initial product excited state of homolecular TTA in C_{60}. In fact, P-type delayed fluorescence due to TTA was detected from a higher fullerene, C_{70}, in toluene; even though E-type delayed fluorescence due to T_1 to S_1 thermal activation complicated this process.[4] C_{60} has closed shells with high symmetry (I_h) which forbids one-photon transitions from the ground state to other "*gerade*" states. This results in a very low S_1 fluorescence quantum yield of C_{60}

($\phi_{f,S1}$ = 3.2 × 10^{-4}).[5] This low quantum yield makes the observation of the delayed fluorescence due to TTA in C_{60} difficult.

We have established[6] that ZnTPP forms ground state aggregates with C_{60} (the sensitizer used in the present study) and when excited in both its Soret and Q-bands, the ZnTPP:C_{60} complex forms charge-separated states (see Chapter 6 of this thesis). The Soret excited species forms the charge-separated species on a subpicosecond time scale. Electron transfer between the triplet states of ZnTPP and fullerenes have been reported previously;[7] direct excitation of ZnTPP resulted in electron transfer from the porphyrin triplet to C_{60} and C_{70}, whereas excitation of the fullerene resulted in electron transfer from the ground state of ZnTPP to the triplet fullerene.[8] Considering the photophysical properties of the porphyrin and fullerene, it might be expected that both the porphyrin and fullerene could be used alone or together as potential sensitizers and upconverters in conjunction with a blue emitting molecule to form efficient NCPU units. However such an assumption may be complicated by the competitive absorption of the excitation light by both porphyrin and fullerene and competitive or sequential electron transfer and energy transfer between the singlet and triplet states of the porphyrin, fullerene and the blue emitter.

In consideration of the prospect of using fullerenes in the NCPU schemes as an efficient stand-alone sensitizer and upconverter or in combination with another sensitizer-upconverter such as ZnTPP, we have attempted to study the spectroscopy and kinetics of the NCPU process in model fullerene – BE systems in both solution and thin polymer

films. In our studies, C_{60} was selected as the sensitizer and perylene (P) and anthanthrene (An) were chosen as the blue emitter molecules. The photophysical properties of C_{60}, P and An are listed in Table 4.1.

Table 4.1 Photophysical properties of C_{60}, P and An in solution.

	C_{60}	Perylene	Anthanthrene	References
$E(S_n)$ (eV) (n ~ first dipole allowed state greater than n = 1)	3.04	-	-	3
$E(S_1)$ (eV)	1.7	2.7	2.8	1,9,10
$E(T_1)$ (eV)	1.5	1.5	1.4	1,11,10
$\tau(S_n)$ (ps)	0.25	-	-	5
$\tau(S_1)$ (ns)	1.2	5.5	(2.8, 3.8)	(5,12),9,(13,14)
$\tau(T_1)$ (ms)	0.14	1.1	0.11	2,9,14
η_{ISC} (direct excited)	1.0	1.0×10^{-2}	-	5,9
$\phi_{f,S1}$ (direct excited)	3.2×10^{-4}	0.98	0.24	5,9,13

Recent research by Wu et al.[15] has shown that C_{60} and its dyads with bodipy can be used as efficient triplet sensitizers for NCPU. These dyads show enhanced molar absorptivities in the 400 – 600 nm spectral region compared to pristine C_{60}. In the presence of the BE, perylene, the dyads exhibit NCPU of greater efficiency. It was demonstrated that the triplet state of C_{60} in toluene is quenched by P with a rate constant $k_q = 0.25 \times 10^9$ $M^{-1}s^{-1}$ which results in a NCPU quantum yield of 2.4 % and an upconversion efficiency of 30.9 %. Steren et al.[16] reported that both energy transfer and electron transfer are possible between triplet C_{60} and P forming triplet perylene and a

charge transfer state ($C_{60}^{\cdot -}...P^{\cdot +}$) respectively with a total quenching constant of (1.4 ± 0.1) × 10^9 $M^{-1}s^{-1}$ in benzonitrile. They estimated that the energy transfer process is more efficient (ϕ_{TTET} = 0.76 ± 0.15) than the electron transfer process (ϕ_{ET} = 0.26 ± 0.03, 0.20 ± 0.07), that the energy transfer process is almost thermoneutral and that despite the reasonably favourable value of ΔG_{ET}, the electron transfer rate (k_{ET} = (3.6 ± 0.4) × 10^8 $M^{-1}s^{-1}$) is slower than the energy transfer rate (k_{TTET} = (1.1 ± 0.2) × 10^9 $M^{-1}s^{-1}$) because of the large reorganization energy barrier of the molecules in the charge transfer state.

The triplet energy of An is slightly lower than the triplet energy of P and C_{60}. However, the triplet state lifetime of An is shorter than that of P and is comparable to the triplet lifetime of C_{60}. To the best of our knowledge, there are no published literature data for the triplet-triplet interaction between C_{60} and An.

4.2 Results and Discussion

Fig. 4.1 displays the absorption spectra of C_{60}, P and An in toluene. They are separately normalized to the respective absorption value of its highest peak. The spectra of these compounds are identical to the previously reported solution state spectra.[1,3,9,13,17] The inset shows the detailed absorption spectra in the region 15,000 – 21,000 cm^{-1}, which shows that the absorption of P and An approaches a value of zero at the excitation wavelength (532 nm, 18,796 cm^{-1}) used for the NCPU experiments in toluene. At this wavelength, the molar extinction coefficient of C_{60} is 1.1 × 10^3 M^{-1} cm^{-1}. Despite the low

value of the molar extinction coefficient, reasonable upconverted emission intensities were observed for C_{60}:BE pairs (*vide infra*).

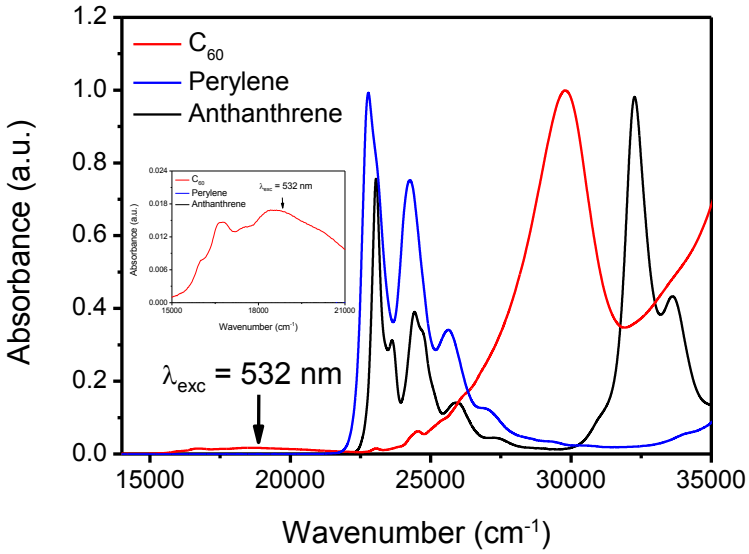

Fig. 4.1 Separately normalized absorption spectra of C_{60} (red curve), perylene (blue curve) and anthanthrene (black curve) measured in toluene. The spectra were normalized with respect to the absorbance of the highest peak. The inset shows the spectral region from 15,000 – 21,000 cm^{-1} in greater detail. The excitation wavelength 532 nm (18,796 cm^{-1}) for the NCPU measurements is shown in the figure as well as in the inset.

Absorption spectra of a constant concentration of C_{60} in toluene with varying concentrations of the BEs were measured. Absorption spectra of the individual BEs in toluene at each of the measured concentrations were subtracted from the corresponding mixture spectra of C_{60} and BEs. The difference spectra exhibit no changes in spectral band shape or in peak intensity, and no additional bands were produced. Slight variations in the spectral intensity with the addition of the BE were attributed to the variations in concentrations of C_{60} and the BE due to the uncertainties associated with the solution

preparation. In any case, the difference spectra suggest that the ground state association between C_{60} and these BEs is negligible in toluene.

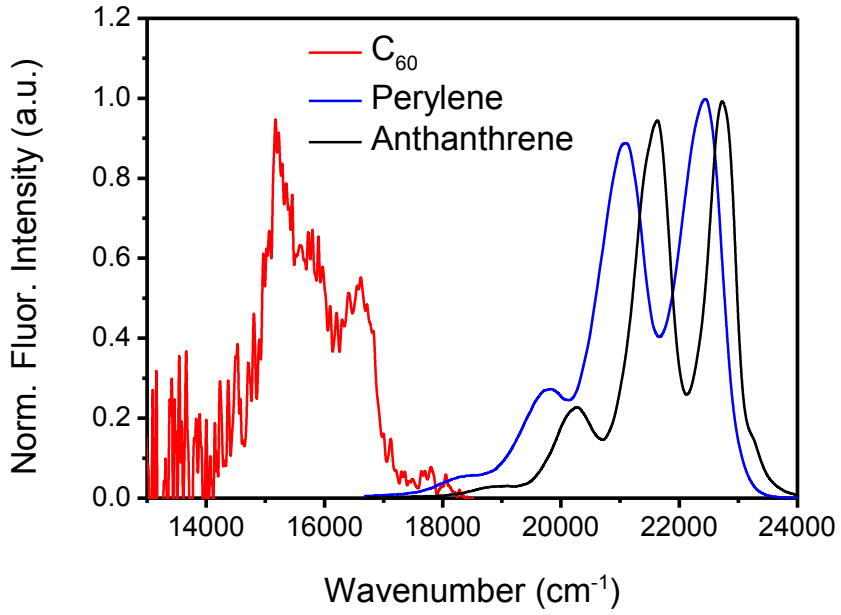

Fig. 4.2 Separately normalized prompt fluorescence spectra of (i) 2.8×10^{-5} M C_{60} in toluene (red curve) excited at 407 nm (2,4570 cm^{-1}), (ii) 1.2×10^{-5} M perylene in toluene (blue curve) excited at 400 nm (25,000 cm^{-1}) and (iii) 1.0×10^{-4} M anthanthrene in toluene (black curve) excited at 400 nm (25,000 cm^{-1}).

Fig. 4.2 displays the corrected fluorescence spectra resulted from prompt, one-photon excitation of C_{60}, P and An which are separately normalized to the highest fluorescence intensity. These spectra are corrected for background scatter from the solvent, fluorescence reabsorption effects, and the variation of the detector sensitivity with wavelength.[18] These spectra resemble the corresponding prompt, one-photon excited fluorescence spectra in solution reported in literature.[1,9,13] Note that the emission

spectrum of C_{60} extends into the near-IR region (550 – 750 nm), and thus overlaps negligibly with the emission spectra of P and An.

Upconverted S_1 fluorescence from both P and An mixed with C_{60} in toluene was obtained upon excitation of C_{60} at 532 nm. The upconverted fluorescence was slightly red-shifted compared to the prompt one-photon actuated S_1 fluorescence spectrum of the BEs because of reabsorption by C_{60} and BE in the solution. Contributions due to this effect and the effects due to solvent background scatter were corrected according to the method reported previously.[18-19] No upconverted fluorescence was observed from an air saturated C_{60}+BE solution in toluene excited at 532 nm because of the quenching of the triplet states of C_{60} and the BE by molecular oxygen. In addition, solutions of C_{60} or BE alone in toluene excited at 532 nm showed no upconverted emission under otherwise identical experimental conditions. These control experiments indicate that the fluorescence observed from the C_{60}+BE solutions is due to the TTA in these molecules.

4.2.1 Photon upconversion in C_{60} and Perylene system in solution

To verify that the fluorescence from P with added C_{60} is due to the TTA process, the $\log_{10}$ of the observed fluorescence intensity from a fixed concentration of C_{60} and P in toluene was plotted against the $\log_{10}$ of the incident laser power density as shown in Fig. 4.3. It should be noted that under low-power irradiation range, the plots are expected to show a slope close to 2 and under high-power irradiation conditions, the slopes tend to deviate to a value closer to 1. In the low-power threshold, processes such as quasi-first order triplet deactivation processes (e.g., relaxation of the triplet state to the ground

singlet state through either radiative or nonradiative channels) and triplet quenching dominate, thus resulting in a slope close to 2. However, at higher laser power, the annihilation efficiency is maximized because of the higher probability of TTA due to a high triplet concentration, which results in a slope closer to 1.[20]

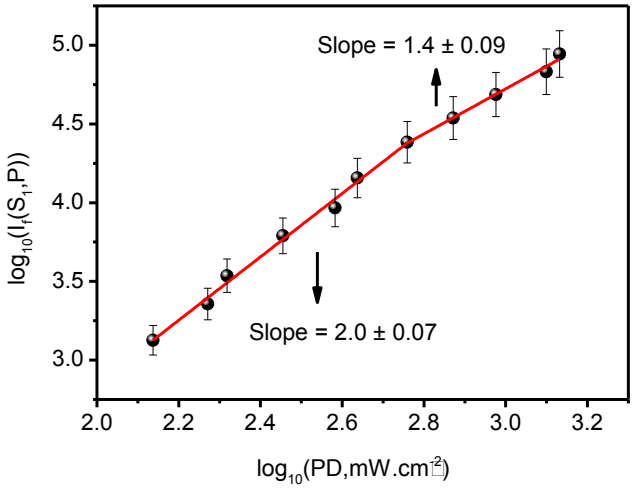

Fig. 4.3 Double logarithmic plot of the upconverted fluorescence intensity *vs.* incident laser density for an equimolar (1.0×10^{-4} M) mixture of C_{60} mixed with P. All the samples were excited with a cw 532 nm laser, the excitation monochromator band width was fixed at 2.0 nm and the emission band pass was fixed at 4.0 nm. R^2 = 0.99 for the least-squares fit.

Because the laser power corresponding to the point of deviation from a slope of 2 is reported to cause the highest TTA efficiency,[20a,b] a laser power density of 0.28 W. cm^{-2} was used for further steady state upconversion measurements. However, multi-photon ionization spectra of 5 micromolar perylene in n-hexane demonstrated that simultaneous two-photon, three-photon and four-photon absorption processes could occur at laser excitation powers as low as 0.5 mW.[21] In our case, the excitation power density used was

greater than this lower limit. Therefore it can be suspected that multi-photon absorption processes may have complicated the kinetics of the NCPU processes in our studies (*vide infra*).

The triplet energy of C_{60} and P are almost the same (1.5 eV, 12,098 cm^{-1}).[1,11] Considering the uncertainties associated with the measurements of these values, it can be reasonably assumed, for the following reaction under continuous irradiation conditions,

$$T_1(C_{60}) + S_0(BE) \underset{k_{TTBET}}{\overset{k_{TTET}}{\rightleftharpoons}} S_0(C_{60}) + T_1(BE) \qquad \text{(i)}$$

that the fractional population of the triplets of C_{60} and P would be controlled by the ratio of the triplet energy transfer rate constant (k_{TTET}) and the triplet back energy transfer rate constant (k_{TTBET}) according to the following relation,

$$\frac{k_{TTET}}{k_{TTBET}} = \exp\left(-\frac{\Delta H}{k_B T}\right) \qquad (4.1)$$

where ΔH is the enthalpic cost associated with the triplet energy transfer and back energy transfer, k_B is the Boltzmann constant and T is the temperature in K. For C_{60} and P, ΔH is nearly zero and therefore, $k_{TTET} \approx k_{TTBET}$, i.e., the triplet back energy transfer can be nearly as efficient as the triplet energy transfer.

According to Schmidt et al.,[22] the entropy change associated with triplet energy transfer and triplet back energy transfer are given by,

$$(\Delta S)_{TTET} = k_B \ln\left(\frac{[T_1(C_{60})][S_0(BE)]}{[T_1(BE)][S_0(C_{60})]}\right) \qquad (4.2)$$

$$(\Delta S)_{TTBET} = k_B \ln\left(\frac{[T_1(BE)][S_0(C_{60})]}{[T_1(C_{60})][S_0(BE)]}\right) \qquad (4.3)$$

These equations had been derived using Stirling's approximation and because this approximation holds only for large numbers of species, equations (4.2) and (4.3) do not hold for any of the triplet concentrations approaching zero.

(A) **(B)**

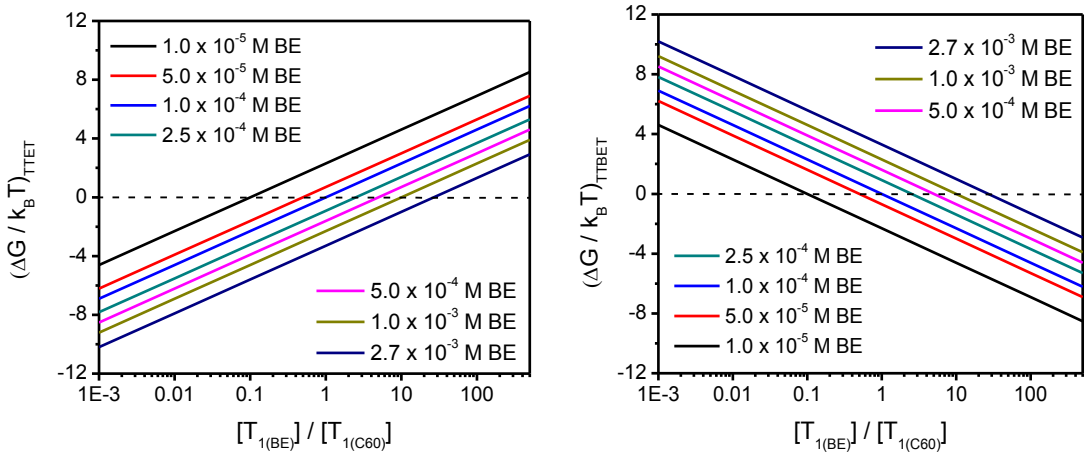

Fig. 4.4 Gibbs free energy change (ΔG) associated with TTET and TTBET according to the process proposed by Schmidt et al.[22] and given by equations (4.4) and (4.5). The concentration of C_{60} was kept at a constant value, $[S_0(C_{60})] = 1.0 \times 10^{-4}$ M and the concentrations of the blue emitters (P) are the experimental concentrations used in Fig. 4.5.

The value of ΔS will be large at the beginning of energy transfer because at this point $[T_1(C_{60})] \gg [T_1(BE)]$. However, as time elapses, triplet energy transfer will result in decay of the triplet population of C_{60} with a concomitant build-up of the population of the T_1 state of P, which would decrease the value of ΔS. However, as $[T_1(BE)]$ starts to increase, triplet back energy transfer will start depopulating the T_1 state of P. This will

increase [$T_1(C_{60})$], thus increasing the ΔS. Both C_{60} and P are rigid molecules, therefore changes in entropy due to differences in intermolecular vibrational freedom can be assumed to be negligible. Since the value of ΔH associated with TTET and TTBET is close to zero, we can reasonably assume that the free energy changes associated with TTET and TTBET is dependent upon the entropy factor which again depends on the concentrations of C_{60} and P in the ground singlet state and the triplet states.

The free energy changes associated with TTET and TTBET are thus given by,

$$(\Delta G/k_B T)_{TTET} = -\ln\left(\frac{[T_1(C_{60})][S_0(BE)]}{[T_1(BE)][S_0(C_{60})]}\right) \quad (4.4)$$

$$(\Delta G/k_B T)_{TTBET} = -\ln\left(\frac{[T_1(BE)][S_0(C_{60})]}{[T_1(C_{60})][S_0(BE)]}\right) \quad (4.5)$$

where T is the temperature in K.

The dependence of ΔG for TTET and TTBET on the branching ratios of the triplet population of the BE and C_{60} at a constant concentration of C_{60} and varying concentrations of BE are demonstrated in Fig. 4.4 (A) and (B) respectively. Note that at lower singlet emitter concentrations ([S_0(P)] < [$S_0(C_{60})$]), TTET becomes exergonic (ΔG < 0) for branching ratios of the triplets [T_1(P)]/[$T_1(C_{60})$] < 1. For [S_0(P)] > [$S_0(C_{60})$], TTET is exergonic only for [T_1(P)]/[$T_1(C_{60})$] < 50. For triplet branching ratios > 50, TTET is endergonic (ΔG > 0) at all the concentrations employed. Under identical experimental conditions, the sign of ΔG just reverses for TTBET. For [S_0(P)] < [$S_0(C_{60})$], TTBET is endergonic for [T_1(P)]/[$T_1(C_{60})$] < 1 and starts to become exergonic only for

$[T_{1(P)}]/[T_{1(C60)}] > 1$. For $[S_0(P)] > [S_0(C_{60})]$, TTBET is predominantly endergonic for $[T_1(P)]/[T_1(C_{60})] < 50$. However for branching ratios above 50, TTBET is exergonic for all the concentrations of the blue-emitter used. However, it should be noted that the triplet lifetime of P (τ_T = 1.1 ms)[9] is much greater than the triplet lifetime of C_{60} (τ_T = 0.13 ms).[2] Therefore the triplet state of P could act as a reservoir of the triplet population and therefore on longer timescales TTBET from this state can be significant.

Fig. 4.5 displays the $\log_{10}$-$\log_{10}$ plot for upconverted fluorescence from varying concentrations of P with added C_{60} in toluene excited at 532 nm under constant irradiation power. The plot has a slope of 2 in the lower concentration range of P whereas the slope decreases to around 1 at P concentrations approaching 1 mM. This is consistent with the predictions by equations (4.4) and (4.5).

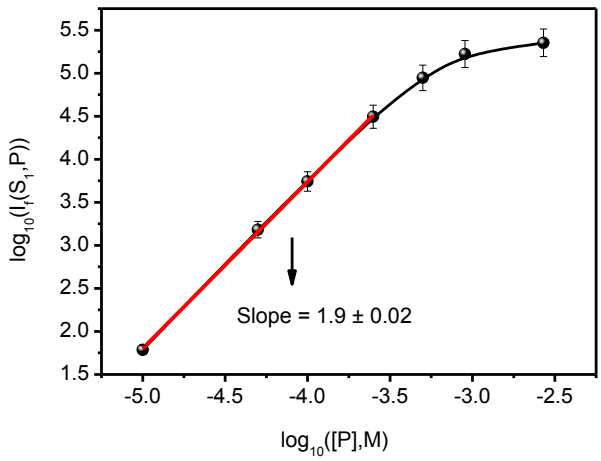

Fig. 4.5 Double logarithmic plot of upconverted fluorescence intensity *vs.* the concentration of the BE in 1.0×10^{-4} M C_{60} and various concentrations of P. Excitation was with a cw 532 nm laser and the laser power was fixed at 0.28 W/cm^2. The emission band pass was fixed at 0.4 nm. R^2 = 0.99 for the least-squares fit.

At lower concentrations of P, the process of NCPU is dominated by the unimolecular decay processes and the quenching of the triplet state of C_{60}. However at higher concentrations of P, triplet quenching of C_{60} by P will result in a high yield of triplet P. This would maximise the probability of TTA in P and thus would result in a slope close to 1. Above a 1 mM P concentration, a slope of about 0.3 is observed, presumably because at this concentration TTET is nearly quantitative resulting in saturation of the triplet concentration of P. Therefore, above this threshold, further increases in the concentration of P do not influence the rate of TTA in P, but rather could increase the probability of reabsorption by P. The nonlinearity of the dependence of the upconverted intensity on the emitter concentration was previously observed in the upconverted fluorescence from ZnTPP+P in benzene excited at 532 nm.[19] It should be noted that a higher concentration of triplet P could be achieved at higher concentrations of P and that could enhance TTBET from triplet P to C_{60}. In addition, ground state depletion of P by triplet C_{60} via electron transfer[16] could complicate the kinetics (*vide infra*).

In order to examine the kinetics of processes associated with NCPU for C_{60}+P in toluene, triplet-triplet transient absorption spectra of C_{60}, P and C_{60}+P in toluene and the corresponding transient kinetics were measured. Fig. 4.6 demonstrates the $T_1 \rightarrow T_n$ transient absorption spectrum of 1×10^{-4} M C_{60} in toluene excited at 532 nm. The spectrum is similar to the spectra reported in literature[5,23] except for a narrow dip in the absorbance at around 420 nm. The spectral band at 750 nm was observed earlier and was attributed to the absorption from the lowest lying triplet state of C_{60}. The molar extinction coefficient of this state is 16,100 $M^{-1}cm^{-1}$ at this wavelegnth.[5]

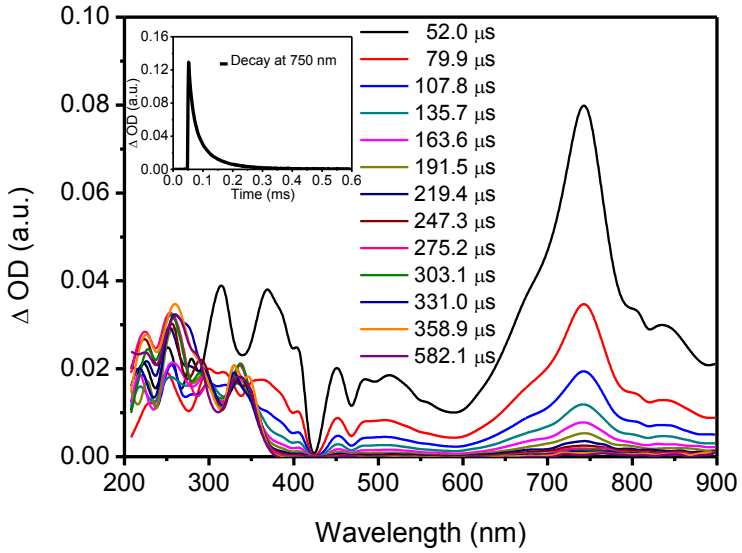

Fig. 4.6 $T_1 \rightarrow T_n$ transient absorption spectrum of 1×10^{-4} M C_{60} in toluene excited at 532 nm. Inset shows the transient absorption decay measured at 750 nm. The laser pulse width was 5 ns and the laser power density at the sample was 0.34 $W.cm^{-2}$.

The inset of Fig. 4.6 shows the transient absorption decay of the triplet measured at 750 nm. The rate of this decay is very similar to the decay in toluene measured by Fujitsuka and Ito,[5] but shorter than the decay in toluene measured by Weisman. Weisman measured a unimolecular triplet lifetime of C_{60} ~ 133 μs under conditions which suppressed bimolecular processes.[2a] But the triplet decay was found to be strongly quenched with an increase in C_{60} concentration because of an increase in the rate of TTA in C_{60}. Fujitsuka and Ito[5] reported an intrinsic first-order triplet decay rate constant to be $k_1 \sim 4 \times 10^4$ s^{-1} and the rate constant of bimolecular TTA to be $k_{TTA} \sim 1.1 \times 10^9$ M^{-1} s^{-1} respectively. Ebbesen et al.[12] reported a bimolecular TTA rate constant of $k_{TTA} \geq 4.8 \times 10^9$ $M^{-1}s^{-1}$ for C_{60} in toluene. This shows that TTA in C_{60} is a very efficient process.

(A)

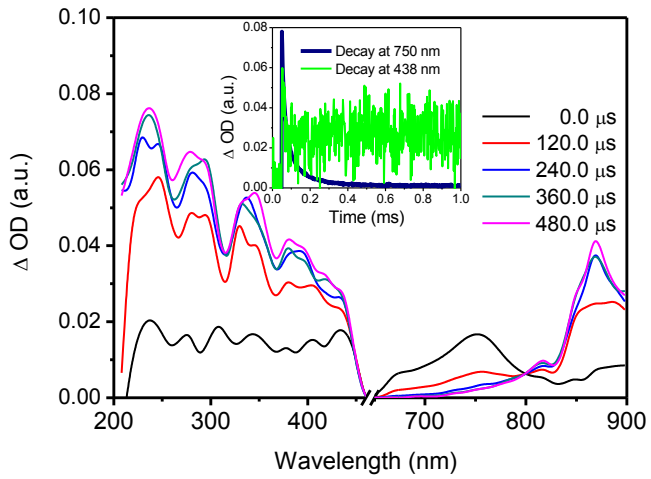

(B)

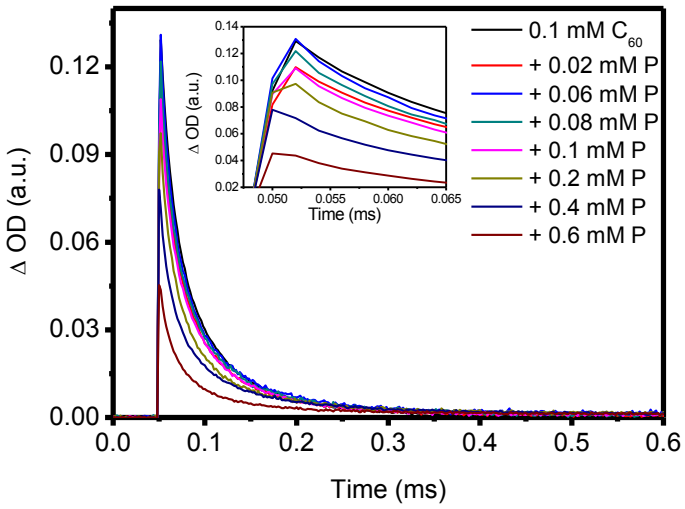

Fig. 4.7 (A) $T_1 \rightarrow T_n$ transient absorption spectrum of 1×10^{-4} M C_{60} and 1×10^{-4} M P in toluene excited at 532 nm. The inset shows the transient absorption decay measured of C_{60} at 750 nm and the transient absorption build-up of P at 878 nm. (B) Transient absorption decay of C_{60} at 750 nm measured as a function of P concentration. The laser pulse width was 5 ns and the laser power on density on the sample was 0.34 W.cm^{-2}.

Fig. 4.7 (A) demonstrates the triplet transient absorption spectrum of C_{60} with added P in toluene. With increasing concentrations of P, the peak absorbance at t = 0 for the $T_1 \rightarrow T_n$ absorption of C_{60} observed at 750 nm is reduced with a concomitant build-up of two peaks at around 818 and 878 nm. These peaks can be identified as the blue-edge shoulders of a broad peak corresponding to the formation of $C_{60}^{\cdot -}$ due to electron transfer from the perylene ground state to triplet C_{60}.[16] The spectra corresponding to the build-up of ^3P and $P^{\cdot +}$ in benzonitrile were reported and their absorption maxima were found at 485 and 555 nm respectively.[16]

Our experiments of the transient absorption of ^3P obtained by exciting perylene in toluene at 532 nm showed an absorption peak at 438 nm, corresponding to the $T_1 \rightarrow T_n$ absorption of P. However the signature absorption band of the ^3P species was overlapped with the absorption of $^3C_{60}$ in Fig. 4.7 (A). Nevertheless, the transient absorption kinetics measured at 438 nm showed a rapid decay in the initial time-period followed by a transient build-up corresponding to the population of the triplet state of P. Negligible absorption was obtained between 450 – 650 nm where the transient absorption due to $P^{\cdot +}$ should be observed. This could be due to the fact that $P^{\cdot +}$ abstracts hydrogen from toluene solvent forming PH^+, thus reducing the concentration of $P^{\cdot +}$.[21]

Fig. 4.7 (B) shows the transient absorption kinetic signals of 532 nm excited $^3C_{60}$ in toluene with added P. The data clearly show a reduction in the initial concentration of $^3C_{60}$ at t = 0 as well as quenching of the temporal decay upon adding P, in agreement with the results of Wu et al.[15] A number of kinetic processes are possible when P is added to

C_{60}. They are unimolecular decay of $^3C_{60}$ (k_1), homomolecular TTA in C_{60} ($k_{TTA(1)}$), heteromolecular TTA between C_{60} and P ($k_{TTA(2)}$), quenching of $^3C_{60}$ by P (k_q) through electron transfer from P to $^3C_{60}$ (k_{ET}) and energy transfer from $^3C_{60}$ to P (k_{TTET}) ($k_q = k_{ET} + k_{TTET}$) and triplet back energy transfer from ^{3}P to C_{60} at longer time scales (k_{TTBET}). The rate of decay of $^3C_{60}$ with added P after excitation is represented by the equation,

$$\frac{\mathrm{d}[T_1(C_{60})]_t}{\mathrm{dt}} = -k_1[T_1(C_{60})]_t - k_{TTA(1)}[T_1(C_{60})]_t^{\,2} - k_{TTA(2)}[T_1(C_{60})]_t[T_1(P)]_t - k_q[T_1(C_{60})]_t[S_0(P)]_t + k_{TTBET}[S_0(C_{60})]_t[T_1(P)]_t \quad (4.6)$$

In the initial times of $^3C_{60}$ decay, the unimolecular decay, homomolecular TTA in C_{60} and the triplet quenching of C_{60} by P dominate over other bimolecular processes such as heteromolacular TTA. At times approaching zero, the rate of decay of the initial triplet concentration of C_{60} normalized to the triplet concentration at t = 0 can be given by,[22]

$$\frac{\left.\frac{\mathrm{d}[T_1(C_{60})]_t}{\mathrm{dt}}\right|_0}{[T_1(C_{60})]_0} = -\left\{\left(k_1 + k_q[S_0(P)]_0\right) + k_{TTA(1)}[T_1(C_{60})]_0\right\} \quad (4.7)$$

Thus, following the procedure proposed by Schmidt et al.,[22] a fit of equation (4.7) as a tangent through the initial part of the decay can provide the terms, ($k_1 + k_q[S_0(P)]$) and $k_{TTA(1)}$ at each of the concentrations of P. The rate constants obtained are tabulated in Table 4.2.

Table 4.2 Quasi-first order rate constants for the decay of the triplet state of C_{60} as a function of P concentration.

Concentration of P added (M)	$k_1+k_q[S_0(P)]_0 / 10^4$ (s^{-1})	$k_{TTA(1)} / 10^9$ ($M^{-1}s^{-1}$)
0	2.24 (k_1)	1.07
2×10^{-5}	2.56	1.30
6×10^{-5}	2.87	1.49
8×10^{-5}	2.91	1.52
1×10^{-4}	2.98	1.57
2×10^{-4}	3.39	1.92
4×10^{-4}	3.46	1.98
6×10^{-4}	3.99	2.96

It should be noted that both the first order rate constants and the rate constant of TTA from the triplet state of C_{60} increases as a result of an increase in the concentration of added P. A plot of ($k_1+k_q[S_0(P)]$) versus the concentration of P is shown in Fig. 4.8.

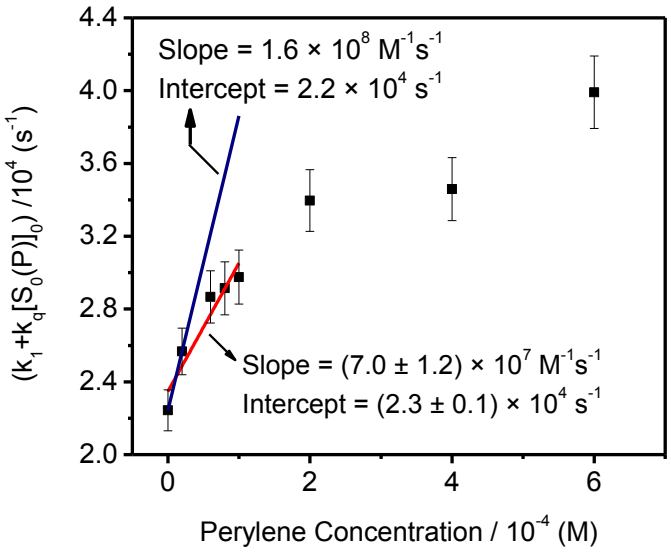

Fig. 4.8 Dependence of the quasi-first order rate constants of the decay of $^3C_{60}$ on the concentration of added P. R^2 = 0.89 for the least-squares fit.

The slope and intercept of a linear fit through the low perylene concentration region provided the rate constants, k_q = (7.0 ± 1.2) × 10^7 $M^{-1}s^{-1}$ and k_1 = (2.3 ± 0.1) × 10^4 s^{-1}, respectively. However, considering the errors associated with obtaining the (k_1+k_q[S_0(P)]) values by fitting at the very early parts of the decay and by considering the asymptotic nature of the plot in Fig. 4.8, we tend to fit the initial parts of the plot with a tangent and obtained the rate constants through the slope and intercept of the tangent. The obtained rate constants are, k_q = 1.6 × 10^8 $M^{-1}s^{-1}$, two orders of magnitude smaller than the diffusion controlled quenching rate constant k_d =1.1 × 10^{10} $M^{-1}s^{-1}$ and an order of magnitude smaller than the reported literature values of k_q and k_1 = 2.2 × 10^4 s^{-1}, in fair agreement with the reported values.[5,15-16]

Fig. 4.9 (A) shows the time-resolved spectra of the fluorescence from P in the presence of C_{60} in toluene excited at 532 nm. The spectra were not corrected for solvent scattering, excitation light attenuation due to absorption by C_{60}, or for re-absorption of the emitted light by C_{60} and P. Therefore the time-resolved emission bands show considerable distortions, and were severe in the 400-450 nm range because of large molar absorptivity of P in this region. The fluorescence measured at 470 nm showed that the decay persists up to around 300 μs indicating that it is originating from a very slow process rather than from unimolecular radiative decay of the S_1 state of the prompt, one-photon excited P. In addition, the fluorescence signal increases as the concentration of P increases (Fig. 4.9 (B)). Therefore it can be suggested that Fig. 4.9 (A) represents the delayed fluorescence from P due to TTA in ^{3}P which is populated by the TTET from $^3C_{60}$.

(A)

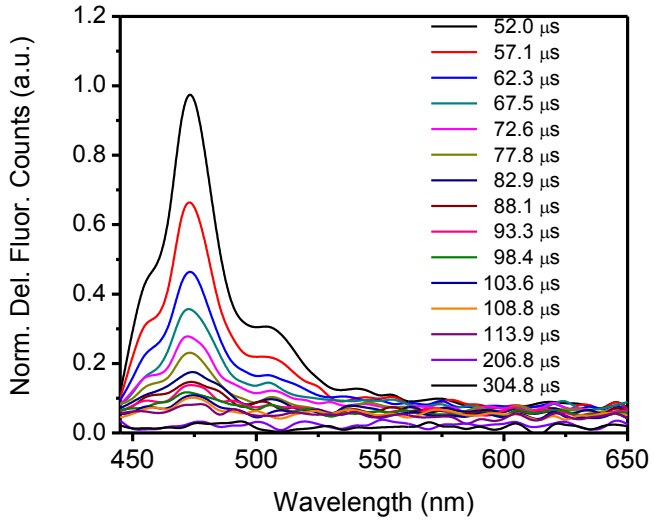

(B)

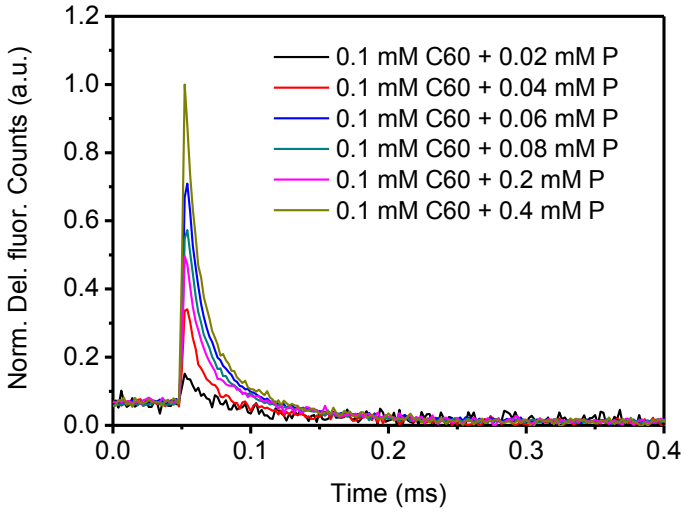

Fig. 4.9 (A) Time-resolved fluorescence spectrum of 1×10^{-4} M C_{60} and 1×10^{-4} M P in toluene excited at 532 nm. (B) Kinetic decay of fluorescence from various concentrations of P in presence of 1×10^{-4} M C_{60} measured at 470 nm. The laser pulse width was 5 ns and the laser power density incident on the sample was 0.34 $W.cm^{-2}$.

Multi-photon excitation processes in P have been reported under irradiation intensities as low as 1 mW.[21] The laser power used in our experiments was 19 mJ / pulse which are much greater than the laser power used in the multi-photon excitation studies of P. In order to assess whether multi-photon excitation processes interfere with the delayed fluorescence from C_{60} + P in toluene, we have tried to calculate the probabilities of absorption of light by P through one-photon (1PA) and two-photon (2PA) processes. The total probability of light absorption by C_{60} and P at 532 nm is given by,[24]

$$P_{total} = (P_{1PA})_{C_{60}} + (P_{1PA})_P + (P_{2PA})_P = 1$$

$$= (\sigma_{1PA} I)_{C_{60}} + (\sigma_{1PA} I)_P + (\sigma_{2PA} I^2)_P \qquad (4.8)$$

where σ_{1PA} and σ_{2PA} are the one-photon and two-photon absorption cross-sections respectively and I is the incident laser intensity.

σ_{1PA} can be calculated from the relation, $\sigma_{1PA} \approx (2.303\varepsilon C)/N$, where ε is the molar extinction coefficient of P at 532 nm (~ 44 $M^{-1}cm^{-1}$), C is the concentration of P (1× 10^{-4} M) and N is the number density of P molecules in unit volume (6.02 × 10^{16} per cm^3). From an estimate of $\sigma_{1PA} \approx 1.7 \times 10^{-19}$ cm^2 and the incident laser intensity, I = 0.34 Wcm^{-2} = 9.1 × 10^{19} photons cm^{-2} s^{-1}, the probability of one-photon absorption was calculated to be $(P_{1PA})_P \approx 0.15$. Makarov measured the two-photon absorption cross-section of P in CH_2Cl_2 within the wavelength range 560 – 1000 nm and found that σ_{2PA} increases from the longer wavelength to the shorter wavelength region and reaches σ_{2PA} = 5.4 × 10^{-50} $photon^{-1}cm^4s$ at 560 nm.[24a] The two-photon absorption cross-section of P in

toluene at 532 nm is not known, however, even for a very large hypothetical value of σ_{2PA} = 5.0 × 10^{-49} photon^{-1}cm^{4}s, $(P_{2PA})_P \approx 2.5 \times 10^{-13}$ is resulted, a very low value of the probability for a two-photon process. Considering these low light absorption probabilities and the facts that there are no immediate accepting singlet energy levels for one-photon absorption of P at 532 nm, it can be safely assumed that the contribution of light absorption by P is negligible in the delayed fluorescence from the S_1 state of P in C_{60}+P system.

A control experiment of P in toluene excited at 532 nm still showed that the fluorescence from P can be observed in the 440 – 500 nm range (appendix Fig. A.4.3). Fluorescence decay of P excited at 532 nm and measured at 470 nm showed a multiexponential decay which extended up to around 150 ns. The fluorescence emission of P excited at 355 nm was very weak and resulted in a very noisy signal. The decay at 470 nm observed for P in toluene excited at 355 nm (appendix Fig. A.4.4) showed a predominantly single exponential decay, the N/e population decay time constant of which was estimated to be around 7 ns which is close to the reported S_1 fluorescence lifetime of P. Therefore the fluorescence from P excited at 532 nm was slightly delayed compared to the one observed at 355 nm excitation but was shorter than the delayed fluorescence observed from C_{60}+P excited at 532 nm by around three orders of magnitude.

These results demonstrate that multi-photon excitation processes in P is not a significant factor when assessing the kinetics of the delayed fluorescence from P in the presence of C_{60} in toluene excited at 532. Therefore, the rate of decay of the

concentration of the S_1 state P with C_{60} excited at 532 as a function of time can be written as,[4,25]

$$\frac{\mathrm{d}[S_1(P)]_t}{\mathrm{dt}} = -k_{S1(P)}[S_1(P)]_t + \frac{1}{2}k_{TTA(P)}[T_1(P)]_t{}^2 \qquad (4.9)$$

which leads to,

$$\frac{\mathrm{d}\sqrt{I_{DF}(t)}}{\mathrm{dt}} = \sqrt{C}\ \frac{\mathrm{d}[T_1(P)]_t}{\mathrm{dt}}$$
$$= -k_{T1(P)}[T_1(P)]_t - k_{TTA(P)}[T_1(P)]_t{}^2 - k_{TTBET}[S_0(C_{60})]_t[T_1(P)]_t \qquad (4.10)$$

where $I_{DF}(t)$ is the time dependent delayed fluorescence intensity and C is a constant related to the instrument sensitivity, the rate constant for the formation of the encounter complex, the efficiency of TTA and the fluorescence quantum yield of the blue emitter.

Assuming that TTBET is negligible at t = 0, it can be written that,

$$\frac{\left.\frac{\mathrm{d}[T_1(P)]_t}{\mathrm{dt}}\right|_0}{[T_1(P)]_0} = -\{k_{T1(P)} + k_{TTA(P)}[T_1(P)]_0\} \qquad (4.11)$$

Fitting the square root of the normalized delayed fluorescence at t = 0 with a tangent can give a slope that is equal to $k_{T1(P)} + k_{TTA(P)}[T_1(P)]_0$. However, separating $k_{T1(P)}$ and $k_{TTA(P)}$ requires a knowledge of $[T_1(P)]_0$. This is difficult to extract because $[T_1(P)]_0$ is a variable in this case which depends upon the rate and efficiency of triplet energy transfer from C_{60} to P.

4.2.2 Photon upconversion in C_{60} and Anthanthrene system in toluene

The delayed fluorescence from C_{60}+An in toluene excited at 532 nm was found to be around 10 times more intense than that from C_{60}+P in toluene measured under identical experimental conditions. Fig. 4.10 (A) shows the $\log_{10}$-$\log_{10}$ plot of the dependence of the upconverted fluorescence from C_{60}+An in toluene excited at 532 nm on the incident laser power. The region of slope close to 2 represents the quasi-first order processes from $^3C_{60}$ whereas the region with slope close to 1 is where the TTA efficiency in An is maximized. The $\log_{10}$-$\log_{10}$ plot of the upconverted fluorescence intensity of C_{60}+An system as function of the concentration of An (Fig. 4.10 (B)) showed a slope = 1.3 below the 100 μM concentration range.

The T_1 state of An lies lower in energy than the T_1 state of C_{60} by a factor of $\Delta H = 800$ cm^{-1}.[1,10] Therefore the fractional population of thermally activated C_{60} triplets would be $[T_1^*]/[T_1] \approx 50$ and this would result in complete quantitative triplet energy transfer to An even at its lowest concentration. A quantitative triplet energy transfer can increase the probability of TTA in An, thus resulting in a slope close to 1. However, above 100 μM concentration of An, the slope diminishes rapidly to 0.6 and then to zero at higher concentrations of An. This may be due to the fact that TTET would be quantitatively complete at higher concentrations of An so that a further increase in the concentration would have no influence on the rate of TTA and rather acts as a photon wasting process.

(A)

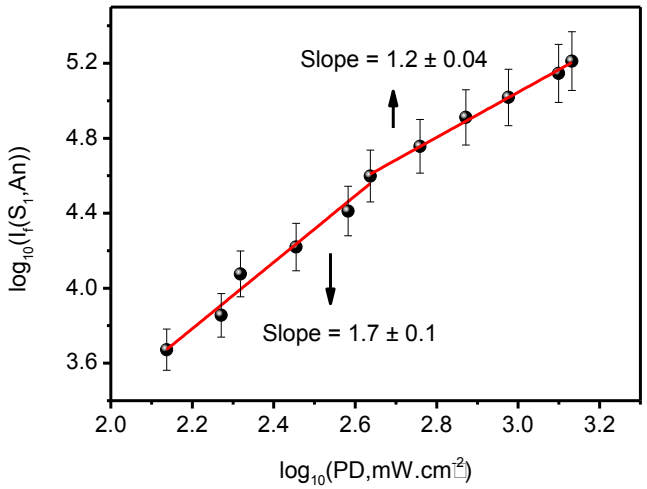

(B)

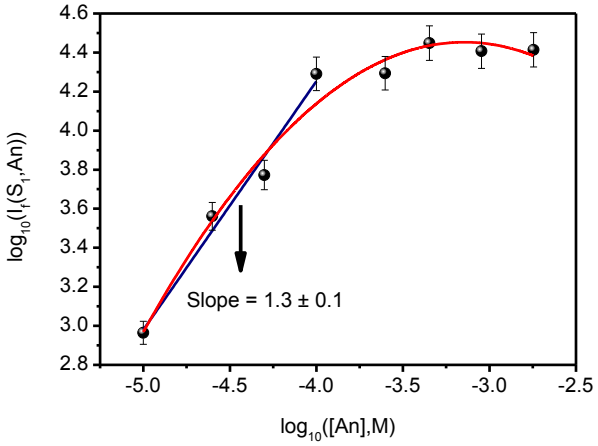

Fig. 4.10 Double logarithmic plot of (A) upconverted fluorescence intensity *vs.* the incident laser power density on an equimolar (1.0×10^{-4} M) mixture of C_{60} mixed with An. All the samples were excited with a cw 532 nm laser, the excitation monochromator band width was fixed at 2.0 nm and the emission band pass was fixed at 4.0 nm. R^2 = 0.97 in the lower intensity region and R^2 = 0.99 in the higher intensity region for the least-squares fit and (B) upconverted fluorescence intensity *vs.* the concentration of the BE in 1.0×10^{-4} M C_{60} and various concentrations of An. Excitation was at 532 nm and the laser power was fixed at 0.28 W/cm^2. Emission band pass was fixed at 0.2 nm. R^2 = 0.97 for both the linear fit and the polynomial fit.

(A)

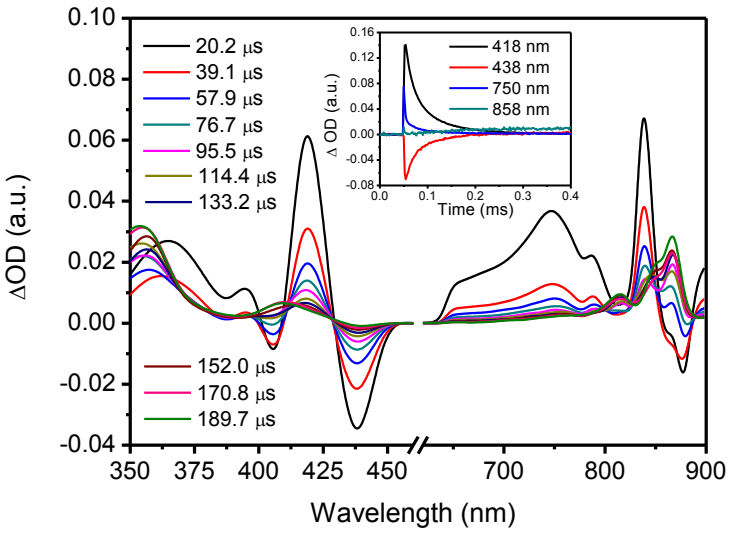

(B)

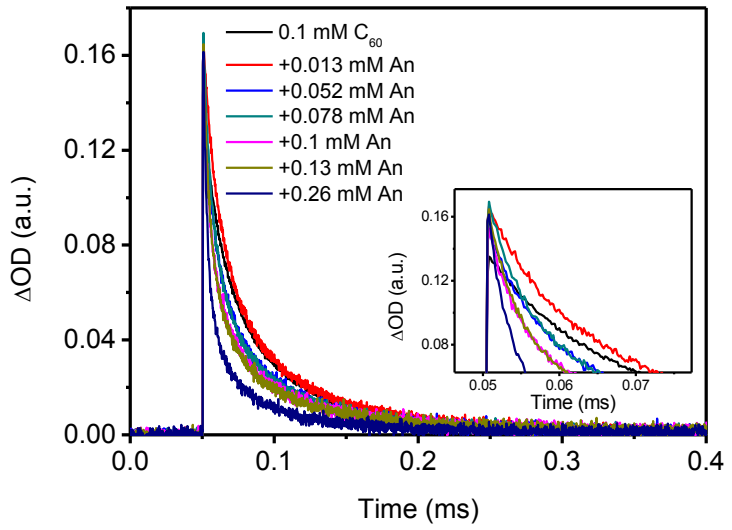

Fig. 4.11 (A) $T_1 \rightarrow T_n$ transient absorption spectrum of 1×10^{-4} M C_{60} + 5.2×10^{-4} M An in toluene excited at 532 nm. The inset shows the transient signals measured at 418, 438, 750 and 858 nm. (B) Transient absorption decay of C_{60} at 750 nm measured as a function of An concentration. The laser pulse width was 5 ns and the laser power density at the sample was 0.34 W.cm^{-2}.

Fig. 4.11 (A) shows the triplet transient absorption spectra of C_{60} excited at 532 nm in the presence of An. The spectra show peaks at 750 nm due to $^3C_{60}$ and at 418, 838 and 868 nm due to ^{3}An. The steady state absorption spectrum of An has maxima at 408 and 438 nm with large molar extinction coefficients and the spectra in Fig.4.13 (A) show bleaching at the these wavelengths. In addition, a small amount of bleaching can be observed at 878 nm. The inset of Fig. 4.11 (A) shows the transient kinetic signals observed at 418, 438, 750 and 858 nm. The transient decay observed at 418 nm and the rise at 438 nm show similar but inverted temporal profiles suggesting that bleaching does occur from the state that corresponds to the transition at 418 nm. The decay observed at 750 nm is quenched and persists only up to 200 μs compared to the decay of C_{60} alone in toluene. The signal observed at 858 nm showed a very sharp decay followed by a rise to 200 μs followed by a further steady rise up to 800 μs. Fig. 4.11 (B) demonstrates the quenching of the triplet absorption decay of C_{60} with added An.

Unlike the C_{60}+P system, the transient absorbance at t = 0 is found not to be reduced significantly with an increase of An concentration. Rather, the temporal decay is found to be quenched on adding An. An energy difference of 800 cm^{-1} between the triplets of C_{60} and An suggests that TTET should be at least 50 times more efficient than TTBET. In this case, the rate of decay of the concentration of triplet C_{60} after excitation will be given by,[22]

$$\frac{\mathrm{d}[T_1(C_{60})]_t}{\mathrm{dt}} = -k_1[T_1(C_{60})]_t - k_{TTA(1)}[T_1(C_{60})]_t^{\,2} - k_q[T_1(C_{60})]_t[S_0(An)]_t \qquad (4.12)$$

which, at t = 0, would lead to the following equation,

$$\frac{\left.\frac{\mathrm{d}[T_1(C_{60})]_t}{\mathrm{dt}}\right|_0}{[T_1(C_{60})]_0} = -\{(k_1 + k_q[S_0(An)]_0) + k_{TTA(1)}[T_1(C_{60})]_0\} \qquad (4.13)$$

Following the method of Schmidt et al.,[22] values of (k_1 + k_q[S_0(An)]$_0$) and $k_{TTA(1)}$ obtained by fitting the early part of the normalized decays shown in Fig. 4.13 (B) with equation (4.13) are given in Table 4.3. A plot of (k_1 + k_q[S_0(An)]$_0$) *versus* [S_0(An)] is shown in Fig. 4.12. This plot provided the rate constants k_1 = (2.2 ± 0.2) × 10^4 s^{-1} and k_q = (2.2 ± 0.2) × 10^8 $M^{-1}s^{-1}$ which is two orders magnitude smaller than the diffusion controlled quenching rate constant k_d =1.1 × 10^{10} M^{-1} s^{-1}. These results show that the quenching is more efficient in the C_{60}+An system than the C_{60}+P system, presumably because of the triplet energy difference between C_{60} and An.

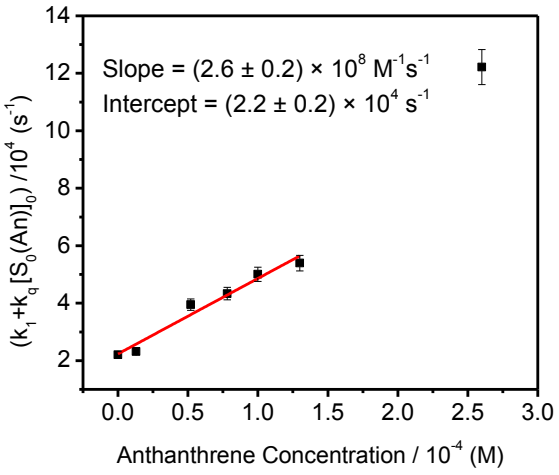

Fig. 4.12 Dependence of the quasi-first order rate constants of the decay of $^3C_{60}$ on the concentration of added An. The fit to the data is according to equation (4.13) which was derived based on the process proposed by Schmidt et al.[22] R^2 = 0.96 for the least-squares fit.

Table 4.3 Quasi-first order rate constants of the triplet state of C_{60} as a function of An concentration.

Concentration of An added (M)	$k_1+k_q[S_0(An)]_0 / 10^4$ (s^{-1})	$k_{TTA(1)} / 10^9$ (M^{-1} s^{-1})
0	2.24 (k_1)	2.60
1.3×10^{-5}	2.32	2.74
5.2×10^{-5}	3.94	2.04
7.8×10^{-5}	4.33	2.22
1.0×10^{-4}	5.00	2.57
1.3×10^{-4}	5.39	2.76
2.6×10^{-4}	12.21	6.16

The time-resolved delayed fluorescence from An+C_{60} in solution is shown in Fig. 4.13 (A). The spectrum closely resembles the one-photon, prompt excited fluorescence spectrum of An[13] except for the segment of the spectrum at $\lambda < 425$ nm where the fluorescence reabsorption effects are significant. In addition to the bands usually observed, the delayed emission showed a weak broad emission centred at around 560 nm. Fig. 4.13 (B) shows the kinetics of the transient emission signal observed at 464 nm as a function of the concentration of An. Obviously, as the concentration of the emitter increases, the intensity of the delayed fluorescence increases.

A control experiment of the time-resolved emission spectrum of An in toluene excited at 532 nm is shown in appendix Fig. A.4.7. The fluorescence decay measured at 468 nm is shown in Fig. A.4.7, and the N/e population decay time estimated from this decay is around 25 ns. This is an order of magnitude greater than the S_1 lifetime of An obtained upon prompt, one-photon excitation.[13] However, the fluorescence decay of An in toluene

at 464 nm measured by exciting at 355 nm, shown in the Fig. A.4.8, showed a single exponential decay behaviour, the N/e decay time of which is estimated to be around 7 ns which is in fair agreement with the actual S_1 lifetime of An.

The delayed fluorescence from An + C_{60} can be related to the triplet concentrations by the equations,[4,25]

$$\frac{\mathrm{d}\sqrt{I_{DF}(t)}}{\mathrm{dt}} = \sqrt{C}\frac{\mathrm{d}[T_1(An)]_t}{\mathrm{dt}} = -k_{T1(An)}[T_1(An)]_t - k_{TTA(An)}[T_1(An)]_t{}^2 \qquad (4.14)$$

which has the solution,

$$\frac{[T_1(An)]_t}{[T_1(An)]_0} = \frac{1-\beta}{\mathrm{e}^{k_{T1(An)}t} - \beta} \qquad (4.15)$$

where $\beta = \alpha/\left(k_{T1(An)} + \alpha\right)$ and $\alpha = k_{TTA(An)}[T_1(An)]_0$.[4]

However, fits of the square root of the normalized delayed fluorescence with equations (4.14) and (4.15) resulted in β values very close to 1. A representative fit of the delayed fluorescence can be seen the inset of Fig. 4.14. A first-order rate constant of $k_{T1(An)}$ = (9.1 ± 0.3) × 10^3 s^{-1} and β = (0.92 ± 0.003) were obtained from the fitted data. This indicates that TTA in An is in the strong annihilation limit.[4] This is apparent from Fig. 4.10 where the log-log plot of the delayed fluorescence intensity has a linear dependence on the concentration of An added. In this case, the first order decay can be assumed to be negligible compared to the second order TTA process, i.e. $k_{T1(An)} \ll k_{TTA(An)}$. Therefore, equation (4.14) is simplified into,[4]

(A)

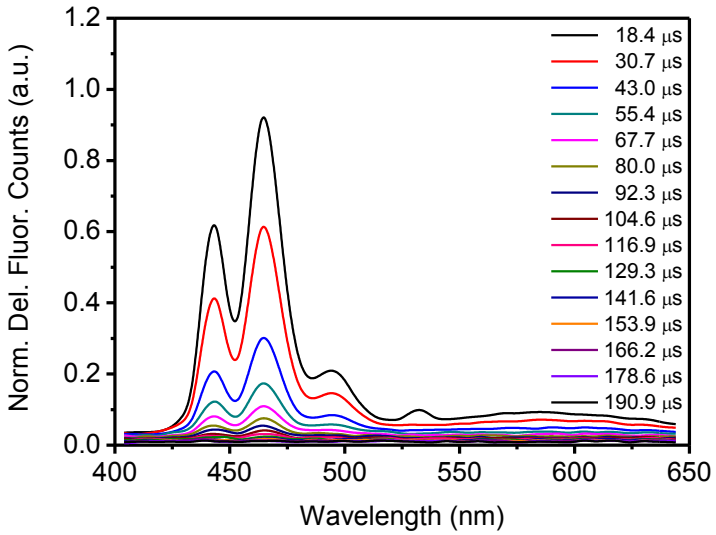

(B)

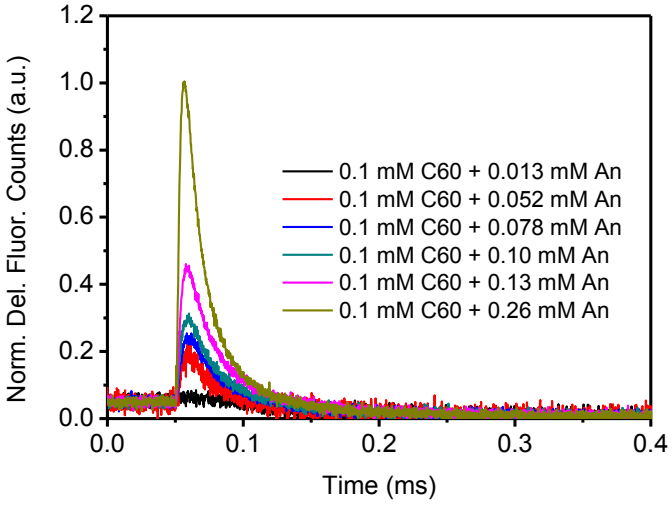

Fig. 4.13 (A) Time-resolved fluorescence spectrum of 1.0×10^{-4} M C_{60} and 1.0×10^{-4} M An in toluene excited at 532 nm. (B) Kinetic decay of fluorescence from various concentrations of An in the presence of 1.0×10^{-4} M C_{60} measured at 464 nm. The laser pulse width was 5 ns and the laser power density at the sample was 0.34 $W.cm^{-2}$.

$$\frac{[T_1(An)]_t}{[T_1(An)]_0} = \frac{1}{1 + K_A t} \qquad (4.16)$$

where $K_A = k_{TTA(An)}[T_1(An)]_0$.

Fitting the square root of the delayed fluorescence using equations (4.14) and (4.16) can, in principle, give the rate constant of TTA in An. Fig. 4.14 shows the delayed fluorescence from C_{60}+An fitted using equation (4.16). The rate constant obtained from the fit is, K_A = (3.1 ± 0.06) × 10^5 s^{-1}.

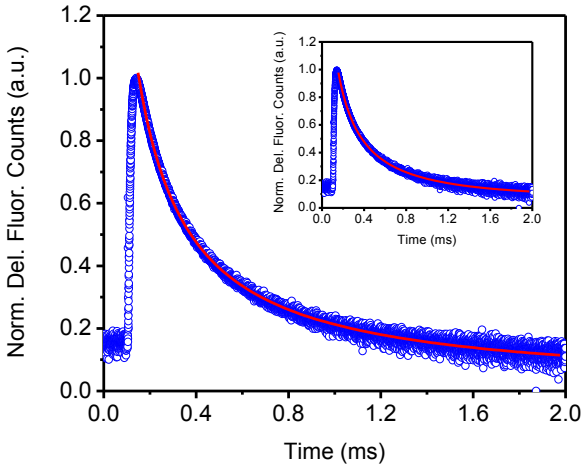

Fig. 4.14 Fit of the square root of the normalized delayed fluorescence from 1.0 × 10^{-4} M C_{60} + 7.8 × 10^{-4} M An in toluene with equations (4.14) and (4.16). The inset shows the fit to the same data using equations (4.14) and (4.15). Experimental conditions are same as that of data in Fig. 4.13 (B) except that a smaller time window is used. The goodness of the fits was decided by assessing the reduced χ^2 value.

Let us assume for argument's sake that the TTA in C_{60} is negligible, that any first order triplet decay process of C_{60} is negligible, and that the quenching of triplet C_{60} by An is rapid and quantitative, then it may be assumed that $[T_1(An)]_0 \approx [T_1(C_{60})]_0$. For

calculating $[T_1(C_{60})]_0$, the molar extinction coefficient of $^3C_{60}$ at 750 nm (16,100 M^{-1} cm^{-1})[5] is used and the light pathlength is approximated as the beam diameter of the excitation laser (0.6 cm), resulting in $[T_1(C_{60})]_0$ = 1.3 × 10^{-5} M. Using this value will result in a second-order rate constant of TTA in An to be $k_{TTA(An)} \approx (2.4 \pm 0.05) \times 10^{10}$ $M^{-1}s^{-1}$. However, because the rate constant of TTA in C_{60} is greater than the rate constant of quenching of triplet C_{60} by An by an order of magnitude, it can be expected that $[T_1(An)]_0 \leq [T_1(C_{60})]_0$. Based on this assumption, it can be estimated that $k_{TTA(An)} \geq (2.4 \pm 0.05) \times 10^{10}$ $M^{-1}s^{-1}$. However, the theoretical diffusion controlled rate constant for the TTA process is approximately 1.1 × 10^{10} $M^{-1}s^{-1}$, therefore the calculated TTA rate constant should be of the required magnitude within experimental error. Based on the above analysis, it can be reasonably concluded that TTA in An is a very efficient process.

4.2.3 Photon upconversion in C_{60} and Anthanthrene system in PMMA thin films

It has been observed that the solution phase delayed fluorescence originating from C_{60} + An is around 10 times more efficient than that from the C_{60}+P system because of the favourable triplet energies of C_{60} and An. We have also undertaken to generate delayed fluorescence due to NCPU in C_{60}+BE in a solid matrix such as PMMA. We have made a thin layer of C_{60}+BE+PMMA on a glass slide and covered it with a thin layer of PVA. PVA was proven to be an efficient barrier towards molecular oxygen which can potentially quench the triplet states and hence can decrease the efficiency of NCPU.[26]

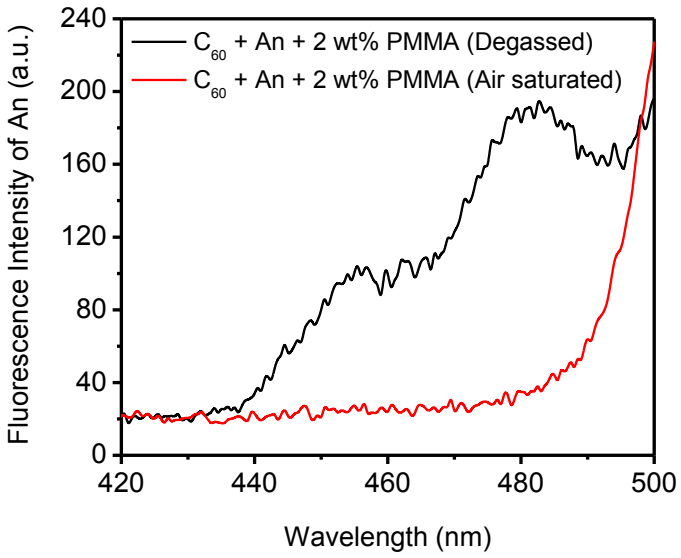

Fig. 4.15 Upconverted S_1 emission observed from An and C_{60} doped in 2.02 Wt% PMMA excited at 532 nm at 0.89 $W.cm^{-2}$. The emission band width was 6 nm. The spectra were measured by Chelsea Greenwald.

Fig. 4.15 shows the proof-of-principle experiment of upconverted fluorescence observed from a sample containing thin layer of C_{60} (2 mM in solution), An (1 mM in solution) and 2 wt% PMMA on a glass slide excited at 532 nm. The spectrum is distorted due to reabsorption by An itself and by C_{60}. Nevertheless, the spectrum looks similar to the solution phase delayed fluorescence spectrum. The scatter from the laser is visible towards the 500 nm region. A spectrum of the same sample taken under identical experimental conditions except that the sample was air saturated showed no emission in the 400 – 500 nm range, confirming that the emission observed from the degassed sample is in fact due to the NCPU process in C_{60}+An. The intensity of fluorescence from the thin film sample is much lower than the emission from the solution phase samples, consistent

with the fact that TTA in solid matrices primarily proceeds through exciton annihilation which largely depends upon the state of aggregation of the sensitizer and the emitter. In the case of C_{60}, P and An, the extent of ground state aggregation was found to be very small in the optical spectra. Finally, C_{60}+P in the PMMA thin film did not produce measurable upconverted emission for a range of C_{60} and P concentrations employed, likely, due to the poor aggregation between C_{60} and P, due to the similar energies of their triplet states, and due to the possibility of TTBET and electron transfer processes.

4.3 Conclusions

The mechanism and kinetics of low-power, noncoherent photon upconversion in two sensitizer+blue emitter systems in nonpolar toluene solution have been studied in detail. In the first system, C_{60} and P, the triplet quenching occurs through energy transfer and electron transfer between $^3C_{60}$ and P. The similar triplet energies of C_{60} and P produce an entropically driven triplet energy transfer from $^3C_{60}$ to P for which the forward TTET is completely exergonic. At longer timescales and at higher concentrations of P, TTBET becomes exergonic and significant. In the second system, C_{60} and anthanthrene, the triplet energy of An is lower than that of C_{60}, making TTBET very inefficient. The triplet quenching constant calculated for the TTET process in the C_{60}+An system was found to be an order of magnitude greater than that calculated for the C_{60}+P system, consistent with the differences in triplet energies of C_{60}, P and An. In addition, TTA in An is found to be very efficient with a rate constant > 10^{10} $M^{-1}s^{-1}$. These factors resulted in an order of magnitude increase of the delayed fluorescence intensity for the C_{60}+An system. Finally,

proof-of-principle measurements demonstrated that the C_{60}+An system in a solid PMMA matrix emits delayed fluorescence whereas the C_{60}+P system does not, consistent with the relative positions of the triplet energies of C_{60}, P and An. However, the fluorescence observed from C_{60}+An in PMMA matrix was found to be weak. Therefore, further investigations are required to increase the efficiency of this system.

References

(1) Accorsi, G.; Armaroli, N. *J. Phys. Chem. C* **2010**, *114*, 1385.

(2) (a) Fraelich, M. R.; Weisman, R. B. *J. Phys. Chem.* **1993**, *97*, 11145. (b) Ausman, K. D.; Weisman, R. B. *Res. Chem. Intermed.* **1997**, *23*, 431.

(3) Orlandi, G.; Negri, F. *Photochem. Photobiol. Sci.* **2002**, *1*, 289.

(4) Bachilo, S. M.; Weisman, R. B. *J. Phys. Chem. A* **2000**, *104*, 7711.

(5) Fujitsuka, M.; Ito, O. In *Encyclopedia of Nanoscience and Nanotechnology*; Nalwa, H. S., Ed., 2004; Vol. 8.

(6) Sugunan, S. K.; Robotham, B.; Sloan, R. P.; Szmytkowski, J.; Ghiggino, K. P.; Paige, M. F.; Steer, R. P. *J. Phys. Chem. A* **2011**, *115*, 12217.

(7) El-Khouly, M. E.; Ito, O.; Smith, P. M.; D'Souza, F. *J. Photochem. Photobiol., C* **2004**, *5*, 79.

(8) (a) El-Khouly, M. E.; Fujitsuka, M.; Ito, O. *J. Porphyr. Phthalocya.* **2000**, *4*, 590. (b) Nojiri, T.; Watanabe, A.; Ito, O. *J. Phys. Chem. A* **1998**, *102*, 5215.

(9) (a) Komfort, M.; Lohmannsroben, H. G.; Salthammer, T. *J. Photochem. Photobiol. A-Chem.* **1990**, *51*, 215. (b) Lewitzka, F.; Lohmannsroben, H. G. *Z. Phys. Chem. Neue. Fol.* **1990**, *169*, 181. (c) Lewitzka, F.; Lohmannsroben, H. G. *Z. Phys. Chem. Neue. Fol.* **1990**, *169*, 203. (d) Lewitzka, F.; Lohmannsroben, H. G.; Strauch, M.; Luttke, W. *J. Photochem. Photobiol. A-Chem.* **1991**, *61*, 191.

(10) Parac, M.; Grimme, S. *Chem. Phys.* **2003**, *292*, 11.

(11) Clarke, R. H.; Hochstrasser, R. M. *J. Mol. Spectrosc.* **1969**, *32*, 309.

(12) Ebbesen, T. W.; Tanigaki, K.; Kuroshima, S. *Chem. Phys. Lett.* **1991**, *181*, 501.

(13) (a) Shah, B. K.; Neckers, D. C.; Shi, J. M.; Forsythe, E. W.; Morton, D. *J. Phys. Chem. A* **2005**, *109*, 7677. (b) Shah, B. K.; Neckers, D. C.; Shi, J. M.; Forsythe, E. W.; Morton, D. *Chem. Mat.* **2006**, *18*, 603.

(14) Carmichael, I.; Hug, G. L. *J. Phys. Chem.* **1985**, *89*, 4036.

(15) Wu, W. H.; Zhao, J. Z.; Sun, J. F.; Guo, S. *J. Org. Chem.* **2012**, *77*, 5305.

(16) Steren, C. A.; vanWilligen, H.; Biczok, L.; Gupta, N.; Linschitz, H. *J. Phys. Chem.* **1996**, *100*, 8920.

(17) Guldi, D. M.; Prato, M. *Acc. Chem. Res.* **2000**, *33*, 695.

(18) (a) Liu, X.; Yeow, E. K. L.; Velate, S.; Steer, R. P. *Phys. Chem. Chem. Phys.* **2006**, *8*, 1298. (b) Lukaszewicz, A.; Karolczak, J.; Kowalska, D.; Maciejewski, A.; Ziolek, M.; Steer, R. P. *Chem. Phys.* **2007**, *331*, 359.

(19) Sugunan, S. K.; Tripathy, U.; Brunet, S. M. K.; Paige, M. F.; Steer, R. P. *J. Phys. Chem. A* **2009**, *113*, 8548.

(20) (a) Monguzzi, A.; Mezyk, J.; Scotognella, F.; Tubino, R.; Meinardi, F. *Phys. Rev. B* **2008**, *78*. (b) Monguzzi, A.; Tubino, R.; Hoseinkhani, S.; Campione, M.; Meinardi, F. *Phys. Chem. Chem. Phys.* **2012**, *14*, 4322. (c) Cheng, Y. Y.; Khoury, T.; Clady, R.; Tayebjee, M. J. Y.; Ekins-Daukes, N. J.; Crossley, M. J.; Schmidt, T. W. *Phys. Chem. Chem. Phys.* **2010**, *12*, 66.

(21) Greever, J. S.; Turner, J. B. M.; Kauffman, J. F. *J. Phys. Chem. A* **2003**, *107*, 4072.

(22) Cheng, Y. Y.; Fuckel, B.; Khoury, T.; Clady, R.; Ekins-Daukes, N. J.; Crossley, M. J.; Schmidt, T. W. *J. Phys. Chem. A* **2011**, *115*, 1047.

(23) (a) Dimitrijevic, N. M.; Kamat, P. V. *J. Phys. Chem.* **1992**, *96*, 4811. (b) Riggs, J. E.; Sun, Y. P. *J. Phys. Chem. A* **1999**, *103*, 485.

(24) (a) Makarov, N. S. Ph.D. Thesis, Montana State University, 2010. (b) Makarov, N. S.; Rebane, A.; Drobizhev, M.; Wolleb, H.; Spahni, H. *J. Opt. Soc. Am. B-Opt. Phys.* **2007**, *24*, 1874.

(25) Cheng, Y. Y.; Fuckel, B.; Khoury, T.; Clady, R.; Tayebjee, M. J. Y.; Ekins-Daukes, N. J.; Crossley, M. J.; Schmidt, T. W. *J. Phys. Chem. Lett.* **2010**, *1*, 1795.

(26) Sugunan, S. K.; Paige, M. F.; Steer, R. P. *Can. J. Chem.-Rev. Can. Chim.* **2011**, *89*, 195.

Chapter 5: Determination of the rate of oxygen diffusion in polymer thin films using upconverted fluorescence from porphyrins

5.1 Introduction

The transport properties of gas molecules through polymer media have been an area of long-standing interest from both fundamental and applied perspectives.[1] In addition to the fundamental interest in the oxidative degradation of polymers,[1b,c] research in this field is motivated by the many potential applications of polymers as protective barriers (for food, chemicals, etc.), as gas separation membranes, as an ingredient in pressure sensitive paints and, most recently, as host materials for organic or organometallic dyes in dye sensitized solar cells.[1b,c,2] Measuring the rate of molecular oxygen transport through polymer materials is therefore important, and devising simple, accurate, rapid methods to make such measurements continues to be an active area of research.

Over the years, many techniques have been developed to measure the diffusion rate of molecular oxygen in polymer thin films. In the time-lag method, a defined pressure of oxygen is applied to one side of a polymer membrane positioned at the center of an evacuated chamber and the buildup of a partial pressure of oxygen on the other side of the membrane is monitored as a function of time. This method suffers from technical difficulties such as the requirements for relatively large, free-standing, defect-free thick films, large chamber volumes and long observation times for polymers having very low values of oxygen permeability.[2e,3] The most widely used alternatives involve methods of

optically sensing the oxygen concentration.[1-4] For most of these methods, an optically excited organic dye molecule or inorganic complex in its singlet or triplet state dissolved or embedded in a polymer thin film is quenched by molecular oxygen introduced into the film, thereby forming the ground state of the dye (plus singlet molecular oxygen in many cases). The rate of oxygen diffusion is monitored by observing either the luminescence quenching of the dye molecule or the rate of singlet oxygen production. The rate of oxygen diffusion across the polymer matrix is then analyzed using either Fick's diffusion kinetics as a function of the time taken to reach a steady state concentration of oxygen in the film or Stern-Volmer and diffusion controlled reaction kinetics once a steady state of oxygen concentration in the film is reached.[3] These methods are particularly attractive because of their high sensitivity, low consumption of oxygen, simple experimental set up, and shorter experimental time.[2f] Typical dye molecules employed in optical oxygen sensing include porphyrins, transition metal complexes, naphthalene, perylene, and triphenylene.[2c,2e,f,3-4] Even though other techniques such as mass spectrometry and fluorescence microscopy can also monitor oxygen transport in polymers,[2b,2f] use of a simple steady state or time-resolved spectrofluorimeter or phosphorimeter remains the simplest and the most popular method.

The method of finding the oxygen permeability of polymer films through steady state Stern-Volmer kinetics was initiated by Jones[5] and was extended by Yekta et al.[3] and Douglas and co-workers.[4d-g] In these cases, a sensor film composed of phosphorescent dye molecules embedded in a polymer film was employed to provide the optical signal. Later, Rharbi et al.[2d] devised a method in which a polymer film was used as the

separating membrane in the time-lag method described earlier, but the build-up of a partial pressure of oxygen in the receiving chamber was monitored by luminescence quenching of a separate sensor film containing a phosphorescent dye. Oxygen permeation through bilayer polymer films was investigated by Paulson and Ogilby.[1c] Here, the polymer film of interest was coated on a sensor layer composed of a porphyrin dissolved in a second polymer. The rate of oxygen permeation through the polymer film was measured by detecting the NIR phosphorescence of singlet oxygen.

The oxygen permeability coefficients of different polymers have been summarized in an article by Hess et al.[2e] The effects of water content on the permeability of poly(vinyl alcohol), PVA, a test material used in the present experiments, has recently been investigated by Lien et al.[6]

In the present study, a proof of principle experiment was conducted to demonstrate that oxygen permeability and diffusion kinetics in polymer films can be measured by observing the quenching of delayed (upconverted) fluorescence in a suitable dye. In this demonstration, oxygen transport through thin layers of PVA coated on a thicker layer of Zn(II) *meso*-tetraphenylporphine (ZnTPP) dissolved in poly(ethyl methacrylate) (PEMA) was examined. It was previously shown that upconverted S_2 (Soret band) fluorescence can be generated relatively efficiently both in solution and in the solid phase by triplet-triplet annihilation (TTA) in ZnTPP upon excitation in its Q band with a cw laser at 532 nm.[7] When molecular oxygen quenches the triplet state of ZnTPP, the S_2 fluorescence of ZnTPP is also quenched. The mechanism of TTA in ZnTPP is shown in Chapter 3 (equations (i),(ii) and (vi)); the oxygen quenching of the triplets is outlined below.

$$T_1(ZnTPP) + O_2(^3\Sigma^-_g) \rightarrow {}^{1,3,5}(ZnTPP\ldots O_2) \rightarrow S_0(ZnTPP) + O_2(^1\Sigma^+_g) \text{ or } O_2(^1\Delta_g) \text{ or } O_2(^3\Sigma^-_g)$$

Note that the triplet-triplet annihilation, step (vi) in Chapter 3, can occur by molecular diffusion in fluid media, but relies on triplet exciton migration in porphyrin aggregates in thin films and other non-fluid media.

By measuring the rate of S_2 fluorescence intensity quenching of ZnTPP upon interaction of the annihilating triplets with different partial pressures of oxygen, one can in principle calculate the rate of oxygen diffusion in the PVA layer. Employing the quenching of TTA-generated upconverted fluorescence from ZnTPP for measuring the diffusion of oxygen in polymers offers two significant advantages over other optical techniques. (i) The S_2-S_0 fluorescence from ZnTPP occurs in the violet region of the spectrum, it is strongly allowed (oscillator strength, f ~ 1) and is therefore very easy to detect, even though the efficiency of the TTA process can be low.[7-8] (ii) The experimental set up required is very simple, involving only a steady state spectrofluorimeter equipped with a vacuum sample chamber and a low power cw visible laser as the excitation source.

5.2 Assumptions, theory and data analysis

PEMA was selected as the host polymer in the sensor layer to dissolve ZnTPP and PVA was selected as the test polymer in this demonstration for the reasons outlined in Chapter 2, section 2.1. It was assumed that the interface between the polymer sensor and

the test layers do not serve as a significant barrier to oxygen diffusion. On this basis it can be reasonably assumed that the concentration of oxygen will be uniform in the sensor PEMA film on the time scale of the experiment and that diffusion of oxygen within the sensor layer will not interfere with measurements of the diffusion properties of oxygen in the PVA test film. It can also be assumed that the oxygen diffusion process can be described by standard models and that once the steady state concentration of oxygen is achieved in the film, the oxygen quenching of the triplet states that participate in the excited state annihilation that produces the observed fluorescence is a pseudo-first order kinetic process. No special steps were taken to control or measure the water content of the PVA film or to determine the degree of crystallinity of the polymer itself. It cannot, therefore, be anticipated that these proof of principle experiments will be able to reproduce exactly any of the previous values of the oxygen diffusion and permeability coefficients that have been correlated with PVA's water content.[6]

The fundamental theories regarding the transport properties of gases in polymers have been summarized in an excellent monograph by Crank et al.[9] The rate of luminescence decay at any time t from a sensor film when one side of a defect-free thin film of a polymer having thickness *l* is exposed to a partial pressure of oxygen is given by,[10]

$$I(t) = \int_0^l I(X,t)\,\mathrm{d}X \qquad (5.1)$$

where I(X,t) is the luminescence intensity as a function of the position within the film, X, and the time of observation is t. X is the normalized depth of oxygen penetration in the film which varies from 0 to 1 and is given by X = x/*l* where x is the perpendicular depth

within the film. Here we assume a uniform distribution of ZnTPP in the PEMA film, a uniform layer of PVA on top of it, uniform laser illumination throughout the film and a uniform rate of oxygen diffusion in the test film and through the interface between the films based on the assumption that the oxygen diffusion in the PVA layer is not affected by that in the PEMA layer. The nonlinear gas solubility model[9,10] can be used to assess the oxygen concentration at any point in the film,

$$\frac{I(X,t)}{I_0} = [\gamma a C^2 + (\gamma + a + b)C + 1]^{-1} \qquad (5.2)$$

where C is the concentration of oxygen, γ, a and b are fitting parameters and I_0 is the unquenched luminescence intensity of the sensor film in the absence of oxygen.

Assuming that the polymer film is uniformly planar throughout the test area, the concentration of oxygen in the polymer film for all time scales is given by,

$$C = C_0 + (C_1 - C_0) \times \left[1 - \frac{4}{\pi} \sum_{1=0}^{\infty} \left(\frac{(-1)^i}{(2i+1)} \right) \exp\left(\frac{-(2i+1)^2 \pi^2 Dt}{4l^2} \right) \cos\left(\frac{(2i+1)\pi X}{2} \right) \right] \quad (5.3)$$

where C_0 is the initial concentration of oxygen in the film, C_1 is the oxygen concentration at the film surface during the diffusion process and D is the diffusion coefficient of oxygen in the film. Since our sample film is allowed to outgas under vacuum prior to introducing oxygen, we reasonably assume that $C_0 = 0$. Because of the oscillatory behavior of this equation and the large computational time required, an alternative form was used for shorter time scales assuming that $C_0 = 0$.

$$C = C_1 \left[\sum_{i=0}^{\infty} (-1)^i \operatorname{erfc} \frac{(2i+1)l + lX}{\sqrt{4Dt}} + \sum_{i=0}^{\infty} (-1)^i \operatorname{erfc} \frac{(2i+1)l - lX}{\sqrt{4Dt}} \right] \qquad (5.4)$$

where erfc is the complimentary error function.

Substituting equation (5.4) into equation (5.2) and subsequently equation (5.2) into equation (5.1) gives the rate of fractional luminescence intensity quenching [$I(t)/I_0$] as a function of time t.

Once the steady state concentration of oxygen is reached in the film, the system should follow Stern-Volmer kinetics,

$$\frac{I_0}{I_q} = 1 + k_q \tau_0 [O_2] \qquad (5.5)$$

where I_q is the luminescence intensity under steady state conditions where the oxygen concentration is $[O_2]$, k_q is the bimolecular quenching rate constant and τ_0 is the lifetime of the excited dye molecule (the lowest triplet state of ZnTPP in our case).

Smoluchowski's diffusional encounter theory can be applied to relate the bimolecular quenching constant to the diffusion coefficient, k_{diff}, which specifies the limiting rate at which the oxygen molecule can form an encounter complex with the excited dye molecule.[2e,3]

$$k_q = \alpha k_{diff} = (\alpha)(4\pi\sigma N_A D) \qquad (5.6)$$

Here the proportionality constant, α, is the luminescence quenching probability in an encounter complex of the dye with oxygen, σ is the diameter of the encounter complex (which should be the sum of the van der Waals radii of the dye molecule and oxygen - a value of 10 Å is used here), N_A is Avogadro's number and D is the diffusion coefficient. Even though α may increase with multiple encounters between the dye molecule and oxygen trapped in the polymer, a value of 1/9 for α was used on the basis that both

ZnTPP and molecular oxygen are in the triplet state prior to forming a diffusional encounter complex and the formation of the product singlet states is limited by a spin statistical factor of 1/9. Likewise, it was assumed that the formation of the fluorescing S_2 excited state of ZnTPP is limited by a spin statistical factor of 1/9 when produced from the TTA encounter complex.[8] The spin statistical factor is determined by the statistical probability that only one of the nine spin states in the encounter complex will yield a singlet product.

Finally, Henry's law can be applied to relate the equilibrium oxygen concentration to the solubility coefficient of oxygen in the film (S) and the partial pressure of oxygen in the low to moderate pressure range.[2e,3]

$$[O_2]_{eq} = SP_{O_2} \qquad (5.7)$$

Combining equations (5.5), (5.6) and (5.7) gives the desired equation relating the steady state luminescence intensity to the permeability (P) of oxygen, which is a product of the diffusion coefficient (D) and the solubility coefficient (S), i.e., P = DS.

$$\frac{I_0}{I_q} = 1 + (\mathrm{P})(4\pi\alpha\sigma N_A\tau_0)(P_{O_2}) \qquad (5.8)$$

Both time-based and steady state data were analyzed in Origin 7.5. Simpson's rule for integration was used to numerically integrate the fitting function in equation (5.2).

5.3 Results and discussion

Fig. 5.1 demonstrates proof-of-principle that variations in the intensity of delayed (upconverted) fluorescence caused by oxygen quenching of the triplet states of an

appropriately chosen fluorescent dye can be used to measure the diffusion kinetics of oxygen in a polymer film. Fig. 5.1 (A) shows the time-of-exposure dependent S_2 fluorescence quenching of ZnTPP resulting when a thin film of PVA spin-cast from a 0.5 wt% solution is brought into contact with an oxygen partial pressure of 13.4 kPa in dry nitrogen at approximately room temperature. The dye luminescence is quenched and attains a constant value after about 500 seconds of exposure to oxygen. The best fit of equation (5.1) to these data yielded a diffusion coefficient $D = 4.5 \times 10^{-9}$ $cm^2.s^{-1}$.

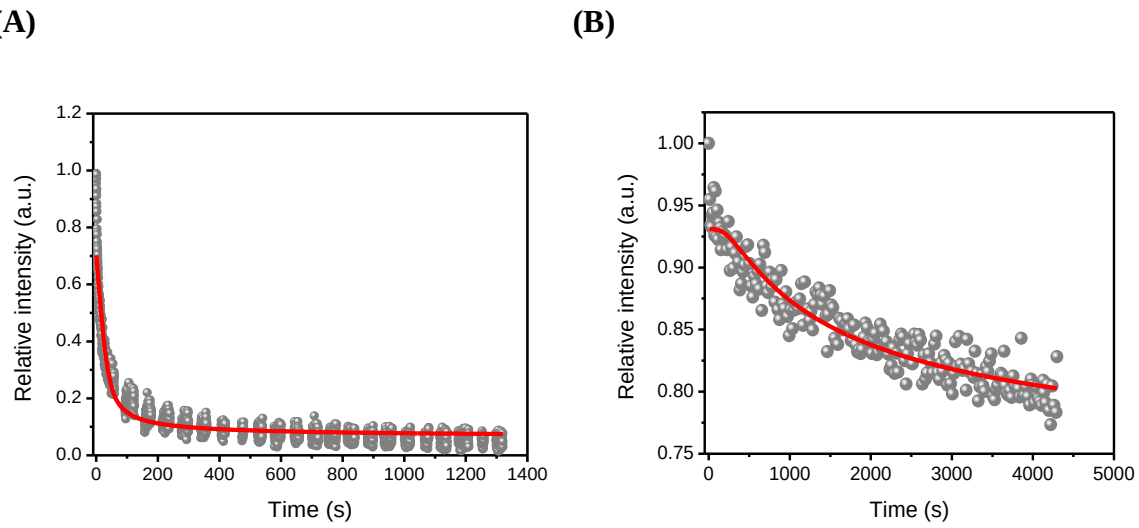

Fig. 5.1 Upconverted luminescence quenching profiles of (A) one thin layer spin cast from 0.5 wt% PVA exposed to a partial pressure of 100 torr of oxygen and (B) one thin layer spin cast from 2.0 wt% PVA exposed to a partial pressure of 200 torr of oxygen. Filled circles represent the data points and the solid curves represent the best fit for the data using equations 5.1, 5.2 and 5.4 and the quality of the fit was determined by the reduced χ^2 values. Data points at t = 0 were omitted while fitting to avoid the function in equation 5.4 encountering ∞ at t = 0.

The time-of-exposure dependent quenching of a thin layer PVA made from a solution having a concentration of 2 wt% PVA in water is shown in Fig. 5.1 (B). Here, the partial

pressure of oxygen is 27 kPa and the luminescence profile reaches a steady state in slightly longer than 4500 seconds, but the relative steady state (equilibrium) intensity is substantially higher than in the previous example. The best fit to these data resulted in a significantly smaller value of the diffusion coefficient, $D = 2.0 \times 10^{-10}$ $cm^2.s^{-1}$. Note that although the fits between the diffusion theory expression and the data are not perfect, two diffusional processes were not needed to obtain the observed agreement, thus substantiating the assumption that the oxygen concentration in the sensor layer is approximately constant on the time scale of the experiment. Note also that these two films were of similar thickness; 6.9×10^{-6} cm for the film cast from the 0.5% solution and 7.1×10^{-6} cm for the film cast from the 2% solution. Both the content and the distribution of the water in these two films, however, are expected to be rather different (*vide infra*).

A difference in the magnitude of the oxygen permeability values for samples prepared from 0.5 wt% and 2.0 wt% solutions was also found in the Stern-Volmer kinetic analysis of the samples under steady state conditions. Here the equilibrium intensity of the dye's upconverted S_2 fluorescence was measured for the same film exposed to different partial pressures of oxygen in dry nitrogen at a total pressure of a little less than 1 atm. The data are amenable to a straightforward Stern-Volmer analysis as shown in Fig. 5.2 (A) for the sample prepared from 0.5 wt% PVA in water. The slope of the curve is 1.3×10^{-3} Pa^{-1} which, when substituted into equation (5.8), gives a permeability coefficient of 2.2×10^{-16} cm^3(gas at STP). $cm.cm^{-2}.s^{-1}.Pa^{-1}$.

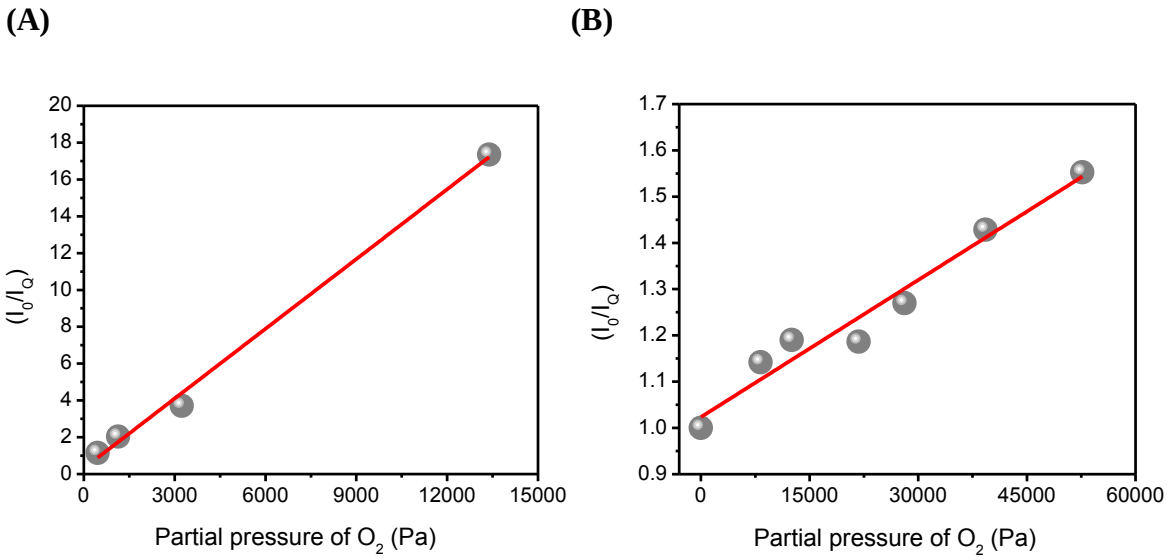

Fig. 5.2 Stern-Volmer kinetic analysis of oxygen quenching data for (A) one layer spin cast from 0.5 wt% PVA, R^2 = 0.99 for the least-squares fit, and (B) one layer spin cast from 2.0 wt% PVA, R^2 = 0.95 for the least-squares fit. Filled circles represent the data points and the solid curves represent the best linear least-squares fit of the data to equation 5.8.

A Stern-Volmer kinetic plot for oxygen diffusion in a thin test layer of PVA made from a 2.0 wt% solution in water, shown in Fig. 5.2 (B), resulted in a slope of 9.9×10^{-6} Pa^{-1} and a permeability coefficient of 1.7×10^{-18} cm^3(gas at STP).cm.cm^{-2}.s^{-1}.Pa^{-1}, which is a factor of 130 lower than that found in the 0.5 wt % sample. Note that the same value of the unquenched lifetime of triplet ZnTPP, $\tau_0 = 6.86 \times 10^{-3}$ s, previously measured[11] for ZnTPP in PMMA, has been used in both of these calculations. The actual triplet lifetime was not measured in these proof-of-principle experiments, and any difference would constitute a source of systematic error in the determination of the values of P reported here.

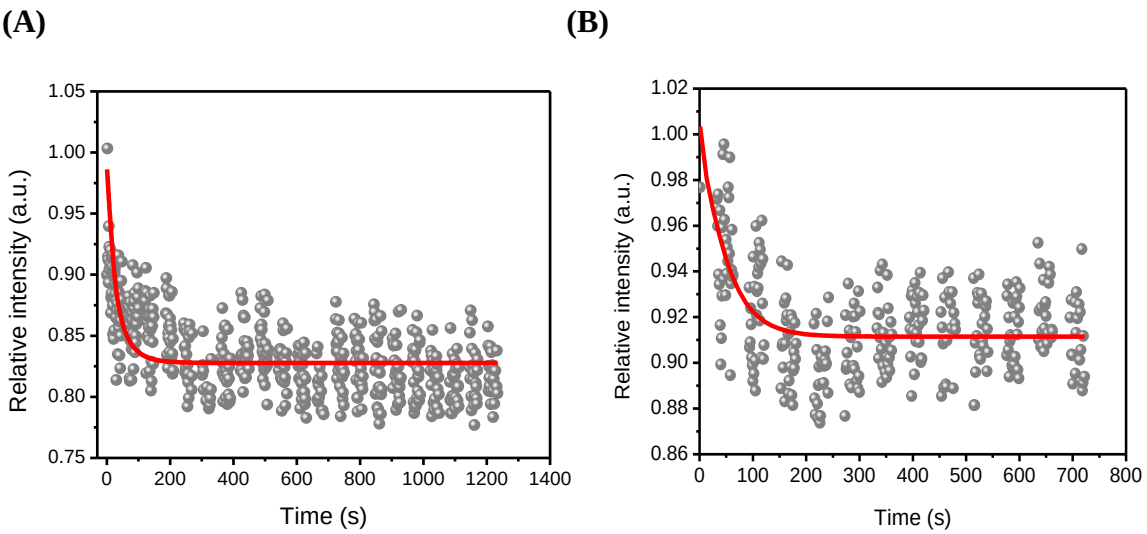

Fig. 5.3 Upconverted luminescence quenching profiles of (A) three layers spin cast from 0.5 wt% PVA exposed to a partial pressure of 100 torr of oxygen and (B) five layers spin cast from 0.5 wt% PVA exposed to a partial pressure of 100 torr of oxygen. Filled circles represent the data points and the solid curves represent the best fit for the data using equations 5.1, 5.2 and 5.4 and the quality of fit was determined by the reduced χ^2 values.

In order to examine the effect of the thickness of the polymer membrane on the measured oxygen permeability of PVA, the temporal luminescence quenching profiles for two different thicknesses of PVA were measured and are shown in Fig. 5.3. The corresponding experimental diffusion coefficients calculated as above are shown in the second column of Table 5.1. Note that the value of the apparent oxygen diffusion coefficient decreases with increasing thickness of the PVA test film. Because both D and P should be independent of film thickness if the films themselves are of the same composition and morphology, this observation implies that at least one uncontrolled variable (in our case the water content and distribution, and perhaps the degree of polymer crystallinity) is responsible for the differences.

Table 5.1 Experimental diffusion coefficients and calculated[12] permeability coefficients for oxygen in PVA membranes having different thickness (μ represents that the calculated values are given as 95% confidence interval, rather than an average value, *vide infra*).

Thickness of thin layers made from 0.5 wt % solution of PVA, *l* (cm)	Experimental diffusion coefficient (D), $cm^2.s^{-1}$	Calculated permeability coefficient (P), cm^3(gas at STP).$cm.cm^{-2}.s^{-1}.Pa^{-1}$
6.9×10^{-6}	4.6×10^{-9}	$2.0\times 10^{-14} < \mu < 2.5 \times 10^{-14}$
5.5×10^{-5}	2.4×10^{-11}	$1.1\times 10^{-16} < \mu < 1.3 \times 10^{-16}$
8.6×10^{-5}	7.8×10^{-11}	$3.4\times 10^{-16} < \mu < 4.2 \times 10^{-16}$

These measured values of D and P can be compared only crudely with literature values because of the largely unknown water contents and distributions of both the samples under evaluation here and those for which data are reported in the literature. Values of D for absolutely dry PVA have been obtained[12a,13] by molecular dynamics simulations for samples at 375 K ($D = 5.0 \times 10^{-7}$ $cm^2.s^{-1}$) and 500 K ($D = 1.6 \times 10^{-6}$ $cm^2.s^{-1}$). However, these values apply to conditions in which PVA will be in its glassy state with a large free volume, where a much faster rate of oxygen diffusion is expected compared with those measured here. The permeability values measured here may be compared to a reported[12b] permeability value for oxygen diffusion in PVA (of unknown water content) of 9.16×10^{-16} cm^3(gas at STP).$cm.cm^{-2}.s^{-1}.Pa^{-1}$, in order-of-magnitude agreement.

The glass transition temperature of PVA is near 358 K, well above the near-room temperatures used in our experiments. When a polymer is in a semi-crystalline state well below its glass transition temperature, nanocrystalline clusters dispersed in a continuous network of a relatively low fraction of amorphous polymer are formed.[14] The crystalline part in the polymer matrix is generally impermeable to gas penetration whereas gas diffusion is relatively facile in the amorphous phase. Moreover, PVA films prepared from aqueous media can contain variable amounts of water and this water can be distributed in a continuum of strongly- to weakly-bound environments.[6] Gas diffusion in the amorphous regions follows the free-volume model,[14b] and whereas the diffusive motion of gas molecules is generally faster than the mobility of the polymer segments, the polymer does respond to provide space to accommodate the diffusing gas.[15] It is not unreasonable to assume that the free volume in the polymer thin film, and hence the water content and distribution in our films, will depend on the initial concentration of the polymer in solution and the exact conditions used to cast the film. All other factors remaining the same, the number density of the polymer molecules should be expected to increase with increasing concentration of the polymer in the spin-cast solution. The relation between the initial polymer concentration in aqueous solution and the resulting free volume and distribution of water in the thin film should explain why the measured diffusion coefficient and permeability are substantially reduced when the polymer concentration in the spin-cast solution is increased. We proceed with a largely empirical analysis based on this hypothesis.

Consider two different samples, 1 and 2, of the same polymer film that are formed from two different concentrations of the polymer in solution. The resulting films have different water contents and hence different oxygen solubilities, S_1 and S_2. Let the measured oxygen diffusion coefficients in the two films be D_1 and D_2 respectively and let the measured permeability coefficients be P_1 and P_2 respectively. Since P = DS, the ratios of the values of P and D will give an estimate of the differences in oxygen solubilities in the two films. Using the data for D and P presented above, for the two starting PVA concentrations employed we find that $S_1 = 5.7S_2$ – i.e. using this analysis oxygen would be about six times more soluble in the PVA made from the lower concentration solution. Since the two films are of approximately the same thickness, the pore sizes of the film made from the lower concentration solution must be significantly larger and contain more bulk-like water than those in the film formed from the higher concentration solution. Since water can dissolve oxygen and hence the oxygen solubility increases with the bulk-like water content of PVA,[6] this interpretation is qualitatively consistent with the above starting hypothesis.

The solubility of oxygen in the PVA thin film can be computed by correlating the equilibrium concentration of the oxygen dissolved in the polymer film (C) with the partial pressure, P_{O2} of the gas at the polymer surface using the dual-mode theory,[12b,16]

$$C = K_H P_{O_2} + C_\infty \frac{b P_{O_2}}{1 + b P_{O_2}} \qquad (5.9)$$

Here K_H is the Henry's law constant (Pa^{-1}), which characterizes the first term in equation (5.9) as a Henry's isotherm. The second term, which contains C_∞, the steady state concentration of oxygen in the polymer film, and b the ratio of the rates of the

adsorption/desorption processes, is a Langmuir-type isotherm. When using this model, it must be assumed that the absorption/desorption processes do not alter the PVA matrix, that the matrix is homogeneous and that only one oxygen molecule occupies a given site in the polymer matrix at a time.

In addition, because oxygen is a small, rapidly-diffusing molecule and the pressures of oxygen applied in the experiments are less than 1.0 atm, ideal gas behavior for the dissolution of oxygen in the polymer can be assumed. If one can neglect the Langmuir-type isotherm part in equation (5.9), as is the usual case,[12b] then the solubility of oxygen in the PVA polymer matrix is governed by Henry's law for the gas pressures applied here. Using these assumptions and approximations, the solubility coefficient can be computed by using the simple equation,

$$S = K_H (T / T_0) P_0 \qquad (5.10)$$

where T = 298 K is the experimental temperature, P_0 = 1.0 atm and T_0 = 273 K.

The Henry's constant K_H for dry PVA has been computed using Monte Carlo simulations by Cozmuta et al.[12b] Due to the complex dynamics of oxygen in the voids and channels of the polymer and due to the possible structural modifications of the polymer matrix during the adsorption process, K_H was calculated as a 95 % confidence interval rather than as an average value and was reported as ($0.4 < \mu < 0.5$) $cm^3/cm^3/atm$. The lower and upper limits of this range of K_H values were used to compute a theoretical solubility coefficient of oxygen in dry PVA, also expressed as a 95% confidence interval (Table 5.2). This calculated solubility coefficient range together with the values of the experimentally observed diffusion coefficients was then used to calculate a range of

values of the permeability coefficient. These values are compared with the experimentally determined values of the permeability coefficients. The experimental permeability coefficients and experimental diffusion coefficients measured for PVA containing residual amounts of water are compared with the calculated solubility coefficient and the calculated permeability coefficients for dry PVA in Tables 5.1 and 5.2. The calculated permeability coefficients are two to three orders of magnitude larger than the experimentally observed ones (Table 5.2).

Table 5.2 Experimental and calculated[12] (*vide supra*) diffusion coefficients and permeability coefficients of oxygen in thin films of PVA cast from two different concentrations of PVA in water.

Concentration of PVA, wt% in aqueous solution	Experimental permeability coefficient (P), cm^3(gas at STP). cm. $cm^{-2}.s^{-1}.Pa^{-1}$	Experimental diffusion coefficient (D), $cm^2\ s^{-1}$	Calculated solubility coefficient (S), cm^3(gas at STP).$cm^{-3}.Pa^{-1}$	Calculated permeability coefficient (P), cm^3(gas at STP).cm. $cm^{-2}.s^{-1}.Pa^{-1}$
0.5	2.2×10^{-16}	4.5×10^{-9}	$4.4\times 10^{-6} < \mu < 5.4 \times 10^{-6}$	$2.0\times 10^{-14} < \mu < 2.5 \times 10^{-14}$
2.0	1.7×10^{-18}	2.0×10^{-10}		$8.9\times 10^{-16} < \mu < 1.1\times 10^{-15}$

Although some of this discrepancy could be due to experimental uncertainties in the measured values of D and S, a more likely source is the presence of water in the polymer. It should be noted that severe discrepancies exist in the literature regarding the magnitudes of the oxygen permeation coefficients of a wide range of polymers.[2e] For PVA, however, Lien et al.[6] have shown that the oxygen permeability is a strong function

only of the water content of the films, and increases rapidly by over a factor of 100 as the water content increases by a few wt. percent.

5.4 Conclusions

A proof-of-principle experiment was devised and conducted to demonstrate that quenching of delayed fluorescence in a visible light absorbing system that exhibits photon upconversion can be used to measure the diffusion properties of oxygen in thin polymer films. Although the upconverted fluorescence from the S_2 state of ZnTPP as the reporting luminescence was used in this demonstration, other molecular systems exhibiting photon upconversion by TTA or by triplet-singlet annihilation could also be employed and might be useful in overcoming some of the limitations encountered in the present study. Here, the choice of polymer matrices have been limited by the fact that the capping test film must be chosen so that spin casting it onto the porphyrin-containing sensor film does not dissolve the porphyrin so that it becomes embedded in the test film. Although reliable diffusion and permeability coefficients cannot be claimed to have been measured with the system reported here, the data obtained were readily interpretable using standard gas transport and luminescence quenching methodology. Time-of-exposure luminescence decay data were amenable to analysis using standard diffusion models; luminescence quenching at equilibrium oxygen concentrations produced excellent linear Stern-Volmer plots. Order-of-magnitude agreement with literature data was obtained.

The discrepancies between the values of the diffusion and permeability coefficients for oxygen in PVA obtained by spin-casting from aqueous solutions of different PVA

concentrations have been rationalized by considering how the differences in film structure and water content affect the solubility of oxygen in the films. Water content and distribution in the PVA films were not controlled or measured. Future work, based on the useful report of Lien et al.[6] that identifies the role of water in the gas transport properties of PVA should be expected to resolve the serious discrepancies that currently exist in the literature. Better results using the system described here might be obtained by using a sensor-containing polymer that has a glass transition temperature below room temperature. Such an arrangement would permit the test polymer layer to be deposited in intimate contact with the sensor layer and then, as needed for PVA, pre-equilibrated with water vapour at various partial pressures. Nevertheless, the existing information is extremely useful in assessing the viability of proposed photon upconversion schemes for the improving the efficiencies of dye-sensitized solar cells, in which oxygen quenching of triplet states must be avoided.

References

(1) (a) Cisse, A. L.; Grossman, E.; Sibener, S. I. *J. Phys. Chem. B* **2008**, *112*, 7166. (b) Poulsen, L.; Zebger, I.; Tofte, P.; Klinger, M.; Hassager, O.; Ogilby, P. R. *J. Phys. Chem. B* **2003**, *107*, 13885. (c) Poulsen, L.; Ogilby, P. R. *J. Phys. Chem. A* **2000**, *104*, 2573.

(2) (a) Bowyer, W. J.; Xu, W. Y.; Demas, J. N. *Anal. Chem.* **2004**, *76*, 4374. (b) Kneas, K. A.; Demas, J. N.; DeGraff, B. A.; Periasamy, A. *Microsc. microanal.* **2000**, *6*, 551. (c) Obata, M.; Matsuura, N.; Mitsuo, K.; Nagai, H.; Asai, K.; Harada, M.; Hirohara, S.; Tanihara, M.; Yano, S. *J. Polym. Sci. Pol. Chem.* **2010**, *48*, 663. (d) Rharbi, Y.; Yekta, A.; Winnik, M. A. *Anal. Chem.* **1999**, *71*, 5045. (e) Hess, S.; Becker, A.; Baluschev, S.; Yakutkin, V.; Wegner, G. *Macromol. Chem. Phys.* **2007**, *208*, 2173. (f) Lopez-Gejo, J.; Haigh, D.; Orellana, G. *Langmuir* **2010**, *26*, 2144.

(3) Yekta, A.; Masoumi, Z.; Winnik, M. A. *Can. J. Chem.-Rev. Can. Chim.* **1995**, *73*, 2021.

(4) (a) Tian, Y. Q.; Shumway, B. R.; Meldrum, D. R. *Chem. Mat.* **2010**, *22*, 2069. (b) Mills, A.; Lepre, A. *Anal. Chem.* **1997**, *69*, 4653. (c) Xu, W. Y.; McDonough, R. C.; Langsdorf, B.; Demas, J. N.; Degraff, B. A. *Anal. Chem.* **1994**, *66*, 4133. (d) Evans, R. C.; Douglas, P. *Anal. Chem.* **2006**, *78*, 5645. (e) Eaton, K.; Douglas, B.; Douglas, P. *Sens. Actuator B-Chem.* **2004**, *97*, 2. (f) Douglas, P.; Eaton, K. *Sens. Actuator B-Chem.* **2002**, *82*, 200. (g) Douglas, P.; Eaton, K. *Sens. Actuator B-Chem.* **2002**, *82*, 48. (h) Hartmann, P.; Leiner, M. J. P.; Lippitsch, M. E. *Anal. Chem.* **1995**, *67*, 88. (i)

Oige, K.; Avarmaa, T.; Suisalu, A.; Jaaniso, R. *Sens. Actuator B-Chem.* **2005**, *106*, 424. (j) Badocco, D.; Pastore, P. *Anal. Chem.* **2008**, *80*, 2091.

(5) Jones, P. F. *J. Polym. Sci., Part B: Polym. Lett* **1968**, *6*, 487.

(6) Lien, L.; Fellows, C. M.; Copeland, L.; Hawkett, B. S.; Gilbert, R. G. *Aust. J. Chem.* **2002**, *55*, 507.

(7) (a) Sugunan, S. K.; Tripathy, U.; Brunet, S. M. K.; Paige, M. F.; Steer, R. P. *J. Phys. Chem. A* **2009**, *113*, 8548. (b) O'Brien, J. A.; Rallabandi, S.; Tripathy, U.; Paige, M. F.; Steer, R. P. *Chem. Phys. Lett.* **2009**, *475*, 220.

(8) Turro, N. J.; Ramamurthy, V.; Scaiano, J. C. *Principles of Molecular Photochemistry : An Introduction*; University Science Books: Sausalito, California, 2009.

(9) Crank, J.; Park, G. S. *Diffusion in Polymers*; Academic Press: London and New York, 1968.

(10) Kneas, K. A.; Demas, J. N.; Nguyen, B.; Lockhart, A.; Xu, W. Y.; DeGraff, B. A. *Anal. Chem.* **2002**, *74*, 1111.

(11) Furuto, T.; Lee, S. K.; Amao, Y.; Asai, K.; Okura, I. *J. Photochem. Photobiol. A-Chem.* **2000**, *132*, 81.

(12) (a) Karlsson, G. E.; Gedde, U. W.; Hedenqvist, M. S. *Polymer* **2004**, *45*, 3893. (b) Cozmuta, I.; Blanco, M.; Goddard, W. A. *J. Phys. Chem. B* **2007**, *111*, 3151.

(13) Karlsson, G. E.; Johansson, T. S.; Gedde, U. W.; Hedenqvist, M. S. *J. Macromol. Sci.-Phys.* **2002**, *B41*, 185.

(14) (a) Hiltner, A.; Liu, R. Y. F.; Hu, Y. S.; Baer, E. *J. Polym. Sci. Pt. B-Polym. Phys.* **2005**, *43*, 1047. (b) Horas, J. A.; Rizzotto, M. G. *J. Polym. Sci. Pt. B-Polym. Phys.* **1996**, *34*, 1541. (c) Biscoglio, M. *J. Phys. Chem. B* **1999**, *103*, 9070. (d) Van der Bruggen, B.; Jansen, J. C.; Figoli, A.; Geens, J.; Van Baelen, D.; Drioli, E.; Vandecasteele, C. *J. Phys. Chem. B* **2004**, *108*, 13273.

(15) Budd, P. M.; McKeown, N. B.; Fritsch, D. *J. Mater. Chem.* **2005**, *15*, 1977.

(16) Muller-Plathe, F. *Macromolecules* **1991**, *24*, 6475.

Chapter 6: Photophysical studies of a self-assembled metalloporphyrin-fullerene system in solution

6.1 Introduction

As noted in Chapter 1, section 1.8 of this thesis, a myriad of articles deal with electron transfer and energy transfer processes between metalloporphyrins (MPs) and fullerenes in self-assembled and covalently linked dyads, triads and supramolecular structures.[1] These systems are known to generate long-lived, charge-separated species efficiently and therefore have been proposed to be useful in constructing optoelectronic devices and organic solar cells.[2]

MPs and fullerenes are reported to form self-assembled aggregates in both solution and the solid states, normally facilitated *via* the interaction between electron rich 6:6 π bonds of C_{60} and the metal center of the MP.[3] Efficient electron transfer and energy transfer between the triplet states of MP and C_{60} in such self-assembled systems have been reported.[1b] Nanosecond transient absorption spectroscopy of ZnTPP and C_{60} or C_{70} in benzonitrile[4] has demonstrated that selective excitation of concentrated solutions of ZnTPP results in electron transfer from the porphyrin triplet to the C_{60} and C_{70} fullerenes with rates ranging from (5–7) $\times$ 10^8 $M^{-1}s^{-1}$. However, when the fullerene is exclusively excited in benzonitrile, electron transfer from the ground state of ZnTPP to the triplet state of fullerene with rate constants in the (8–10) $\times$ 10^8 $M^{-1}s^{-1}$ range are measured.

The triplet states of ZnTPP and C_{60} are fairly long-lived with lifetimes of the order of ~ 1.2 ms[5] and ~ 0.13 ms[6] respectively. Therefore, electron transfer or energy transfer associated with these states could occur at rates that are potentially competitive with the

rates of other triplet deactivating processes. However, when a porphyrin in close proximity to a potential electron or energy acceptor molecule such as a fullerene is excited in its Soret region, the fate of the locally excited, short-lived (τ_{S2} = 1.4 ps for ZnTPP)[7] S_2 state of the porphyrin can be entirely different. In this case, if energy transfer or electron transfer is to occur from the S_2 state of the MP to C_{60}, it has to occur with rates that are significantly greater than the rate of any other radiative and non-radiative processes from this state.

It was well-established[8] that Soret excitation of a MP-fullerene dyad can rapidly populate the S_1 state of the porphyrin because of its rapid S_2-S_1 internal conversion rate. However, the S_2 state of porphyrin in MP-fullerene constructs can also relax through either energy transfer or electron transfer processes. Thus the fate of the S_2 state of the porphyrin in these dyads is largely governed by the electronic energies and the reduction potential of the electron acceptor, the ground state interaction energy between the porphyrin and the fullerene and the solvation environment.[9] Both energy transfer and electron transfer have been reported in Soret excited porphyrins in covalently-linked dyads and larger supramolecular structures.

Ultrafast electron transfer from the S_2 state of the Soret-excited porphyrins in dyads has been reported by Mataga et al.[10] They proposed that electron transfer occurs from the S_2 state of the porphyrin to various imide acceptors in covalently linked porphyrin–imide dyads with a maximum rate of 7×10^{12} s^{-1} in the barrierless region of the Marcus parabola. On the other hand, the S_2 states of Soret-excited covalently linked porphyrin-C_{60} or –C_{70} dyads have been reported by Kesti et al.[11] relax primarily by $S_2 - S_1$ internal

conversion (60%) within the excited porphyrin moiety and by parallel intramolecular energy transfer to the fullerene (40%). In these latter systems, electron transfer from the locally excited S_2 state of the porphyrin to the fullerene was reported to be highly unlikely in the C_{70} dyads.

One of the primary objectives of our studies using metalloporphyrins as dual absorber-upconverters in TTA schemes is to make use of the energy pooled in the S_2 state of the MP as a result of TTA.[5,7,12] One way of doing this is to couple the MP covalently or noncovalently with electron acceptors to facilitate electron transfer from the MP S_2 state to achieve a long-lived charge transfer state in the complex. This state should then, in turn, be able to inject electrons to the conduction bands of materials such as TiO_2 nanoparticles. In order for facilitating electron transfer efficiently, the S_2 state has to be sufficiently long-lived to allow electron transfer and charge separation processes to compete with other parallel intramolecular and intermolecular decay processes. Nevertheless, ultrafast electron transfer from porphyrin S_2 states with rates approaching 10^{13} s^{-1} has been measured[10] and an investigation to understand the dynamics of such processes, although difficult due to the short lifetime of the S_2 state of porphyrins, is required.

Fullerenes can be used as efficient electron acceptors from triplet MPs in covalent or coordinate structures; however, information about the fate of the initial locally-excited Soret state of MP self-assembled with untethered, unsubstituted fullerenes is scarce. Such an investigation can be complicated by the fact that the quenching of the excited porphyrin proceeds through weak interactions between the MP and fullerene. Such

interactions are usually characterized by a distribution of intermolecular distances.[10b] Nevertheless, investigation of the interactions and dynamics of the excited states of self-assembled MP and fullerenes is required if they are to be used in photon-actuated devices, especially devices in which TTA could be used to enhance the efficiency. In the present study, the photophysical properties of Soret-excited and Q-band excited ZnTPP self-assembled with unsubstituted C_{60} have been examined in both aerated toluene (nonpolar) and benzonitrile (polar) to unravel the mechanism of the relaxation of the locally excited S_2 state and S_1 state of ZnTPP in the aggregate.

6.2 Results and Discussion

6.2.1 Steady state absorption spectral measurements

Fig. 6.1 shows the uv-visible absorption spectra of ZnTPP, C_{60} and their mixtures measured in toluene at room temperature. The spectra of ZnTPP and C_{60} alone in toluene reproduce the literature spectra reported previously.[1,5,7,12-13] The synthesized spectrum obtained by adding the spectra of pure ZnTPP and C_{60} resembles the absorption spectrum of a mixture of the same concentration of ZnTPP and C_{60} as in the individual samples in agreement with reported data.[11,14] The difference spectrum obtained by subtracting the individual spectra of the components from the absorption spectrum of the mixture of ZnTPP and C_{60} essentially produced the instrument baseline, suggesting that the interaction between ZnTPP and C_{60} is very weak in their electronic ground states. This interpretation is supported by the observations that no band shift or band broadening occurred and no measurable additional peaks were formed. This contradicts a recent report of a gradual reduction in the Soret band absorbance of zinc tetrahexylporphine

with the addition of fullerene, resulting in an association constant 1.0 - 3.2 × 10^3 M^{-1}.[15]

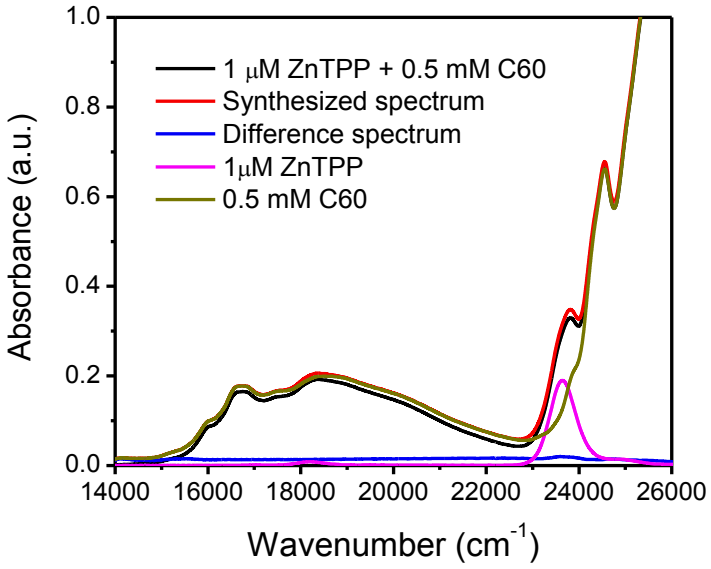

Fig. 6.1 Normalized absorption spectra of (i) 1 μM ZnTPP, (ii) 0.5 mM C_{60}, (iii) a mixture of 1 μM ZnTPP + 0.5 mM C_{60}, (iv) a synthesized spectrum of (i) + (ii), and (v) the difference between (iii) and (iv), all in toluene at room temperature. The spectral bandpass is 2.0 nm. Spectrum (iv) is displaced by 0.01 a.u. relative to spectrum (iii) and (v) is displaced relative to (i) for clarity of comparison.

To confirm that the addition of fullerene has negligible effects on the absorption spectra of ZnTPP, both the Soret and Q-band absorption spectra of a constant concentration of ZnTPP titrated against varying concentrations of fullerene in toluene were measured with a narrow spectral bandwidth and a small data acquisition step size and are shown in Fig. 6.2 (A) and (B), and (C) respectively.

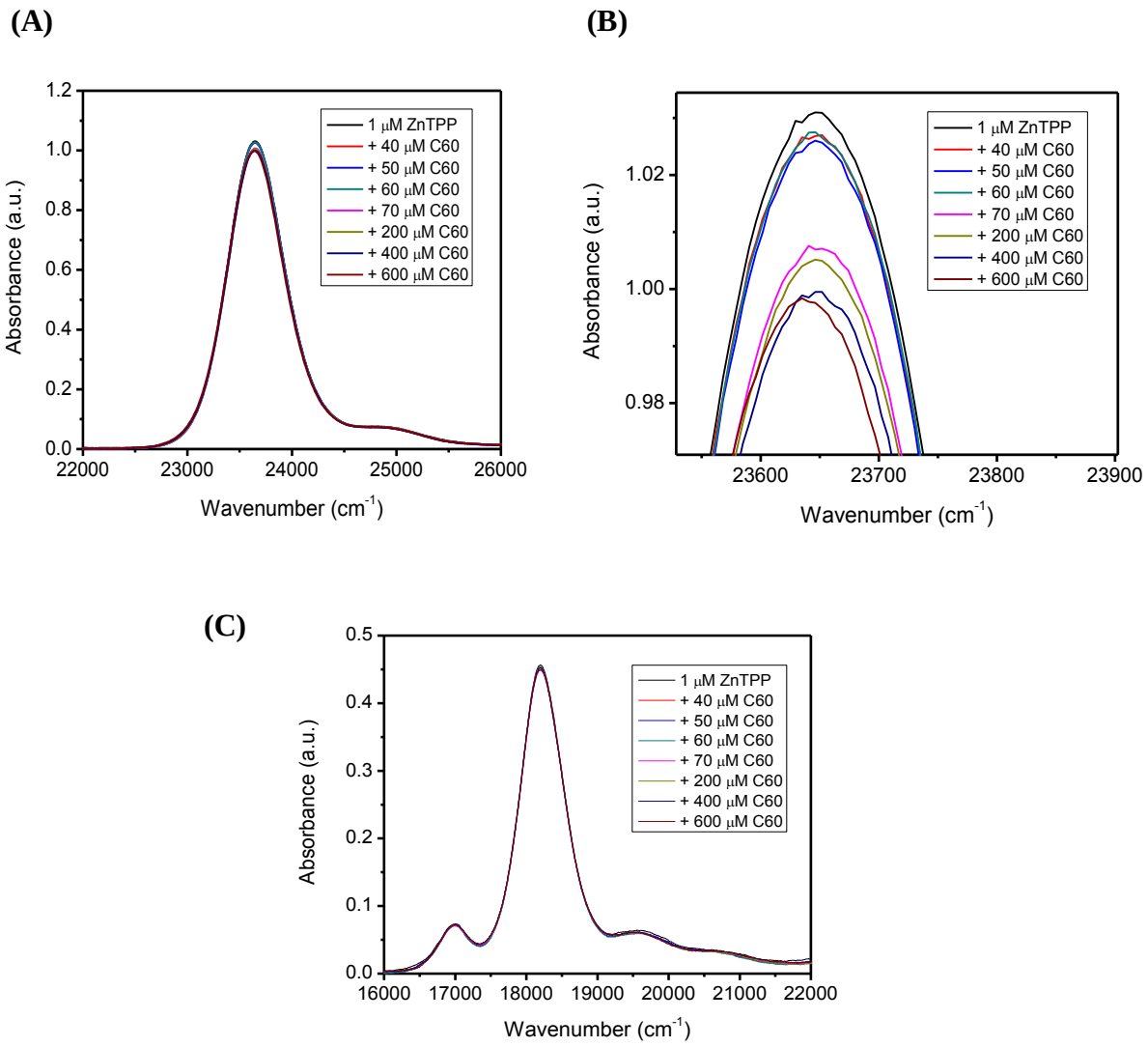

Fig. 6.2 (A) Absorption spectral changes of 20.0 μM ZnTPP with added C_{60} in toluene taken with a 0.5 × 10 mm cuvette. The inset shows the changes in the absorption values in greater detail. (B) Expanded version of Fig. (A). (C) Absorption spectral changes of 20.0 μM ZnTPP with added C_{60} in toluene taken with a 4.0 × 10 mm cuvette. Spectra were collected with a band pass of 0.1 nm and with a step size of 0.1 nm. The matched reference cuvette contained only C_{60} in toluene at the same concentration as that in the sample cuvette.

Any changes in the peak absorbance value were found to be random within a range, $\Delta A = 0.035$ for the Soret band and $\Delta A = 0.02$ for the Q-band. These variations were attributed to random differences in concentration and were much smaller than those reported previously due to the narrow bandwidth and the small step size used. These measurements indicate that there are no statistically significant changes in the peak absorbance and peak shapes in both the Soret and Q band regions of ZnTPP when C_{60} is added.

All of the above absorption measurements were also carried out in the polar solvent benzonitrile which has the ability to stabilize possible charge transfer products. The solubility of C_{60} in benzonitrile is very poor (0.41 mg/mL),[16] which limited the range of concentrations that could be investigated. Poor data were obtained; however, the results were qualitatively similar to those obtained in toluene.

These absorption measurements provide no direct evidence for ground state association between ZnTPP and C_{60}, which might prompt one to conclude that the ground state association constant of ZnTPP and C_{60} is negligibly small. However, literature data supporting the efficient binding of ground state ZnTPP and C_{60} are available. Mutual upfield ring current shifts observed in the NMR spectra of mixtures of metalloporphyrin and fullerenes in arene solutions suggest that association of porphyrin and fullerene in nonpolar solvents does occur.[14] The binding energy between ZnTPP and C_{60} was calculated using TDDFT methods and was reported to be 0.5 eV,[3] suggesting that ground state association should be significant. The enthalpy change associated with the formation

of the ground state complex of ZnTPP with C_{60} in toluene was reported to be -6 kJ mol^{-1}, which could be interpreted as the net enthalpy change associated with displacing solvent toluene molecules from both ZnTPP and C_{60} while forming the complex.[1a,17] Assuming that net entropic effects are significantly small for this process, an association constant for a pure enthalpic controlled complexation can be calculated[18] to be $K_a = 3 \times 10^4$ M^{-1} which is similar to the association constants for other ZnTPP-ligand interactions.

The absorption spectra of a compound often show marked changes in peak shape, in relative intensity, and sometimes new spectral bands upon addition of a second compound capable of forming ground state complexes. This is usually the case when porphyrins bind through axial coordination of the central metal to dative ligands attached to fullerenes and such binding usually results in large values of the association constants of the order of > 10^3 M^{-1}.[2,19] Even though ZnTPP is capable of forming ground state complexes with C_{60} with an association constant of the order of 10^3 - 10^4 M^{-1}, no measurable changes in the absorption spectral features were observed in the present study. However, this could be due to the fact that the ground and excited states of ZnTPP are similarly affected upon addition of fullerene, i.e., that the binding energy of ZnTPP with C_{60} is similar in both the ground state and excited states. This would result in almost perfectly overlapping absorption spectra of ZnTPP+C_{60} in both the complexed and uncomplexed form and could also result in the same magnitude of the molar absorptivity of the complexed and uncomplxed ZnTPP. This would result in oscillator strengths for the transitions in either the Soret band or Q-band that are the same for both complexed and uncomplxed ZnTPP. Based on the above reasoning, it can be postulated that ZnTPP

can undergo ground state self-assembly with C_{60} despite the lack of modified uv-visible absorption spectra. Here, an association constant of *ca*. 10^4 M^{-1} and a binding energy of -6 *kJ mol*$^{-1}$ in both the ground state and excited state of ZnTPP are reasonable.

6.2.2 Fluorescence quenching: Static *vs*. dynamic quenching mechanisms

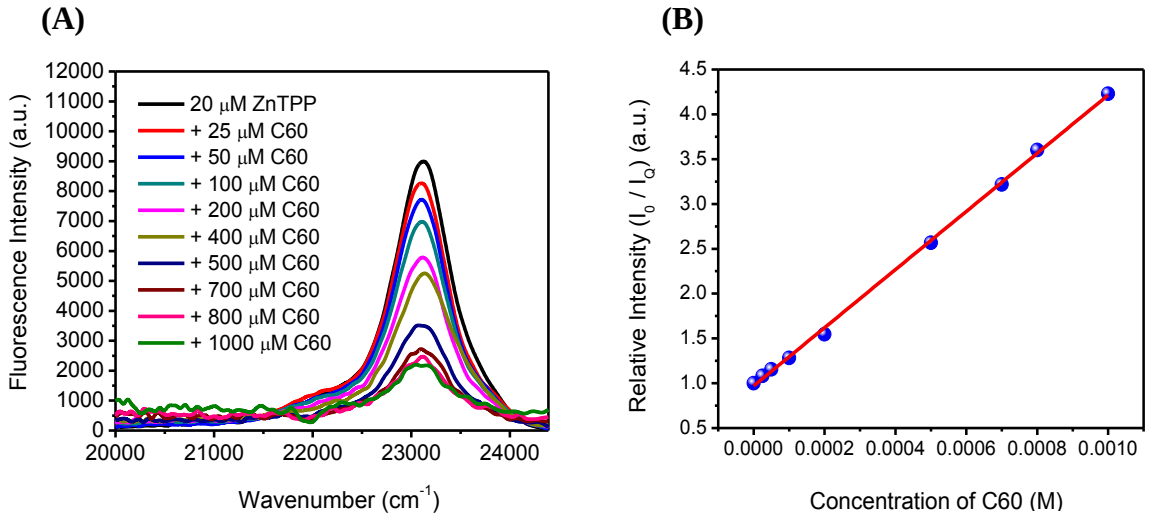

Fig. 6.3 (A) S_2 fluorescence quenching of 20.0 μM ZnTPP obtained upon addition of increasing concentrations of C_{60} when excited at 400 nm. Both excitation and emission band passes were fixed at 2.0 nm. (B) Stern-Volmer plot derived from Fig. 6.3 (A). Excitation at 400 nm and emission monitored at 432 nm. Slope = $(3.24 \pm 0.04) \times 10^3$ M^{-1}. R^2 = 0.99 for the least-squares fit.

Solutions of constant concentrations of ZnTPP were titrated with varying concentrations of C_{60} to observe the effect of adding fullerene on the S_2 fluorescence obtained upon Soret band excitation and S_1 fluorescence obtained upon both Soret and Q-band excitation. Fig. 6.3 (A) demonstrates quenching of the Soret excited (400 nm) S_2 fluorescence of ZnTPP with increasing concentrations of C_{60}. The spectra were corrected for the contribution of background scatter from the solvent, fluorescence reabsorption by

ZnTPP and C_{60} and competitive absorption by C_{60} at the excitation wavelength. Note that with an excess concentration (1mM) of C_{60} in solution, the S_2 fluorescence of ZnTPP is quenched to ~ 28 % of its initial value without added C_{60}. A Stern-Volmer plot constructed by plotting the ratio of the unquenched intensity to the quenched intensities against the concentration of added C_{60} is shown in Fig. 6.3 (B) which yielded a slope of $(3.24 \pm 0.04) \times 10^3\ M^{-1}$.

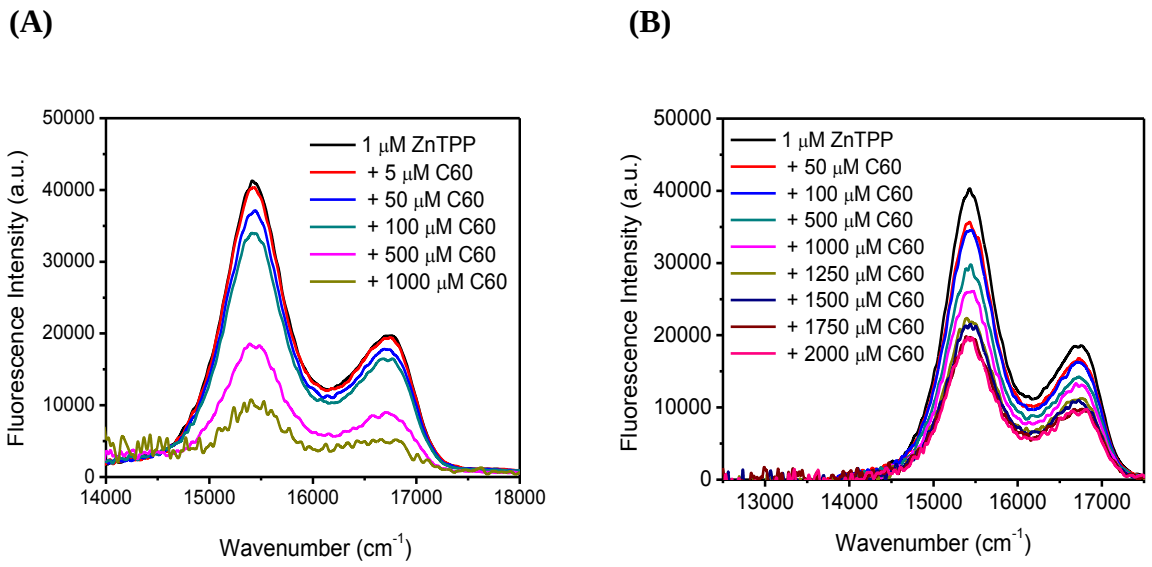

Fig. 6.4 (A) S_1 fluorescence quenching of 1.0 μM ZnTPP upon addition of increasing concentrations of C_{60} when excited at 407 nm. Both excitation and emission band passes were fixed at 2.0 nm. (B) S_1 fluorescence quenching of 1.0 μM ZnTPP obtained upon addition of increasing concentrations of C_{60} when excited at 550 nm. Excitation and emission band passes were fixed at 2.0 nm and 4.0 nm respectively.

Fig. 6.4 (A) and (B) show the quenching of the S_1 fluorescence of ZnTPP obtained when increasing concentrations of C_{60} are added and when excited at 400 nm and 550 nm respectively. Again, these spectra are corrected for solvent background, reabsorption by

ZnTPP and C_{60} in the emission range and competitive absorption by C_{60} at their respective excitation wavelength. It can be observed that the net rate of quenching of the S_1 fluorescence of ZnTPP is higher when the sample is excited to the Soret band, *i.e.* at 400 nm than when it is excited to the Q-band, *i.e.* at 550 nm. For example, when 1 mM of C_{60} is added to 1 µM ZnTPP, the Soret excited sample shows an S_1 fluorescence that is quenched to ~ 25 % of the initial, unquenched intensity obtained by excitation of 1 µM ZnTPP in the Soret band whereas the Q-band excitation of 1 mM of C_{60} added to 1 µM ZnTPP resulted in a reduction in the fluorescence intensity only to ~ 62 % of the unquenched intensity obtained under otherwise identical conditions.

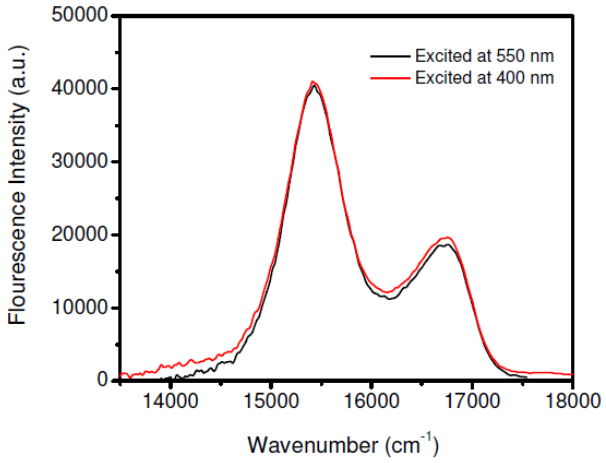

Fig. 6.5 Normalized S_1 fluorescence of 1.0 µM ZnTPP with a 100-fold excess of C_{60} when excited at 400 nm (red curve, both excitation band pass and emission band pass are at 2.0 nm) and at 550 nm (black curve, excitation band pass at 2.0 nm and emission band pass at 4.0 nm).

However, a comparison of the corrected S_1 fluorescence spectra obtained by exciting in the Soret and Q bands (Fig. 6.5) demonstrates that the shapes and relative intensities of the emission bands are identical. The apparent differences in the quenching rates were

immediately obvious when these quenching data were displayed in the form of Stern-Volmer plots. The Stern-Volmer plot for the quenching of the Soret excited ZnTPP:C_{60} mixtures, shown in Fig. 6.6 (A), produced a slope of $(2.72 \pm 0.06) \times 10^3\ M^{-1}$ whereas the quenching plot of Q-band excited mixtures, as shown in Fig. 6.6 (B), yielded a slope of $(0.55 \pm 0.03) \times 10^3\ M^{-1}$.

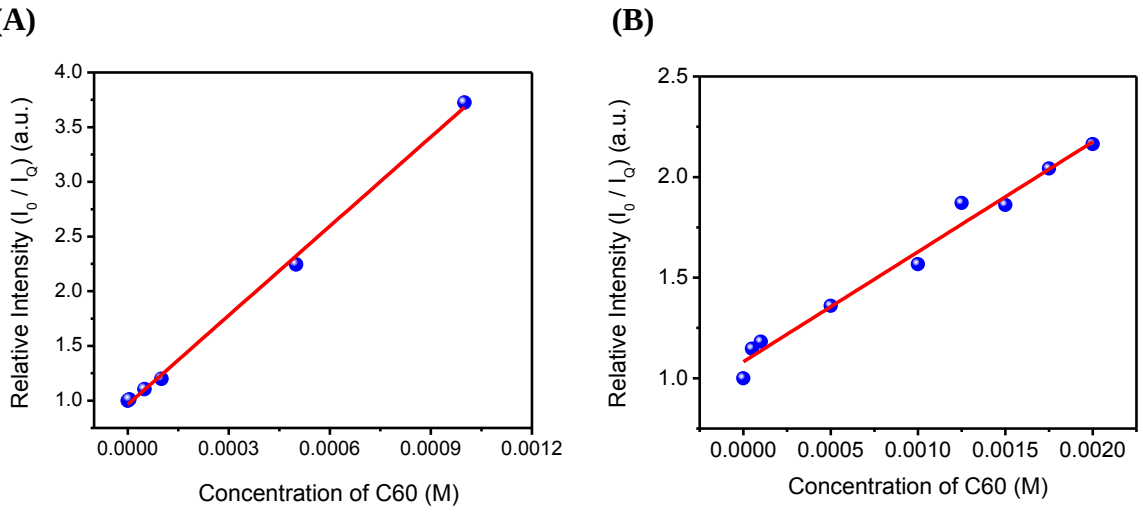

Fig. 6.6 (A) (A) Stern-Volmer plot derived from Fig. 6.4 (A). Excitation at 407 nm and emission monitored at 655 nm. Slope = $(2.72 \pm 0.06) \times 10^3\ M^{-1}$. R^2 = 0.99 for the linear fit. (B) Stern-Volmer plot derived from Figure 6.4 (B). Excitation at 550 nm and emission monitored at 655 nm. Slope = $(0.55 \pm 0.03) \times 10^3\ M^{-1}$. R^2 = 0.98 for the linear fit.

It should be noted that a weak emission in the 15,000 cm^{-1} to 12,000 cm^{-1} region due to the emission from the excited singlet C_{60} itself was observed. Contribution from this emission was much more significant when the sample was excited at 400 nm than when it was excited at 550 nm, and this emission was digitally subtracted from the corresponding spectra after fluorescence corrections. After this subtraction, even at the highest concentration of C_{60} employed, none of these spectra exhibited any additional emission

bands due to the singlet excited state of C_{60} that could possibly originate due to energy transfer between ZnTPP and C_{60} or a radiative charge transfer state formed after electron transfer between ZnTPP and C_{60}.

The spectral emission measurements were carried out in benzonitrile under the same experimental conditions as in toluene. Similar to the absorption measurements carried out in benzonitrile, the data obtained were of poor quality because of the low solubility of C_{60} in benzonitrile.[16] However, the emission data in benzonitrile were qualitatively similar to those in toluene, suggesting similar photophysics in both the solvents. In any case, the steady state absorption and emission spectral measurements of ZnTPP and C_{60} in toluene and benzonitrile did not provide any direct evidence of the possibility of photo-induced electron transfer.

Fluorescence quenching in solution usually follows one of the well-known mechanisms; the static quenching, dynamic quenching, or a combination of both.[20] In the static quenching process, the fluorophore and quencher are complexed in the ground state and the excited state, whereas dynamic quenching follows a diffusion controlled process. Both these quenching mechanisms can be differentiated through the following methods:[20] (i) The Stern-Volmer plots derived from the luminescence quenching data are usually linear for dynamic and static quenching whereas a combination of both results in an upward curved Stern-Volmer plot which is quadratic in the concentration of the quencher. (ii) The lifetime of the emitting state is quenched in the dynamic mechanism whereas it is unaltered in static quenching because only uncomplexed molecule emits fluorescence. (iii) Dynamic quenching shows an increase in rate with increased temperature whereas

static quenching shows a decreased rate of quenching with increased temperature. In order to elucidate the mechanism of quenching, the ps S_2 fluorescence lifetimes, ps S_1 fluorescence rise times and the ns S_1 fluorescence lifetimes of ZnTPP with and without added C_{60} were measured in toluene at a fixed temperature of 295 K.

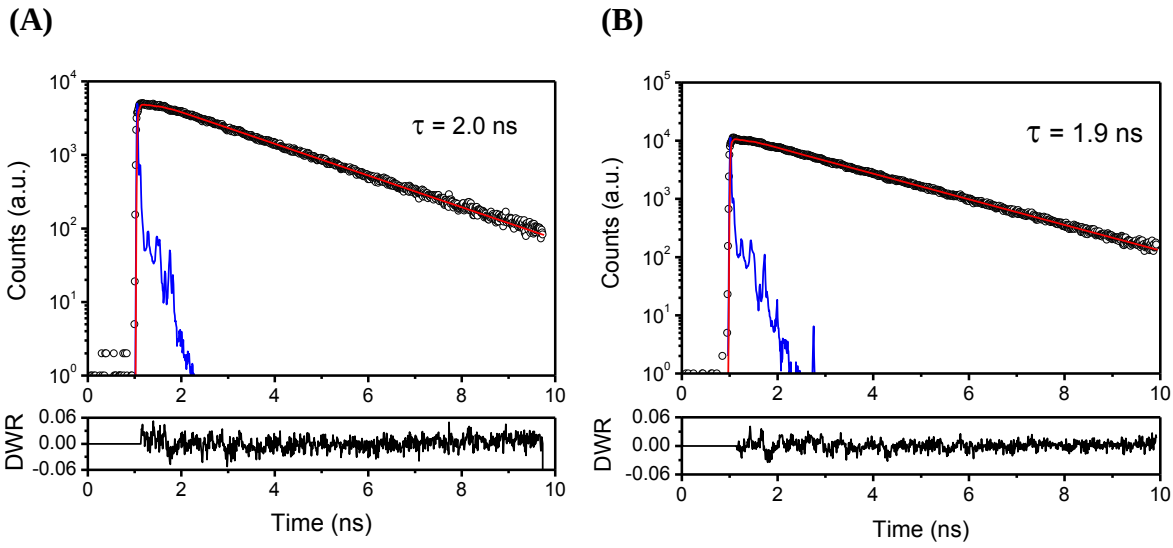

Fig. 6.7 (A) S_1-S_0 fluorescence decay of 1.0 μM ZnTPP. (B) S_1-S_0 fluorescence decay of 1.0 μM ZnTPP with 1.0 mM added C_{60}. Both the samples were excited at 407.0 nm and the emission was monitored at 650.0 nm. Open circles are the data points (9.7 ps per channel) and the solid blue line is the instrument response function. The solid red line is the best single exponential fit to the data determined by the reduced χ^2 value. The lower panel shows the distribution of the weighted residuals.

Figures 6.7 (A) and 5.7 (B) demonstrate the apparent negligible effect of adding large excesses of C_{60} (upto *ca*. 2 mM) on the ns S_1 fluorescence decay of ZnTPP measured at 650 nm. There was a small background emission from C_{60} alone which extended beyond the longest time window of 50 ns and which could not be fitted using a four-exponential decay model and this background was subtracted from the measured decay of the

C_{60}:ZnTPP mixture. The corrected decay curves were well-modeled by single exponential decay functions even after adding a large excess of C_{60}, and yielded a decay time constant of 2.00 ± 0.05 ns. More than half of the ZnTPP will be complexed with C_{60} in the ground state at the highest concentration employed, which should result in a reduction of the S_1 fluorescence intensity by about a factor of two. The observed fluorescence lifetimes of the C_{60}:ZnTPP mixtures represent the unquenched S_1 state lifetime of ZnTPP.[5,21] A very minor shorter-lived decay component (< 2% of the total emission at all C_{60} concentrations up to 1 mM) was observed at this emission wavelength, the apparent amplitude of which increases with increasing the concentration of C_{60}. However, at these highest concentrations subtraction of the C_{60} component resulted in very noisy, imprecise data which is of less significance. The fitting parameters obtained are tabulated in Table 6.1. In this table, τ is the lifetime constant, a is the pre-exponential factor and F is the fraction of the total emission due to each component.

Table 6.1 Time-correlated single photon counting data for the temporal fluorescence profile obtained by exciting 1 μM ZnTPP with added C_{60} in aerated toluene at 407 nm and observing emission in the porphyrin Q band region.

concentration	τ_1 (ns)	a_1	F_1	τ_2 (ns)	a_2	F_2
1 μM ZnTPP	2.05	1.0	1.0			
	2.05	1.0	1.0	-	-	-
	2.06	1.0	1.0			
+ 50 μM C_{60}	2.04	0.92	0.99	0.25	0.08	0.01
	2.04	0.95	0.99	0.25	0.05	0.01
	2.04	0.94	0.99	0.25	0.06	0.01
+ 100 μM C_{60}	2.02	0.97	0.99	0.29	0.03	0.01
	2.02	0.95	0.99	0.26	0.05	0.01
	2.02	0.95	0.99	0.26	0.05	0.01
+ 240 μM C_{60}	2.00	0.93	0.99	0.29	0.07	0.01
	2.00	0.94	0.99	0.28	0.06	0.01
+ 500 μM C_{60}	2.00	0.94	0.99	0.33	0.06	0.01
	2.00	0.95	0.99	0.35	0.05	0.01
	1.99	0.96	0.99	0.32	0.04	0.01
+1000 μM C_{60}	1.97	0.90	0.98	0.37	0.08	0.02
	1.97	0.91	0.98	0.38	0.09	0.02
	1.97	0.90	0.98	0.38	0.10	0.02
+2500 μM C_{60}	1.7	0.7	0.8	0.7	0.3	0.1
	1.7	0.7	0.8	0.7	0.3	0.1
	1.7	0.7	0.8	0.7	0.3	0.1

Measured and analyzed by Dr. Jędrzej Szmytkowski (Department of Chemistry, University of Saskatchewan), Figure 6.8 (A) and (B) illustrate that the addition of a large excess of C_{60} also has no significant effect on the ps S_2 fluorescence decay of ZnTPP in toluene. A time constant, 1.40 ± 0.05 ps is obtained, a value characteristic of an unperturbed, unquenched S_2 excited state of uncomplexed ZnTPP in toluene.[5,7] The S_1 fluorescence rise profiles (measured and analyzed by Dr. Jędrzej Szmytkowski) (see appendix, Fig. A.6.1 and Fig. A.6.2) are much noisier due to the smaller oscillator

strength of the $S_1 - S_0$ transition. Nonetheless, they also remain unaltered after adding a large excess of C_{60} and the rise time remains equal (within ca. ± 0.1 ps) to the S_2 fluorescence decay time of unquenched ZnTPP at all added C_{60} concentrations.

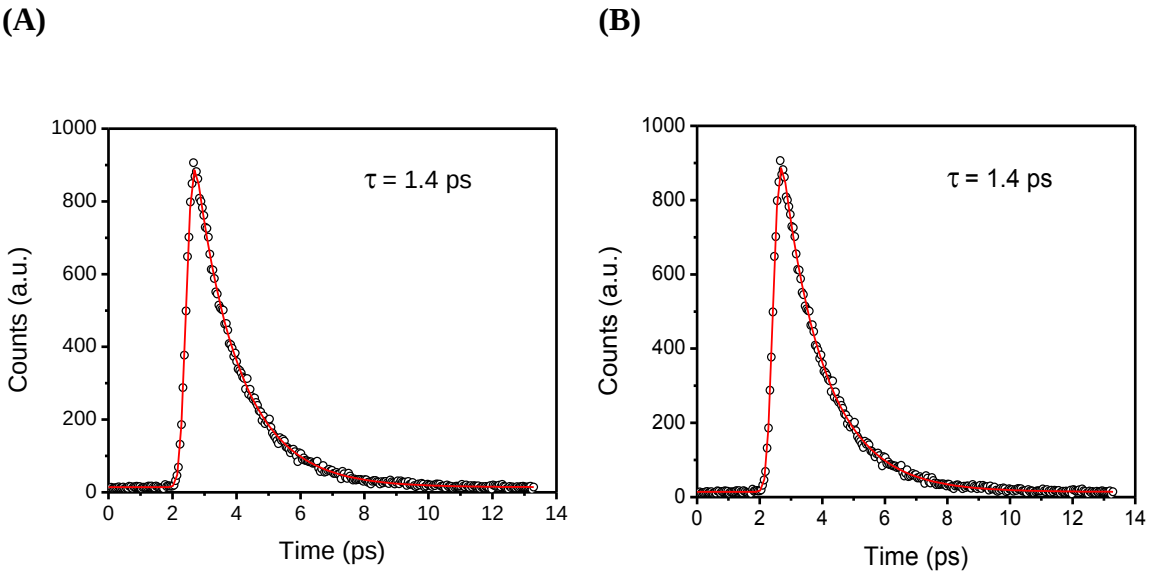

Fig. 6.8 (A) Temporal S_2 fluorescence decay of 180 μM ZnTPP with 27.5 μM added C_{60} in toluene. (B) Temporal S_2 fluorescence decay of 180 μM ZnTPP with 900 μM added C_{60} in toluene. Both the samples were excited at 400 nm and the emission was monitored at 433 nm. The red curve shows the best single exponential fit to the data. The data were obtained at 46 fs per point. The data were measured and analyzed by Dr. Jędrzej Szmytkowski.

In order to determine the quenching mechanism of the Soret excited ZnTPP, the average diffusional displacement of ZnTPP and C_{60} during the S_2 lifetime can be computed using, $\langle x \rangle = (2D\tau_{S2})^{1/2} = (2 \times 1 \times 10^{-9}\ m^2\ s^{-1} \times 1.4 \times 10^{-12}\ s)^{1/2} = 0.06$ nm, where $D = 1 \times 10^{-9}\ m^2\ s^{-1}$ is the diffusion coefficient of a ZnTPP and C_{60} mixture in toluene at room temperature[22] and $\tau_{S2} = 1.4$ ps is the S_2 state lifetime of a ZnTPP.[5,7] This

calculated value of diffusional displacement is much smaller than the average van der Waals spacing between ZnTPP and C_{60}. Therefore during the quenching process, both ZnTPP and C_{60} should be almost stationary within its van der Waals distance during the lifetime of the S_2 state of ZnTPP, which suggests that a purely static process operates for the quenching of the S_2 fluorescence of ZnTPP with C_{60}. This observation is supported by the fact that the measured S_2 state lifetime of ZnTPP remains the same even after adding a large excess of C_{60} (a 1000:1 molar ratio of C_{60}:ZnTPP) and the emission observed was from porphyrin molecules that were not complexed with C_{60} in the ground state. That is, the S_2 fluorescence quenching by C_{60} follows the mechanism,[23]

$$\frac{I_0}{I_Q} = (1 + K_S[Q]) \qquad (6.1)$$

where I_0 is the unquenched S_2 fluorescence intensity, I_Q is the quenched fluorescence intensity obtained upon adding C_{60}, [Q] is the molar concentration of the quencher and K_S is the static quenching constant and is represented as, $K_S = K_{SVS2} = 3.24 \times 10^3\ M^{-1}$. On the basis of the quenching data, it can be inferred that the quenching of the S_2 state of ZnTPP is extremely rapid and occurs with a rate constant that is larger than the rate of decay of the S_2 state of uncomplexed ZnTPP. Thus, Soret excitation of the ZnTPP+C_{60} complex produces a species that is nonradiative and the emission observed is only from porphyrins that are uncomplxed with C_{60} in the ground state. The Stern-Volmer constant or the static quenching constant can be identified as the association constant for ZnTPP and C_{60} in the ground state, i.e.,

$$K_A = [ZnTPP^{\cdots}C_{60}]/([ZnTPP][C_{60}]) = (3.24 \pm 0.04) \times 10^3\ M^{-1} \qquad (6.2)$$

When considering the S_1 fluorescence quenching data, it should be noted that the S_1 fluorescence lifetimes remain unaltered even after adding a large molar excess of C_{60} and this suggests that the emission is arising from ZnTPP that is not complexed with C_{60} in the ground state. This result suggests that the fluorescence quenching proceeds mainly through a pure static mechanism. Apart from an extremely feeble, short-lived emission component observed in the ns time-resolved S_1 fluorescence decays (which contribute only 2% to the total emission at a C_{60}:ZnTPP ratio of 1000:1 and which was ignored due to the inaccuracy of assigning any meaning to this component at the highest concentrations), the only fluorescence decay observed was due to the emission from the S_1 state of the Q band-excited uncomplexed porphyrin. In order for a pure static mechanism to be operative, the quenching rate of the S_1 state of porphyrin in the complex should be greater than the rate of decay of the locally excited S_1 state of ZnTPP which demands that the ZnTPP$^{\cdots}$C$_{60}$ distance should be almost stationary during the quenching process and the species produced upon excitation of the ground state complex should be almost completely dark.

However, the average C$_{60}^{\cdots}$ZnTPP diffusional displacement during the S_1 state lifetime of ZnTPP is $\langle x \rangle = (2D\tau_{S1})^{1/2} = 2$ nm, if the diffusion coefficient for ZnTPP+C_{60} mixture in toluene is assumed to be $D = 1 \times 10^{-9}$ m^2 s^{-1} at room temperature and the lifetime of the ZnTPP S_1 state, $\tau_{S1} = 2.0$ ns in solution.[5,21] This computed displacement is considerably greater than the van der Waals spacing between ZnTPP and fullerene, which range from 0.29 nm to 0.35 nm in co-crystallized zinc metalloporphyrin+C_{60} and +C_{70} aggregates.[24] Therefore, significant diffusional displacement of ZnTPP and C_{60} could be

expected during the lifetime of the S_1 state of ZnTPP which, therefore, suggests that a combination of static and dynamic quenching mechanisms will be needed to explain the observed quenching kinetics. Consider the following equation,[23]

$$\frac{I_0}{I_Q} = (1 + K_D[Q])(1 + K_S[Q]) \qquad (6.3)$$

where K_S and K_D are the static and dynamic quenching constants respectively. If both static and dynamics quenching constants have the same magnitude, then equation (6.3) is quadratic in [Q], which should result in a curved Stern-Volmer plot. If $K_D >> K_S$, then $K_{SV} = K_D = k_Q\tau^0$ and this should yield a value of $k_Q = K_D/\tau^0 = 2.8 \times 10^{11}$ $M^{-1}s^{-1}$. This calculated value of the quenching rate constant is at least 15 times larger than the diffusion controlled quenching rate constant for a bimolecular reaction in toluene at room temperature (obtained using the Stokes–Einstein equation and a toluene solvent viscosity of 0.587 cP at 293K). In addition, the linear Stern-Volmer plot obtained from the steady state quenching and the unquenched S_1 lifetimes suggest that $K_S >> K_D$. Therefore, equation 6.3 can be reduced to equation 6.1, where the static quenching constant, K_S is obtained from the measured Stern-Volmer constant K_{SV}.

The Stern-Volmer constant for S_1 fluorescence quenching upon excitation in the Q-band is given by, $K_{SVS1} = (5.5 \pm 0.3) \times 10^2$ M^{-1}, which poses a puzzle if assigned as the association constant for the aggregation of ZnTPP with C_{60} in the ground state according to the following equation,

$$K_A = [ZnTPP^{\cdots}C_{60}]/([ZnTPP][C_{60}]) = (5.5 \pm 0.3) \times 10^2\ M^{-1} \qquad (6.4)$$

Note that the Stern-Volmer constant (association constant) calculated from the quenching of the S_2 emission of ZnTPP by C_{60} was around 6 times larger than that for quenching the S_1 fluorescence obtained under identical experimental conditions. If both S_1 and S_2 of the ZnTPP in the locally-excited ZnTPP$^{\cdots}C_{60}$ complex are quenched by C_{60} through a pure static mechanism, the same value of K_{SV} and hence the same value of the ground state association constant, K_A, would result. The fact that two different quenching constants were obtained suggests that the differences in the rates of quenching from the first and second singlet excited states of the porphyrin cannot be entirely attributed to excitation of the ground state ZnTPP$^{\cdots}C_{60}$ complex and subsequent quenching in the excited states. It should be mentioned that the relatively small value of K_{SV} obtained for quenching of the Q band excited porphyrin cannot be attributed to an averaging of quenching rates over an increasing range of C_{60} – ZnTPP distances because quenching of the locally-excited species in the S_1 state must occur on a time scale that is very fast compared with the rate of diffusional displacement of C_{60} and ZnTPP.

6.2.3 Mechanisms of fluorescence quenching: electron transfer *vs*. energy transfer

At this point, it is important to examine which mechanisms could be responsible for the apparent differences in the rates of quenching of the excited electronic states of ZnTPP by C_{60}. Both electron transfer and energy transfer pathways have been found to be important in the excited state relaxation pathways in many tethered porphyrin-fullerene complexes. It can be assumed that both these processes are also possible in the self-assembled ZnTPP-C_{60} system, considering the positions of the excited state energy

levels, spectral overlaps and favorable redox parameters of ZnTPP and C_{60}. However, the overlap of the emission bands of ZnTPP and the absorption bands of C_{60} is small and the oscillator strength of the C_{60} bands are very small in regions where spectral overlap occurs. This probably makes dipole-dipole induced Förster resonance energy transfer inefficient. However, many reports suggest that the distance between a porphyrin and fullerene in solution and in solid state aggregates can be as short as the van der Waals distance. If the MP and C_{60} in the untethered 1:1 complexes in solution are separated by van der Waals spacing, both short-range electron transfer and Dexter-type energy transfer can be possible. However, could these processes occur at rates that are competitive with the rate of decay of the S_2 state of ZnTPP? In order to delineate the underlying mechanism of the quenching of the S_2 state of the complex and to determine whether the difference in S_2 and S_1 quenching rates is due to Dexter energy transfer or electron transfer from the S_2 state, picosecond transient absorption spectra of ZnTPP with and without added C_{60} were measured in collaboration with Benjamin Robotham and Prof. Kenneth P. Ghiggino of School of Chemistry, University of Melbourne, Australia.

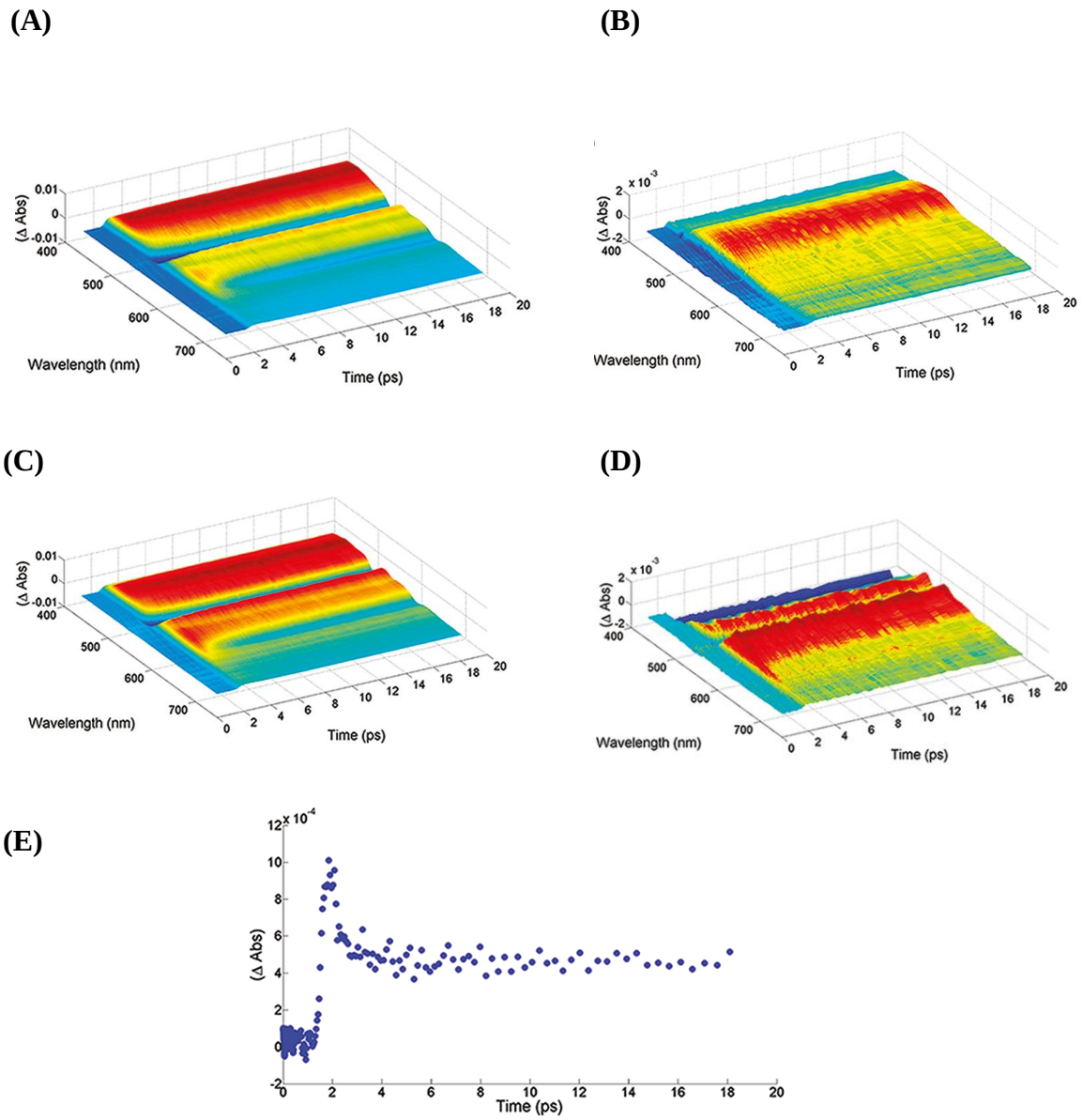

Fig. 6.9 (A) Transient absorption spectrum of 100 μM ZnTPP in toluene excited at 415 nm. (B) Transient absorption spectrum of 1 mM C_{60} in toluene excited at 415 nm. (C) Transient absorption spectrum of 100 μM ZnTPP with 1 mM added C_{60} in toluene excited at 415 nm. (D) Absorbance adjusted difference spectrum of (C) (ZnTPP + C_{60}) - (A) (ZnTPP) - (B) (C_{60}) in toluene. (E) Kinetic trace of the absorbance adjusted difference spectrum (D) at 650 nm. Data were measured and analyzed by Benjamin Robotham, School of Chemistry, University of Melbourne.

Fig. 6.9 (A) shows the picosecond transient absorption of a 100 μM concentration of ZnTPP alone in toluene excited to the Soret band at 415 nm using a train of fs pulses. It can be seen that the spectra in the 400 nm - 500 nm range are dominated by strong absorptions centered at around 470, 575, 610 nm and a weak feature at 676 nm which are due to the transient absorption from the S_1 state of ZnTPP.[10,23,25] A weak spectral feature can also be observed at 650 nm which decays with the same rate as that of the S_2 state of ZnTPP revealed by the picosecond fluorescence upconversion measurements (Fig. 6.8 (A)). Therefore the spectral peak at 650 nm was attributed to the transient absorption by the S_2 state of ZnTPP to some higher excited singlet states (S_n).

The transient absorption spectrum of C_{60} in toluene shown in Fig. 6.9 (B) exhibited broad absorptions peaked at around 544 and 648 nm which were characterized by long decay times. These peaks were assigned to the transient absorptions of the S_1 state of C_{60}. Fig. 6.9 (C) shows the transient absorption spectrum of a mixture of ZnTPP and C_{60} in toluene. This spectrum is qualitatively similar to the transient absorption spectrum of ZnTPP shown in Fig. 6.9 (A). However, the amplitudes of the spectral bands below 500 nm were found to be reduced with an increase in the amplitude of the bands at $\lambda > 500$ nm, with significant increase in the amplitude for the band at 650 nm. In order to understand the spectrum in detail, a transient difference spectrum was constructed by subtracting the relative absorbance corrected transient spectra of ZnTPP and C_{60} from the spectrum of the mixture and this is shown in Fig. 6.9 (D).

It is obvious that the amplitudes of the bands towards the blue end of the spectrum decrease with an apparent increase in the amplitude of the bands beyond 500 nm. The

difference spectrum shows marked spectral features at 525 and 569 nm and a weak feature at 650 nm. Both the bands at 525 and 569 nm are extremely long-lived. They show almost no decay even after scanning over a long delay range, up to 900 ps. This indicates that the states corresponding to these bands have a much longer lifetime than the S_1 lifetimes of ZnTPP and C_{60}, i.e., >>1 ns. The kinetic decay measured at 650 nm was found to decay very rapidly and is limited by the instrument temporal resolution. This extremely short-lived spectral feature starts to overlap with the longer-lived spectral features in the 550 to 700 nm range. The decay of this spectral feature is faster than the S_2 fluorescence decay of ZnTPP itself, which of necessity, is consistent with the rate requirements of the quenching processes from the S_2 state.

The transient absorption spectrum of ZnTPP in benzonitrile is shown in Fig. 6.10 (A) and it is characterized by the signature S_1 transient absorption bands of ZnTPP at 537, 582 and 623 nm. The spectrum displays a weaker absorption with a maximum at 660 nm which decays with the same rate of decay of the S_2 state of ZnTPP and is assigned as the transient absorption of the S_2 state. Fig. 6.10 (B) displays the transient absorption spectrum of C_{60} in benzonitrile with a broad band with a peak maximum around 555 nm and a short-lived weak broader feature with a maximum around 563 nm both of which are attributed to the S_1 absorption of C_{60}. The transient absorption of a mixture of ZnTPP and C_{60}, as shown in Fig. 6.10 (C), is very similar to the spectrum of ZnTPP itself, but with a reduction in the amplitude below *ca*. 520 nm and an enhancement in the amplitude beyond that spectral range.

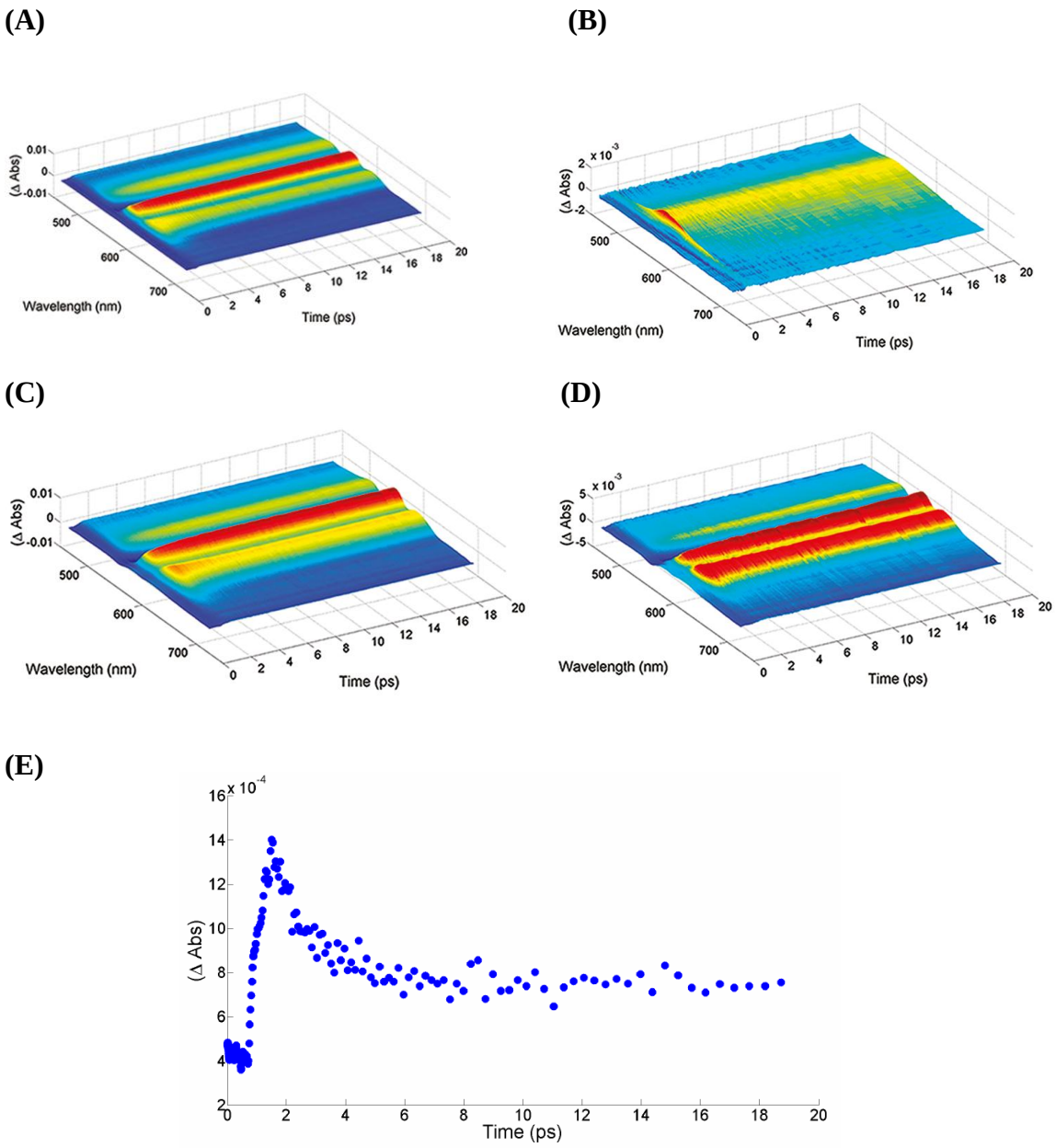

Fig. 6.10 (A) Transient absorption spectra of 100 μMZnTPP in benzonitrile excited at 415 nm. (B) Transient absorption spectra of 200 μM C_{60} in benzonitrile excited at 415 nm. (C) Transient absorption spectra of 100 μM ZnTPP with 200 μM added C_{60} in benzonitrile excited at 415 nm. (D) Absorbance adjusted difference spectrum of (C) (ZnTPP + C_{60}) - (A) (ZnTPP) - (B) (C_{60}) in benzonitrile. (E) Kinetic trace of the absorbance adjusted difference spectrum (D) at 660 nm. Data were measured and analyzed by Benjamin Robotham, School of Chemistry, University of Melbourne.

The relative absorbance-corrected difference spectrum, shown in Fig. 6.10 (D), exhibits a significant reduction of the amplitude in the blue region of the spectrum with a significant increase in the amplitudes towards the red region. The kinetic traces of the transients observed at 534, 580 and 619 nm were not decaying within the temporal pump pulse separation time (10.6 μs). The amplitude and shape of the spectral data collected at any point before the experimental time zero matched those of the data collected afterward time zero, indicating that these bands originate from an extremely long-lived species (lifetime >> 10 μs). The kinetic trace observed at 660 nm showed a very fast decay which is instrument time-resolution limited and which is much faster than the S_2 population decay of ZnTPP molecule itself. This is again consistent with the rate requirements of the quenching of the S_2 state of ZnTPP by C_{60}.

In order to understand the dynamics of the Soret-excited porphyrin self-assembled with C_{60} and the observed differences in the quenching rate constants, we first consider short-range Dexter energy transfer, which depends on the extent of overlap of the electronic wavefunctions of the donor and the acceptor molecules.[26] In order for Dexter energy transfer to be responsible for the enhanced rate of quenching of the S_2 state of ZnTPP compared to its S_1 state, the extent of electronic wavefunction overlap of ZnTPP with C_{60} should be greater than its S_2 state than the S_1 state, i.e.,

$$\left\langle \Psi(ZnTPP^{*}_{(S_2)})\Psi(C_{60(S_0)})\left|\hat{\mathrm{H}}_{\mathrm{e}}\right|\Psi(ZnTPP_{(S_0)})\Psi(C_{60}{}^{*}_{(S_n)})\right\rangle^2$$

$$> \left\langle \Psi ZnTPP^{*}_{(S_1)}\Psi(C_{60(S_0)})\left|\hat{\mathrm{H}}_{\mathrm{e}}\right|\Psi(ZnTPP_{(S_0)})\Psi(C_{60}{}^{*}_{(S_n)})\right\rangle^2 \qquad (6.5)$$

where Ψ represents the electronic orbital wavefunction, $\hat{H}_e$ represents the Hamiltonian for the electronic exchange interaction between ZnTPP and C_{60} and $n \geq 1$ in this case.

The Soret band or Q-band excitation of the ground state complex should instantaneously form a weakly bound exciplex of the same geometry.[10]. It should be noted that ZnTPP is a centrosymmetric molecule and that the same set of molecular orbitals *viz*. nearly-degenerate HOMO and HOMO-1 (symmetry: a_{2u} and a_{1u} in D_{4h}) and the strictly doubly degenerate LUMO (symmetry: e_g in D_{4h}) contribute towards the S_1 and S_2 excited states of ZnTPP.[27] A TDDFT calculation predicts that >95% and >85% of the oscillator strengths of the $S_1 - S_0$ and $S_2 - S_0$ optical transitions respectively are contributed by a sum of the allowed $a_{2u} - e_g$ and $a_{1u} - e_g$ one-electron promotions.[28] Therefore the spatial extent of the electronic wavefunctions of ZnTPP in its S_1 and S_2 states will be very similar and the extent of overlap of these orbitals with the orbitals of C_{60} can also be expected to be similar. However, the polarizability of ZnTPP in its S_2 state is considerably greater than that in the S_1 state as revealed by a linear decrease in the $S_2 - S_1$ electronic energy gap of ZnTPP and other metalloporphyrins with increasing solvent Lorenz-Lorentz polarizability function.[13] Therefore it is reasonable to expect that there would be a slightly greater excited donor-acceptor wavefunction overlap when the complex is excited in the Soret band of ZnTPP and a slightly enhanced rate of Dexter-type energy transfer from the S_2 state of ZnTPP than its S_1 state. If this is true, emission in the NIR region from the excited C_{60} in the ZnTPP:C_{60} species should be observable. However, no direct evidence of enhanced emission due to the excited species in the 13,000 cm^{-1} to 16,000 cm^{-1} region in either toluene or benzonitrile was observed relative

to the emission of C_{60} alone. The emission spectra therefore provide no direct evidence of either Dexter-type short-range energy transfer from ZnTPP to C_{60} or the population of excited C_{60} due to charge recombination within an intermediate charge-separated species.[1i] However, based on this observation, the involvement of the short-range energy transfer process cannot be ruled out because of the following reasons, (i) the fluorescence quantum yield of C_{60} is very low in this spectral range (of the order of ~ 10^{-4})[1i] and (ii) the possibility that only a small fraction of the C_{60} in solution complexes with ZnTPP in the ground state and acts as the energy acceptor for the Soret excited ZnTPP.

Given that both long-range resonance energy transfer and short-range Dexter energy transfer cannot adequately explain the observed differences in the quenching rates of the S_2 and S_1 states of ZnTPP, an alternative possible mechanism to be considered is the short-range electron transfer from ZnTPP to C_{60} in the ZnTPP+C_{60} exciplex. Electron transfer from the Soret band or Q-band excited ZnTPP (donor) to ground state of C_{60} (acceptor) is energetically favorable with a $\Delta G_{ET} < 0$.[10,29] The differences in the net rate of quenching of fluorescence of the S_2 and S_1 states of ZnTPP by C_{60} may be reasonably correlated with the differences in the driving forces of electron transfer from these states to C_{60}. Rehm-Weller equation[19a,30] (described in detail in Chapter 1, section 1.6) can be used to estimate the change in free energy associated with electron transfer from these states and is given as equation 6.6.

$$\Delta G_{ET} = E_{ox}(D) - E_{red}(A) - E^* + \lambda_o \qquad (6.6)$$

where $E_{ox}(D)$ is the oxidation potential of the donor, $E_{(red)}(A)$ is the reduction potential of

the acceptor, E^* is the 0-0 excitation energy of ZnTPP complexed with C_{60} which is greater for the Soret-band excitation compared to the Q-band excitation by a factor of ~ 0.8 eV.[19a] In this equation, λ_o is the solvent reorganization-stabilization energy and is given as,[19a]

$$\lambda_o = \frac{e}{8\pi\varepsilon_0}\left(\frac{1}{r_+} - \frac{1}{r_-}\right)\left(\frac{1}{\varepsilon_s} - \frac{1}{\varepsilon_m}\right) - \frac{e}{4\pi\varepsilon_0}\left(\frac{1}{\varepsilon_s d}\right) \qquad (6.7)$$

where e is the charge of the electron, ε_0 is the permittivity of free space, r_+ and r_- are the ionic radii of the radical cation and the anion respectively, ε_s is the dielectric constant of the solvent in which charge separation occurs, ε_m is the dielectric constant of the medium in which the redox potentials of the donor and the acceptor are measured and d is the interionic distance.

Incorporating the redox potentials of ZnTPP and C_{60} in toluene and assuming that the radical anion $C_{60}^{\cdot -}$ and/or cation $ZnTPP^{\cdot +}$ are produced in the same electronic state in both cases, it can be shown that $\Delta G_{ET,S2} - \Delta G_{ET,S1} = \Delta\Delta G_{ET} = -\Delta E(S_2 - S_0) = -0.81$ eV. Assuming that the radical anion, $C_{60}^{\cdot -}$ is produced in its ground state, the free energy changes associated with electron transfer from both states can be computed as $-\Delta G_{ET,S2} = (1.3 + \lambda_o)$ eV and $-\Delta G_{ET,S1} = (0.5 + \lambda_o)$ eV where λ_o is the solvent stabilization energy given by equation 6.7. In the case of a nonpolar solvent such as toluene λ_o can be as large as 1 eV.[19a,30] However, it was already shown that quenching of the S_2 state of ZnTPP occurs on a sub-ps time scale and both ZnTPP and C_{60} would be almost stationary during this time scale, it can then be reasonably assumed that at least the dipolar solvent

stabilization energy λ_o approaches zero for an electron transfer from Soret excited ZnTPP in toluene.[12a]

The thermodynamic driving force for electron transfer and charge recombination can be mapped out using a Marcus plot where the natural log of the rate of electron transfer is plotted against the free energy required for the electron transfer process. Marcus predicted a "normal region" where the rate of reaction increases with an increase in free energy of reaction and an "inverted region" where the reaction rate decreases with increase in free energy.[31] For a covalently linked ZnTPP-C_{60} dyad in a nonpolar solvent,[10] the calculated free energies of energy transfer would normally imply that electron transfer from the S_2 state would be in the inverted region of the Marcus parabola with the S_1 electron transfer near the maximum of the parabola. This would imply that the rate of electron transfer from S_2 should be slowed down compared to that from S_1. This observation contradicts the observed faster rate of S_2 fluorescence quenching. However, one cannot confidently assign the ground state of $C_{60}^{\cdot -}$ as the initial product state because a variety of electronically excited states are likely to be available to the product radical ions. If the lowest excited doublet state of $C_{60}^{\cdot -}$ rather than the ground state is the product state of electron transfer, then the driving force for electron transfer would be reduced by a factor of 1.55 eV, the electronic excitation energy of the radical anion for the uncomplexed species in CH_2Cl_2/toluene.[32] Therefore, it could be possible that the rate of electron transfer in the Q-band excited complex would fall in the normal Marcus region with that of the Soret-band excited species falling near the barrierless region (similar to the porphyrin-imide dyad). This would result in a faster net rate of electron transfer from

the Soret-excited species compared with the Q band excited species. This possibility is supported by a recent report by Hammarström et al.[33] in which forward electron transfer in a Soret-excited water-soluble zinc porphyrin-viologen complex produces an electronically excited charge transfer state.

Spectroscopic evidence for distinguishing electron transfer and energy transfer mechanisms in donor-acceptor systems can be obtained from their ps transient absorption spectra. Electron transfer process can be exclusively identified by the formation of typically broad absorption bands in the near-IR and IR regions corresponding to a charge separated species due to the radical cation and the anion. The benchmark absorption spectra of the ZnTPP radical cation,[34] $ZnTPP^{\cdot+}$, and the C_{60} radical anion,[32] $C_{60}^{\cdot-}$ are well characterized both as individual species and as ion pairs, and are observed in the ns transient absorption spectra of the charge-separated state obtained after charge transfer from the lowest triplet state of MP to C_{60} in the ground electronic state.[1b,4] The spectral detection limit of the instrument used for acquiring the ps transient absorption in the present study didn't allow observation of the band in the near infrared region corresponding to the ground state of $C_{60}^{\cdot-}$ formed following charge transfer from ZnTPP triplet state. Therefore the only method to characterize the possibility of electron transfer mechanism was to identify the formation of the porphyrin radical cation in the near-IR region, well within the detection range of the instrument used. The presence of both complexed and uncomplexed absorbing products in the ZnTPP+C_{60} mixture produced overlapping spectral features and thus complicated the ps transient absorption spectra. However, the difference spectra shown in Figures 6.9 (D) and 6.10 (D), together with the

corresponding kinetic traces gave the required information about the transient species formed following Soret-band excitation of ZnTPP in ZnTPP+C_{60} mixture.

From the ps transient difference spectrum of ZnTPP and C_{60} in toluene, it is discernible that the amplitudes of the transient absorption signals in the 460 nm region and in the region above 530 nm have similar but inverted temporal kinetic traces. This suggests that the species that absorbs near 460 nm is the precursor of another species that absorbs above 530 nm, hence suggesting a reactant-product relationship. In order to assess this possible reactant-product states, let us consider two possible relaxation paths associated with the S_2 state of Soret excited porphyrin in ZnTPP:C_{60} mixture: (i) ultrafast internal conversion of the Soret excited S_2 state population of ZnTPP to its S_1 state on a sub-ps time scale followed by electron transfer from the S_1 state of ZnTPP to C_{60}, and (ii) ultrafast electron transfer from the S_2 state of ZnTPP to C_{60} on a time scale that is competitive with the internal conversion rate from S_2 to S_1 state. It can be observed from the kinetic trace recorded at 650 nm that the short lived component builds up faster than the spectral features corresponding to the S_1 state of ZnTPP and that this short-lived component decays faster than the unquenched S_2 state lifetime of ZnTPP. This suggests that the 650 nm spectral feature could be the product of electron transfer from the S_2 state to C_{60} in the ZnTPP:C_{60} complex which forms on a faster time scale than the internal conversion time scale. This should create a dark electronically excited charge separated state with a slightly shifted band with enhanced molar absorptivity compared to the lowest energy charge separated state. The fact that this feature decays faster than the decay of the charge separated state originating in the S_1 state suggests that it may be

relaxing by charge recombination to a vibrationally hot excited ground state, thus bypassing the S_1 state.

The long-lived transient spectral features observed in benzonitrile extended to times beyond the excitation pulse separation. This shows that the species formed upon Soret-excitation of the porphyrin in the complex is stabilized by the polar solvent benzonitrile. When the diffusion rates are taken into consideration, it is difficult to interpret as whether these transients originate from the excitation of a ground state complex or from interactions during the long lifetime of the triplet state of ZnTPP. The very short-lived component observed around 660 nm suggests that rapid electron transfer does occur from the S_2 state of ZnTPP to C_{60} to form an excited charge separated state, which then undergoes rapid charge recombination to a vibrationally excited ZnTPP ground state. However, the solubility of C_{60} is low in benzonitrile, the range of concentrations that can be measured is limited, and this resulted in poor signal to noise ratios and lower intensities of the transient absorption bands.

The relative amounts of the various species observed cannot be estimated directly from the transient absorption measurements in the present study and the possibility of simultaneous energy and electron transfer relaxation channels for the excited states of ZnTPP cannot be ruled out. Nevertheless, qualitative spectroscopic evidence for the formation on a sub-ps time scale of charge-transfer species that undergo recombination to a vibrationally excited ground state was obtained when untethered self-assembled porphyrin-fullerene complexes are excited in the Soret band. Qualitative support for this mechanism was obtained in measurements of the extent of photodegradation of the

ZnTPP during the transient absorption experiments. When ZnTPP alone in the aerated toluene and benzonitrile solvents was irradiated, it degraded to a greater extent than when the same concentration of ZnTPP in the same solvent containing a large excess of C_{60} was subjected to the same total radiant exposure. This suggests that C_{60} acts as a photoprotective agent in these experiments by acting as a sink for the energy of the excited state population of ZnTPP *via* the mechanisms outlined above.

It should be noted that the features peaking around 650 nm in the ps transient absorption spectra of uncomplexed ZnTPP that relax with the same rate of decay of the S_2 fluorescence of ZnTPP arise from the transient absorption of the S_2 state of the porphyrin itself. Assuming that this transition is facilitated by an allowed one-photon transition having substantial oscillator strength from the S_2 (2^1E_u) state to a higher *gerade* singlet state of ZnTPP, the energy of this product state populated by transient absorption from the S_2 state can be predicted to be around 4.9 eV (253 nm). This is obtained by adding the one electron transition energy (the pump frequency) to the S_2 state (3.0 eV) and the peak energy of the transition at 650 nm (1.9 eV). Time-dependent density functional theory calculations[28] predict the presence of several *gerade* singlet electronic states lying above the 2^1E_u state of ZnTPP, but these calculations do not extend above 3.5 eV. Two-photon absorption measurements of ZnTPP would help to reveal its $g - g$ electronic spacing and thus extract information about the *gerade* singlet state lying at around 4.9 eV.

6.3 Conclusions

The photophysical properties of the model donor-acceptor system, ZnTPP-C_{60} has been studied in a nonpolar solvent, toluene and a polar solvent, benzonitrile using steady state absorption and fluorescence spectroscopy, nanosecond time-correlated single photon counting, ps fluorescence upconversion and ps transient absorption spectroscopy. It is confirmed that ZnTPP and C_{60} aggregate in the ground state. Simultaneous excitation of uncomplexed and complexed ZnTPP complicates the photophysical behavior of this system. The steady state spectroscopic data are qualitatively similar in both nonpolar toluene and polar benzonitrile solvents and show that quenching occurs faster when exciting to S_2 of the porphyrin, compared with S_1. However, evidence for distinguishing between Dexter-type short-range energy transfer process and photo-induced electron transfer could not be found. Both steady state fluorescence quenching data and fluorescence lifetime measurements suggested that the apparent differences between the quenching constants of the Soret-excited and the Q-band excited complexes cannot be attributed to the quenching of an exciplex formed from the ground state complex of ZnTPP and C_{60}. The possibility of long-range Förster-type energy transfer from the S_2 and S_1 state of ZnTPP to C_{60} can be ruled out based on the poor spectral overlap between ZnTPP and C_{60}. Nevertheless, definitive evidence of ultrafast quenching of the locally excited S_2 state of ZnTPP in the ZnTPP$^{\cdots}C_{60}$ complex was obtained from both steady state and ps transient absorption measurements. Either or both short-range electronic energy transfer and electron transfer are possible in the excited complex and the feasibility of these mechanisms has been examined. Formation of long-lived transients,

on a sub-ps time scale, representing the charge-separated states has been observed for the first time in the ps transient absorption spectra. The possibility of parallel energy and electron transfer relaxation processes cannot be ruled out. Nevertheless, relaxation processes which by-pass the locally-excited S_1 state have been observed. Soret excitation of ZnTPP in the complex does not result in a quantitative yield of the S_1 state of the species. Finally, a transient absorption feature centered around 650 nm was observed which was never reported previously and was attributed to the absorption of the S_2 state of ZnTPP itself to a higher *gerade* singlet excited state.

References

(1) (a) Orlandi, G.; Negri, F. *Photochem. Photobiol. Sci.* **2002**, *1*, 289. (b) El-Khouly, M. E.; Ito, O.; Smith, P. M.; D'Souza, F. *J. Photochem. Photobiol., C* **2004**, *5*, 79. (c) Boyd, P. D. W.; Reed, C. A. *Acc. Chem. Res.* **2005**, *38*, 235. (d) D'Souza, F.; Ito, O. *Coord. Chem. Rev.* **2005**, *249*, 1410. (e) Thomas, K. G.; George, M. V.; Kamat, P. V. *Helv. Chim. Acta* **2005**, *88*, 1291. (f) Tashiro, K.; Aida, T. *Chem. Soc. Rev.* **2007**, *36*, 189. (g) Drain, C. M.; Varotto, A.; Radivojevic, I. *Chem. Rev.* **2009**, *109*, 1630. (h) Beletskaya, I.; Tyurin, V. S.; Tsivadze, A. Y.; Guilard, R.; Stern, C. *Chem. Rev.* **2009**, *109*, 1659. (i) Accorsi, G.; Armaroli, N. *J. Phys. Chem. C* **2010**, *114*, 1385. (j) Grimm, B.; Hausmann, A.; Khant, A.; Seitz, W.; Spänig, F.; Guldi, D. M. *Handbook of Porphyrin Science, Vol. 1, Supramolecular Chemistry*; World Scientific: Singapore, 2010. (k) D'Souza, F.; Ito, O. *Handbook of Porphyrin Science, Vol. 1, Supramolecular Chemistry*; World Scientific: Singapore, 2010.

(2) (a) Bell, T. D. M.; Ghiggino, K. P.; Jolliffe, K. A.; Ranasinghe, M. G.; Langford, S. J.; Shephard, M. J.; Paddon-Row, M. N. *J. Phys. Chem. A* **2002**, *106*, 10079. (b) Milanesio, M. E.; Gervaldo, M.; Otero, L. A.; Sereno, L.; Silber, J. J.; Durantini, E. N. *J. Phys. Org. Chem.* **2002**, *15*, 844. (c) Vail, S. A.; Tome, J. P. C.; Krawczuk, P. J.; Dourandin, A.; Shafirovich, V.; Cavaleiro, J. A. S.; Schuster, D. I. *J. Phys. Org. Chem.* **2004**, *17*, 814. (d) Imahori, H. *Org. Biomol. Chem.* **2004**, *2*, 1425. (e) Nierengarten, J.-F. *New J. Chem.* **2004**, *28*, 1177. (f) Günes, S.; Neugebauer, H.; Sariciftci, N. S. *Chem. Rev.* **2007**, *107*, 1324. (g) Imahori, H.; Umeyama, T. *J. Phys. Chem. C* **2009**, *113*, 9029. (h) Megiatto, J. D.; Schuster, D.

I.; Abwandner, S.; de, M. G.; Guldi, D. M. *J. Am. Chem. Soc.* **2010**, *132*, 3847. (i) Pal, S. K.; Kesti, T.; Maiti, M.; Zhang, F.; Inganaas, O.; Hellstroem, S.; Andersson, M. R.; Oswald, F.; Langa, F.; Oesterman, T.; Pascher, T.; Yartsev, A.; Sundstroem, V. *J. Am. Chem. Soc.* **2010**, *132*, 12440.

(3) (a) Liao, M.-S.; Watts, J. D.; Huang, M.-J. *Phys. Chem. Chem. Phys.* **2009**, *11*, 4365. (b) Liao, M.-S.; Watts, J. D.; Huang, M.-J. *J. Phys. Chem. B* **2007**, *111*, 4374.

(4) (a) Nojiri, T.; Watanabe, A.; Ito, O. *J. Phys. Chem. A* **1998**, *102*, 5215. (b) El-Khouly, M. E.; Fujitsuka, M.; Ito, O. *J. Porphyr. Phthalocya.* **2000**, *4*, 590.

(5) Sugunan, S. K.; Tripathy, U.; Brunet, S. M. K.; Paige, M. F.; Steer, R. P. *J. Phys. Chem. A* **2009**, *113*, 8548.

(6) Fraelich, M. R.; Weisman, R. B. *J. Phys. Chem.* **1993**, *97*, 11145.

(7) Steer, R. P. *J. Appl. Phys.* **2007**, *102*, 076102/1.

(8) (a) Kesti, T. J.; Tkachenko, N. V.; Vehmanen, V.; Yamada, H.; Imahori, H.; Fukuzumi, S.; Lemmetyinen, H. *J. Am. Chem. Soc.* **2002**, *124*, 8067. (b) Yamada, H.; Ohkubo, K.; Kuzuhara, D.; Takahashi, T.; Sandanayaka, A. S. D.; Okujima, T.; Ohara, K.; Ito, O.; Uno, H.; Ono, N.; Fukuzumi, S. *J. Phys. Chem. B* **2010**, *114*, 14717.

(9) Sugunan, S. K.; Robotham, B.; Sloan, R. P.; Szmytkowski, J.; Ghiggino, K. P.; Paige, M. F.; Steer, R. P. *J. Phys. Chem. A* **2011**, *115*, 12217.

(10) (a) Mataga, N.; Chosrowjan, H.; Shibata, Y.; Yoshida, N.; Osuka, A.; Kikuzawa, T.; Okada, T. *J. Am. Chem. Soc.* **2001**, *123*, 12422. (b) Mataga, N.; Chosrowjan,

H.; Taniguchi, S. *J. Photochem. Photobiol. C* **2005**, *6*, 37. (c) Mataga, N.; Chosrowjan, H.; Taniguchi, S.; Shibata, Y.; Yoshida, N.; Osuka, A.; Kikuzawa, T.; Okada, T. *J. Phys. Chem. A* **2002**, *106*, 12191. (d) Mataga, N.; Taniguchi, S.; Chosrowjan, H.; Osuka, A.; Yoshida, N. *Photochem. Photobiol. Sci.* **2003**, *2*, 493. (e) Mataga, N.; Taniguchi, S.; Chosrowjan, H.; Osuka, A.; Yoshida, N. *Chem. Phys.* **2003**, *295*, 215.

(11) Kesti, T.; Tkachenko, N.; Yamada, H.; Imahori, H.; Fukuzumi, S.; Lemmetyinen, H. *Photochem. Photobiol. Sci.* **2003**, *2*, 251.

(12) (a) Maiti, M.; Danger, B. R.; Steer, R. P. *J. Phys. Chem. A* **2009**, *113*, 11318. (b) O'Brien, J. A.; Rallabandi, S.; Tripathy, U.; Paige, M. F.; Steer, R. P. *Chem. Phys. Lett.* **2009**, *475*, 220.

(13) (a) Liu, X.; Tripathy, U.; Bhosale, S. V.; Langford, S. J.; Steer, R. P. *J. Phys. Chem. A* **2008**, *112*, 8986. (b) Tripathy, U.; Kowalska, D.; Liu, X.; Velate, S.; Steer, R. P. *J. Phys. Chem. A* **2008**, *112*, 5824.

(14) (a) Boyd, P. D. W.; Hodgson, M. C.; Rickard, C. E. F.; Oliver, A. G.; Chaker, L.; Brothers, P. J.; Bolskar, R. D.; Tham, F. S.; Reed, C. A. *J. Am. Chem. Soc.* **1999**, *121*, 10487. (b) Wahadoszamen, M.; Nakabayashi, T.; Kang, S.; Imahori, H.; Ohta, N. *J. Phys. Chem. B* **2006**, *110*, 20354.

(15) Bhattacharya, S.; Ujihashi, N.; Aonuma, S.; Kimura, T.; Komatsu, N. *Spectrochim. Acta A* **2007**, *68*, 495.

(16) Ruoff, R. S.; Tse, D. S.; Malhotra, R.; Lorents, D. C. *J. Phys. Chem.* **1993**, *97*, 3379.

(17) Xiao, J.; Meyerhoff, M. E. *J. Chromatog. A* **1995**, *715*, 19.

(18) Hosseini, A.; Taylor, S.; Accorsi, G.; Armaroli, N.; Reed, C. A.; Boyd, P. D. W. *J. Am. Chem. Soc.* **2006**, *128*, 15903.

(19) (a) Danger, B. R.; Bedient, K.; Maiti, M.; Burgess, I. J.; Steer, R. P. *J. Phys. Chem. A* **2010**, *114*, 10960. (b) Flamigni, L.; Ventura, B.; Oliva, A. I.; Ballester, P. *Chem.--Eur. J.* **2008**, *14*, 4214.

(20) Lakowicz, J. R., *Principles of Fluorescence Spectroscopy*; Springer: New York, 2006.

(21) Kowalska, D.; Steer, R. P. *J. Photochem. Photobiol., A* **2008**, *195*, 223.

(22) Saiki, H.; Takami, K.; Tominaga, T. *Phys. Chem. Chem. Phys.* **1999**, *1*, 303.

(23) Lukaszewicz, A.; Karolczak, J.; Kowalska, D.; Maciejewski, A.; Ziolek, M.; Steer, R. P. *Chem. Phys.* **2007**, *331*, 359.

(24) Konarev, D. V.; Kovalevsky, A. Y.; Li, X.; Neretin, I. S.; Litvinov, A. L.; Drichko, N. y. V.; Slovokhotov, Y. L.; Coppens, P.; Lyubovskaya, R. N. *Inorg. Chem.* **2002**, *41*, 3638.

(25) Yu, H.-Z.; Baskin, J. S.; Zewail, A. H. *J. Phys. Chem. A* **2002**, *106*, 9845.

(26) Dexter, D. L. *J. Chem. Phys.* **1953**, *21*, 836.

(27) Tripathy, U.; Steer, R. P. *J. Porphyr. Phthalocya.* **2007**, *11*, 228.

(28) Liu, X.; Yeow, E. K. L.; Velate, S.; Steer, R. P. *Phys. Chem. Chem. Phys.* **2006**, *8*, 1298.

(29) Imahori, H.; El-Khouly, M. E.; Fujitsuka, M.; Ito, O.; Sakata, Y.; Fukuzumi, S. *J. Phys. Chem. A* **2001**, *105*, 325.

(30) (a) Rehm, D.; Weller, A. *Ber. Bunsenges. Phys. Chem.* **1969**, *73*, 834. (b) Weller, A. *Z. Phys. Chem. (Wiesbaden)* **1982**, *133*, 93.

(31) Kavarnos, G. J.; Turro, N. J. *Chem. Rev.* **1986**, *86*, 401.

(32) Greaney, M. A.; Gorun, S. M. *J. Phys. Chem.* **1991**, *95*, 7142.

(33) (a) Andersson, M.; Davidsson, J.; Hammarstroem, L.; Korppi-Tommola, J.; Peltola, T. *J. Phys. Chem. B* **1999**, *103*, 3258. (b) Petersson, J.; Eklund, M.; Davidsson, J.; Hammarstroem, L. *J. Phys. Chem. B* **2010**, *114*, 14329.

(34) Fajer, J.; Borg, D. C.; Forman, A.; Dolphin, D.; Felton, R. H. *J. Amer. Chem. Soc.* **1970**, *92*, 3451.

Chapter 7: Conclusions and suggestions for future work

7.1 Conclusions

With the global production and supply of fossil fuels declining exponentially,[1] the search for alternative energy sources has mainly converged to green energy sources such as solar energy. Conventional silicon-based solar cells are efficient, but they are relatively expensive to manufacture, and are rigid, thick and fragile. Dye-sensitized solar cells (DSSCs) are proposed as inexpensive, thin and flexible alternatives. Efficiencies of up to 12% have been achieved for DSSCs.[2] Dyes that are usually used in DSSCs do not absorb light efficiently in the near-IR region of the solar spectrum where the photon flux is significant. Some dyes are capable of absorbing in this range and upconverting the absorbed energy through TTA and this NCPU scheme has been proposed as a viable method to utilize the near-IR part of the solar spectrum. However, when the light absorber itself can act as an upconverter, TTA populates a higher excited singlet state that is usually very short-lived. Therefore it is essential to utilize the energy deposited into these higher excited states before it is wasted through non-productive photophysical processes. This requires a detailed understanding of the mechanisms of TTA, the properties of the excited states accessible through TTA, and further photophysical processes.

In order to contribute towards our understanding of the involvement of higher excited singlet states produced by TTA, we have selected diamagnetic metalloporphyrins and

fullerenes as models for further investigation. The model metalloporphyrin ZnTPP undergoes efficient TTA to populate its short-lived S_2 state from which it fluoresces. It was demonstrated that the TTA-produced, short-lived S_2 state cannot act as an electron or energy donor to an acceptor molecule unless strong ground state interaction exists between the porphyrin and the acceptor. The second candidate, C_{60}, acts as efficient triplet energy donor to a BE followed by annihilation of the triplet BE molecules to form the S_1 state of the BE which emits fluorescence. The S_n ($n > 1$) electronic energy levels of C_{60} are closely spaced and rapidly decay to the S_1 state. Therefore, it is unlikely that these states could act as an energy or electron donor in the absence of aggregation. However, we have demonstrated that C_{60} can act as an efficient electron acceptor for Soret-excited ZnTPP in solution. Therefore a combination of ZnTPP and C_{60} may be used as a candidate for NCPU in a DSSC scheme. Finally, TTA has been used as a tool to measure the oxygen permeabilities of a polymer thin film, which is of importance considering the need to eliminate oxygen from devices based on TTA.

The studies presented in this thesis address the possibility of using the higher excited singlet states (S_n, $n \geq 2$) produced from TTA in metalloporphyrins and fullerenes as electron and energy donors in a DSSC. The ultimate challenges to achieve this goal are associated with the inherent photophysical properties of these molecules. However, the studies described in this thesis provide a fundamental perspective of the photophysical events of TTA. Further extensive studies are required to make the short-lived S_n product state of TTA in metalloporphyrins and fullerenes a viable source of electronic energy in a DSSC scheme. The key issues to be addressed are: (i) optimization of the yield of the

product state (S_n) of TTA, (ii) choice of suitable electron acceptors for the S_n state produced from TTA, (iii) manufacture of solar cells based on TTA, and their testing and optimization. A discussion about possible ways to handle these issues forms the following future work proposal of this thesis.

7.2 Suggestions for future work

The yield of the S_n state produced on homomolecular TTA depends mainly upon the efficiency of the TTA process. Having proved that the efficiency of TTA can surpass 40% by removing the spin statistics restriction, room is available for further improvements. The first and foremost challenge is to improve the ability of the upconverter molecule to absorb the maximum number of photons that can be utilized in TTA. The molar extinction coefficients of metalloporphyrins and fullerenes are small in the near-IR to IR region. This can be enhanced by taking advantage of the structure-property relationships of these molecules in different ways: (i) Breaking the symmetry of the molecule through chemical functionalization can help. However, this could also affect the relative energies of the singlet and triplet states of these molecules and hence their rates of radiative and nonradiative transitions; (ii) It will be possible to functionalize the upconverter molecule with light harvesting antenna chromophores possessing large absorption cross-sections and molar extinction coefficients[3] that can transfer the harvested energy to the upconverter through a Förster or Dexter type mechanisms. However, this can work in part at the cost of changing the electronic energy levels of the upconverter molecule; (iii) Upconverter molecules with large absorption cross-sections

and molar extinction coefficients in the red and NIR of the electromagnetic spectrum can be synthesized by extending their π-electron conjugation.

Secondly, the annihilation probability should be maximized to optimize the yield of the product state. This can be achieved by increasing the probability that a triplet annihilator molecule finds its partner to annihilate before it gets a chance to decay by other processes. This can be achieved by controlling the concentration of the annihilator molecules and by restricting these molecules so that they are close to each other in a confined space. We have demonstrated that TTA occurs through a Dexter mechanism, so that the extent of solute aggregation (which in turn is controlled by its concentration) is a fundamental criterion to maximize such interactions. This is especially important for TTA in the solid state where TTA is controlled by triplet exciton diffusion and the annihilation probability is controlled by the degree of solute aggregation. It was demonstrated that the annihilation probability can be enhanced by trapping the molecules in a nanoparticle.[4] We propose that this could also be achieved by using yoctowells, gaps having yoctolitre volumes (1 yL = 10^{-24} L) created by molecular walls,[5] which can trap the triplet annihilator molecules.

For solid state DSSC devices that are designed to perform for long periods of time, keeping the device oxygen free is a tedious task and may not be practically 100% efficient. Instead of allowing for leaked oxygen to decrease the long-term efficiency and stability of these devices, strategies must be made to take advantage of the oxygen

leaking into these devices, such as utilizing a NCPU system proposed by Schmidt et al.[6] in which molecular oxygen is utilized as a mediator for triplet energy transfer and NCPU.

The S_n states of the proposed molecules are short-lived and may undergo rapid decay before injecting electrons into the conduction band of a semiconductor in a DSSC device. Therefore it may be necessary to use an intermediate molecule which can accept electronic energy from the absorbing molecule in the S_n state through energy transfer or electron transfer. If the intermediate molecule is an electron acceptor, in order to be efficient, the electron transfer between the S_n state of the upconverter and this molecule should be very fast, the charge recombination of the upconverter cation and the intermediate molecular radical anion should be very slow. Finally the electron transfer from the intermediate molecule to a semiconductor should be rapid. We have demonstrated that C_{60} can be used as an intermediate molecule to generate a charge-separated state by accepting the electrons from Soret-excited ZnTPP. However C_{60} itself absorbs at the excitation wavelength used for our model molecule ZnTPP and C_{60} could undergo TTA within itself. This would complicate the photophysical processes and would affect the efficiency of these processes. Therefore, new molecules including higher order fullerenes must be tested to overcome these issues which oppose the efficient generation of charge transfer states.

Finally, once the efficiencies are optimized in the lab, it is then necessary to manufacture the DCCSs to test them in real life situations, and to optimize their performance before commercialization. The absorption spectra of most of the molecules

used as absorbers / upconverters in TTA do not cover the entire solar spectrum. Therefore it is essential to tune the absorption spectra of these molecules by chemical and structural modifications. Once a library of these molecules is available, a hybrid sandwich structure can be made in which each layer of the structure consists of different upconverter/absorber and each upconverter/absorber absorbs a different part of the solar spectrum so that the whole solar spectrum can be utilized. The performance of DSSCs fabricated based on these principles may depend upon several factors such as the long-term photochemical stability of the upconverter molecule, selection of the semiconductor, electron transport within the semiconductor, nature of the redox electrolyte, etc. Ionic liquids can be proposed as non-volatile, stable, inert electrolytes; however, the implications of using them on the performance of DSSCs based on TTA need to be evaluated.

References

(1) Kamat, P. V. *J. Phys. Chem. C* **2007**, *111*, 2834.

(2) (a) Oregan, B.; Gratzel, M. *Nature* **1991**, *353*, 737. (b) Yella, A.; Lee, H. W.; Tsao, H. N.; Yi, C. Y.; Chandiran, A. K.; Nazeeruddin, M. K.; Diau, E. W. G.; Yeh, C. Y.; Zakeeruddin, S. M.; Gratzel, M. *Science* **2011**, *334*, 629.

(3) Ceroni, P. *Chem. Eur. J.* **2011**, *17*, 9560.

(4) Monguzzi, A.; Frigoli, M.; Larpent, C.; Tubino, R.; Meinardi, F. *Adv. Funct. Mater.* **2012**, *22*, 139.

(5) Bhosale, S. V.; Hackbarth, S.; Langford, S. J. *Chem. Asian J.* **2012**, *7*, 176.

(6) Fuckel, B.; Roberts, D. A.; Cheng, Y. Y.; Clady, R.; Piper, R. B.; Ekins-Daukes, N. J.; Crossley, M. J.; Schmidt, T. W. *J. Phys. Chem. Lett.* **2011**, *2*, 966.

Appendices

Chapter 3

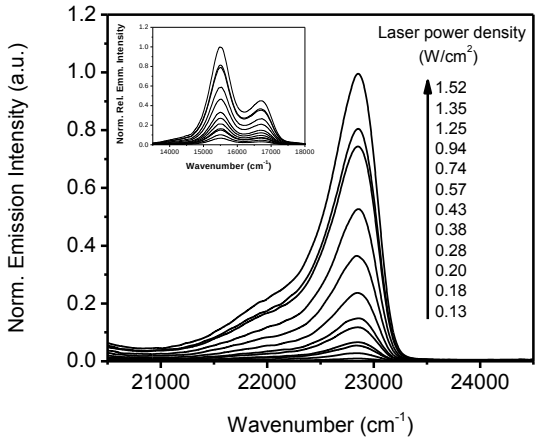

Fig. A.3.1 Upconverted S_2 fluorescence obtained from 1.0×10^{-4} M ZnTPP in benzene as function of incident laser power. Samples were excited in the front face geometry with a 532 nm cw laser and a spectrometer with a 3.6 nm emission band pass. The inset shows the prompt S_1 fluorescence from the same sample as a function of the laser power.

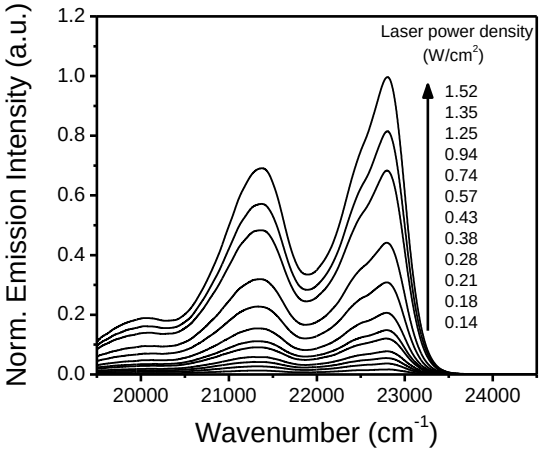

Fig. A.3.2 Upconverted S_1 fluorescence obtained from 1.0×10^{-4} M perylene in a solution containing 1.0×10^{-4} M ZnTPP in benzene as function of incident laser power. Samples were excited in the front face geometry with a 532 nm cw laser and a spectrometer with a 3.6 nm emission band pass.

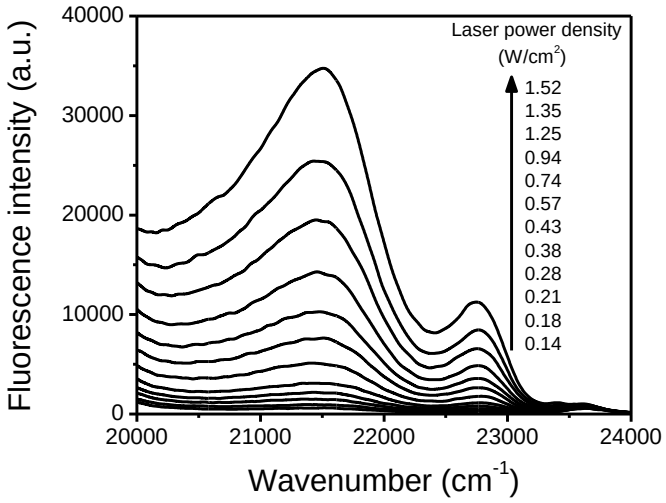

Fig. A.3.3 Upconverted S_1 fluorescence obtained from 5.0×10^{-5} M of C343 in a solution containing 1.0×10^{-4} M ZnTPP in benzene as a function of incident laser power. Samples were excited in rectangular geometry with a 532 nm cw laser and a spectrometer with a 3.6 nm emission band pass.

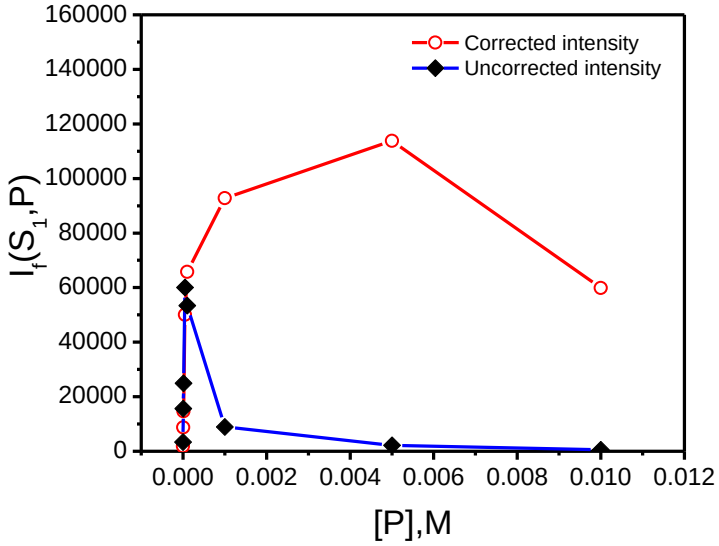

Fig. A.3.4 Comparison of corrected and uncorrected S_1 fluorescence intensities of P. The corrected intensities were obtained using equation 2.6 in Chapter 2.

Derivation of kinetic equation for TTA-S_2 fluorescence *versus* prompt S_1 fluorescence of ZnTPP as a function of incident laser power

The rate equation for the production of the S_2 state of ZnTPP as a result of TTA under steady state excitation conditions is given as,

$$\frac{\mathrm{d}[S_2]}{\mathrm{dt}} = \frac{1}{2}k_{TTA}[T_1]^2 - \left(k_{r,S_2} + k_{nr,S_2}\right)[S_2] = 0 \qquad (1)$$

where k_{TTA} is the rate constant of TTA, k_{r,S_2} and k_{nr,S_2} are the radiative and the nonradiative rate constants of the S_2 state of ZnTPP, respectvely. Therefore,

$$[S_2] = \frac{k_{TTA}}{2\left(k_{r,S_2} + k_{nr,S_2}\right)}[T_1]^2 \qquad (2)$$

Similarly, the steady state approximation for the triplet concentration of ZnTPP is given by,

$$\frac{\mathrm{d}[T_1]}{\mathrm{dt}} = \varepsilon(\bar{\nu})I_{exc}\phi_{ISC} - \left(k_{r,T_1} + k_{nr,T_1}\right)[T_1] - k_{TTA}[T_1]^2 = 0 \qquad (3)$$

where $\varepsilon(\bar{\nu})$ is the molar extinction coefficient at the excitation wavelength, I_{exc} is the incident laser intensity and ϕ_{ISC} is the S_1-T_1 intersystem crossing quantum yield. It is reasonable to assume that $\varepsilon(\bar{\nu})I_{exc}$ is proportional to the S_1 state concentration, $[S_1]$.

Under low illumination intensities in the weak annihilation limit where $\left(k_{r,T_1} + k_{nr,T_1}\right)[T_1] \gg k_{TTA}[T_1]^2$, equations (2) and (3) give,

$$[S_2] = \frac{k_{TTA}\varepsilon(\bar{\nu})^2 {I_{exc}}^2 {\phi_{ISC}}^2}{2\left(k_{r,S_2} + k_{nr,S_2}\right)\left(k_{r,T_1} + k_{nr,T_1}\right)^2} \propto [S_1]^2 \qquad (4)$$

which will give a slope = 2 if log[S_2] is plotted against log[S_1].

At high excitation conditions (strong annihilation limit) where $\left(k_{r,T_1} + k_{nr,T_1}\right)[T_1] \ll k_{TTA}[T_1]^2$, equations (2) and (3) give,

$$[S_2] = \frac{\varepsilon(\bar{\nu}) I_{exc} \phi_{ISC}}{2\left(k_{r,S_2} + k_{nr,S_2}\right)} \propto [S_1] \qquad (5)$$

which gives a slope = 1 for a plot of log[S_2] *versus* log[S_1].

At the threshold excitation intensity (I_{th}) when the plot starts to deviate from a slope = 2 to slope = 1, equations (4) and (5) are equal. Therefore, the threshold intensity is given by,

$$I_{th} = \frac{\left(k_{r,T_1} + k_{nr,T_1}\right)^2}{\phi_{TTA} k_{T_1} \varepsilon(\bar{\nu}) \phi_{ISC}} \qquad (6)$$

where the efficiency of the TTA process, $\phi_{TTA} = k_{TTA}/k_{T_1}$, where k_{T_1} is the total decay rate constant of the triplet state.

Derivation of kinetic equation for K_{as} between ZnTPP and C343 triplets

Various possible photophysical processes associated with TTA are given below.

$$S_0(MP) + h\nu_{vis} \rightarrow S_1(MP) \qquad (1)$$

$$S_1(MP) \rightarrow T_1(MP) \quad (\eta_{isc} \sim 1) \qquad (2)$$

$$2\ T_1(MP) \rightarrow S_2(MP) + S_0(MP) \qquad (3)$$

$$T_1(MP) + S_0(BE) \leftrightarrows {}^3(MP\cdots BE) \qquad (4)$$

$${}^3(MP\cdots BE) + T_1(MP) \rightarrow 2\ S_0(MP) + S_1(BE) \qquad (5)$$

Under steady state conditions, the intensity of fluorescence from the S_2 state of ZnTPP is $I_{f,S2} = k_{r,S2}[S_2(MP)]$; that from the blue emitter C343 is $I_{f,BE} = k_{r,BE}[S_1(BE)]$ where the k_r are the respective radiative decay constants of the fluorescent species. The concentrations of the fluorescing intermediates can be obtained by solving differential equations for $d[S_2(MP)]/dt$ and $d[S_1(MP)]/dt$ in the steady state limit. i.e.

$$[S_2(MP)]_{SS} = \frac{k_7[T_1(MP)]^2}{(k_{r,S_2} + k_{nr,S_2})} \qquad (6)$$

$$[S_1(BE)]_{ss} = \frac{k_{13}[T_1(MP)][{}^3(MP\cdots BE)]}{(k_{r,BE} + k_{nr,BE})} \qquad (7)$$

where k_r and k_{nr} are the radiative and nonradiative rate constants respectively for the two fluorescing species. The desired ratio, R_f, is then obtained by noting that $\phi_{f,S2} = k_{r,S2}/(k_{r,S2} + k_{nr,S2})$, $\phi_{f,BE} = k_{r,BE}/(k_{r,BE} + k_{nr,BE})$, and $[T_1(MP)]/[{}^3(MP\cdots BE)] = 1/(K_{as}[BE])$.

$$R_f = \frac{I_{f,S_2}}{I_{f,BE}} = \frac{\phi_{f,S_2}}{\phi_{f,BE}} \cdot \frac{k_3}{k_5} \cdot \frac{1}{K_{as}[BE]} \qquad (8)$$

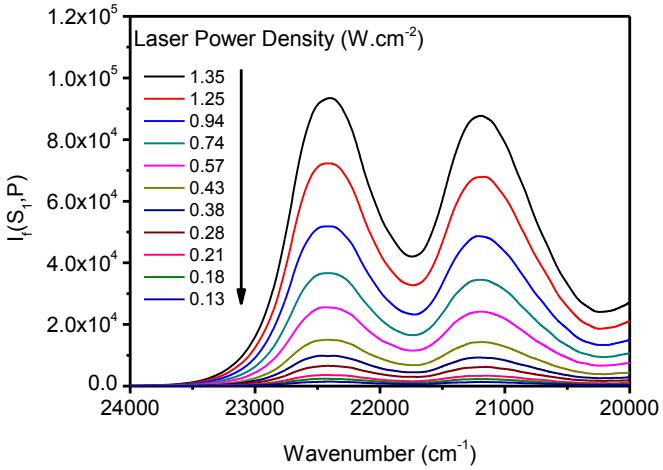

Fig. A.4.1 Plot of the upconverted fluorescence as a function of the incident laser density on an equimolar (1.0×10^{-4} M) mixture of C_{60} mixed with P. All the samples were excited with 532 nm laser, the excitation monochromator band width is fixed at 2.0 nm and the emission band pass was fixed at 4.0 nm.

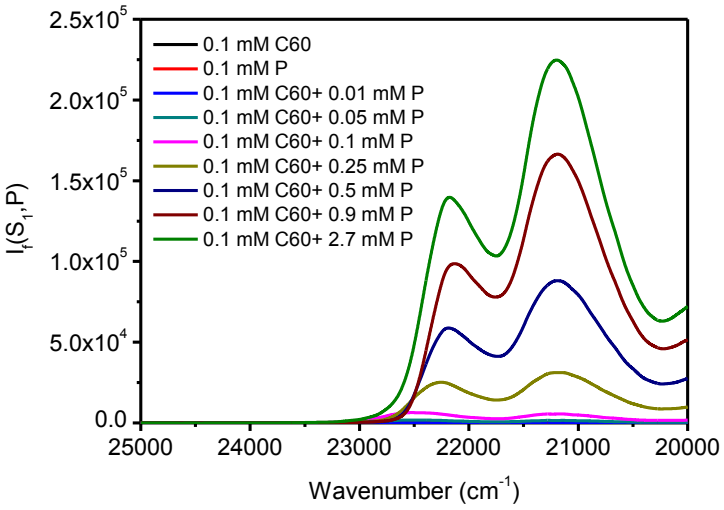

Fig. A.4.2 Plot of upconverted fluorescence from 1.0×10^{-4} M of C_{60} mixed with various concentration of P. All the samples were excited with 532 nm laser, the excitation monochromator band width is fixed at 2.0 nm and the emission band pass was fixed at 0.4 nm.

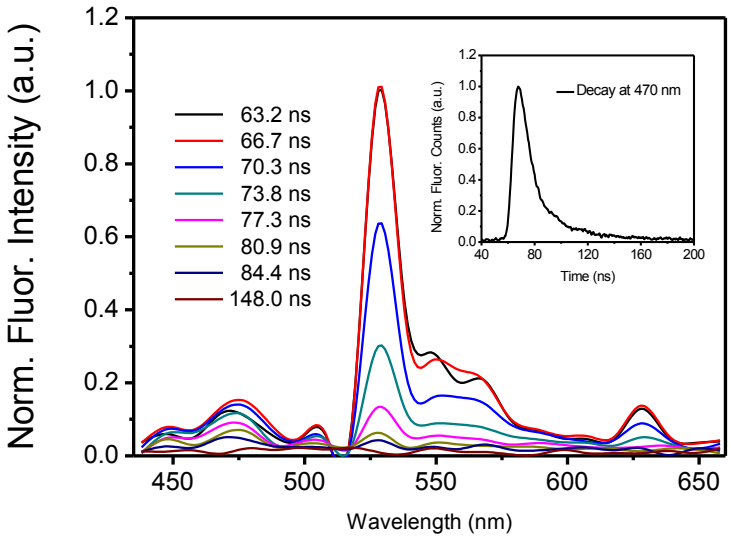

Fig. A.4.3 Fluorescence spectrum of 1×10^{-4} M P in toluene excited at 532 nm. The inset shows the fluorescence decay of P measured at 470 nm. The laser pulse width was 5 ns and the laser power on density on the sample was 0.34 $W.cm^{-2}$.

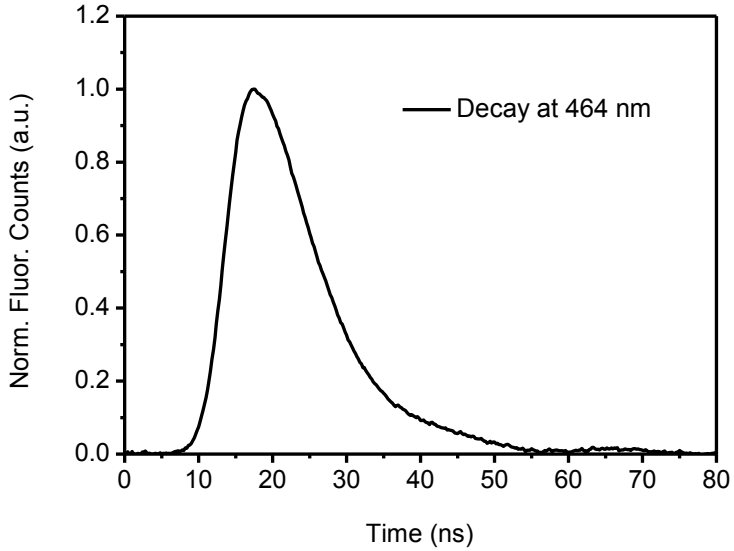

Fig. A.4.4 Fluorescence decay of 1.2×10^{-4} M P in toluene excited at 355 nm. The decay was observed at 464 nm. The laser pulse width was 5 ns.

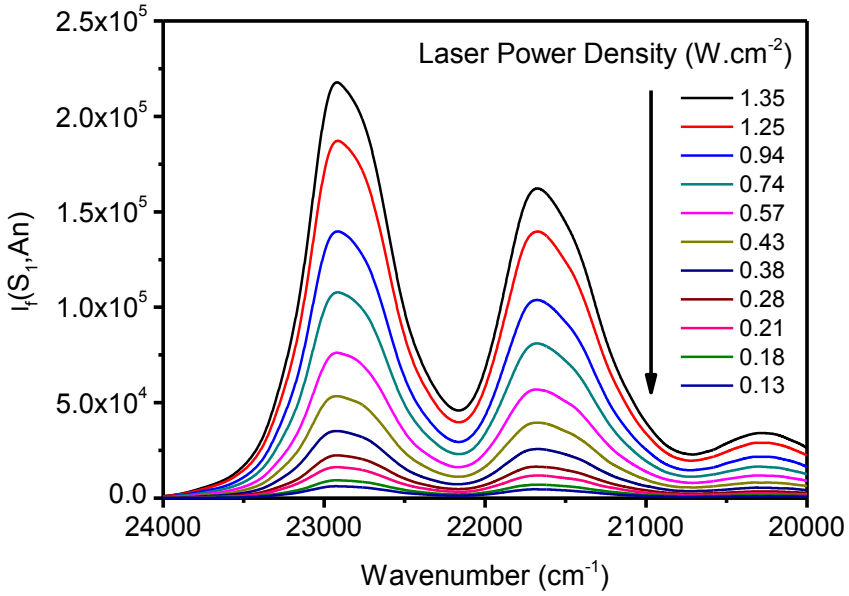

Fig. A.4.5 Plot of the upconverted fluorescence *vs.* the incident laser density on an equimolar (1.0×10^{-4} M) mixture of C_{60} mixed with An. All the samples were excited with 532 nm laser, the excitation monochromator band width is fixed at 2.0 nm and the emission band pass was fixed at 4.0 nm.

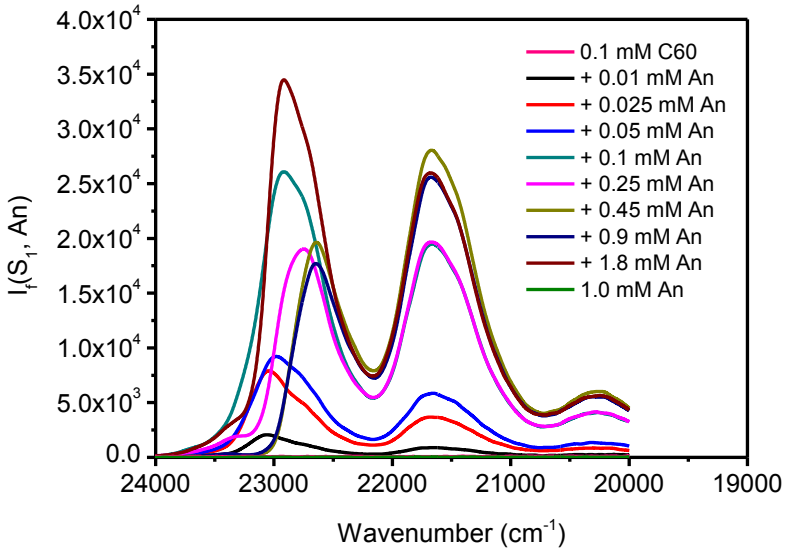

Fig. A.4.6 Plot of upconverted fluorescence from 1.0×10^{-4} M of C_{60} mixed with various concentration of An. All the samples were excited with 532 nm laser, the excitation monochromator band width is fixed at 2.0 nm and the emission band pass was fixed at 0.2 nm.

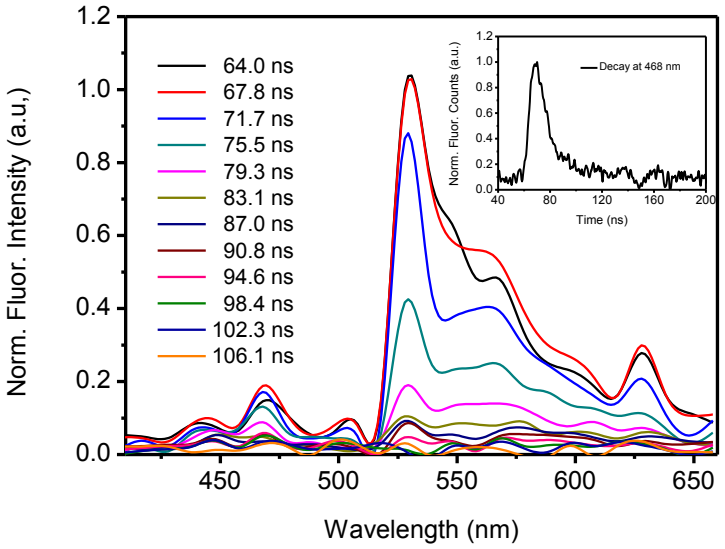

Fig. A.4.7 Time-resolved fluorescence spectrum of 1×10^{-4} M An in toluene excited at 532 nm. The inset shows the kinetic decay measured at 468 nm. The laser pulse width was 5 ns and the laser power on density on the sample was 0.34 $W.cm^{-2}$.

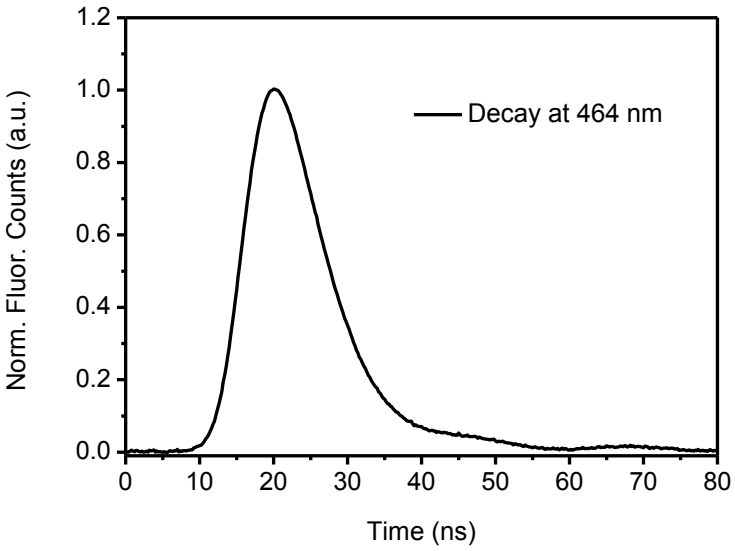

Fig. A.4.8 Fluorescence decay of 1.3×10^{-4} M An in toluene excited at 355 nm. The decay was observed at 464 nm. The laser pulse width was 5 ns.

Chapter 5

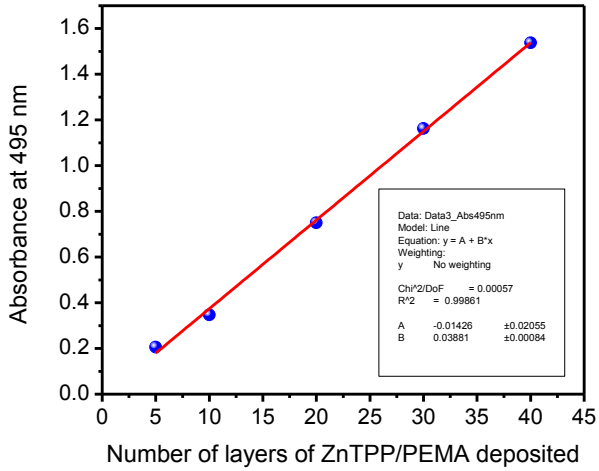

Fig. A.5.1 Absorbance of ZnTPP in PEMA versus the number of layers of sample deposited. R^2 = 0.99 for the least-squares fit.

Program for fitting the oxygen diffusion data

The oxygen diffusion data was fitted using equations (4.1), (4.2) and (4.4). The program was written in Origin 7.0 C-compiler by Dr. Jędrzej Szmytkowski. The fitting was started from time, t > 0. The integration was performed using Simpson's rule of definite integrals according to the following equation,

$$\int_a^b \mathrm{f}(x)\mathrm{d}x \approx \frac{h}{3}\left[\mathrm{f}(x_0) + 2\sum_{i=1}^{n/2-1}\mathrm{f}(x_{2i}) + 4\sum_{i=1}^{n/2}\mathrm{f}(x_{2i-1}) + \mathrm{f}(x_n)\right]$$

The program is outlined below.

Parameter names: C1,l,eps,D,A,B,be
Independent variable: t

Dependent variable: y

Program code:

```
double X1,X2,h,sum1,sum2,pom;
int m,j;
double integ,integ1,integ2,C,suma1,suma2,CX1,CX2;
double suma1X1,suma1X2,suma2X1,suma2X2;
int i,n;
X1=0;
X2=1;
n=50;
m=50;
h=(X2-X1)/m;
sum1=0;
j=2;
do
{
pom=X1+j*h;
suma1=0;
for(i=0; i<=n; ++i)
suma1=suma1+((-1)^i)*(1-erf(((2*i+1)*l-l*pom)/(2*sqrt(D*t))));
suma2=0;
for(i=0; i<=n; ++i)
suma2=suma2+((-1)^i)*(1-erf(((2*i+1)*l+l*pom)/(2*sqrt(D*t))));
C=C1*(suma1+suma2);
integ=(10^(eps*l))/(1+(A+B+be)*C+(A*be)*C^2);
sum1=sum1+integ;
j=j+2;
}while(j<=m);
sum2=0;
j=1;
do
{
pom=X1+j*h;
```

```
suma1=0;
for(i=0; i<=n; ++i)
suma1=suma1+((-1)^i)*(1-erf(((2*i+1)*l-l*pom)/(2*sqrt(D*t))));
suma2=0;
for(i=0; i<=n; ++i)
suma2=suma2+((-1)^i)*(1-erf(((2*i+1)*l+l*pom)/(2*sqrt(D*t))));
C=C1*(suma1+suma2);
integ=(10^(eps*l))/(1+(A+B+be)*C+(A*be)*C^2);
sum2=sum2+integ;
j=j+2;
}while(j<=m);
suma1X1=0;
suma1X2=0;
for(i=0; i<=n; ++i){
suma1X1=suma1X1+((-1)^i)*(1-erf(((2*i+1)*l-l*X1)/(2*sqrt(D*t))));
suma1X2=suma1X2+((-1)^i)*(1-erf(((2*i+1)*l-l*X2)/(2*sqrt(D*t))));
}
suma2X1=0;
suma2X2=0;
for(i=0; i<=n; ++i){
suma2X1=suma2X1+((-1)^i)*(1-erf(((2*i+1)*l+l*X1)/(2*sqrt(D*t))));
suma2X2=suma2X2+((-1)^i)*(1-erf(((2*i+1)*l+l*X2)/(2*sqrt(D*t))));
}
CX1=C1*(suma1X1+suma2X1);
CX2=C1*(suma1X2+suma2X2);
integ1=(10^(eps*l))/(1+(A+B+be)*CX1+(A*be)*CX1^2);
integ2=(10^(eps*l))/(1+(A+B+be)*CX2+(A*be)*CX2^2);
y = (h/3)*(integ1 + 2*sum1 + 4*sum2 + integ2);
```

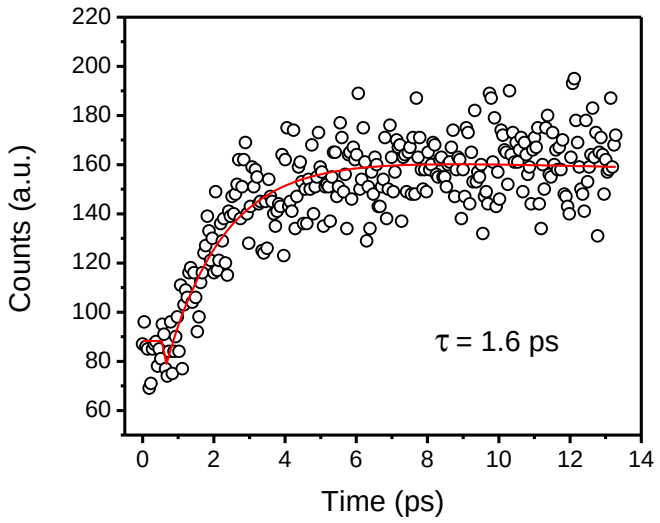

Fig. A.6.1 S_1 rise of 200μM ZnTPP + 300μM C_{60} in toluene. Excitation was at 400 nm and the S_1 fluorescence rise was monitored at 655 nm. The time delay per data point is 47 fs. Measured and analyzed by Dr. Jędrzej Szmytkowski.

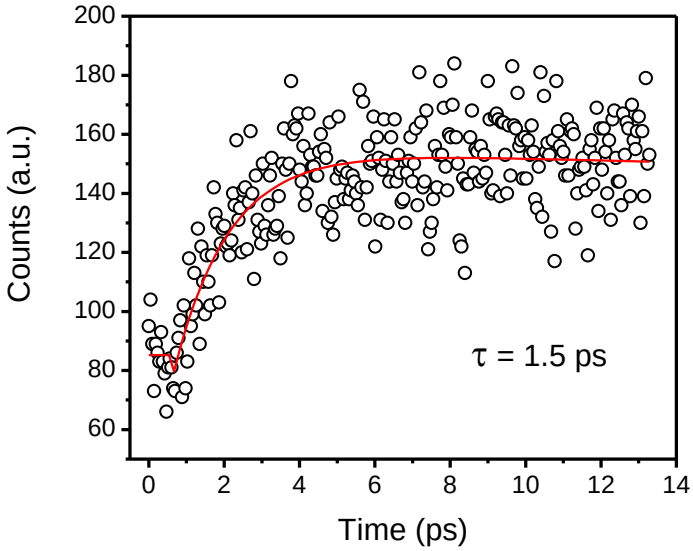

Fig. A.6.2 S_1 rise of 200μM ZnTPP + 1000μM C_{60} in toluene. Excitation was at 400 nm and the S_1 fluorescence rise was monitored at 655 nm. The time delay per data point is 47 fs. Measured and analyzed by Dr. Jędrzej Szmytkowski.

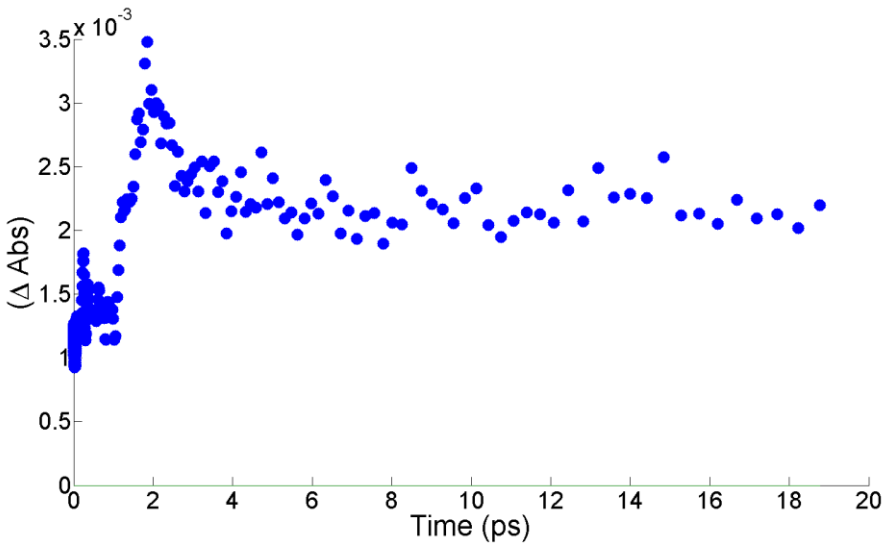

Fig. A.6.3 Kinetic trace of the formation on a ps time scale of a long-lived transient observed at 660 nm of the absorbance adjusted difference spectrum of ZnTPP + C_{60} system in benzonitrile. Measured and analyzed by Benjamin Robotham of School of Chemistry, University of Melbourne, Australia.

Program for fitting the fluorescence upconversion data

Paramater names: sigma, e1, e2, e3, e4, e5, e6, e7, e8

Variables: tzero, fwhm, c0, c1, tau1, c2, tau2, c3, tau3, c4, tau4

Independent variable: t

Dependent variable: f(t)

Program code:

```
fwhm=fwhm
tzero=t0
c0=c0
c1=c1
tau1=tau1
c2=c2
```

```
tau2=tau2
c3=c3
tau3=tau3
c4=c4
tau4=tau4
sigma=fwhm/(2*sqrt(2*ln(2)))
// sigma is the standard deviation for the gaussian (function of the fwhm)
e1= exp(-(t-tzero)/tau1)*exp((sigma/tau1)^2/2)
e2= (1-erf((sigma/tau1-(t-tzero)/sigma)/sqrt(2)))/2
//e1*e2 for exp(-t/tau1)
e3= exp(-(t-tzero)/tau2)*exp((sigma/tau2)^2/2)
e4= (1-erf((sigma/tau2-(t-tzero)/sigma)/sqrt(2)))/2
//e3*e4 for exp(-t/tau2)
e5= exp(-(t-tzero)/tau3)*exp((sigma/tau3)^2/2)
e6= (1-erf((sigma/tau3-(t-tzero)/sigma)/sqrt(2)))/2
//e5*e6 for exp(-t/tau3)
e7= exp(-(t-tzero)/tau4)*exp((sigma/tau4)^2/2)
e8= (1-erf((sigma/tau4-(t-tzero)/sigma)/sqrt(2)))/2
//e7*e8 for exp(-t/tau4)
f(t) = (c0+c1*e1*e2+c2*e3*e4+c3*e5*e6+c4*e7*e8)
```

Picosecond transient absorption spectroscopy at University of Melbourne, Australia

"The following details were provided by Benjamin Robotham, School of Chemistry, University of Melbourne."

Picosecond transient absorption spectra were recorded using an ultrafast excitation source consisting of a Ti:sapphire laser (Coherent, Mira) combined with a regenerative amplifier (Coherent, RegA 9050) operating at a 94 kHz pulse repetition rate at an output average power of ~500 mW at 830 nm. Half of the amplified output was directed to an OPA (Coherent, OPA 9400) and the second harmonic output at 415 nm was used as the pump beam with an average power of ~70 mW. This pump beam was modulated with a light chopper (Thorlabs, MC1000/MC1F60) before passing through a variable optical

delay line (Newport, UTS150PP with ESP 300 controller) and a Berek compensator (New Focus, 5540) to the sample cell (Starna, 2 mm path length). The other half of the amplified laser output was focused into a 3 mm sapphire crystal (Crystalsystems) to provide a continuum probe beam with an employed range of 460 to 760 nm.

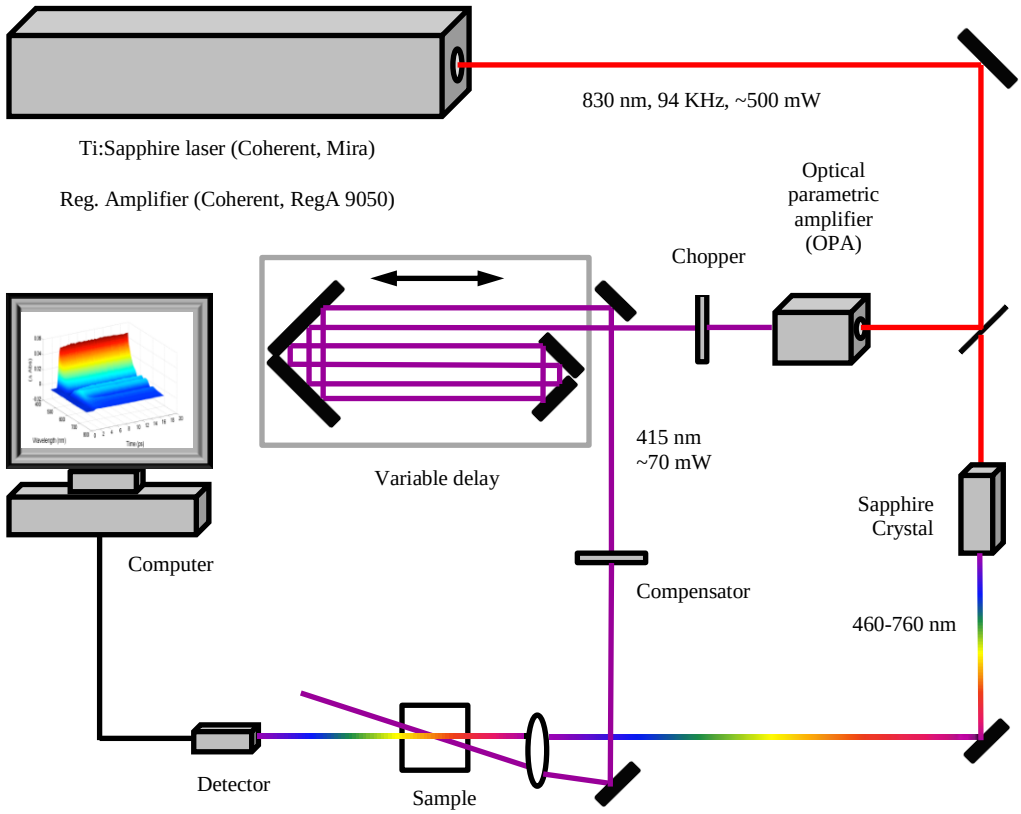

Fig A.6.4 General optical scheme of a picosecond transient absorption spectrophotometer used by Benjamin Robotham of School of Chemistry, University of Melbourne, Australia.

The relative polarization of the pump and probe beams were set to 54.7 degrees (the magic angle) to remove any decay artifacts due to molecular rotation. After passing

through the sample the probe beam was delivered to a CMOS detector (Ultrafast Systems) by a 200 μm fiber (Ocean Optics, P200-2-UV-VIS). Data acquisition was controlled by a MATLAB (Mathworks) program developed in-house. All spectra were corrected for the chirp of the probe continuum. The time resolution of the system was approximately 200 fs.

Samples of ZnTPP (100 μM in both toluene and benzonitrile), C_{60} (1 mM in toluene, 0.2 mM in benzonitrile) and a mixture of both with identical respective concentrations were excited with 415 nm pulses and probed as described above in the 460 to 760 nm region. An interval of 20 ps was scanned with 200 logarithmically spaced delay positions and the spectra collected were averaged over 20 scans. All measurements were carried out in aerated solutions to minimize the build-up of long-lived triplet species. The solutions in the sample cell were stirred continuously during measurement by a magnetic stirrer bead.